

**Evaluation of the Seismic Design Methods for Steel Multi-Tiered Concentrically Braced
Frames**

by

Pablo Antonio Cano

A thesis submitted in partial fulfillment of the requirements for the degree of

Master of Science

in

STRUCTURAL ENGINEERING

Department of Civil and Environmental Engineering
University of Alberta

© Pablo Antonio Cano, 2019

Abstract

Multi-tiered concentrically braced frames (MT-CBFs) are widely used in North America as the lateral load-resisting system of tall single-storey buildings such as airplane hangars, recreational facilities, shopping centres, and industrial buildings. MT-CBFs consist of multiple concentrically braced panels along the height of the frame separated by horizontal struts. Multi-tier arrangements are typically used when it is not practical nor economical to use a single bracing panel along the height of the frame between the ground and roof levels. In multi-tiered braced frames, the length of braces is reduced, which allows the selection of smaller brace sizes and easily satisfying code-specified brace slenderness limits. The column buckling length in the in-plane direction is also reduced due to the application of intermediate horizontal struts, which permits selection of a smaller column section. When using shorter braces, result in smaller design forces on the adjacent forced-controlled members including struts, beams, columns, and connections.

Past studies have shown that inelastic frame deformations tend to concentrate in one of the tiers over the frame height, which induces large in-plane bending moments in braced frame columns and high deformation demands in braces. This behaviour may lead to column buckling and/or brace fracture. Design requirements have been included in the Canadian steel design standard (CSA S16) and the U.S. Seismic Provisions to prevent such limit states. In the U.S., the Seismic Provisions have included the design of multi-tiered ordinary and special concentrically braced frames (MT-OCBFs and MT-SCBFs). However, there are no detailed numerical models or experimental research to validate the design requirements.

This M.Sc. thesis research focuses on the evaluation of the seismic behaviour and design methods for MT-CBFs. A two-tiered CBF prototype frame was first designed as a special concentrically

braced frame using the 2010 and 2016 AISC Seismic Provisions. Then, a detailed numerical model was developed and was analyzed using the cyclic pushover (static) analysis and the nonlinear response history (dynamic) analysis. The global and local response of the prototype frames together with the force demands in the columns were examined using the results obtained from the numerical analyses. Special attention was paid to the stability condition of the column as well as in-plane and out-of-plane moments induced in this member.

Results obtained for the prototype frame designed excluding the special seismic design provisions confirmed column buckling and nonuniform distribution of the frame inelastic lateral deformations in the tier where brace tensile yielding takes place first. A total of 13 column buckling cases were observed using the dynamic analysis method among an ensemble of 40 ground motion records. Moreover, excessive deformations, which is an indication of brace low-cycle fracture, were observed in the yielding tier of this prototype frame. In contrast, the prototype braced frame that was designed in accordance with the recent special seismic design provisions performed satisfactorily. No column buckling occurred and the frame lateral response was stable. Braces in both tiers yielded under most ground motion records and frame inelastic lateral deformations were shared between both tiers. It was found that the column moment demands prescribed by the current design provisions over estimates the moment demands obtained under a major earthquake event. Additionally, expected storey drift was found to be higher than the code-specified design storey drift, which resulted in large ductility demands in braced tiers, which poses concerns regarding the adequacy of the current drift requirements. New brace force adjustment factors are proposed to achieve more realistic brace nonlinear forces when computing column force demands and tier drifts.

Preface

This thesis is an original work by Pablo A. Cano. Parts of Chapters 3, 4, and 5 were presented at the 2018 Annual Structural Stability Research Council (SSRC) conference held in Baltimore, Maryland, U.S. and submitted to the 2019 American Society of Civil Engineers Structures Congress to be held in Orlando, Florida, U.S. The work presented at these two conferences was co-authored with Dr. Ali Imanpour. The conference paper published in the 2018 SSRC conference proceeding associated with this research has been invited to be published in the American Institute of Steel Construction (AISC) Engineering Journal, which will be submitted for publication.

Dedication

To the victims of the 1999 Armenia earthquake

and

to my parents for encouraging me to strive to surpass myself each day.

Acknowledgements

First, I would like to express my most profound gratitude to my supervisor, Dr. Ali Imanpour. His crucial guidance and continuous encouragement have led me to progress as an academic and as a professional, but more important—as a person. Thank you for sharing your knowledge and passion about seismic engineering. It is a privilege to continue my doctoral studies with you as my supervisor. Many thanks to Dr. Robert G. Driver and Dr. Douglas Tomlinson for their time in reviewing this thesis. I would also like to thank Dr. Robert Tremblay for his input in this research. I am very thankful for the advice provided by Dr. Cristopher Stoakes in the development of the numerical model used in this thesis. I am very grateful with Yan Jiang for sharing the experimental data of the bracing member and Dr. Ali Davaran for the advice provided.

Furthermore, I would like to express my genuine appreciation to the Steel Centre for providing unique learning opportunities and encouragement to challenge traditional boundaries. Additionally, I would like to thank my colleagues from the Steel Centre for their advice throughout this project.

I would like to acknowledge the financial support from the Natural Sciences and Engineering Research Council (NSERC), American Institute of Steel Construction (AISC), Canadian Institute of Steel Construction (CISC), and the faculties of Engineering and Graduate Studies and Research at the University of Alberta.

I would also like to thank my family, who have supported me throughout this journey and have given me their perpetual love.

Last, but certainly not least, I would like to thank my beloved girlfriend, Paula, for believing in me and always being there for me. Words do not exist to express how thankful I am for the unremitting love and support that I have felt.

Contents

Chapter 1 – Introduction	1
1.1 Background.....	1
1.2 Research Problem	3
1.3 Objectives	6
1.4 Methodology.....	7
1.5 Thesis Organization	8
Chapter 2 – Literature Review	9
2.1 General.....	9
2.2 Seismic Behaviour of Steel Braces.....	9
2.3 Seismic Behaviour of Steel Concentrically Braced Frames	17
2.4 Seismic Behaviour of Steel MT-CBFs	21
2.5 Design of MT-CBFs	35
Chapter 3 – Design of Steel Multi-Tiered Concentrically Braced Frames	42
3.1 General.....	42
3.2 Building and Frame Geometry.....	42
3.3 Gravity and Seismic Loads	44
3.4 Brace Design.....	45
3.5 Column Design	46
3.6 Strut Design	54

3.7 Drift Check.....	56
3.8 Design Summary.....	58
Chapter 4 – Numerical Model of the Braced Frames	60
4.1 General.....	60
4.2 Model Development.....	60
4.3 Analysis.....	74
Chapter 5 – Seismic Response of Two-Tiered Steel Concentrically Braced Frames.....	81
5.1 General.....	81
5.2 Pushover Analysis.....	81
5.3 Nonlinear Response History Analysis	88
5.4 Summary.....	109
Chapter 6 – Design Recommendations	110
6.1 General.....	110
6.2 Strength Requirements.....	110
6.2 Drift Requirement.....	115
6.3 Case Study	118
Chapter 7 – Conclusions and Recommendations.....	124
7.1 Summary.....	124
7.2 Limitations	126

7.3 Conclusions.....	126
7.4 Recommendations for Further Research.....	129
Bibliography	131

List of Tables

Table 3.1: Summary of design calculations for the prototype frame.....	59
Table 4.1: Selected ground motions for dynamic analysis (Dehghani 2016).....	76
Table 5.1: Tier drifts at a storey drift 2.0%.....	84
Table 5.2: Statistics of the global response of the 2010 design	91
Table 5.3: Statistics of global response of the 2016 design	93
Table 5.4: Statistics of column demands for 2010 design	99
Table 5.5: Statistics of column demands for 2016 design	100
Table 6.1: Statistics of column axial force and biaxial moment demands plus brace forces at the maximum interaction ratio.....	111
Table 6.2: Statistics of brace forces at the maximum storey drift	117

List of Figures

Figure 1.1: a) four-tiered concentrically braced frame in an industrial building; b) two-tiered concentrically braced frame in an industrial building.....	2
Figure 1.2: MT-CBFs configurations a) X-shape; b) V-shape; c) diagonals; d) chevron; and e) split-X	2
Figure 1.3: Inelastic response of a) K-type CBF; and b) standard CBF	5
Figure 2.1: Hysteretic response of steel bracing members	10
Figure 2.2: Influence of global slenderness ratio on the hysteretic response of steel braces (Ziemian 2010).....	11
Figure 2.3: Inelastic response of chevron braced frame when plastic hinge forming in the beam11	
Figure 2.4: HSS brace out-of-plane buckling (Sabelli et al. 2013).....	13
Figure 2.5: Effect of loading velocity (v in mm/s) on the steel brace buckling capacity (Kazemzadeh Azad et al. 2018).....	14
Figure 2.6: Hysteretic response of a steel bracing member obtained from a) quasi-static loading, and b) dynamic loading with $v = 300\text{mm/s}$ (Kazemzadeh Azad et al. 2018).....	14
Figure 2.7: HSS members under cyclic loading: a) Local buckling; and b) fracture of (Fell et al. 2009)	15
Figure 2.8: Influence of the brace slenderness on the fracture life of HSS members (Tremblay 2001).....	16
Figure 2.9: rotation at fracture: test data versus values predicted (Tremblay et al. 2003).....	16

Figure 2.10 Brace fracture limit varying with a) brace width-to-thickness ratio ($KL/r = 52.6$ and $E/F_y = 446$ MPa); and b) brace slenderness ratio ($b/t = 11.3$ and $E/F_y = 446$ MPa) (Hsiao et al. 2013)	17
.....	
Figure 2.11: Single-storey steel concentrically braced frame.....	18
Figure 2.12: Progression of seismic behaviour of single-storey CBF	19
Figure 2.13: Linear hinge zone for out-of-plane buckling of steel braces (Sabelli et al. 2013) ...	20
Figure 2.14: Typical MT-CBF configurations (AISC 2016a)	22
Figure 2.15: Comparison between Multi-tiered CBFs and Multi-storey CBF	23
Figure 2.16: Drift in individual braced panels of a two-tiered CBF and column in-plane bending demand recorded between the braced panels (Imanpour and Tremblay 2012)	24
Figure 2.17: Two-tiered concentrically braced frame geometry (Imanpour and Tremblay 2012)	24
Figure 2.18: Normal stress contour (ksi, where 1 MPa = 0.145 ksi) of the column at maximum Tier 1 drift (Imanpour et al. 2013).....	25
Figure 2.19: Frame deformed shape at the instant of column buckling (Imanpour et al. 2016a).	27
Figure 2.20: Improved lateral response of a two-tiered steel CBF: a) Brace yielding and buckling in Tier 1 and initiation of brace tensile yielding in Tier 2; and b) Proposed brace force scenario to trigger yielding in the noncritical tier (critical tier: Tier 1; and noncritical tier: Tier 2)	28
Figure 2.21:a) Column free-body diagram under unbalanced brace story shear; b) column shear force diagram; and c) column bending moment diagram	29
Figure 2.22: Three-tiered steel braced frame with adjacent gravity columns.....	30
Figure 2.23: W250x101 column part of a two-tiered CBF in the multi-directional hybrid testing system (Imanpour et al. 2017)	32

Figure 2.24: Local buckling of Wide-flange steel columns as part of multi-storey CBFs (Newell and Uang 2008).....	32
Figure 2.25: Lateral instability of steel Wide-flange column as part of MRFs (Elkady and Lignos 2018).....	33
Figure 2.26: Failure modes observed in wide-flange steel MRF columns: a) symmetric flange buckling; b) anti-symmetric local buckling; c) and coupled buckling (Ozkula et al. 2017)	34
Figure 2.27: Out-of-plane notional load applied at the tier level.....	36
Figure 2.28: Analysis cases prescribed by AISC Seismic Provisions for columns, beams, and connections	38
Figure 2.29: Progression of brace buckling and yielding in MT-SCBFs (AISC 2016a).....	40
Figure 2.30: Forces arise from out-of-plane brace buckling (AISC 2016a).....	41
Figure 3.1: Three-dimensional schematic of a single storey building with two-tiered CBFs (roof trusses not shown), figure not to scale	43
Figure 3.2: Geometry of the prototype frame	43
Figure 3.3: Design response spectrum	45
Figure 3.4: Brace loading scenarios: a) Analysis case A; and b) Analysis case B.....	48
Figure 3.5: Column buckling mode shapes: a) In-plane mode; and b) out-of-plane mode	49
Figure 3.6: Brace loading scenario for Analysis case C	51
Figure 3.7: Analysis case C: a) frame deformed shape ; b) frame free-body diagram; c) column free-body diagram; d) column shear force diagram; and e) column bending moment diagram under ΔV_{br}	53
Figure 3.8: Strut-to-column connection a) 2010 design; and b) 2016 design.....	55

Figure 3.9: Frame deformed shape at expected storey drift from analyses	58
Figure 3.10: Prototype frame designed in accordance with the a) 2010 AISC Seismic Provisions; and b) 2016 AISC Seismic Provisions.....	59
Figure 4.1: Three-dimensional 4-node general-purpose shell element with reduced integration.	61
Figure 4.2: One-dimensional representation of the hardening in the nonlinear isotropic/kinematic model (Adopted from Dassault Systèmes 2014)	63
Figure 4.3: Finite element model of the isolated HSS 127×127×7.9 member	64
Figure 4.4: HSS brace mesh across the section wall with various divisions a) one shell element; b) two shell elements; c) four shell elements; d) eight shell elements; e) and twelve shell elements	64
Figure 4.5: Axial force–axial deformation response of the HSS127×127×7.9 brace under incremental cyclic loading (test data by Jiang 2012).....	65
Figure 4.6: Lateral displacement at buckling using different mesh size elements	66
Figure 4.7: Simulation of flexural plastic hinging and local buckling of HSS127×127×7.9 $\delta = 4.5\delta_y$	67
Figure 4.8: Finite element model of the steel two-tiered concentrically braced frame	67
Figure 4.9: Constraint applied at the base of the frame	68
Figure 4.10: Boundary conditions assigned to the columns a) in the plane of the frame; and b) out of the plane of the frame	69
Figure 4.11: Two-tiered CBF with adjacent leaning column	70
Figure 4.12: In-plane and out-of-plane initial geometric imperfections: a) CBF elevations; and b) CBF side view (deformations magnified).....	71
Figure 4.13: Residual stress pattern assigned to Wide-flange sections	73

Figure 4.14: Gravity analysis step	73
Figure 4.15: Pushover loading protocol.....	74
Figure 4.16: Inertia point masses assigned to the braced frame model	77
Figure 4.17: HSS 89×89×6.4 brace hysteretic response under 1980 Irpinia, Italy (SCC1) ground motion record using a) full density; and b) 0.1% density	78
Figure 4.18: Influence of column density on the out-of-plane moment under the 1980 Irpinia, Italy (SCC1) ground motion record	79
Figure 5.1: Normalized lateral load–lateral displacement response: (a) 2010 design; and (b)2016 design, (V is the design base shear as defined in Section 3.3).....	82
Figure 5.2: Frame deformed shape: (a) 2010 design: column buckling at story drift 2.0%; and (b) 2016 design final deformed shape at story drift 2.1%	83
Figure 5.3: Tier drifts: a) 2010 design; and b) 2016 design.....	84
Figure 5.4: Normalized brace axial force: (a) continuous braces of the 2010 design; (b) discontinuous braces of the 2010 design; (c) continuous braces of the 2016 design; (d) discontinuous braces of the 2016 design	85
Figure 5.5: Column in-plane bending moments for a) 2010 design; and b) 2016 design.....	87
Figure 5.6: Deformed shape with Von-Mises stress contour at the verge of RHS column buckling at 2.0% storey drift.....	87
Figure 5.7: Column out-of-plane bending moments for a) the 2010 design; and b) the 2016 design	88

Figure 5.8: 2010 frame deformed shape under 1994 Northridge (SCC14) ground motion record: a) onset of LHS column buckling at $t = 4.70$ s and story drift of 1.7%; b) LHS column buckling at $t = 5.38$ s; and c) frame collapse at $t = 5.49$ s	89
Figure 5.9: 2010 design a) maximum storey drift under 40 ground motion records; and b) storey drifts at buckling under 13 collapsed ground motion records.....	90
Figure 5.10: 2010 design response under 2007 Pisco, Peru (SCI7) ground motion record: a) axial force–axial displacement response of LHS column; and b) base shear–storey drift response(frame lateral shear force is normalized by the design base shear, V ; and dots represent the instant of column buckling)	92
Figure 5.11: 2010 design: LHS column buckling at 34.7 s and 1.6% storey drift under 2007 Pisco, Peru (SCI7) ground motion record	94
Figure 5.12: 2016 design: maximum storey drifts under the 40 ground motion records.....	94
Figure 5.13: 2010 design a) Tier 1 drift; and b) Tier 2 drift	95
Figure 5.14: 2016 design a) Tier 1 drift; and b) Tier 2 drift	96
Figure 5.15: Brace axial force response in Tier 1 and Tier 2 under 2007 Pisco, Peru (SCI7) ground motion record: a) 2010 design; and b) 2016 design.....	97
Figure 5.16: Local buckling of the first tier brace in 2010 design under 2011 Tohoku, Japan (SCI3) ground motion record at 9.7 s 1.5% storey drift and 2.6% tier drift.....	98
Figure 5.17: Column in-plane bending moment demand under the 2011 Southern Peru (SCI16) ground acceleration record: a) 2010 design; and b) 2016 design	101

Figure 5.18: Column in-plane bending moments for the LHS column under a) the 1994 Northridge (SCC14) ground motion record; and b) the 2001 Southern Peru (SCI16) ground motion record	103
Figure 5.19: Column in-plane bending moments for 2016 design	104
Figure 5.20: Column out-of-plane bending moments for a) 2010 design; and b) 2016 design..	104
Figure 5.21: Brace out-of-plane buckling (deformations magnified).....	105
Figure 5.22: Moments in the X- and Y-directions produced by plastic hinging of the brace gusset plate.....	106
Figure 5.23: History of column out-of-plane bending moment under 1980 Irpinia, Italy (SCC1) ground motion record.....	107
Figure 5.24: Column out-of-plane moment history under the 1980 Irpinia, Italy (SCC1) ground motion record	107
Figure 5.25: Column out-of-plane bending moment for the 2016 design under the 2011 Tohoku, Japan (SCI6) ground motion record.....	108
Figure 5.26: Column axial force for a) 2010 design; and b) 2016 design	108
Figure 6.1: Proposed adjusted brace resistances when yielding propagates between tiers: a) brace tensile yielding has just initiated in Tier 2; and b) brace tensile yielding has just initiated in Tier 1	113
Figure 6.2: Slenderness effect on the difference between C_{exp} and C'_{exp}	114
Figure 6.3: a) Deformed shape of MT-CBF; b) deformed shape of compression column caused by the notional out-of-plane load; c) column out-of-plane shear diagram; and d) column out-of-plane moment diagram	115

Figure 6.4: Proposed adjusted brace force scenario to verify tier drifts 118

Figure 6.5: Proposed analysis case C for the moment calculation including..... 119

List of Symbols

A	Cross-sectional area
A_g	Gross cross-sectional area
B_1	Multiplier for P - δ effects (AISC 360)
B	Width of flange
C_d	Deflection amplification factor (ASCE 7)
C_{exp}	Brace expected strength in compression (AISC 341)
C'_{exp}	Brace expected post-buckling strength (AISC 341)
C_s	Seismic response coefficient (ASCE 7)
D	Depth of the section
F_a	Acceleration-based site coefficient
F_{cr}	Column inelastic buckling stress (AISC 360)
F_e	Column elastic buckling stress (AISC 360)
F_{cre}	Inelastic buckling stress for brace flexural buckling using expected yield strength (AISC 360)
F_v	Velocity-based site coefficient
F_y	Yielding stress of steel

h	Height of column or frame
h_i	Height of tier
I_e	Importance factor of the structure (ASCE 7)
K	Effective length factor of member
Kl	Effective length
Kl/r	Effective slenderness ratio or Brace slenderness limit
M_c	Column seismic induced in-plane flexural bending moment
M_n	Nominal flexural strength
M_p	Nominal plastic flexural strength
M_v	Higher mode effect factor
P	Column axial force
P_n	Column nominal compressive strength
P_y	Column nominal axial yield strength
R	Response modification factor (ASCE 7)
r	Radius of gyration
R_d	Ductility related force modification factor (NBCC)
R_o	Overstrength-related force modification factor (NBCC)
S_{DS}	Design spectral response acceleration parameter for short periods (ASCE 7)

S_{D1}	Design spectral response acceleration parameter at 1 s (ASCE 7)
S_{MS}	MCE_R spectral response acceleration parameter for short periods (ASCE 7)
S_{M1}	MCE_R spectral response acceleration parameter at 1 s (ASCE 7)
T_{exp}	Brace expected strength in tension (AISC 341)
T_a	Fundamental period of vibration of the structure
t_f	Thickness of the flange
t_w	Thickness of the web
V	Design storey shear
V_c	Column shear force
W	Seismic weight
Z	Plastic section modulus of the column
β	Coefficient for bending in beam-columns
λ	Slenderness parameter
ϕ	Resistance factor

Abbreviations

AISC	American Institute of Steel Construction
ASCE	American Society of Civil Engineers
BFCs	Braced Frame Columns
BFs	Braced frames
BRBF	Buckling restraint braced frames
CBFs	Concentrically braced frames
CSA	Canadian Standards Association
EBFs	Eccentrically braced frames
GCs	Gravity columns
HSS	Hollow Square Section
LD	Limited ductility
LHS	Left-hand-side
MD	Moderately ductile
OCBF	Ordinary concentrically braced frames
MCE _R	Maximum considered earthquake
MPa	Mega Pascal

MRFs	Moment resisting frames
MT-BFs	Multi-tiered braced frames
MT-BRBFs	Multi-tiered buckling restraint braced frames
MT-CBFs	Multi-tiered concentrically braced frames
MT-OCBFs	Multi-tiered ordinary concentrically braced frames
MT-SCBFs	Multi-tiered special concentrically braced frames
NBCC	National Building Code of Canada
NLRH	Nonlinear response history
OpenSees	Open system for earthquake engineering simulation
RHS	Right-hand-side; Rectangular Hollow Section
SCBF	Special concentrically braced frames
SDOF	Single-Degree-Of-Freedom

Chapter 1 – Introduction

1.1 Background

Multi-tiered concentrically braced frames (MT-CBFs) are widely used in North America as the lateral load-resisting system of tall single-storey buildings such as airplane hangars, recreational facilities, shopping centres, and industrial buildings (Figure 1.1). MT-CBFs consist of multiple concentrically braced tiers along the height of the frame separated by horizontal strut members. Various bracing configurations can be used in MT-CBFs including X-, V-, diagonal, chevron, and split-X bracing (Figure 1.2). Bracing members of MT-CBFs can be designed as a tension/compression (T/C) or tension-only (T/O) member. Multi-tier arrangements are typically used when it is not practical or economical to use a single bracing panel along the height of the frame between the ground and roof levels. By introducing multiple bracing tiers stacked on top of each other, the length of braces is reduced, which allows smaller brace sizes to be used and easily satisfy code-specified brace slenderness limits. The column buckling length in the in-plane direction is also reduced due to the application of intermediate horizontal struts, which permits selection of a smaller column section. From the seismic design perspective, the stringent limits on width-to-thickness and global slenderness ratios can be easily satisfied when using shorter braces. Moreover, when capacity design is imposed, reduced brace sizes result in smaller design forces on the adjacent forced-controlled members including struts, beams, columns, and connections.

a)

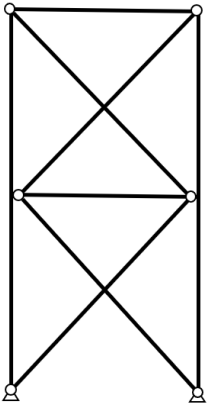


b)

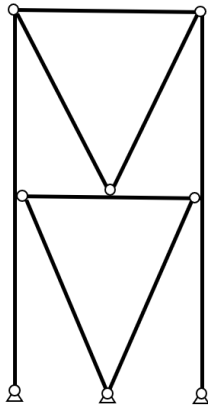


Figure 1.1: a) *four-tiered concentrically braced frame in an industrial building; b) two-tiered concentrically braced frame in an industrial building.*

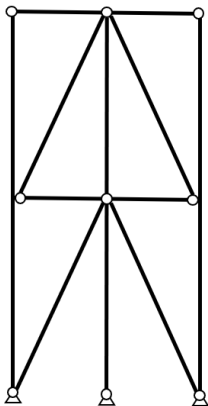
a)



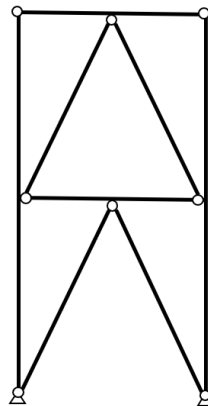
b)



c)



d)



e)

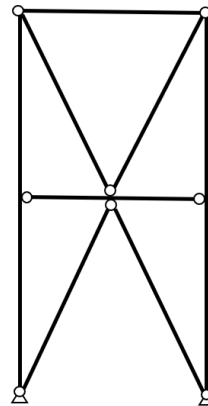


Figure 1.2: *MT-CBFs configurations a) X-shape; b) V-shape; c) diagonals; d) chevron; and e) split-X*

MT-CBF columns are typically wide-flange (W-shape) sections oriented such that out-of-plane bending moments act about the major axis of the section to resist the out-of-plane wind load along the full height of the frame. No out-of-plane bracing exists along the height of the column, and the column buckling length is taken equal to the full frame height in this direction. However, the columns can be considered braced in the plane of the frame because of horizontal struts. It should be noted that hollow structural sections (HSSs) are also used in multi-tiered braced frames as columns in low and moderate seismicity regions of Canada.

1.2 Research Problem

Previous studies on the seismic performance of multi-tiered concentrically braced frames have shown that frame lateral deformations under seismic loads are not uniformly distributed along the height. Rather, the lateral deformation tends to concentrate in the tier where the brace tensile yielding takes place first (Imanpour et al. 2012a; 2012b; and Imanpour and Tremblay 2012). Such differential drift demands cause high in-plane flexural demands on the columns, which may lead to flexural yielding, column buckling and even frame collapse. Additionally, past studies showed that the tier where tensile yielding occurs first (i.e. critical tier) can be identified by comparing the storey shear resistance obtained from probable brace resistance. The tier with the least shear resistance will often yield first and prevent the increase in the lateral-load carrying capacity of the frame, which in turn prevents the initiation of tensile yielding in other (non-critical) tiers. Non-uniform yielding is also expected when identical tiers with the same storey shear resistance are used. This is because of the variations in the brace geometry, initial out-of-straightness and material properties between tiers that can affect the sequence of brace yielding and buckling.

Special seismic design provisions were introduced for the first time in the 2009 edition of the Canadian steel design standard (CSA S16) (CSA 2009). The requirements were updated in 2014 edition of the S16 standard (CSA 2014) to reflect the findings of the numerical studies reported in Imanpour et al. (2012a; 2012b) and Imanpour and Tremblay (2012). Based on these provisions, in addition to considering the axial force, MT-CBF columns are required to resist in-plane and out-of-plane flexural demands arising from the difference in tier-drifts and column initial imperfections and brace out-of-plane buckling, respectively.

In the 2010 AISC Seismic Provisions (AISC 2010a), MT-CBFs were classified as K-type braced frames, a braced-frame configuration in which the braces connect to a column at a location with no out-of-plane support. K-type frames were not permitted for seismic applications due to the unbalanced brace force induced on the columns between supports, which can result in large in-plane bending moments. This response is illustrated in Figure 1.3a. However, designers were able to mitigate this effect by including struts between columns (Figure 1.3b), and design MT-CBFs as conventional multi-storey CBFs. The columns of such MT-CBFs were designed *only for axial compression force* resulting from gravity loads plus brace axial forces due to seismic load effects as required by 2010 AISC Seismic Provisions

The results obtained from past numerical studies in Canada and the U.S. (Imanpour et al. 2016a; Imanpour and Tremblay 2016; Stoakes and Fahnestock 2016) have been adopted by the 2016 edition of the AISC Seismic Provisions (AISC 2016a). In this standard, new seismic design requirements were introduced for the first time for multi-tiered ordinary concentrically braced frames (MT-OCBFs), multi-tiered special concentrically frames (MT-SCBFs), and multi-tiered buckling-restrained braced frames (MT-BRBFs). The 2016 AISC Seismic Provisions introduce a

set of design requirements for struts and columns of MT-SCBFs to protect the columns and force yielding of braces in more than one braced panel. Similar to the Canadian standard, in addition to considering the axial force, the MT-CBF columns are required to resist in-plane bending moment demands arising from the difference in tier drifts and out-of-plane bending moment demands due to column initial imperfections and brace out-of-plane buckling. Furthermore, columns are required to be torsionally braced at each tier level to reduce the tendency of the column to twist at the strut level.

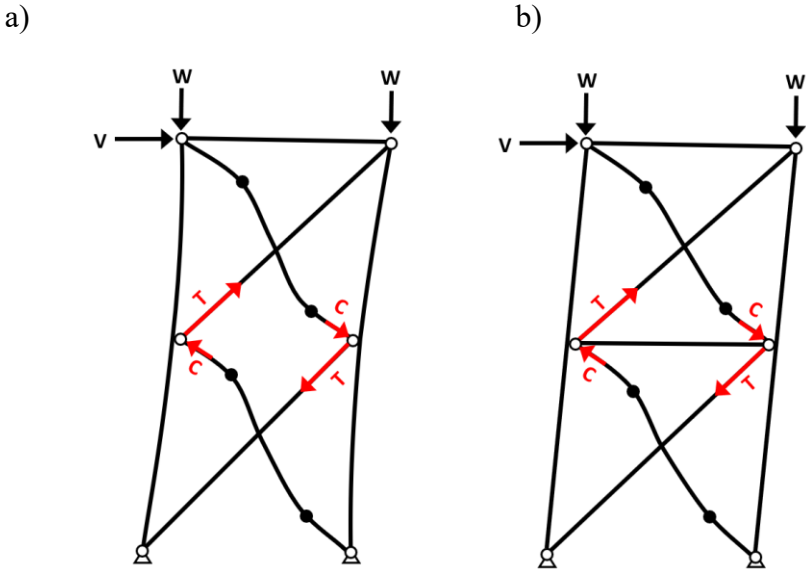


Figure 1.3: Inelastic response of a) K-type CBF; and b) standard CBF

Although significant improvements have been made over the past decade to develop seismic design procedures for steel MT-CBFs, there is still a lack of background research into seismic response and design of such frames. In particular, there is very limited detailed nonlinear numerical analysis and no full-scale experimental test data to fully understand the instability observed in MT-CBF columns designed excluding the special seismic provisions. Furthermore, the moments

induced in the columns as a result of the non-uniform yielding need to be characterized, and the adequacy of the design requirements adopted by North American design standards (CSA 2014; AISC 2016a) should be validated.

1.3 Objectives

The objective of this M.Sc. research is to evaluate the seismic performance of steel multi-tiered concentrically braced frames with the focus on frames designed in accordance with the provisions prescribed by the U.S. steel design standard (2016 AISC Seismic Provisions) for multi-tier special concentrically braced frames (MT-SCBFs) using numerical methods. A set of special objectives were defined as follows:

- To conduct a literature survey on the seismic response of steel CBFs and stability response of steel wide-flange columns.
- To review the guidelines prescribed in the Canadian Steel Design Standard and the U.S. Seismic Provisions.
- To examine the seismic behaviour of MT-SCBFs designed in accordance with 2010 and 2016 AISC Seismic Provisions using nonlinear static and dynamic analyses.
- To characterize the in-plane and out-of-plane bending moments induced in MT-SCBF columns under seismic loads.
- To validate the seismic design requirements prescribed for the columns of MT-SCBFs in 2016 AISC Seismic Provisions including flexural bending moment demands and stiffness requirements.
- To propose design recommendations to improve design practices for MT-SCBFs.

- To produce nonlinear seismic analysis data for future research studies such as experimental testing of MT-SCBFs.

Note that this research does not include the experimental testing of full-scale MT-SCBF frames; however, this research lays the foundation for future experimental work.

1.4 Methodology

The objectives of this research were accomplished through five phases as follows:

- **Phase 1:** An extensive review of the existing literature was performed at the beginning and throughout the course of the work to understand the seismic behaviour of steel concentrically braced frames, multi-tiered braced frames, and steel wide-flange columns.
- **Phase 2:** A prototype frame consisting of a two-tiered SCBF was designed in accordance with the 2010 and 2016 American Seismic Provisions to evaluate its global and local response.
- **Phase 3:** A detailed numerical model using a finite element program was developed to examine the behaviour of MT-SCBFs. Special considerations were made to simulate the nonlinear response of the members including braces, columns, beams, and struts.
- **Phase 4:** A cyclic nonlinear static (pushover) analysis and a nonlinear response history analysis were performed on the prototype frames of Phase 2.
- **Phase 5:** The results obtained from numerical analyses were examined to evaluate the seismic response of the prototype frames, determine the seismic demands on the columns, validate the current design requirements for MT-SCBFs and where possible, make recommendations to enhance the design procedure.

1.5 Thesis Organization

This M.Sc. thesis is presented in seven chapters. Chapter 1 consists of the introduction and background information. In Chapter 2, a survey of past studies on the seismic response of conventional steel CBFs, MT-CBFs, steel wide-flange columns as well as a review of current design requirements are presented. Chapter 3 discusses the design of a prototype frame in accordance with the 2010 and 2016 AISC Seismic Provisions. The development of the numerical model including the element type, material model, imperfections and analysis methods are then outlined in Chapter 4. In Chapter 5, the results from the cyclic pushover analyses and the nonlinear response history analyses are presented. In Chapter 6 recommendations for the design of MT-CBFs are proposed. Finally, a summary of the work completed and the main conclusions are outlined in Chapter 7; in addition, recommendations for future research are made in this chapter. Appendix A contains the data corresponding to each ground motion for the nonlinear response history analysis.

Chapter 2 – Literature Review

2.1 General

The objective of this Chapter is to review past studies on the seismic response of steel concentrically braced frames (CBFs) plus the seismic design provisions currently used in Canada and the U.S. to design steel multi-tiered concentrically braced frames (MT-CBFs). The nonlinear cyclic behaviour of steel braces used in CBFs is described first. The seismic response of conventional steel CBFs with the focus on MT-CBFs is then presented. Finally, the seismic design provisions for steel MT-CBFs as prescribed by the Canadian steel design standard CSA S16 and the AISC Seismic Provisions are presented.

2.2 Seismic Behaviour of Steel Braces

2.2.1 Brace Hysteretic Response

The bracing members of CBFs are an essential component of the seismic-force-resisting system (SFERS). The bracing members have two main purposes 1) to transfer lateral loads from the top of the frame to the foundation, and 2) to dissipate the energy introduced into the SFERS from an earthquake. Several studies have examined the cyclic behaviour of steel bracing members (Jain et al. 1980; Popov and Black 1981; Lee and Goel 1987; Bertero et al. 1989; Shaback 2001; and Tremblay et al. 2003). The cyclic behaviour of steel braces is characterized by a non-symmetrical hysteretic behaviour as illustrated in the axial force–axial deformation curve shown in Figure 2.1, where P is the axial load and δ is the axial displacement. As shown, the compression capacity of

the brace is considerably lower than the tension capacity. The compression capacity degrades significantly after its first buckling point (C_{exp}) is reached until reaching the expected post-buckling load (C'_{exp}). In comparison, once a brace reaches its tensile yielding load ($A_g F_y$), the brace can uphold the high-tension load even after further axial displacement is applied.

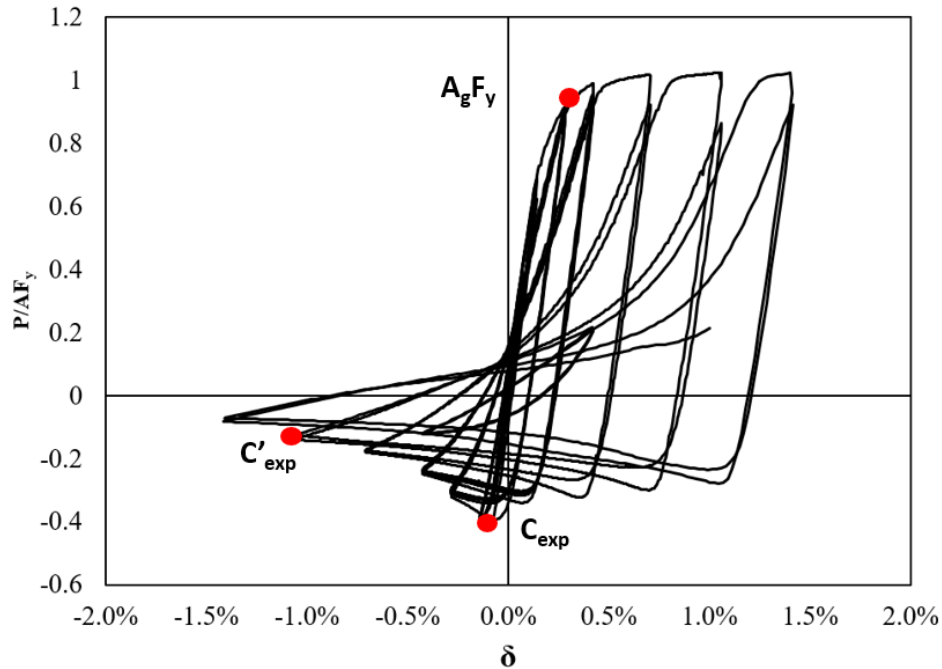


Figure 2.1: Hysteretic response of steel bracing members

There are different factors that can influence the hysteretic behaviour of the bracing members, such as slenderness, width-to-thickness, type of loading, and connection details. The slenderness is the most influential parameter that dictates the overall behaviour of bracing members and its energy dissipation capacity when subjected to cyclic loading as shown in Figure 2.2 (Tremblay 2002). Past experimental studies have also shown a strong correlation between slenderness and the

capacity of a member to dissipate energy. When the brace slenderness increases, the dissipation capacity decreases.

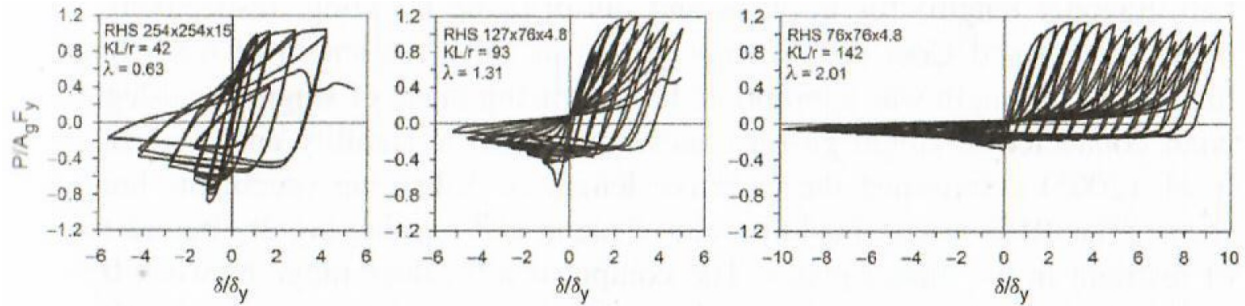


Figure 2.2: Influence of global slenderness ratio on the hysteretic response of steel braces (Ziemian 2010)

2.2.2 Bracing Configuration

The type of framing system can also affect the hysteretic behaviour of the bracing members. Plastic hinge forming in the middle of the beam of chevron frames upon compression brace buckling (Figure 2.3) can lead to more pronounced buckling and yielding in bracing members (Tremblay 2002). In X-braced frames, braces tend to undergo larger deformations over a shorter length in contrast to single-bracing, resulting in higher plastic rotation of the braces (Tremblay et al. 2003).

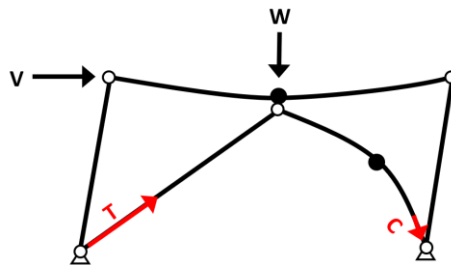


Figure 2.3: Inelastic response of chevron braced frame when plastic hinge forming in the beam

2.2.3 Brace Cross-section

Singly-symmetric, doubly symmetric, and built-up shapes can be used as bracing members of CBFs. The type of cross-section has a significant effect on the hysteretic behaviour of steel bracing members. Singly-symmetric braces such as T and C shapes have been found to be less efficient due to their susceptibility to buckling in a torsional-flexure mode (Black et al. 1980). Similarly, built-up shapes (e.g. double angles) are less effective in resisting compression load and dissipating energy than doubly-symmetric shapes, due to early buckling of individual members (Astaneh-Asl and Goel 1984; Astaneh-Asl et al. 1985). In regions of high seismicity, doubly-symmetric shapes such as hollow structural sections (HSSs) are commonly used due to their effectiveness in resisting compression loads (Lee and Goel 1987; Liu 1987; Tang and Goel 1987; and Foutch et al. 1986). Although, past experimental studies have shown that square or rectangular HSSs exhibit a limited inelastic deformation capacity under cyclic loading. This limitation is caused by the high strains that are developed in the corners of the cross section upon local buckling of the member (Gugerli 1982; Lee and Goel 1987; Leowardi and Walpole 1996; and Liu 1987). Other doubly symmetric shapes such as round HSS and W-sections have shown to be less prone to local buckling (Fell et al. 2009).

Rectangular and square HSS members are a popular choice for bracing members in North America largely because low-cycle fatigue fracture can be mitigated using appropriate slenderness and width-to-thickness ratios (Tremblay 2002); furthermore, rectangular HSS members lend themselves to convenient connections to gusset plates. Depending on the connections and orientation of the member, the bracing member made of HSSs can buckle in-plane or out-of-plane. A typical connection detail is to slot the connecting gusset plate to the end of the HSS section and

connect the two members using a fillet weld or bolt at the intercepting regions. This connection generally results in the braces buckling out-of-plane (Figure 2.4) by developing a flexural plastic hinge at each of the gusset plates and at the middle of the brace.



Figure 2.4: HSS brace out-of-plane buckling (Sabelli et al. 2013)

2.2.4 Dynamic Buckling

Buckling of steel braces under real-time dynamic loading have a significant effect on the hysteretic response of braces (Kazemzadeh Azad et al. 2018). It was shown that the buckling resistance of a brace under dynamic loading can exceed its static buckling capacity. This is because of higher loading-velocities, as illustrated in Figure 2.5. This phenomenon can result in significant variations of the hysteretic response of a member, as shown in Figures 2.6a and 2.6b.

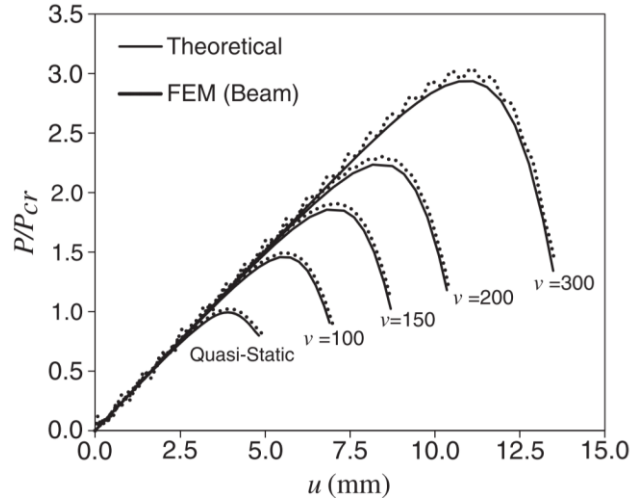
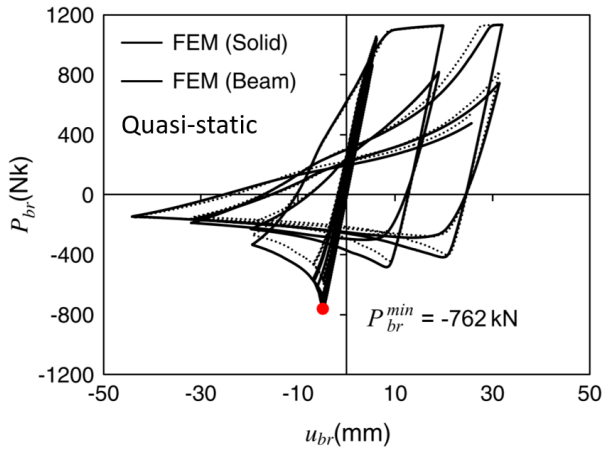


Figure 2.5: Effect of loading velocity (v in mm/s) on the steel brace buckling capacity (Kazemzadeh Azad et al. 2018)

a)



b)

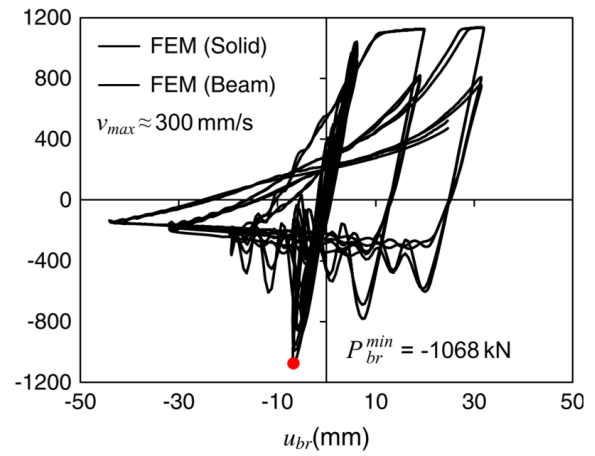


Figure 2.6: Hysteretic response of a steel bracing member obtained from a) quasi-static loading, and b) dynamic loading with $v = 300$ mm/s (Kazemzadeh Azad et al. 2018)

2.2.5 Brace Fracture under Cyclic Loading

There have been several studies that have examined brace fracture under cyclic loading including Goel 1987; Lee 1988; Hassan and Goel 1991; Archambault 1995; Tremblay 2002; Tremblay et al. 2003; Shaback and Brown 2003; Fell et al. 2009; and Haddad et al. 2011. Fracture under cyclic loading typically occurs in the following tension cycle after the member has suffered severe local buckling (Figure 2.7) under the previous compression cycle. When HSS members are used, fracture initiates at the corners where plastic strains are the highest, then, it propagates across the cross-section as shown in Figure 2.7 (Tremblay et al. 2003). It is concluded from these studies that the most influential factors that affect the fractured life of a section are the slenderness, width-to-thickness ratio, the yield stress, and section geometry. It was also found that slender members tend to perform better than non-slender members as shown in Figure 2.8, where λ is the slenderness parameter and ductility value is determined the ratio between the maximum displacement and the displacement at yield. Tests by Tremblay et al. (2003) showed that higher width-to-thickness ratios can result in fracture of the member at low levels of ductility because of severe local buckling expected in such cross-sections. Fell et al. (2009) reported fracture initiation for HSS members in the range from 2% to 3% of the storey drift.

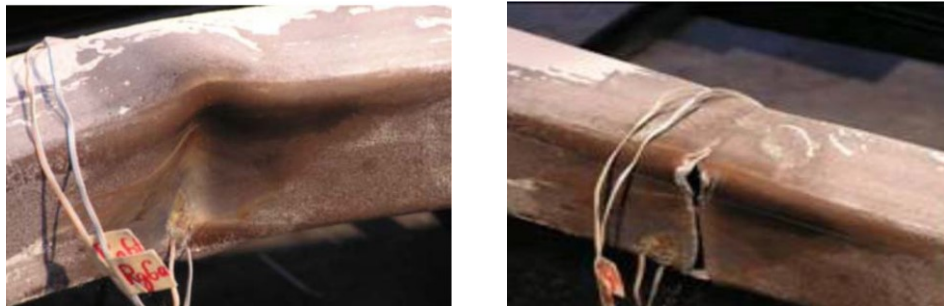


Figure 2.7: HSS members under cyclic loading: a) Local buckling; and b) fracture of (Fell et al. 2009)

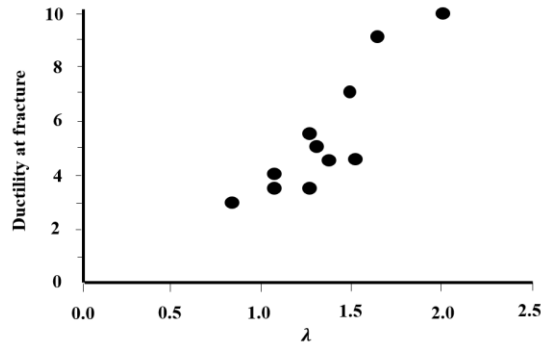


Figure 2.8: Influence of the brace slenderness on the fracture life of HSS members (Tremblay 2001)

There are several models that have been proposed to predict the fracture life of HSS members (Lee and Goel 1987; Tang and Goel 1987; Hassan and Goel 1991, Archambault 1995; Fell et al. 2009; Hsiao et al. 2013). Tremblay (2002) proposed a relationship between total ductility reached at fracture and the brace slenderness ratio where the total ductility is the sum of the peak ductility reached in tension and the peak ductility reached in compression. This model estimates the fracture life of diagonal bracing members well; however, it was found to be unconservative for X-bracing configurations (Tremblay et al. 2003). Instead, Tremblay et al. (2003) proposed to use the rotation experienced at the brace plastic hinging as an indicator of fracture life rather than a ductility-related parameter. As shown in Figure 2.9, rotation values at fracture can be well estimated.

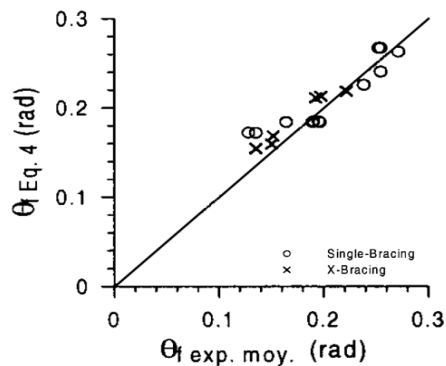


Figure 2.9: rotation at fracture: test data versus values predicted (Tremblay et al. 2003)

Hsiao et al. 2013 proposed a fracture model for nonlinear modelling of SCBFs with HSS members. This model accounts for the width-to-thickness ratio of the cross-section, overall slenderness ratio of the brace, and yield strength of the bracing members. It was found that the maximum strain can be used as the best variable to predict brace fracture as shown in Figure 2.10. It is confirmed that the maximum storey drift before fracture occurs for square HSS braces satisfies a drift of approximately 2%.

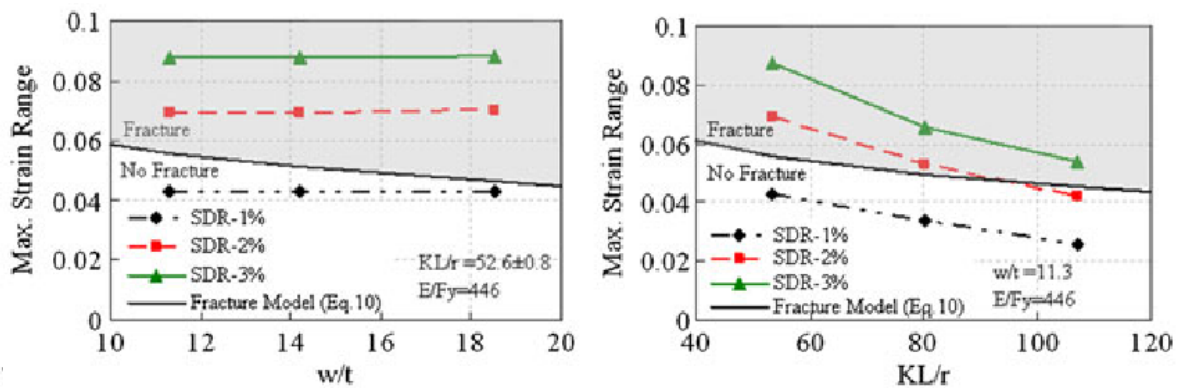


Figure 2.10 Brace fracture limit varying with a) brace width-to-thickness ratio ($KL/r = 52.6$ and $E/F_y = 446$ MPa); and b) brace slenderness ratio ($b/t = 11.3$ and $E/F_y = 446$ MPa) (Hsiao et al. 2013)

2.3 Seismic Behaviour of Steel Concentrically Braced Frames

Steel concentrically braced frames (CBFs) consist of vertical, horizontal, and diagonal members that resist lateral wind and seismic loads through vertical truss action. An example of such braced frames is shown in Figure 2.11. Similar to other seismic force resisting systems, the main objective of CBFs is to prevent structural collapse and maintain the integrity of gravity load-carrying system under major earthquake events. In steel CBFs, bracing members are designed as sacrificial elements (seismic fuses) to yield and buckle under earthquake loads and safely dissipate seismic

energy. The other elements of the structure including beams, columns, roof diaphragm, footing, anchor rods and connections are intended to remain elastic (Filiatrault et al. 2013). This design methodology is referred to as capacity design where weaker elements are engineered in the structure to respond in the nonlinear range of the material while the rest of the structure are designed stronger than those elements and must remain elastic under major earthquake events.

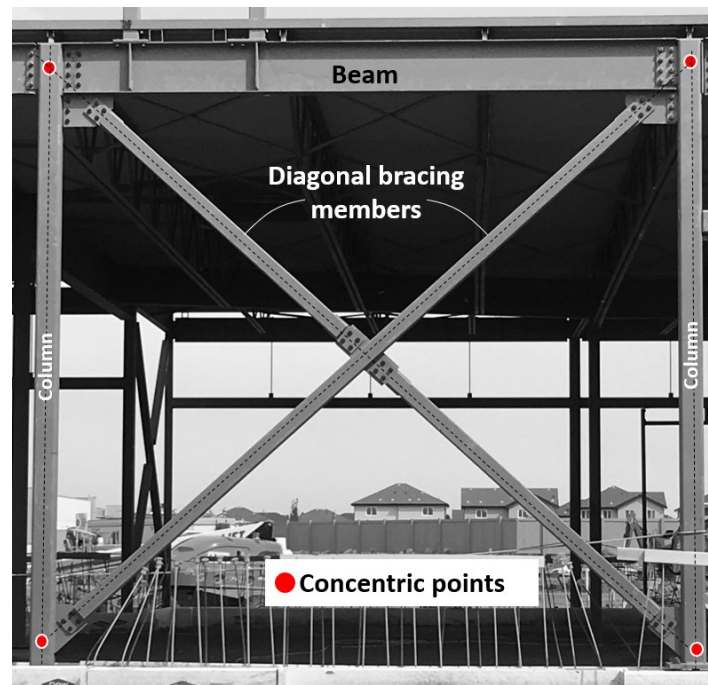


Figure 2.11: Single-storey steel concentrically braced frame

Steel concentrically braced frames are categorized in seismic design provisions by their ductility, which is defined as the system capability to undergo inelastic deformation and dissipate seismic-input energy. The ductility-related force modification factor R_d in Canada and the response modification factor R in the U.S. are used to represent this aspect of the structure in seismic design. In Canada, steel concentrically braced frames are categorized into two ductility levels: limited-ductility (LD) and moderately-ductile (MD) systems. In the U.S. there are two ductility levels for

concentrically braced frames: ordinary concentrically braced frames (OCBFs) and special concentrically braced frames (SCBFs).

The expected seismic behaviour of CBFs and the concept of capacity design is described using a single-storey chevron braced frame shown in Figure 2.12a. Under a lateral seismic load, one of the braces will act in tension, and the other one responds in compression (Figure 2.12b). By increasing the lateral load (Figure 2.12c), the compression member reaches its maximum compression capacity and subsequently buckles. Beyond this point, the compression brace force will begin to degrade. As the lateral load increases, the tension brace achieves its maximum tension capacity, and beyond this point, tensile yielding is initiated in the tension brace. The reduction in the compression brace force continues until the force reaches the brace post-buckling strength (Figure 2.12d).

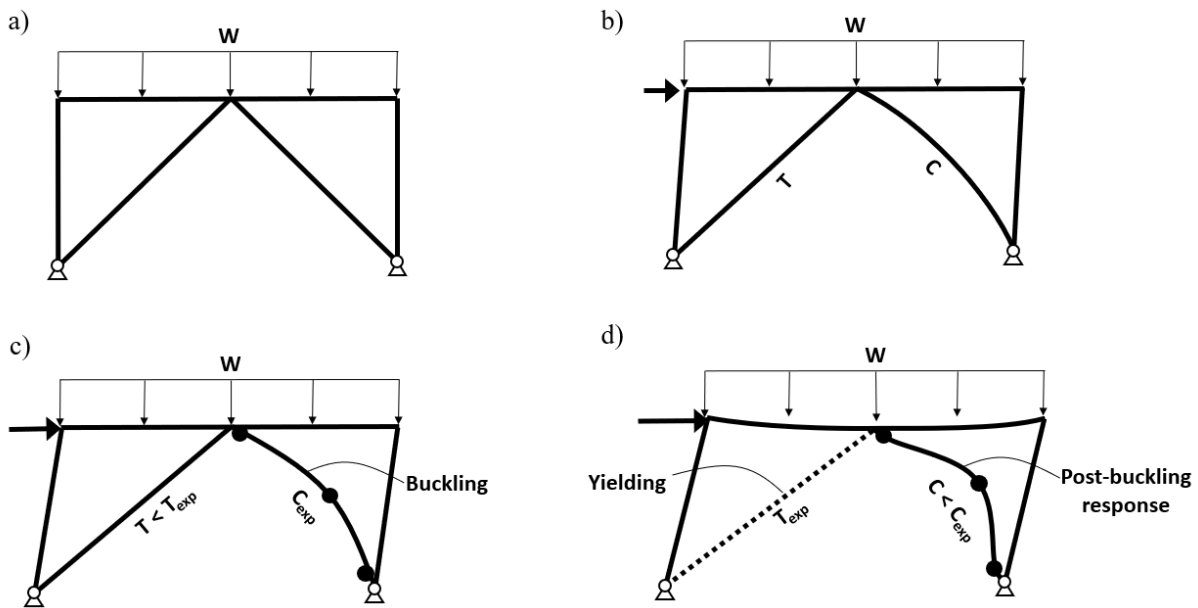


Figure 2.12: Progression of seismic behaviour of single-storey CBF

To ensure that the expected forces are achieved in the bracing members of CBFs, columns, beams and adjacent connections must resist the forces arising from the yielding and buckling of the bracing members.

Brace connections should be designed and detailed so that braces can develop a stable cyclic response under reversal loads expected in a major seismic event. Brace gusset plates should be designed to allow the development of plastic rotations when the brace buckles in-plane or out-of-plane. For out-of-plane buckling, the connection detail with a fold line on the gusset plate shown in Figure 2.13 is recommended (AISC 2016a). The clear spacing at the end of the brace is to be taken equal to 2 times the thickness of the gusset plate as recommended by Astaneh-Asl et al. (1986).

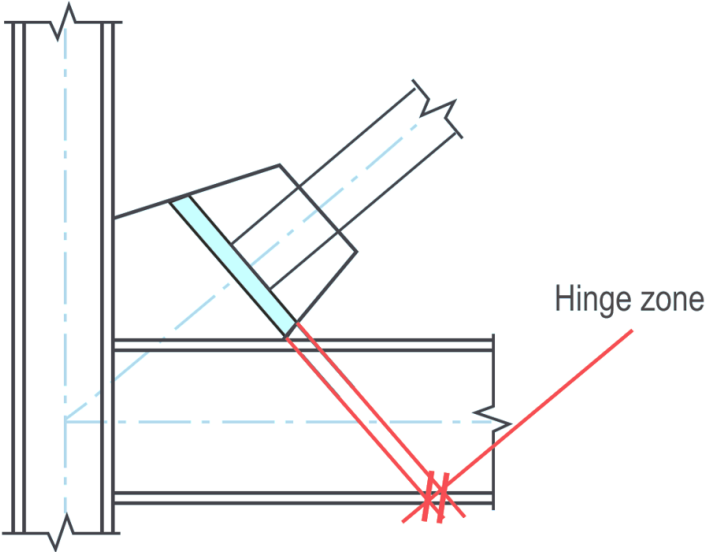


Figure 2.13: Linear hinge zone for out-of-plane buckling of steel braces (Sabelli et al. 2013)

2.4 Seismic Behaviour of Steel MT-CBFs

Multi-tiered concentrically braced frames (MT-CBFs) are commonly used in tall single-storey buildings, such as airport hangers, industrial warehouses, and recreation centres or tall-storey-buildings such as hotels, residential, and office buildings. MT-CBFs are made of multiple panels of CBFs stacked on top of each other along the height of a storey.

Different configurations of MT-CBFs exist as illustrated in Figure 2.14. Although MT-CBFs appear to be similar to multi-storey concentrically braced frame (MS-CBFs), there are two major distinctions between the two frames: 1) MT-CBFs lack floor diaphragms between the ground and roof levels (Figure 2.15), which creates a single-degree-of-freedom (SDOF) system, and 2) MT-CBF columns lack out-of-plane bracing along the height of the frame, which poses concerns on the out-of-plane stability of such members (Figure 2.15).

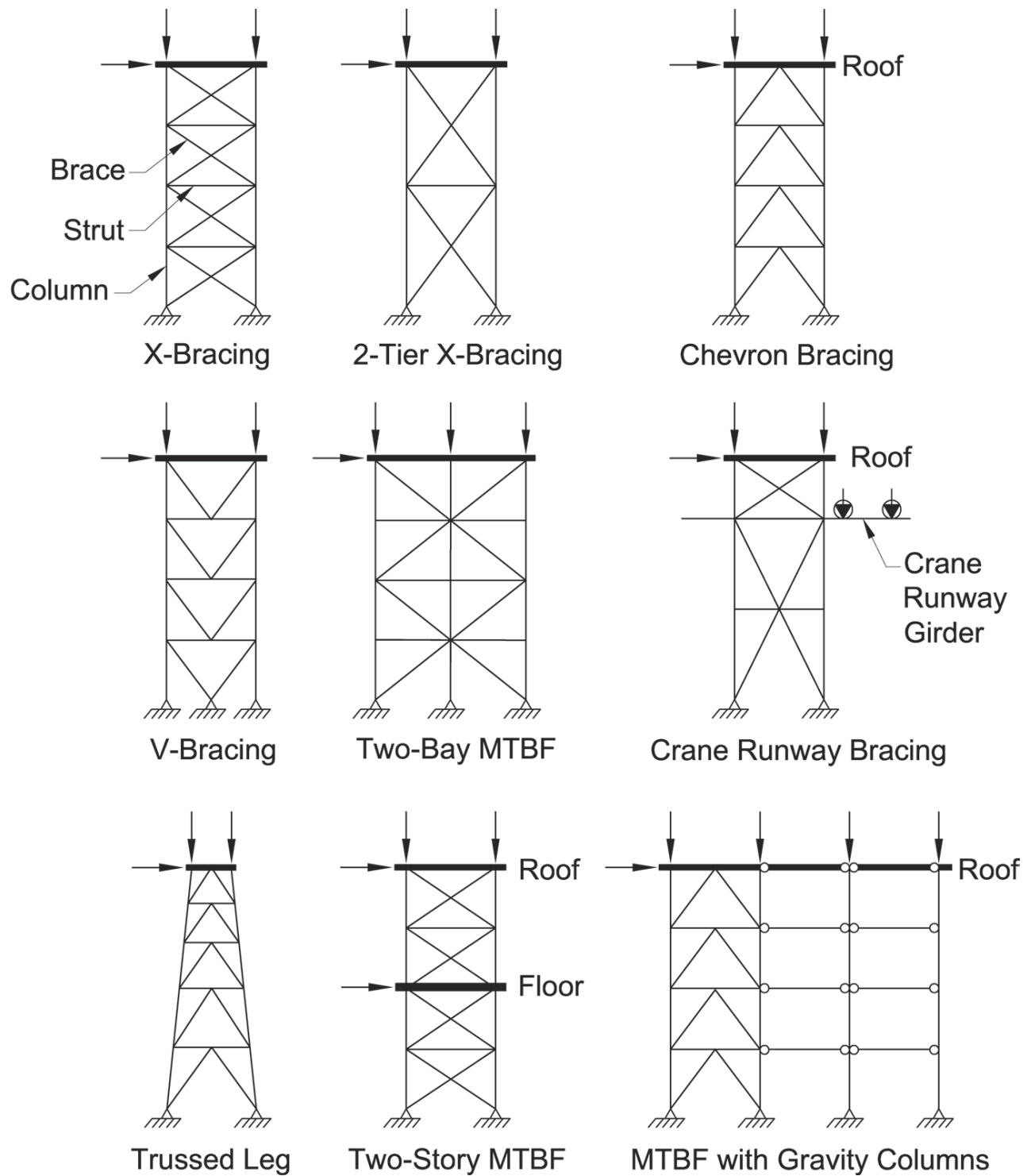


Figure 2.14: Typical MT-CBF configurations (AISC 2016a)

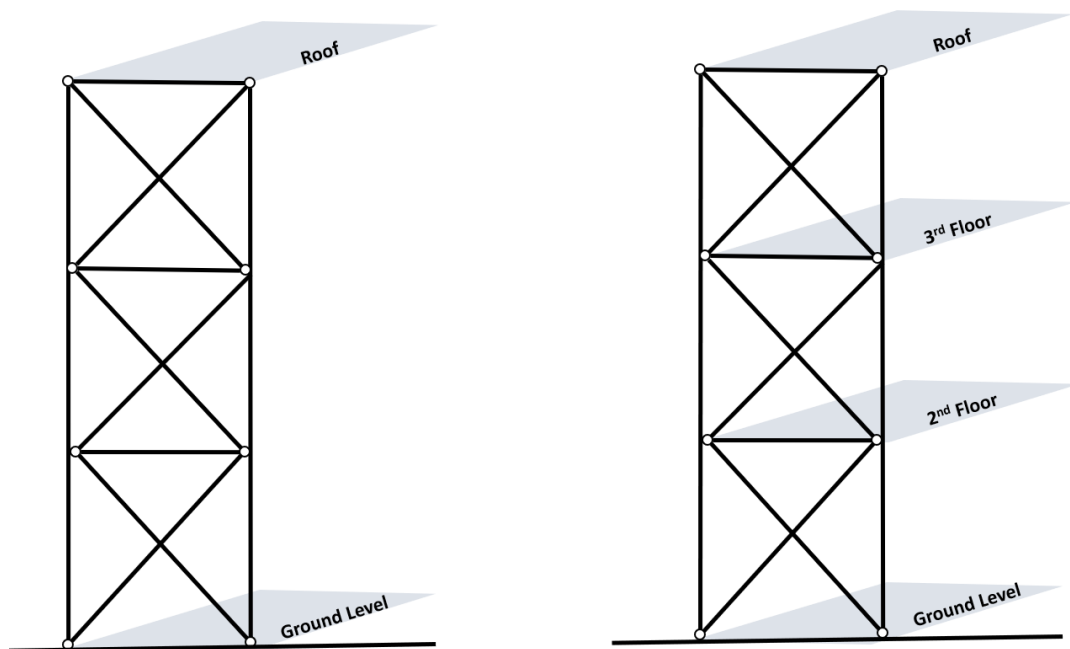


Figure 2.15: Comparison between Multi-tiered CBFs and Multi-storey CBF

2.4.1 Expected Seismic Behaviour

The seismic behaviour of MT-CBFs was the focus of several research programs in recent years. The numerical seismic response evaluation using the OpenSees platform (McKenna and Fenves 2004) showed that the lateral frame deformations are not uniformly distributed along the frame height, but rather concentrated in one of the tiers, which produces in-plane bending moments on the columns as shown in Figure 2.16 for a two-tiered frame studied shown in Figure 2.17 (Imanpour and Tremblay 2012; Imanpour et al. 2012b).

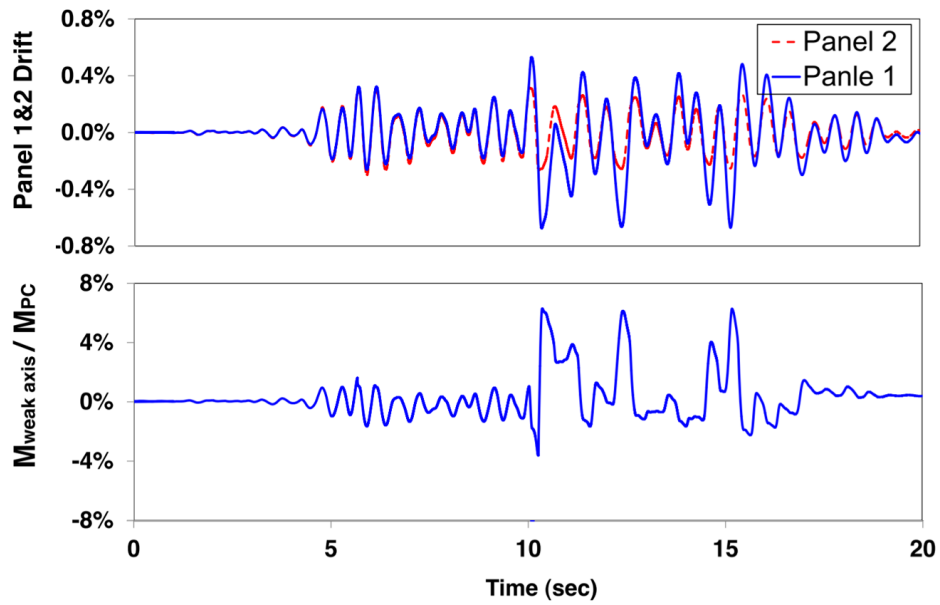


Figure 2.16: Drift in individual braced panels of a two-tiered CBF and column in-plane bending demand recorded between the braced panels (Imanpour and Tremblay 2012)

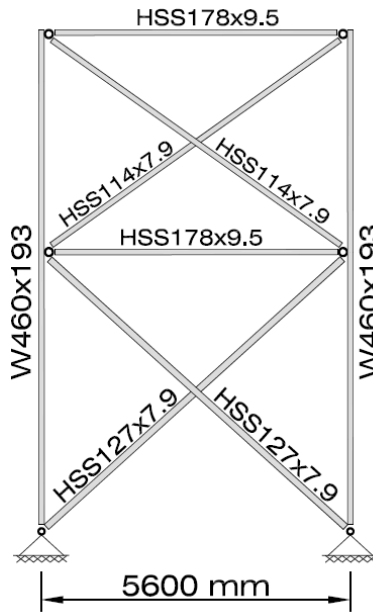


Figure 2.17: Two-tiered concentrically braced frame geometry (Imanpour and Tremblay 2012)

Imanpour et al. (2013) examined the seismic stability response of columns in a four-tier braced frame designed in accordance with the 2010 AISC Seismic Provisions (AISC 2010a). The frame was analyzed using the nonlinear response history method in OpenSees (McKenna and Fenves 2004). The study also examined the response of an isolated columns part of the four-tiered CBF using the Abaqus program (Dassault Systèmes 2012) under the displacements obtained from the nonlinear response time history analysis in OpenSees. It was found that the frame designed according to the 2010 AISC Seismic Provisions is prone to a concentration of inelastic drift in one of the bracing tiers. A significant in-plane flexural demand was observed in the columns of the frame (Figure 2.18). The study found that flexural yielding of the column could compromise the stability condition of the column. Additionally, this study identified excessive ductility demands on the bracing members of the tier where large inelastic deformations are concentrated.

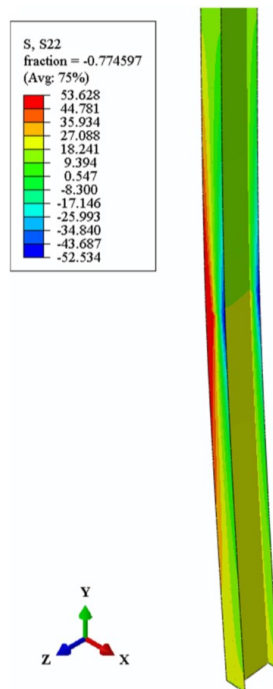


Figure 2.18: Normal stress contour (ksi, where 1 MPa = 0.145 ksi) of the column at maximum Tier 1 drift (Imanpour et al. 2013)

Stoakes and Fahnestock (2014) examined the seismic stability of the steel MT-CBF columns using a three-dimensional finite element model. Columns were subjected to realistic axial loads and torsional rotation due to the buckling of braces. This study was able to reassure the positive effects of providing a torsional restraint on the columns at the tier levels; however, large tier drifts were observed in the analyses, which could lead to brace brittle fracture due to low cycle fatigue.

Imanpour et al. (2016a) conducted a numerical parametric study to analyze the behaviour of MT-CBFs designed in accordance with the 2010 AISC Seismic Provisions. In this study, the number of tiers ranged between two and six, and the height ratio between tiers was also varied. Furthermore, this study investigated the effects of column base fixity and low-ductile steel MT-CBFs. The seismic behaviour of three braced frames was also analyzed using a three-dimensional finite element model. The results of these three analyses were used to validate a computationally efficient approach fibre-based numerical model to perform the parametric study. This study found a concentration of inelastic lateral deformations that led to high in-plane flexural demands on the columns. In several cases, column buckling was observed as shown in Figure 2.19. The buckling mode took place about the weak-axis of the column section and changed to torsional-flexural buckling as a result of the out-of-plane displacement mainly at the mid-height of the column as the column has no lateral out-of-plane support along the frame height. The study showed that the MT-CBFs designed in accordance with the 2010 AISC Seismic Provisions can exhibit an unsatisfactory seismic response. This study also found that the use of higher seismic forces in design did not have a significant benefit to the flexural demand produced on the columns nor prevented column buckling. Nonetheless, using a fixed condition at the base of the column improved the seismic response of the column and prevented column instability.



Figure 2.19: Frame deformed shape at the instant of column buckling (Imanpour et al. 2016a)

Imanpour et al. (2016b) proposed new design requirements to improve the seismic response of MT-CBFs to prevent column instability and brace fracture by propagating brace tensile yielding between the braced panels. Based on the proposed design method, an in-plane flexural bending moment should be included in the column design. To determine the column in-plane moment, the tier where brace yielding takes place first should be identified. The critical tier can be identified by comparing the storey shear resistance at brace yielding and buckling. The tier with the lowest storey shear resistance is identified as the critical tier. Then, the column in-plane moment demand can be estimated using the brace force scenario shown in Figure 2.20 where the tension brace in the critical tier (Tier 1) reaches its expected tensile resistance T_{exp} , brace force in the compression member of the critical tier reaches the post-buckling compression resistance C'_{exp} , while in the adjacent tier, the tension brace is assumed to reach its expected tensile resistance T_{exp} and the compression brace force in the noncritical tier is set equal to the buckling resistance C_{exp} . If

multiple tiers have the same storey shear resistance, multiple analyses where the critical tier location varies by slightly reducing (e.g. 20%) the brace yield strength. This analysis results in an unbalanced brace storey shear force that should be resisted by the columns:

$$\Delta V_{br} = V_{br\ 1} - V_{br\ 2}$$

where,

$$V_{br\ 1} = \cos\theta_1(T_{exp} + C'_{exp}) \text{ and } V_{br\ 2} = \cos\theta_2(T_{exp} + C'_{exp}).$$

The design in-plane bending moment of the column can be calculated based on the shear force diagram under ΔV_{br} as shown in Figure 2.21. The required strength of the column should be verified using the interaction equation specified in the AISC Specification (AISC 2010a) under axial compression force and weak-axis bending moment demands.

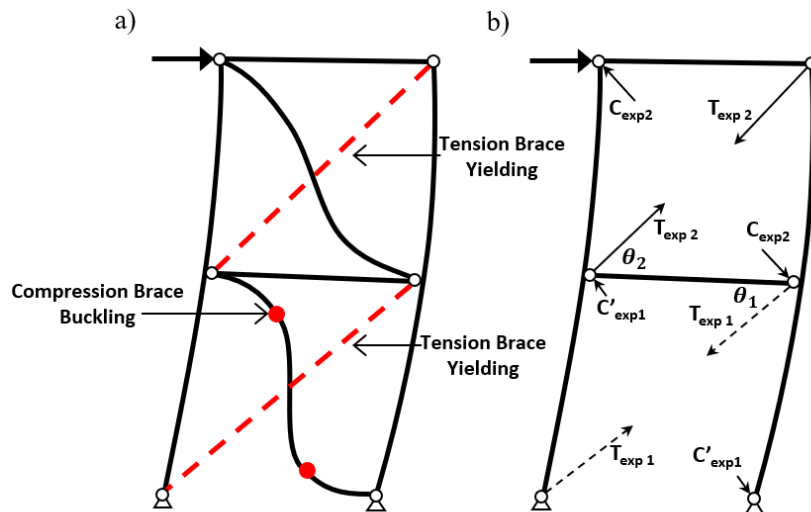


Figure 2.20: Improved lateral response of a two-tiered steel CBF: a) Brace yielding and buckling in Tier 1 and initiation of brace tensile yielding in Tier 2; and b) Proposed brace force scenario to trigger yielding in the noncritical tier (critical tier: Tier 1; and noncritical tier: Tier 2)

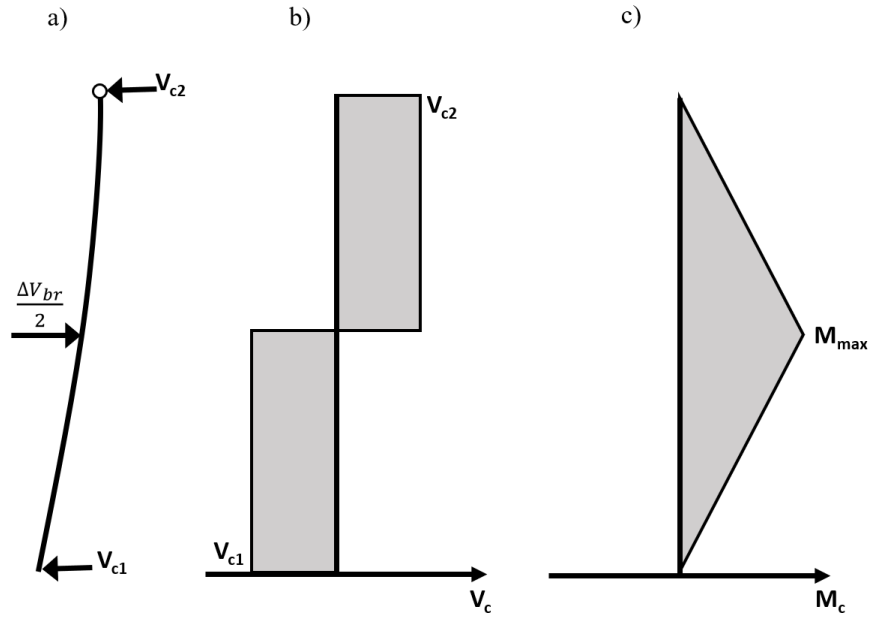


Figure 2.21: a) Column free-body diagram under unbalanced brace story shear; b) column shear force diagram; and c) column bending moment diagram

The second requirement that Imanpour et al. (2016b) proposed was to limit the tier drift to avoid brace fracture due to excessive deformation demands in bracing tiers. This was achieved by providing the column with sufficient in-plane flexural stiffness. This study proposed a tier drift limit of 2% when the storey drift is equal to an expected storey drift, Δ_{exp} , of 2.0Δ , where Δ is the design storey drift predicted in accordance with the applicable building code (ASCE 2010). A prototype frame designed in accordance with the proposed requirements was analyzed using OpenSees and it was shown that the proposed requirements can effectively prevent undesirable limit states observed in the frames designed excluding such provisions.

In another study, the seismic behaviour of MT-CBFs was examined by involving the contribution from the adjacent gravity columns in the lateral-load carrying capacity as shown in Figure 2.22. It

was found that the involvement of the gravity columns can improve the seismic response of MT-CBFs (Imanpour et al. 2016c).

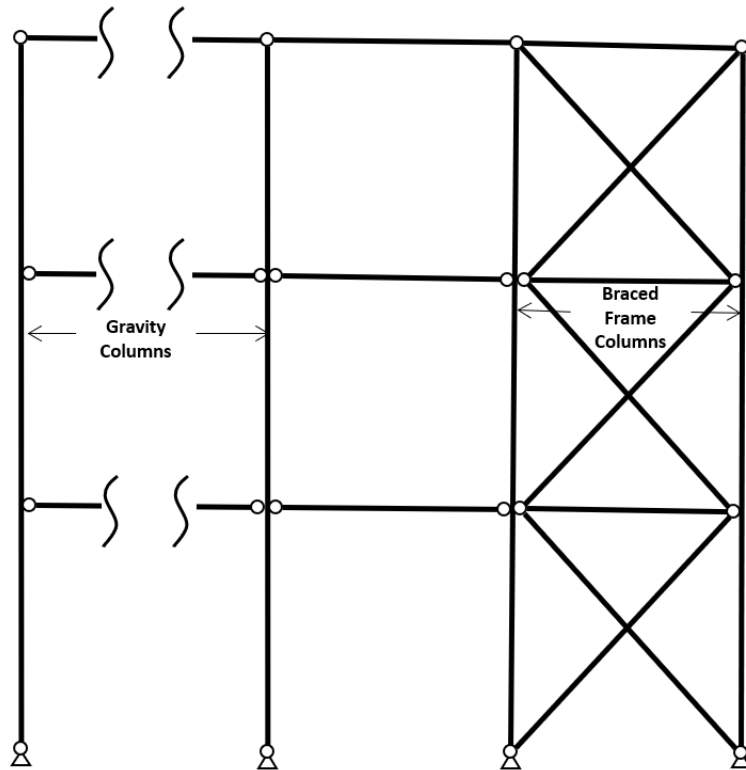


Figure 2.22: Three-tiered steel braced frame with adjacent gravity columns

Two analysis methods were proposed by Imanpour and Tremblay (2016a) to predict the seismic induced in-plane bending moment of the columns and tier drifts in tall MT-CBFs with three or more tiers. The first method is the extension of the method initially proposed for two-tiered CBFs and can be used when yielding propagates from the bottom tier to the top one or from top tier to the bottom one. However, the second method involves a more general stiffness-based analysis that can be used for various yielding scenarios.

2.4.2 Seismic Behaviour of Wide-Flange Steel Columns

Limited research has been conducted to understand the seismic behaviour of steel wide-flange columns in MT-CBFs. Stoakes and Fahnestock (2012; 2016) evaluated the seismic behaviour of isolated columns using numerical analyses. Various limit states were identified, which includes strong axis flexural buckling, weak-axis flexural buckling, flexural-torsional buckling due to biaxial moment demands, and flange and web local buckling. It was found that the governing limit state depends on the force distribution on the columns. Furthermore, it was shown that weak-axis flexural yielding of a column can significantly degrade the strong-axis buckling strength of a column. Sections with large slenderness ratios are prone to strength degradation when weak-axis flexural yielding has occurred.

More recently, Imanpour et al. (2017) experimentally tested wide-flange columns, which was part of a two-tiered CBFs, using a pseudo-dynamic hybrid simulation method. The column testing machine is shown in Figure 2.23. A W250x101 column was physically tested using the input produced by the finite element analysis under a ground motion record. The study successfully simulated column instability observed in the past numerical simulations.

Newell and Uang (2008) experimentally studied the cyclic behaviour of wide-flange steel columns in multi-storey CBFs. Nine full-scale wide-flange specimens were tested under various axial force demands in combination with applied story drifts to examine the column stability response under cyclic loading. The local buckling was the dominant buckling mode as shown in Figure 2.24. No global buckling was observed in any of these tests.

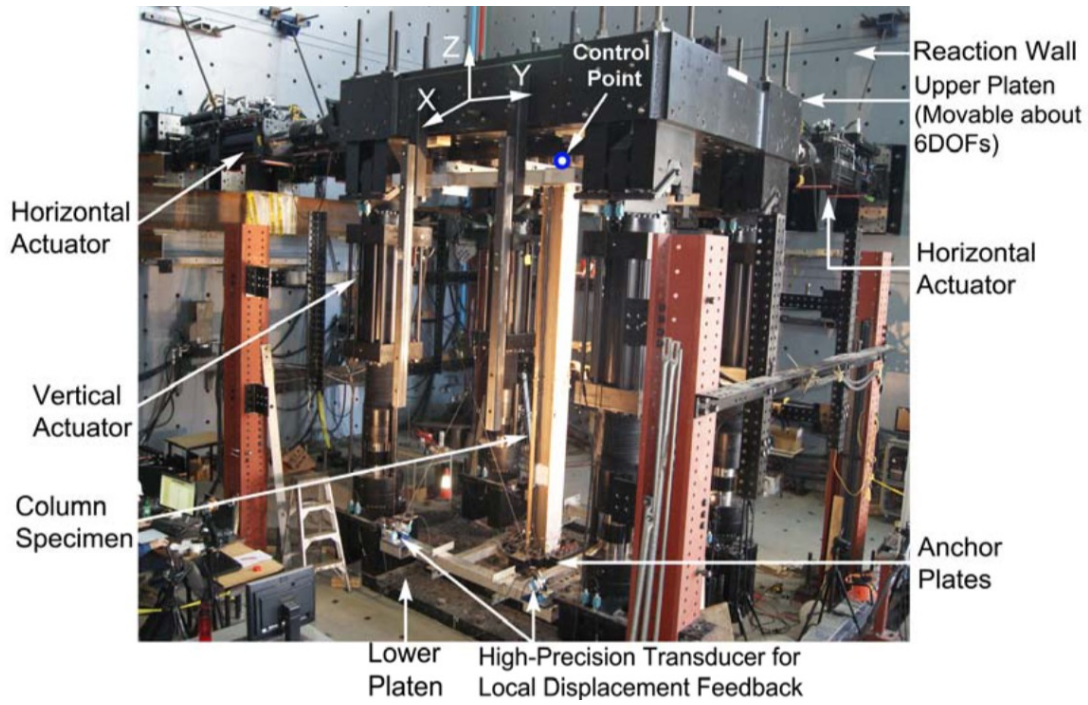


Figure 2.23: W250x101 column part of a two-tiered CBF in the multi-directional hybrid testing system (Imanpour et al. 2017)

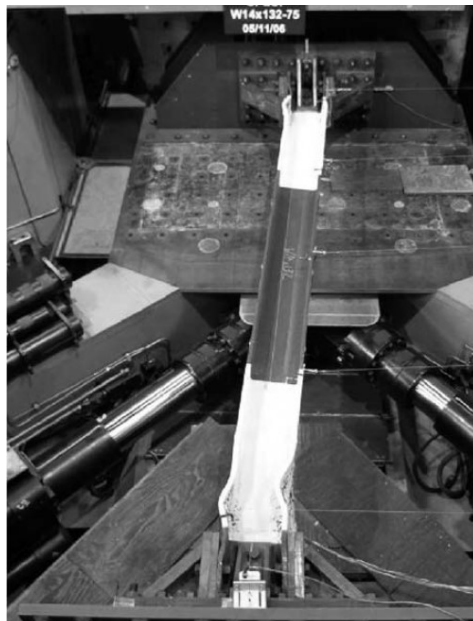


Figure 2.24: Local buckling of Wide-flange steel columns as part of multi-storey CBFs (Newell and Uang 2008)

Elkady and Lignos (2018) performed an extensive experimental study to evaluate the seismic stability of steel wide-flange columns in moment-resisting frames (MRF) under multi-axis cyclic loading. Local flange and web buckling at the column base were observed. Severe local buckling led to large axial shortening and, in some cases, out-of-plane buckling of columns as shown in Figure 2.25. Moreover, column twist was observed at large storey drifts.

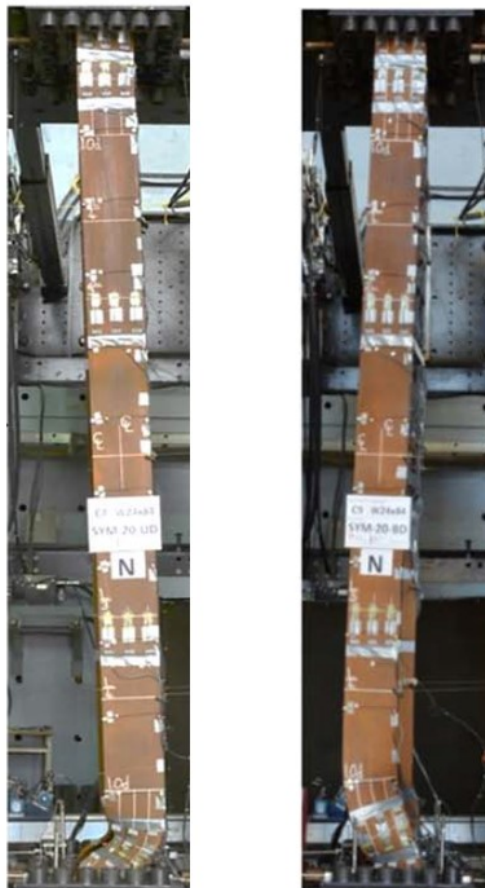


Figure 2.25: Lateral instability of steel Wide-flange column as part of MRFs (Elkady and Lignos 2018)

Ozkula et al. (2017) experimentally tested more than 10 column specimens under various loading conditions to study the seismic response of steel MRF wide-flange columns. Three instability modes were observed: 1) symmetric flange buckling; 2) anti-symmetric local buckling and 3) coupled buckling. An example of each of the buckling modes is presented in Figure 2.26, where the left image is at the west side of the column, the middle image shows the overall column, and the right image is at the east side of the column. A criterion to identify the governing buckling mode and consequently the hysteretic response of the wide-flange steel MRF column subjected to cyclic loading was proposed.

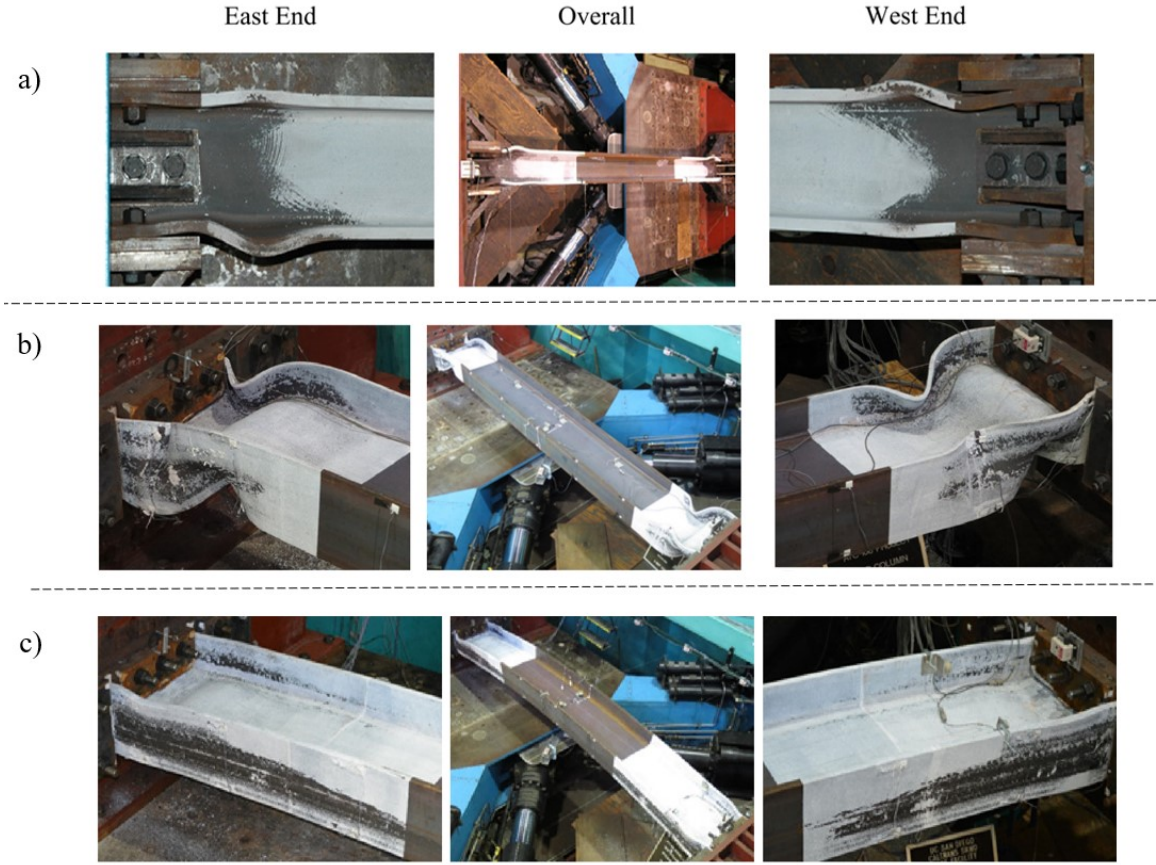


Figure 2.26: Failure modes observed in wide-flange steel MRF columns: a) symmetric flange buckling; b) anti-symmetric local buckling; c) and coupled buckling (Ozkula et al. 2017)

2.5 Design of MT-CBFs

2.5.1 Canadian Design Provisions

2.5.1.1 2009 Canadian steel design standard (S16)

Design requirements and guidelines for the design of columns in MT-CBFs were originally introduced in Canada as part of the 2009 Design of Steel Structures standard, S16-09 (CSA 2009). These requirements were given under Section 27.6.6 titled ‘Columns with Braces Intersecting Between Diaphragms.’ The requirements introduced were applicable only to limited-ductility (LD) MT-CBFs, as these systems are expected to experience limited inelastic behaviour ($R_d R_o = 2.0 \times 1.3 = 2.6$) where R_d is the ductility-related force modification factor, and R_o is the overstrength-related modification factor. The 2009 Design of Steel Structures required a horizontal strut to be placed between the columns at the tier levels to transfer the unbalance force, which is created once the compression braces buckle and the tension forces increase to reach yielding. In addition to the gravity loads, the columns were required to resist the forces induced from the yielding and buckling of the braces at a roof displacement equal to the design storey drift, $R_d R_o \Delta_e$, assuming that yielding has occurred in the tension brace located at any tier of the braced frame (where Δ_e is the elastic storey drift under the base shear of the corresponding building code). Furthermore, columns in MT-CBFs were required to resist the effects of an out-of-plane transverse load acting on the column at each tier level. Each of these loads was equivalent to 10% of the load in the compression member meeting at the intersecting point, as illustrated in Figure 2.27.

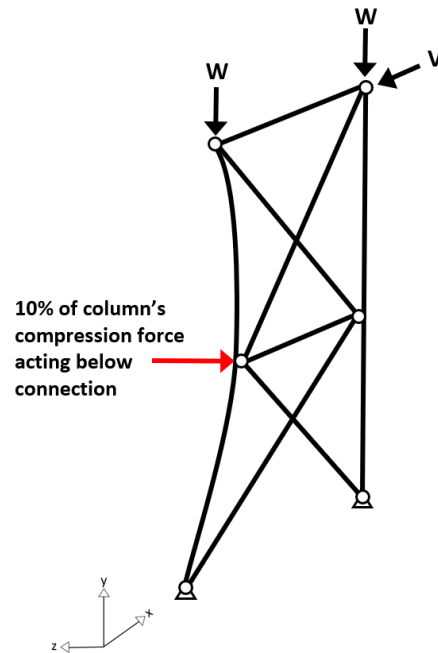


Figure 2.27: Out-of-plane notional load applied at the tier level

2.5.1.2 2014 Canadian steel design standard (S16)

In the latest edition of the Canadian standard, CSA S16-14 (CSA 2014), the provisions to design MT-CBFs have been modified to permitted moderately-ductile (Type MD) ($R_d R_o = 3.0 \times 1.3 = 3.9$) in addition to limited-ductility (Type LD) frames. Type MD frames are allowed to be designed up to three tiers high, and Type LD frames have been extended to five tiers. The design requirements introduced in S16-09 still apply in the latest standard; however, the out-of-plane notional load has been reduced from 10% to 2% of the compression force acting in the column below the brace-to-column connection to reflect the finding of Imanpour and Tremblay (2012). A strut is still required between columns at each tier level in the latest edition; however, the standard suggests using the flexural capacity of the strut to constrain the axial rotation of the columns at

each connection to reduce the effective length of the column against flexural-torsional buckling. Lastly, the 2014 Design of Steel Structures standard advises avoiding tier-drift in excess of 1.5%-2.0%, as this can lead to premature brace fracture caused by ultra-low cycle fatigue.

Imanpour and Tremblay (2016) investigated the seismic response of MT-CBFs designed in accordance with the 2014 Canadian standard (CSA S16-14). A set of prototype frames were analyzed using the nonlinear response history analysis method in OpenSees. The results showed that frames complying to the CSA S16 requirements can develop brace tension yielding in a single tier without excessive tier drifts. The in-plane flexural bending demand can be predicted well using the current CSA S16 requirements. The study suggested that brace tensile yielding can occur in more than one tier and the corresponding force demands should be considered in the column design. This study found that the in-plane flexural demand on the columns is sensitive to the storey drift assumed in the design; therefore, more representative storey drift estimates should be used in design to prevent undervaluing the in-plane moments on the columns. The authors also proposed that further studies should investigate the validity of the out-of-plane notional load imposed on the design of the MT-CBF columns in the current standard, which is evaluated in Chapter 5 of this M.Sc. thesis.

2.5.2 Design Provisions in the U.S.

2.5.2.1 2010 U.S. Seismic Provisions for Structural Steel Buildings (AISC 341)

The 2010 American Institute of Steel Construction (AISC), Seismic Provisions for Structural Steel Buildings (AISC 2010a), did not include design provisions for MT-CBFs. In the absence of special design provisions, MT-SCBFs were designed based on the provisions prescribed for conventional multi-storey braced frames. The required strength of the bracing members was calculated based

on the seismic base shear as determined in the applicable building code. The bracing members were also sized to meet desired energy dissipation capacities and to increase the fracture life by limiting the slenderness ratio ($kL/r \leq 200$) and satisfying the requirements for width-to-thickness ratios as prescribed in section D1.1 of the Seismic Provisions. The design of the other members of the frame, such as columns, struts, and connections, was conducted using the ultimate strengths of the bracing members using capacity design. In the 2010 Seismic Provisions, two analyses were prescribed for SCBFs to determine the forces in the columns, struts, and connections (Figure 2.28). Analysis Case A (Figure 2.8a) represents the brace force scenario where braces reach their expected tensile strength (T_{exp}) and expected compressive strength (C_{exp}). Case B (Figure 2.8b) represents the brace force scenario where the braces achieved their expected tensile strength (T_{exp}) and expected post-buckling strength (C'_{exp}).

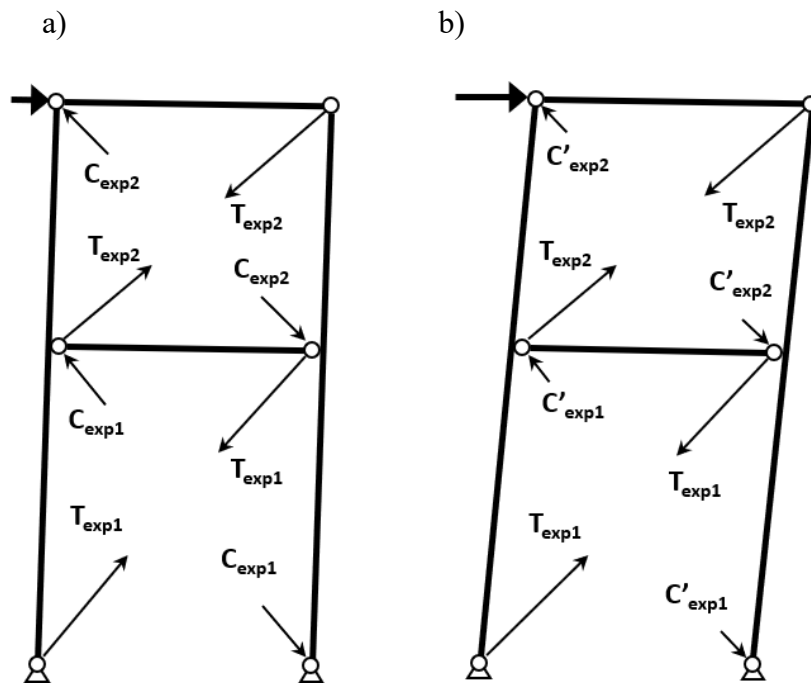


Figure 2.28: Analysis cases prescribed by AISC Seismic Provisions for columns, beams, and connections

2.5.2.2 2016 U.S. Seismic Provisions for Structural Steel Buildings (AISC 341)

Requirements to design MT-CBFs were introduced for the first time in the 2016 Seismic Provisions (AISC 2016a). Special seismic provisions were prescribed for multi-tiered ordinary and special CBFs, as well as multi-tiered buckling-restrained braced frames. Under the current provisions, multi-tiered special concentrically braced frames (MT-SCBFs) are required to be analyzed under three different analysis cases as specified in Chapter F of the 2016 AISC Seismic Provisions. The first two analyses are the same prescribed for CBFs (Figure 2.28). The third analysis case represents the progressive yielding and buckling of braces in MT-SCBFs, which corresponds to the initiation of tensile yielding in the weakest tiers and propagation to the strongest (Figure 2.29). For this analysis, it is assumed that the compression brace in the critical tier (lower tier in this case) has reached its post-buckling strength, C'_{exp} , and the compression brace in the adjacent tier has reached its expected buckling strength, C_{exp} . Concurrently, the tension braces in the critical tier and the adjacent tier are assumed to be at their expected tension strength, T_{exp} . This analysis case is shown in Figure 2.20b for a two-tiered frame. The unbalance storey shear force can be determined by analyzing the frame under applied brace loads. Then, the column in-plane bending demand can be computed for design purposes. This estimate is considered conservative since it is possible that the brace in the adjacent non-critical tier has already experienced several loading cycles, which leads to a decrease in buckling strength at the time when the tension brace yields in the critical tier (Tremblay 2002; Imanpour and Tremblay 2014a).

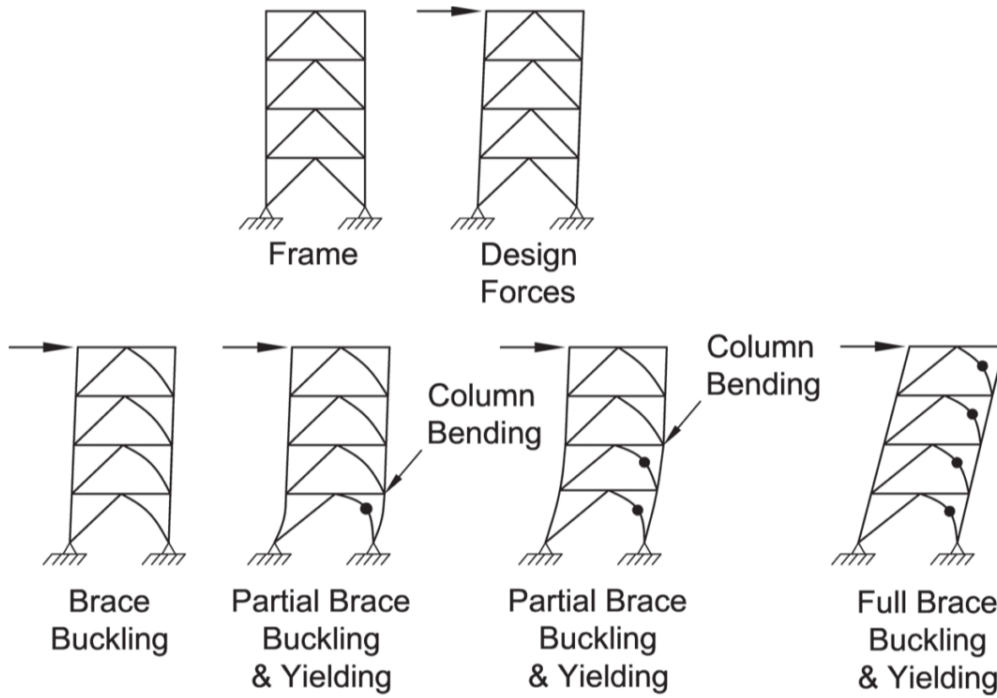


Figure 2.29: Progression of brace buckling and yielding in MT-SCBFs (AISC 2016a)

An out-of-plane bending moment can also be induced on the columns of MT-SCBFs due to initial geometric imperfections in columns, out-of-plane buckling of braces, and plastic hinge forming in the gusset plate (Figure 2.30). To account for such demands, the 2016 AISC Seismic Provisions requires an out-of-plane horizontal notional load be applied on the column at the strut level. The notional load is equal to 0.006 times the vertical component of the compression brace that meets the column at the tier level. In addition, the columns must be designed to resist the out-of-plane moment that the braces produce upon buckling, but less than the maximum bending resistance of the brace connections.

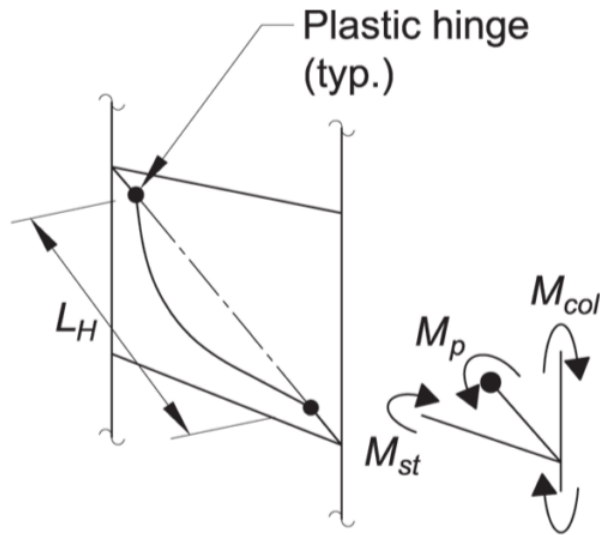


Figure 2.30: Forces arise from out-of-plane brace buckling (AISC 2016a)

Additionally, the 2016 Seismic Provisions require MT-SCBF columns to be torsionally braced at the strut-to-column connections. Stoakes and Fahnestock (2012; 2016) showed that providing rotational bracing, along the height of the column at the strut-to-column connections, can improve the strong-axis buckling strength in the presence of in-plane flexural yielding, particularly when the location of weak-axis flexural moment matches the location of the strong-axis flexural moment (e.g. two-tier braced frame with identical tier heights). The 2016 AISC Seismic Provisions also require that a strut is placed between two tiers to prevent the unsatisfactory K-brace frame response. Finally, the provisions have established a maximum tier drift ratio of 2% to prevent excessive brace deformations that can cause brace fracture (Tremblay et al. 2003).

Chapter 3 – Design of Steel Multi-Tiered Concentrically Braced Frames

3.1 General

The purpose of this chapter is to present the design of a prototype frame using the 2010 and the 2016 AISC Seismic Provisions (AISC 2010a, 2016a). First, the building and frame geometry are introduced, followed by frame loading. Finally, the detailed design calculations for the prototype frame members including braces, columns, and strut are presented.

3.2 Building and Frame Geometry

A single-storey steel building located in Seattle, Washington, U.S., was selected for the case study. The building has plan dimensions of 35 m x 189 m, and a height of 9.0 m. In each principal direction, the building has four concentrically braced frames (two per each exterior walls) as shown in Figure 3.1. The frame height is divided into two tiers with X-bracing configuration. As illustrated in Figure 3.2, the bottom tier, *Tier 1*, is 4.7 m tall, and the top tier, *Tier 2*, is 4.3 m tall. Non-uniform tier heights were selected to intentionally reduce the storey shear resistance of one of the tiers (Tier 1) such that under the lateral load its braces yield first. This tier is referred to as the ‘critical tier’ or the ‘weakest tier.’ This non-uniformity of storey shear resistance may occur in an actual building with identical tier heights as a result of various material properties, brace end conditions or initial geometric imperfections (Schmidt and Barlett 2002). The braced frame was designed as a Special Concentrated Braced Frame (SCBF) system. The braces were sized to carry the lateral seismic load in tension and compression.

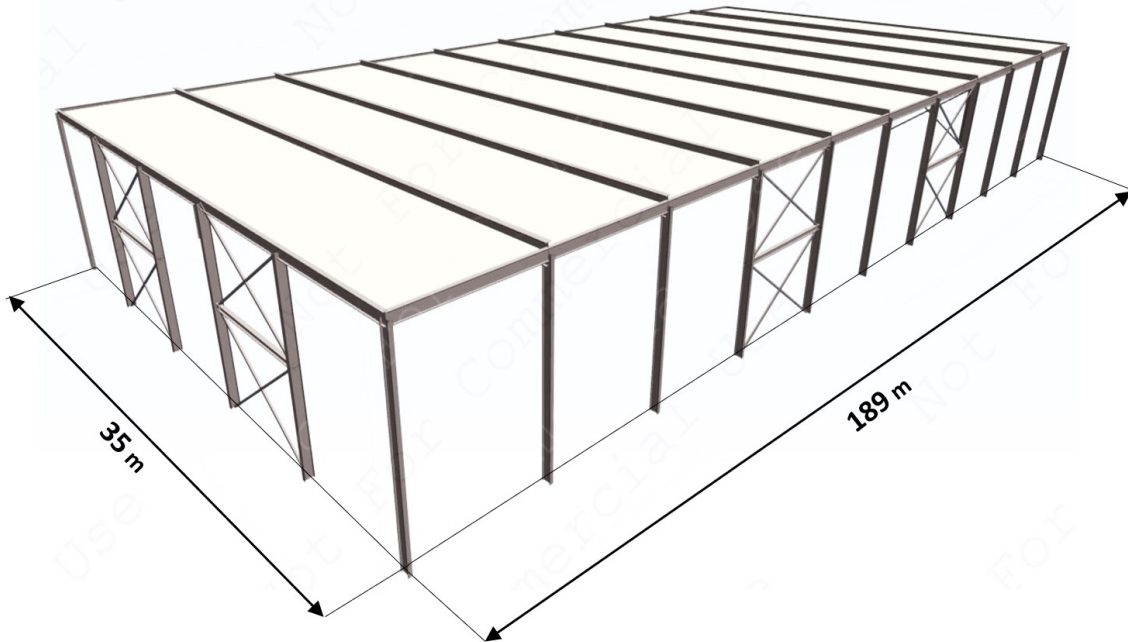


Figure 3.1: Three-dimensional schematic of a single storey building with two-tiered CBFs (roof trusses not shown), figure not to scale

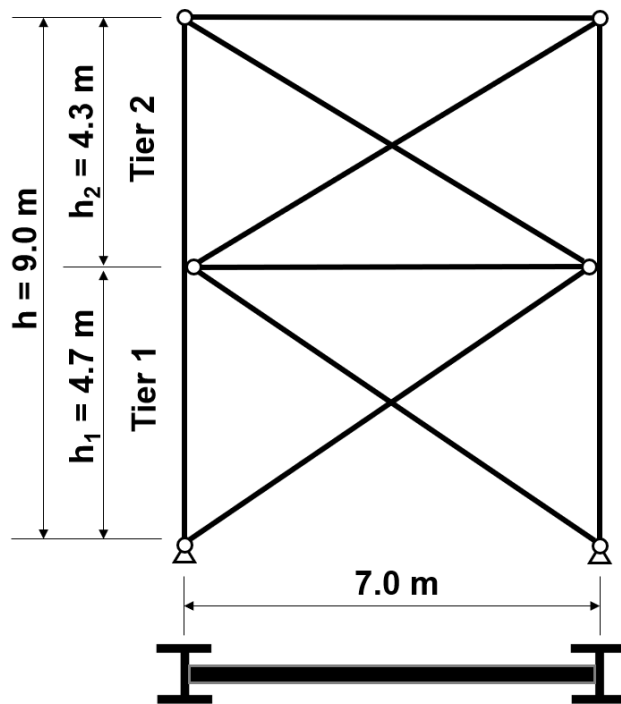


Figure 3.2: Geometry of the prototype frame

The height of each column is 9.0 m. The columns are made of W-shapes and are oriented such that the out-of-plane bending occurs about the strong-axis of the section as seen above in Figure 3.2. A 7.0 m long intermediate horizontal strut is placed between tiers to prevent K-braced frame response (AISC 2010a; 2016a) and ensure the seismic load is properly transferred to the base of the structure through truss-action once the braces respond in inelastic range.

3.3 Gravity and Seismic Loads

The design loads for the selected building were determined in accordance with the ASCE 7-16 standard (ASCE 2016). A Risk Category II was chosen, and it was assumed that the building is located on a Site Class C with a Seismic Design Category D. The gravity loads were calculated using the roof dead load $D_{\text{roof}} = 1.0$ kPa, the exterior wall dead load $D_{\text{wall}} = 0.5$ kPa based on a light cladding structure resting on the ground, and a live load $L = 0.96$ kPa as prescribed by ASCE 7. The tributary area considered per column was calculated on the basis that steel roof trusses support the roof system between the exterior columns of the building. The resulting gravity factored load at the top of each column was then calculated to be 227 kN.

The seismic load parameters include a response modification factor $R = 6.0$, overstrength factor $\Omega_o = 2$, and a deflection amplification factor $C_d = 5.0$. The mapped risk-targeted Maximum Considered Earthquake (MCE_R) ground motion response parameters, $S_S = 1.362g$ and $S_I = 0.458g$ for short and 1.0 s periods, respectively, were used to obtain the design spectral response acceleration parameter $S_{DS} = 0.908g$ and $S_{DI} = 0.458g$. Design Response Spectrum is shown in Figure 3.3. The empirical fundamental period was calculated using $C_t = 0.0488$ and $x = 0.75$, and

is equal to $T_a = 0.25$ s (red dash line in Figure 3.3). Using these values, the seismic design coefficient $C_s = 0.151$ was obtained. The seismic weight of the building W is equal to 7624 kN, based on the roof and the exterior wall dead loads. The equivalent lateral force procedure was used to calculate the frame seismic base shear V , which is the product of the seismic coefficient and the seismic weight tributary of the frame. This force was amplified to account for accidental torsion, resulting in a seismic design base shear equal to 316 kN per frame.

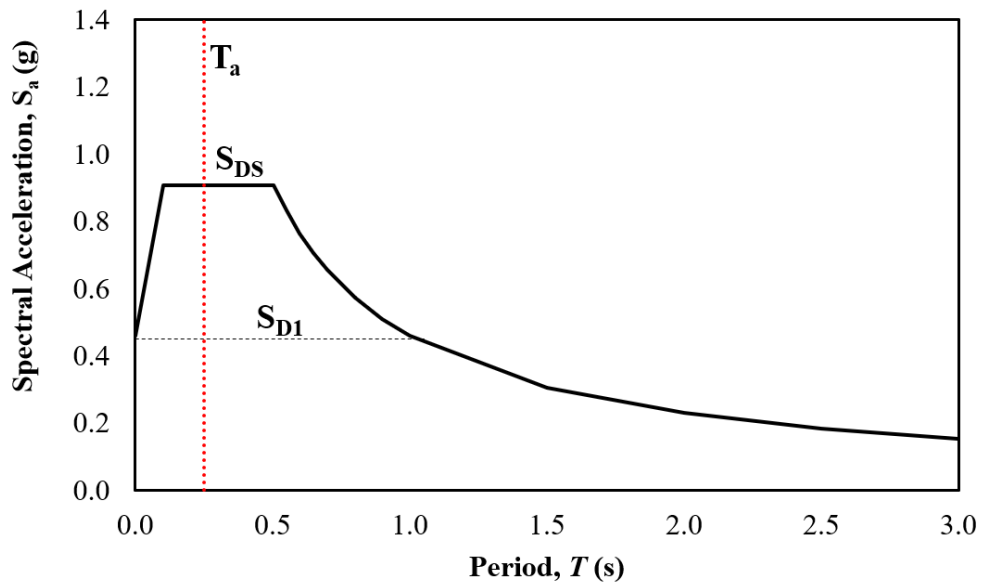


Figure 3.3: Design response spectrum

3.4 Brace Design

The braces in both tiers were designed to resist the seismic load effects in tension and compression. The brace design force in compression is equal to $P_{r,b} = 200$ kN, which includes the seismic-induced axial force $P_{E,b} = 191$ kN plus the gravity induced axial compression force $P_{G,b} = 9$ kN. The braces are designed using square Hollow Structural Section (HSS) members. Such members

are more efficient than singly-symmetric sections as they have an identical radius of gyration about both principal axes of the section (Black et al. 1980). The braces are made of ASTM A1085 Grade A steel (ASTM 2015a) with a yield stress $F_y = 345$ MPa and an expected yield stress $R_y F_y = 431$ MPa as specified in the AISC Seismic Provisions (AISC 2016a). Braces were designed such that they buckle out of the plane of the frame. An effective length of 0.45 times the total length of the brace, which is measured between the brace working points, was used in design to account for the lateral bracing provided by the brace acting in tension and the length of the end connections that do not contribute to brace buckling (Wakabayashi et al. 1974; Nakashima and Wakabayashi 1992; and El-Tayem and Goel 1985; 1986; Sabelli et al. 1999). The brace axial compression resistance in Tier 1 was calculated to equal to $P_{c,bl} = 215$ kN using the AISC Specification for Structural Steel Buildings (AISC 2010b). Although the brace lengths are slightly different between tiers, an identical HSS 89×89×6.4 section was selected for both tiers as typically done in practice to maintain a similar connection size. The selected section complies with the width-to-thickness ratio limit $b/t < 14$ for highly ductile members where b is the effective width of the member and t is the thickness, and with the slenderness limit of $L_c/r \leq 200$, where L_c is the effective length and r is the radius of gyration.

3.5 Column Design

3.5.1 Design in Accordance with the 2010 AISC 341 Seismic Provisions

The columns were first designed in accordance with the 2010 AISC Seismic Provisions. The frame with the selected columns is referred to as the 2010 design. The columns were designed to resist

the gravity loads $P_{G,c} = 227$ kN plus the maximum axial load induced by the summation of the vertical forces due to the brace expected resistances in tension and compression. For the later, two analysis cases, A and B, are prescribed by the 2010 AISC Seismic Provisions as shown in Figures 3.4a and 3.4b with their respective loading. Analysis Case A represents a brace load scenario where braces reach their expected tensile strength (T_{exp}) and expected compression strength (C_{exp}). Case B represents a brace load scenario where braces reach their expected tensile strength (T_{exp}) and expected post-buckling strength (C'_{exp}). The maximum axial compression force, $P_{E,c} = 1103$ kN, was obtained under the first analysis case. The columns are made of ASTM A992 Grade 50 steel (ASTM 2015b) with yield stress $F_y = 345$ MPa. The effective length of the column in the strong-axis $K_x = 0.84h$, weak-axis $K_y = 0.80h_l$, and torsion $K_z = 1.0h_l$ were used in design where h is the total frame height, and h_l is the height of Tier 1 as shown in Figure 3.2. The effective length factors were derived using the structural analysis software (S-Frame 2017) where an individual column was modelled using frame elements, and the corresponding gravity and seismic loads were applied at the top of the column and at the strut level. An elastic Eigen buckling analysis, also referred to as Linear Perturbation Frequency analysis, was then performed (Figure 3.5). The eigenvalues were used to calculate the effective length of the column about its strong and weak axes. An effective length smaller than unity was used to account for the distributed axial load applied on the MT-CBF column segments (Dalal 1969). A W410×67 section was finally selected for the columns of the 2010 design to achieve the most efficient cross-section. The column axial resistance was obtained from the AISC Specification Equation E3-1 is equal to $P_n = 1391$ kN. The web and flange width-to-thickness ratios were verified to comply with a moderately ductile W-shape in

accordance with the 2010 Seismic Provisions, such that $b/t \leq 9.1$ and $h/t \leq 49.3$ were satisfied, for the flange and the web of the section, respectively.

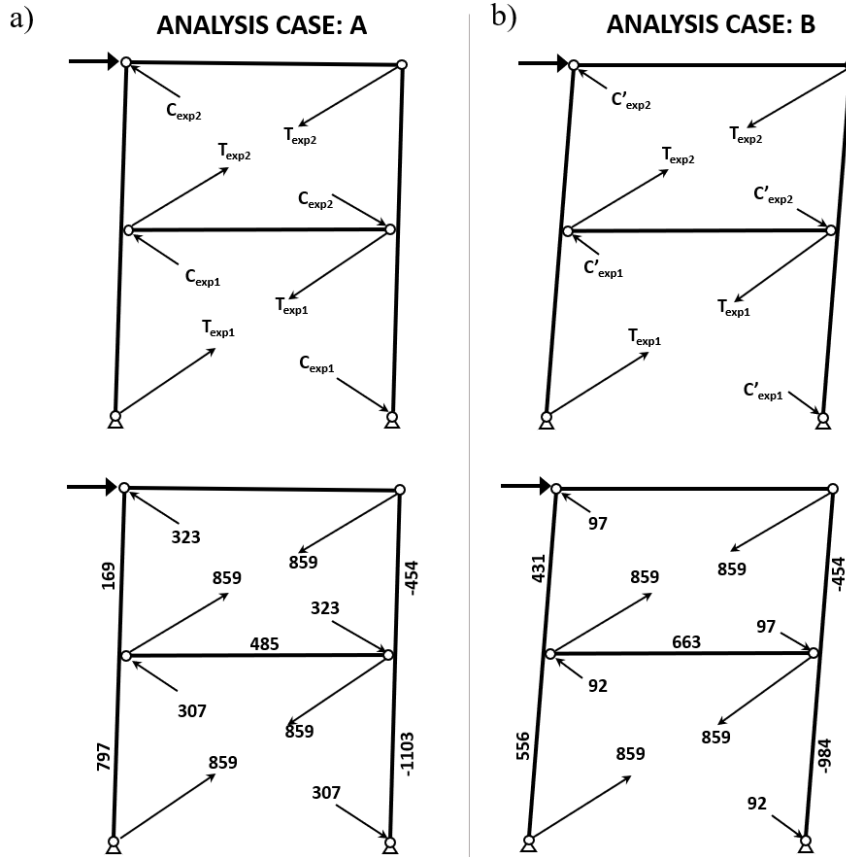


Figure 3.4: Brace loading scenarios: a) Analysis case A; and b) Analysis case B

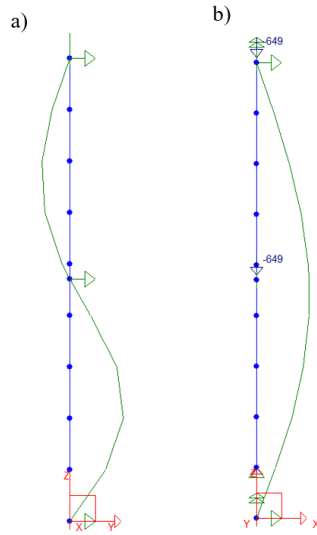


Figure 3.5: Column buckling mode shapes: a) In-plane mode; and b) out-of-plane mode

3.5.2 Design in Accordance with the AISC 341-16 Seismic Provisions

The columns of the prototype frame (Figure 3.2) were redesigned according to the AISC 341-16 Seismic Provisions, which is referred to as the 2016 design. The required strength of columns was determined considering the maximum forces obtained from three analyses cases A, B, and C, as illustrated in Figures 3.4a, 3.4b and Figure 3.6. Analysis case C represents the progressive buckling and yielding of the braces from the critical tier to the non-critical tier, where the bracing members reach their expected tensile strength (T_{exp}) and expected compression strength (C_{exp}) in the non-critical tier and the expected post-buckling strength (C'_{exp}) in the critical tier. This analysis case was introduced in the 2016 AISC Seismic Provisions to address the unsatisfactory limit states observed in the past numerical analyses (Imanpour et al. 2016a; 2016b). Variations in brace material properties, brace slenderness ratio, brace end conditions and initial out-of-straightness can trigger brace buckling and subsequently yielding in one of the braced tiers. It was shown that such response can impose large in-plane flexural bending moment demands on the braced frame

columns, which may lead to column instability in the presence of axial compression force demands if not considered in design. As shown in Analysis case C, the columns should also be verified under the forces arising from the progressive yielding of bracing members along the height of the frame. For the two-tiered CBF studied here, brace tensile yielding is expected to initiate in the first tier, which has a lower expected storey shear resistance (Tier 1) and propagates to Tier 2 with a higher expected storey shear resistance. Under the brace loading scenario corresponding to analysis case C (Figure 3.6), the braced frame column experiences the most critical seismic force demands that includes 1) axial compression force due to the brace expected resistances in tension and compression plus the axial compression force induced by gravity loads; and 2) in-plane bending moment caused by uneven yielding of braces in two adjacent tiers and is obtained from the differences between the expected storey shear resistances of adjacent tiers as described in Section 2.5.2.2. The 2016 AISC Seismic Provisions also requires an additional out-of-plane bending moment demand arising from the brace out-of-plane buckling, flexural plastic hinging of brace connections, column initial out-of-straightness. Similar to the 2010 design, the maximum axial compression force is induced in the first tier segment of the right-hand-side column and is equal to $P_{c,c} = 1330$ kN due to brace expected forces $P_{E,c} = 1103$ kN and the gravity load $P_{G,c} = 227$ kN.

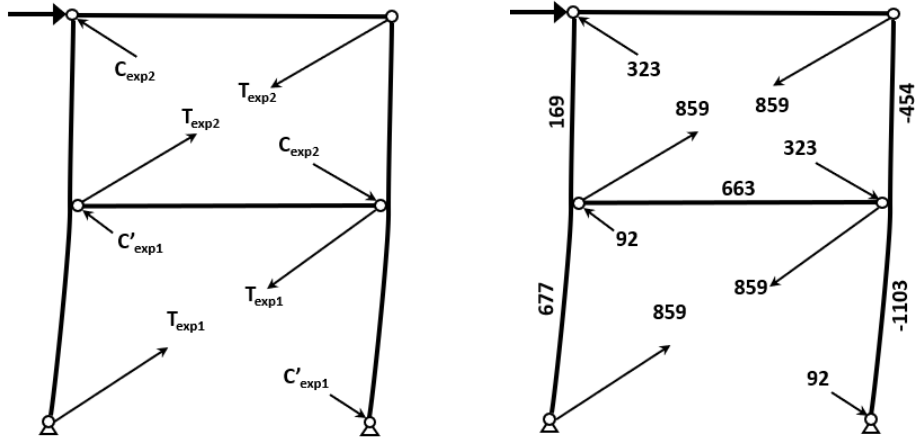


Figure 3.6: Brace loading scenario for Analysis case C

The first step in the calculation of the column in-plane bending moment is to identify the critical tier. The critical (or weakest) tier is the tier with the least expected storey shear resistance. The shear resistance is obtained from the summation of the horizontal components of the brace resistances in tension and compression $V_{exp} = (T_{exp} + C_{exp}) \cos\theta$, where θ is the angle between the brace and the horizontal plane. In cases where tier heights and members are the same, tiers will have different shear resistance due to inherent differences as a result of connection details, material variability (Schmidt and Barlett 2002), or geometric imperfections. In that case, multiple analyses should be performed by switching the critical tier. For the frame of Figure 3.2, expected storey shear resistance in Tier 1 is $V_{exp,1} = 970$ kN, which is smaller than that of Tier 2 $V_{exp,2} = 1014$ kN. The column in-plane bending demand M_{ry} is then calculated using unbalanced brace storey shear force ΔV_{br} using Equation 3.1 as follows:

$$M_{ry} = \frac{\Delta V_{br} h_1 h_2}{2 h} \quad (3.1)$$

where h_1 and h_2 are the height of Tiers 1 and 2, respectively, as shown in Figure 3.2. ΔV_{br} is computed as follows:

$$\Delta V_{br} = (T_{exp} + C_{exp})_2 \cos\theta_2 - (T_{exp} + C'_{exp})_1 \cos\theta_1 \quad (3.2)$$

For Analysis case C, as shown in Figure 3.6, $\Delta V_{br} = 227$ kN and the corresponding in-plane bending moment on the columns is $M_{ry} = 254$ kN-m. Figure 3.7 illustrates how the in-plane flexure demand is derived from Analysis case C.

Column out-of-plane bending moment demand is obtained from two components, the moment induced by applying an out-of-plane horizontal notional load at the strut level that is 0.006 times the vertical load contributed by the compression brace (amplified by multiplier $B_1 = 1.16$ to account for the P- δ effect) and the respective component of the moment caused by the buckling of braces in the out-of-plane direction (Figure 2.30), where the moment induced by the buckling of the braces is equal to $1.1R_y M_p / \alpha_s$ where R_y is the ratio of expected yield stress to the specified minimum yield stress, M_p is the plastic bending moment of the minimum between the compression brace and the brace connection, and α_s is the LRFD force level adjustment factor and is taken equal to 1.0. For the prototype frame, the total out-of-plane bending moment demand is equal to 5.7 kN-m.

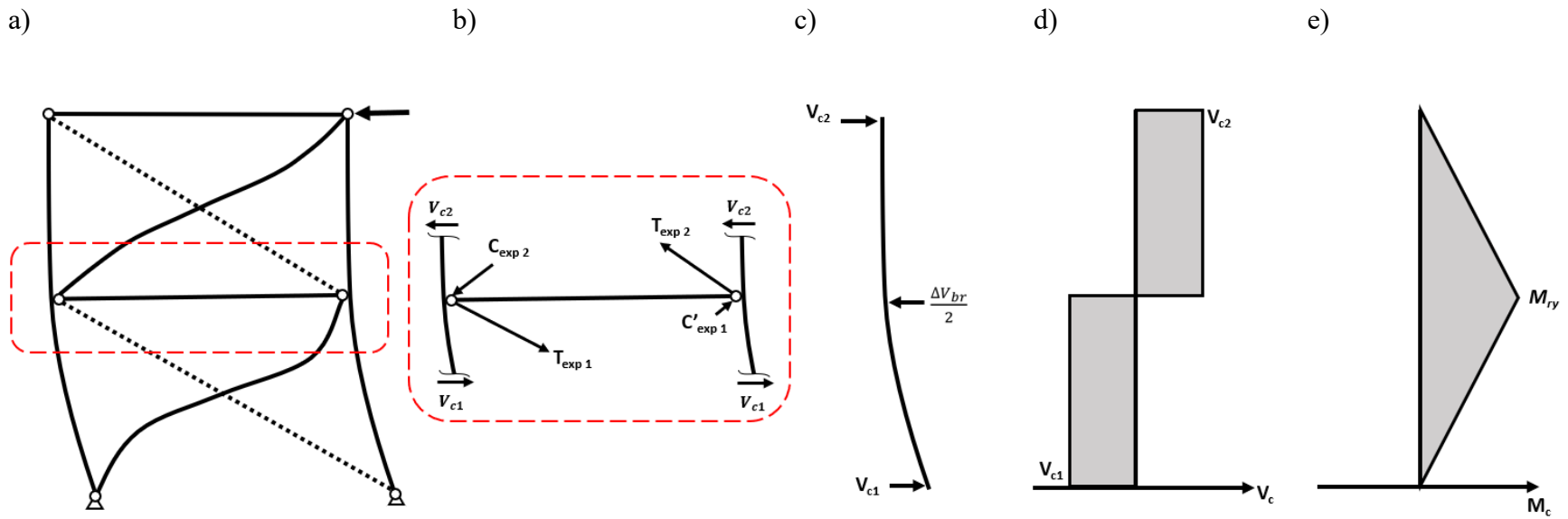


Figure 3.7: Analysis case C: a) frame deformed shape ; b) frame free-body diagram; c) column free-body diagram; d) column shear force diagram; and e) column bending moment diagram under ΔV_{br}

A W310×143 column was selected to carry the gravity, and seismic-induced forces described here. This section was selected as it results in the most efficient cross-section for the column that satisfied the strength requirements in accordance with the interaction equation (Equation 3.3) specified in Chapter H (H1-1a) of the 2016 AISC Specification.

$$\frac{P_r}{P_c} + \frac{8}{9} \left(\frac{M_{rx}}{M_{cx}} + \frac{M_{ry}}{M_{cy}} \right) \leq 1.0 \quad (3.3)$$

The flange and web width-to-thickness ratios were verified using the 2016 AISC Seismic Provisions. The column is classified as a moderately ductile member. The width-to-thickness ratios $b/t \leq 8.6$ and $h/t \leq 52.4$ were satisfied for the flange and the web of the section, respectively.

Comparing the final column sections obtained between the two designs, it is observed that in the 2016 design the presence of combined axial compression force and bi-axial bending moment demands in two-tiered CBF columns leads to a more severe loading scenario.

3.6 Strut Design

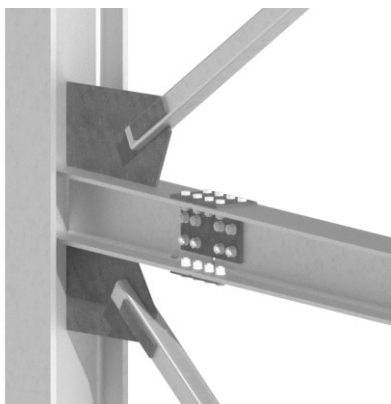
An intermediate horizontal strut was placed between columns at each tier to resist the unbalance load that is developed after brace buckling and yielding. For both 2010 and 2016 designs, the maximum axial design force for the strut is obtained from Analysis case B when the tension braces in both tiers reach T_{exp} and compression brace forces are equal to C'_{exp} as shown in Figure 3.4b. Hence, the strut design force is equal to $P_{r,s} = 663$ kN.

For the 2010 and 2016 designs, the strut was designed assuming that the strut is connected to a stub-section using a set of splice plates (Figure 3.8), which act as a simple connection and prevent the development of in-plane moment due to partial rigidity of the gusset plate connection on the

strut member (Carter et al. 2016). Thus, the in-plane moment acting on the strut was calculated based on the self-weight of the member only for both designs. In addition to the in-plane bending moment, the 2016 Seismic Provisions requires that the strut be designed for an additional out-of-plane bending moment induced by the corresponding component of the minimum value between the plastic moment induced by the brace or the connection, which is caused by brace buckling out-of-plane. This moment was calculated as 4.6 kN-m.

The struts for both designs use a W-shape conforming to ASTM A992 Grade 50 steel with yield stress $F_y = 345$ MPa. A W250×67 strut was selected in both designs to carry the design loads. For the 2010 design, the strut was oriented such that the web is in the plane of the frame as shown in Figure 3.8a; however, the strut web was placed in the horizontal plane for the 2016 design as shown in Figure 3.8b to provide torsional bracing to the column at the strut-to-column connection through the stiffness and strength provided by major axis bending of the strut (Imanpour et al. 2016b; Stoakes and Fahnestock 2014).

a)



b)

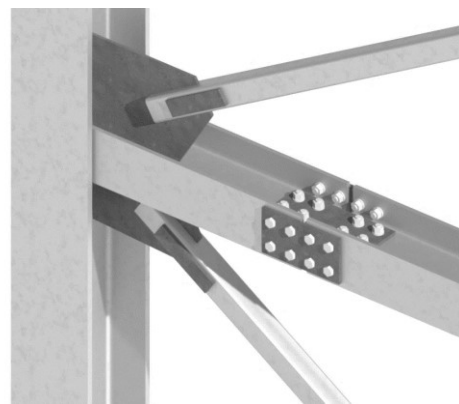


Figure 3.8: Strut-to-column connection a) 2010 design; and b) 2016 design

3.7 Drift Check

As prescribed by ASCE 7, the design storey drift must be limited to 2.5% for an SCBFs with risk category II. This limit was verified for both 2010 and 2016 designs. The elastic drift, Δ_e , can be calculated manually using structural analysis principles or using a structural analysis program where the design seismic base shear is applied at the top of the frame. Thus, the design storey drift, $C_d\Delta_e$, for the 2010 design is 0.60% and for the 2016 design is 0.55%. In both cases, the storey drift limit is satisfied.

The 2016 AISC Seismic Provisions require that in addition to limiting the storey drift to 2.5%, the tier drift be limited to 2% to prevent premature failure of the bracing members (Tremblay et al. 2003; Fell et al. 2009; and Roeder et al. 2011). The 2016 Seismic Provisions require each tier in an MT-SCBF to be subjected to the drift limitation of the applicable building code (ASCE 7), but the drift shall not exceed 2% of the tier height. This requirement was satisfied by verifying the tier drifts at the maximum anticipated storey drift $2.0C_d\Delta_e$, as obtained from the nonlinear response history (NLRH) analyses performed on multi-tiered concentrically braced frames designed in accordance to the 2010 AISC Seismic Provisions (Imanpour et al. 2016b). For the prototype frame studied here, $2.0C_d\Delta_e$ is equal to 1.1%, which corresponds to a lateral displacement of 99.5 mm. To calculate the tier displacement in the critical tier (Tier 1), it is assumed that the tier drift is composed of two components (Figure 3.9): 1) the displacement associated with linear variation over the length of the frame, $\delta_{F,1}$, and 2) the displacement associated with column bending (shear distortion) caused by the unbalanced brace storey shear, $\Delta V'_{br}$ as obtained at the maximum anticipated storey drift $\delta_{C,1}$. Equation 3.4 was used to calculate the tier displacement in Tier 1, δ_1 :

$$\delta_1 = \delta_{F,1} + \left(\frac{\Delta V'_{br}}{2}\right) \left(\frac{h_1^2 h_2^2}{3EI_c h}\right) \quad (3.4)$$

As shown in Figure 3.9, the first component of the drift in Tier 1 is calculated using similar triangles when the storey drift of $2.0C_d\delta_e$ is achieved, which results in $\delta_{F,1} = 2.0C_d\delta_e \left(\frac{h_1}{h}\right) = 52$ mm. For the deflection due to column shear distortion, $\delta_{C,1}$, an unbalanced brace storey force $\Delta V'_{br}$ is calculated when the braces in both tiers have reached their expected post-buckling capacity, C'_{exp} , as expected for well-proportioned frames when they reach the maximum anticipated storey drift (Imanpour et al. 2016a).

Thus,

$$\Delta V'_{br} = (T_{exp} + C'_{exp})_2 \cos\theta_2 - (T_{exp} + C'_{exp})_1 \cos\theta_1$$

For the prototype frame,

$$\Delta V'_{br} = 32 \text{ kN.}$$

Substituting $\Delta V'_{br}$, $\delta_{e,1}$, the tier heights, h_1 and h_2 , the frame height h , and column flexural stiffness in the plane of the frame $EI_{y,c} = 2.26 \times 10^{13} \text{ N} \cdot \text{mm}^2$ into Equation 3.4, the displacement in Tier 1, $\delta_1 = 63 \text{ mm}$, is obtained, which corresponds to a tier drift of 1.33%—satisfying the 2% limit prescribed by the 2016 AISC Seismic Provisions.

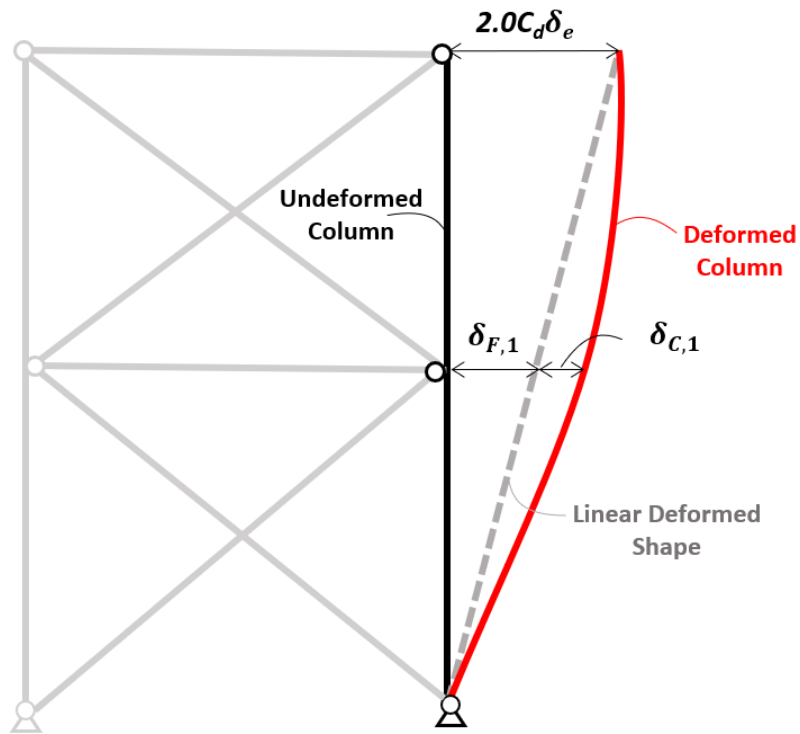


Figure 3.9: Frame deformed shape at expected storey drift from analyses

3.8 Design Summary

Table 3.1 gives a summary of the selected members for the two-tiered CBFs designed in accordance with the 2010 and 2016 AISC Seismic Provisions. The 2010 and 2016 frames are presented in Figure 3.10. The two differences between the two designs are the section of the columns and the orientation of the strut beam.

Table 3.1: Summary of design calculations for the prototype frame

Braces Design								
Tier	Section	L (mm)	b/t	KL/r	P_r/P_c	T_{exp} (kN)	C_{exp} (kN)	C'_{exp} (kN)
Tier 2	HSS 89×89×6.4	8431	12.0	110	0.8	859	323	97
Tier 1	HSS 89×89×6.4	8215	12.0	113	0.9	859	307	92

Column Design							
Frame	Section	$K_x L/r_x$	$K_y L/r_y$	P_r (kN)	M_{rx} (kN m)	M_{ry} (kN m)	$\frac{P_r}{P_c} + \frac{8}{9} \left(\frac{M_{rx}}{M_{cx}} + \frac{M_{ry}}{M_{cy}} \right)$
2010 Frame	W410×67	44.7	100.1	1330	0	0	1.0
2016 Frame	W310×143	54.8	47.9	1330	5.7	254	0.9

Strut Design							
Frame	Section	$K_x L/r_x$	$K_y L/r_y$	P_r (kN)	M_{rx} (kN m)	M_{ry} (kN m)	$\frac{P_r}{P_c} + \frac{8}{9} \left(\frac{M_{rx}}{M_{cx}} + \frac{M_{ry}}{M_{cy}} \right)$
2010 Frame	W250×67	137	63.6	663	4.8	0	0.9
2016 Frame	W250×67	137	63.6	663	4.6	4.8	1.0

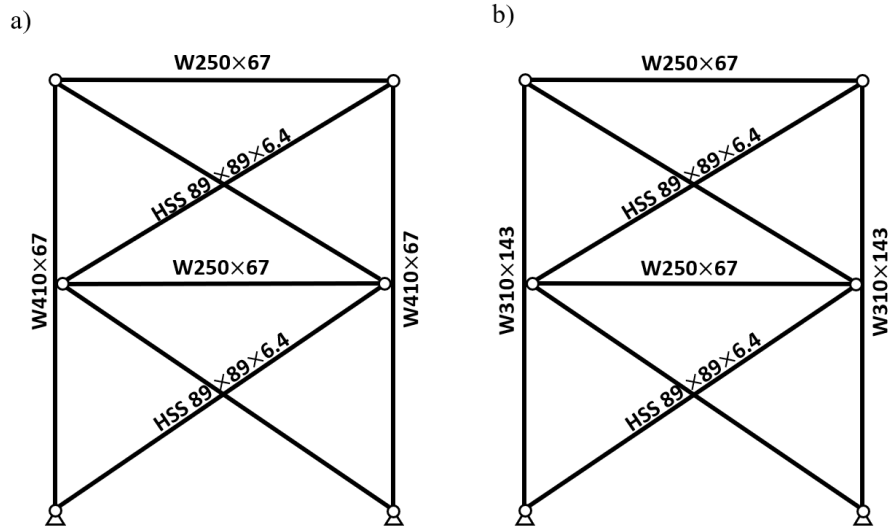


Figure 3.10: Prototype frame designed in accordance with the a) 2010 AISC Seismic Provisions; and b) 2016 AISC Seismic Provisions

Chapter 4 – Numerical Model of the Braced Frames

4.1 General

The numerical models of the prototype frames designed in Chapter 3 were constructed and analyzed using the Abaqus finite element program (Dassault Systèmes 2014) to examine the seismic behaviour of the frames, and evaluate the seismic demands induced in the frame members. The Abaqus program was chosen to conduct this examination because of its ability to efficiently simulate complex nonlinearities including material, geometry, interactions between different members, and loading. Furthermore, the program can appropriately simulate initial geometric out-of-straightness and residual stresses while capturing the local response of the frame such as local buckling, twist, and connection behaviour. This chapter presents modelling assumptions and analysis techniques used for nonlinear pushover (static) and nonlinear response history (dynamic) analyses.

4.2 Model Development

4.2.1 Element

The three-dimensional deformable quadrilateral (4-node), stress/displacement shell elements with reduced integration and a large-strain formulation shell element (S4R) were used to simulate the braces, columns, strut, connections, and roof beam of the prototype frames. The geometry and integration point of the selected element are shown in Figure 4.1. Shell elements are more computationally-efficient than other three-dimensional (solid) elements because of the lesser number of integration points; however, they provide slightly less accurate measurements

particularly across the thickness of the elements. Nonetheless, this type of element is capable of estimating displacements and strains well (Dassault Systèmes 2014) and consequently the forces and stresses of a given discretized part. Therefore, due to the large size of the model produced, three-dimensional shell elements were considered as the best option based on a mixed criterion between computational efficiency and accuracy.

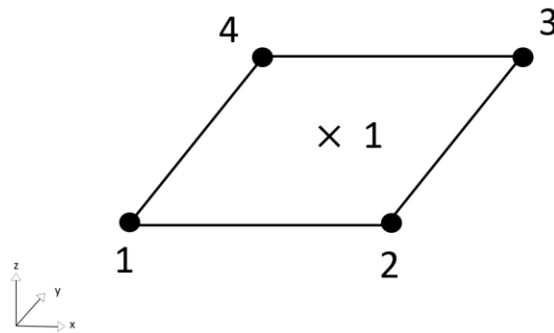


Figure 4.1: Three-dimensional 4-node general-purpose shell element with reduced integration

4.2.2 Material Properties and Plasticity Model

The elastic behaviour was simulated using Young's modulus equal to $E = 200,000$ MPa and the Poisson's ratio $\nu = 0.3$. Under seismic loading, it is expected that the braced frame members experience severe yielding and undergo large plastic deformations. Hence, a material model that could accurately simulate the cyclic inelastic behaviour of the steel material while considering the kinematic and cyclic hardening was selected.

Kinematic/isotropic plastic material model was chosen from the the Abaqus material library to simulate the inelastic response of the material. This allows to use the kinematic formulation to track the yield surface shift, and the isotropic formulations to define the uniform expansion of the yield surface. The parameters used to describe the combined hardening response of the steel

material in the Abaqus model were obtained from the calibration performed by Suzuki and Lignos (2015). Although these parameters were only calibrated for ASTM A992 steel, they were used here to describe the material properties of the other steel grades due to limited access to cyclic coupon test data. Within the Abaqus model, there are three parameters that define the kinematic/isotropic material model: yield stress at zero strain (F_y), initial kinematic hardening (C_I), and the rate at which C_I decreases (γ) with increasing plastic deformation, ε^{pl} . Figure 4.2 shows how the back stress, α , is defined using C_I and γ , and combined with the F_y to determine the envelop of the yield surface. The kinematic component of the material model was defined as $C_I = 3378$ MPa and $\gamma = 20$. A nominal yield stress $F_y = 345$ MPa was used for the beam, strut and columns made of ASTM A992 steel. The yield stress equal to 300 MPa was assigned to connection plates conforming to CSA G40.21 300W. For HSS braces selected from ASTM A1085 steel, the expected yield stress $R_y F_y = 431$ MPa where R_y is the ratio between the measure and nominal yield stresses ($R_y = 1.25$ as per the 2016 AISC Seismic Provisions) was used.

Cyclic hardening of steel was defined using the maximum change in the size of the yield surface Q_∞ and the rate at which the yield surface changes with plastic deformation b , as shown in Figure 4.2. The cyclic hardening parameters equal to $Q_\infty = 90$ MPa and $b = 12$ were used.

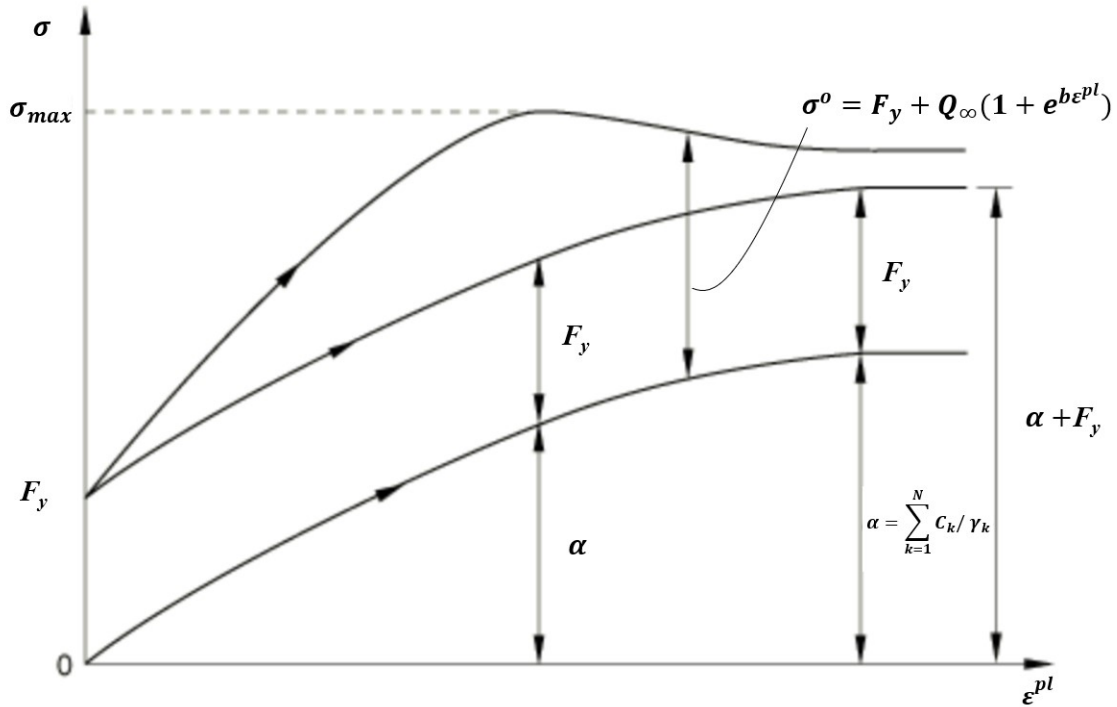


Figure 4.2: One-dimensional representation of the hardening in the nonlinear isotropic/kinematic model (Adopted from Dassault Systèmes 2014)

4.2.3 Mesh analysis and calibration

An independent model was constructed using a 4.5 m long isolated HSS127×127×7.9 member to determine an appropriate size of the shell elements and ensure that brace flexural plastic hinging and local buckling can be reproduced using the selected brace elements upon global buckling (Figure 4.3). Then, the analysis results were compared against experimental data conducted by Jiang (2012). This calibration was beneficial not only to determine an appropriate size of mesh but also to validate the use of the parameters obtained from Suzuki and Lignos (2015) used to define the plastic material model for the brace.

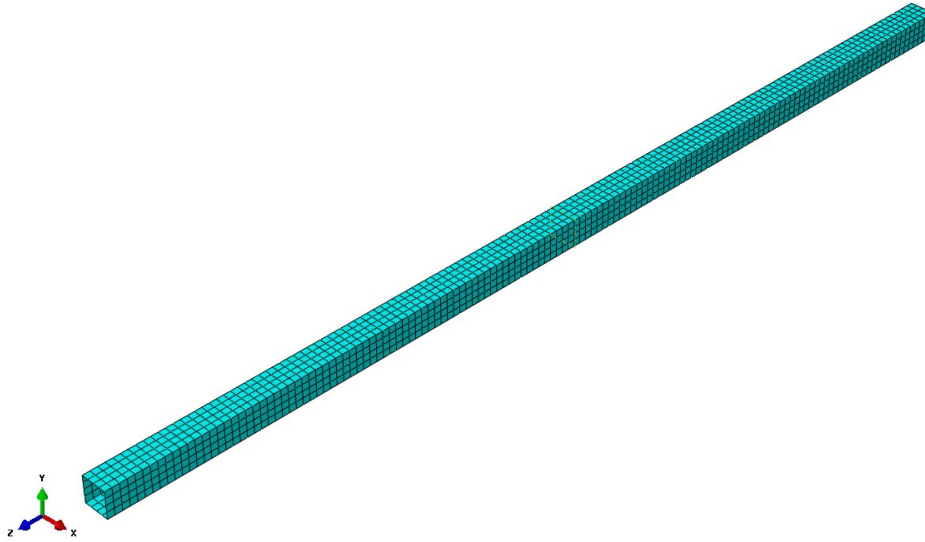


Figure 4.3: Finite element model of the isolated HSS 127×127×7.9 member

Five mesh sizes were studied using the isolated brace model as shown in Fig. 4.4: a single element, two elements, four elements, eight elements, and twelve elements across the width of the section.

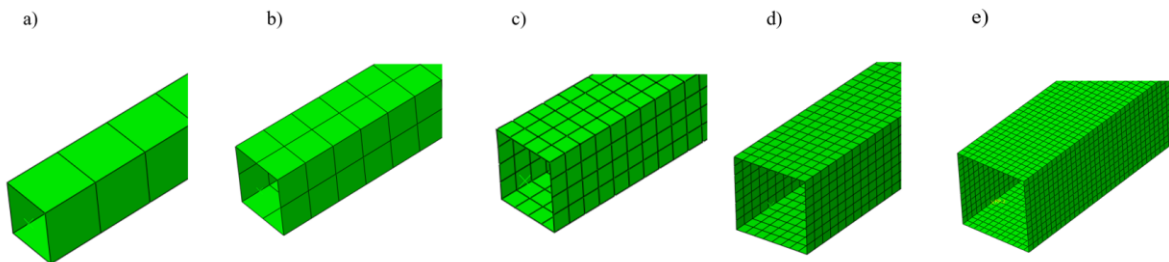


Figure 4.4: HSS brace mesh across the section wall with various divisions a) one shell element; b) two shell elements; c) four shell elements; d) eight shell elements; e) and twelve shell elements

The hysteretic response from the finite element analysis was compared against the test data, as shown in Figure 4.5. As shown, a good agreement was obtained between the experimental results and numerical prediction. A slightly higher compressive capacity by the numerical model can be

attributed to the fact that residual stresses were neglected in the numerical model and since the global slenderness ratio ($KL/r = 93$) of the selected brace falls under inelastic buckling range it is expected that residual stresses reduce the buckling load.

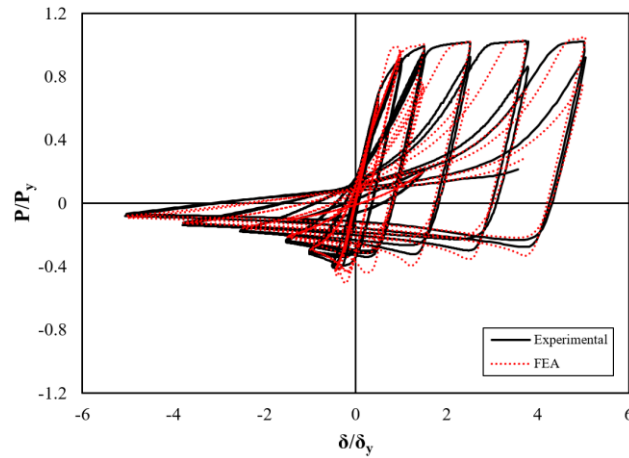


Figure 4.5: Axial force–axial deformation response of the HSS127×127×7.9 brace under incremental cyclic loading (test data by Jiang 2012)

Then, the lateral displacement of the member at buckling was obtained to study the computational efficiency and convergence rate of the finite element model. It can be observed in Figure 4.6 that the lateral displacement at buckling tends to converge when using more than four elements across the width of the section. Additionally, a higher number of elements allows for better prediction of local buckling.

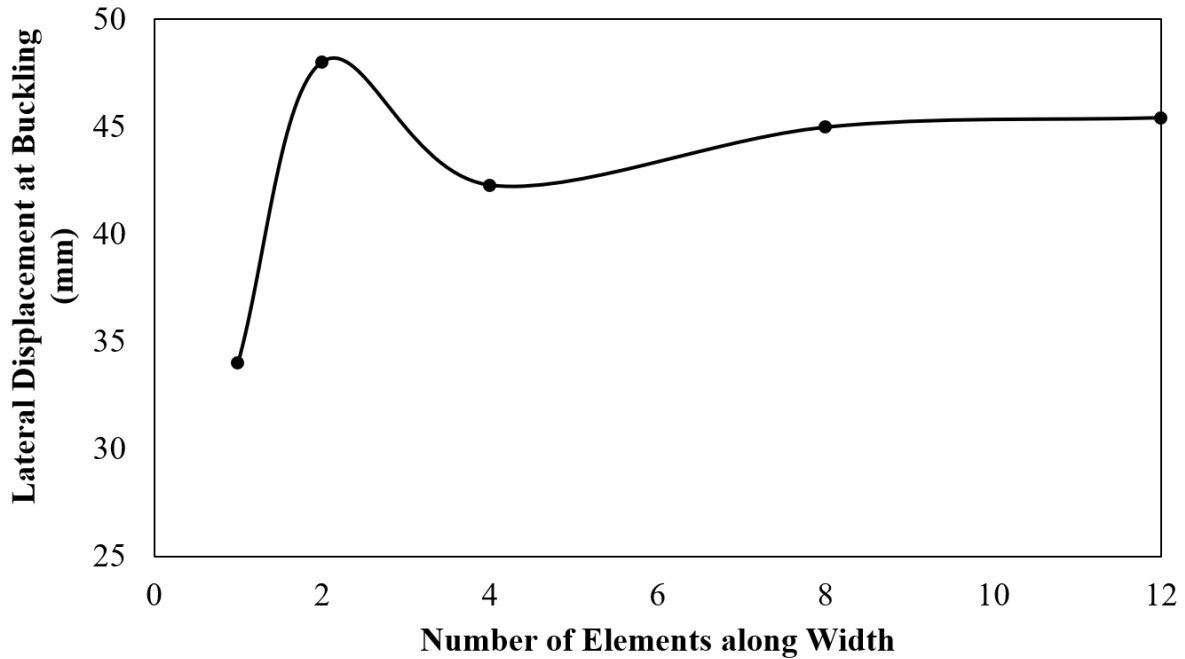


Figure 4.6: Lateral displacement at buckling using different mesh size elements

A flexural plastic hinge and a local buckling were properly captured in the analysis when using four elements across the width of the section, as shown in Figure 4.7.

As shown in Figure 4.8, a finer mesh density (approximately 25 mm square mesh) was used around the connections to better capture the interaction between members and resulting complex stress state at connection plates and parts of the members adjacent to the connections. The remaining parts of the columns, strut, and beam were assigned coarser elements (25-30 mm in length) as shown in Figure 4.8, based on the convergence analysis performed on four W-sections by Stoakes and Fahnestock (2016).

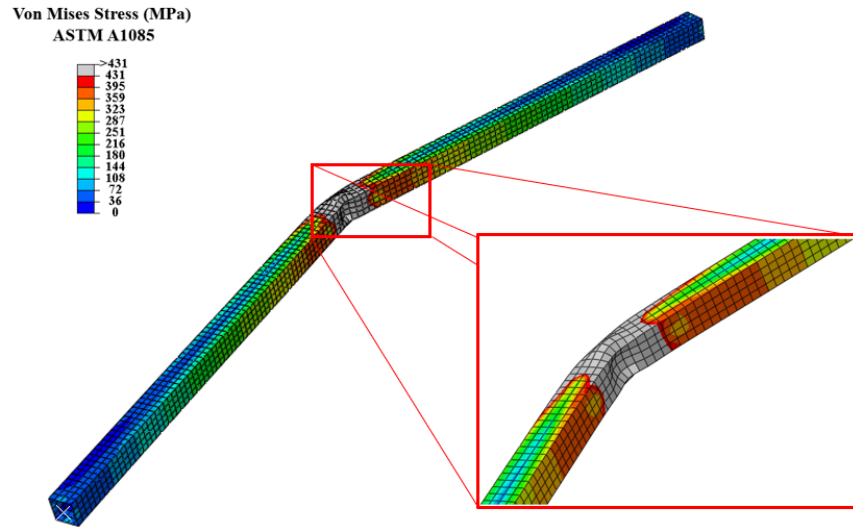


Figure 4.7: Simulation of flexural plastic hinging and local buckling of HSS127×127×7.9 $\delta = 4.5\delta_y$

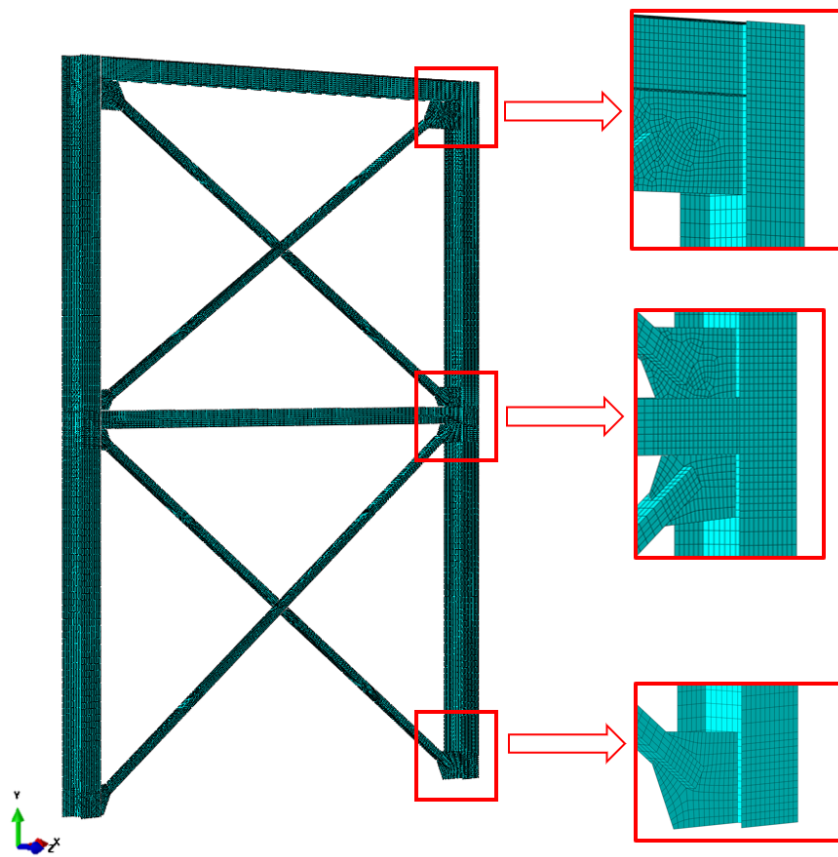


Figure 4.8: Finite element model of the steel two-tiered concentrically braced frame

4.2.4 Boundary Conditions

The base of the columns and bottom-edge of the base-gusset-plates were constrained to a reference point at the centre of the column as shown in Figure 4.9. The translational degrees-of-freedom of this reference point were fixed in all three principal directions. Also, a torsional constraint was defined at the reference point. The reference point was free to rotate in and out of the plane of the frame (UR3 and UR1) to simulate a pinned base condition. Similarly, at the top of each column, the web and flanges were constrained to a reference point at the middle of the column web. These reference points at the top of the columns were restrained from out-of-plane movement and torsional rotation. Similar to the base of the frame, the reference points at the top were free to rotate in and out of the plane of the frame to simulate a pinned-roller condition as shown in Figure 4.10.

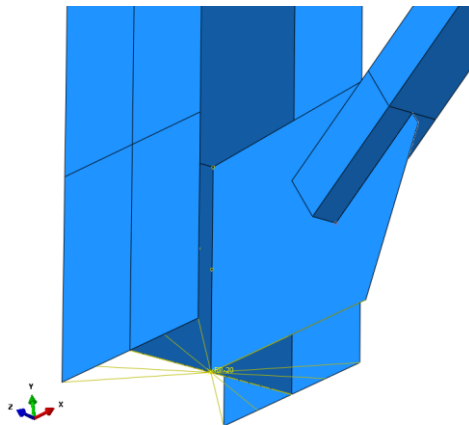


Figure 4.9: Constraint applied at the base of the frame

4.2.5 Geometric nonlinearity

4.2.5.1 P- Δ Simulation

Nonlinear analyses are load path dependent, and the results depend on the combined gravity and lateral load effects. Therefore, the vertical gravity loads acting on the entire structure, not only on

the braced frame, should be simulated in the numerical model in order to capture destabilizing $P-\Delta$ effects. As shown in Figure 4.11 a leaning column with gravity loads tributary to the gravity-load-resisting system was included in the model to represent the proportion effects of the corresponding gravity columns, which relies on the seismic-force-resisting system for lateral stability. The leaning column was linked to the braced frame at the roof level to represent in-plane rigidity of the roof diaphragm. Note that although the performance of multi-tiered braced frames can be improved by involving gravity columns in the lateral load-carrying capacity as shown by (Imanpour et al. 2016c), the effect of gravity columns in providing the lateral stiffness was not considered in this numerical analysis to portray the worst scenario possible.

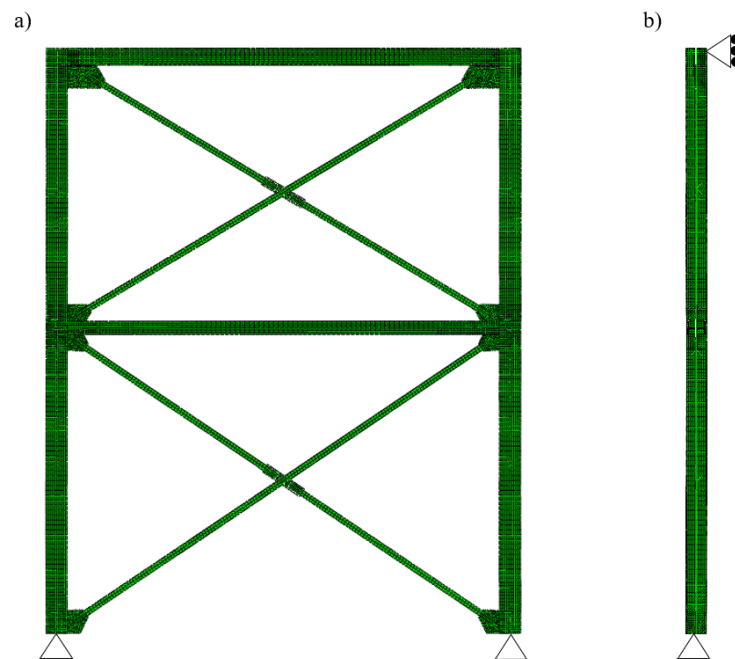


Figure 4.10: Boundary conditions assigned to the columns a) in the plane of the frame; and b) out of the plane of the frame

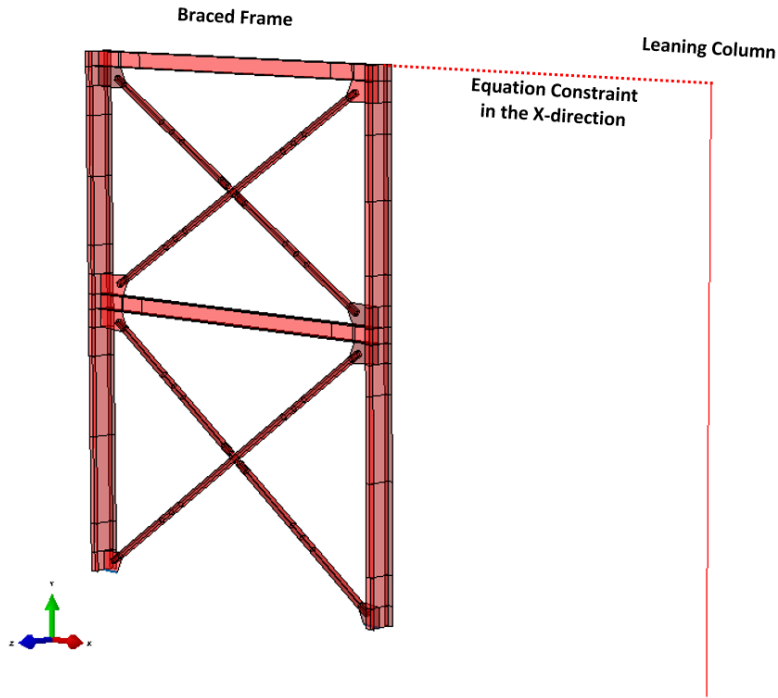


Figure 4.11: Two-tiered CBF with adjacent leaning column

A three-dimensional deformable wire element was used to simulate the leaning column. The benefit of using this element is the low computational effort required when performing nonlinear dynamic analyses. Within the model, the leaning column was pinned at the base, and the top was constrained to the top of the braced frame in the plane of the frame using an equation-constraint. The leaning column was also torsionally fixed at both ends, and its out-of-plane movement was constrained. P- Δ tributary to the braced frame was simulated by applying the braced frame tributary gravity loads on top of its columns.

4.2.5.2 P- δ Simulation

To simulate the effects of axial forces on the braces and columns, initial geometric imperfections, specifically out-of-straightness, were explicitly considered in the numerical model. Initial

geometric imperfections corresponding to the first buckling mode of the bracing members and columns, which were obtained from an Eigen buckling analysis, were assigned to these members. The amplitude of the initial imperfections was taken equal to 1/1000 times the unbraced length of the member in the direction of buckling as allowed in construction (AISC 2016c). For the columns, the total height of the frame was considered as the unbraced length in the out-of-plane direction, and the corresponding tier heights were considered as the unbraced length in the in-plane direction as shown in Figure 4.12. For the braces, 0.45 times the length of each brace was considered as the unbraced length (Wakabayashi et al. 1974; Nakashima and Wakabayashi 1992; and El-Tayem and Goel 1985; 1986; Sabelli et al. 1999) to account for the lateral support provided by the other bracing member of the tier and the restraints imposed by brace end connections. The directions of the imperfections were set to initiate the in-plane bending of the columns towards the negative X-direction in the bottom tier and towards the positive X-direction in the top tier (Figure 4.12a). The direction of the out-of-plane imperfections applied on the braces and columns were set to produce the maximum out-of-plane bending moment on the column upon brace buckling and yielding as shown in Figure 4.12b.

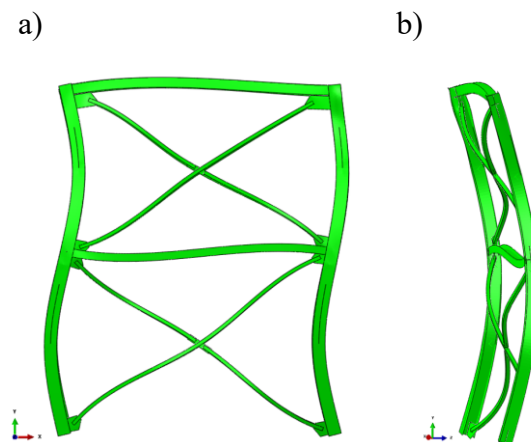


Figure 4.12: In-plane and out-of-plane initial geometric imperfections: a) CBF elevations; and b) CBF side view (deformations magnified)

4.2.6 Residual Stress

Residual stresses, which are produced due to the differential cooling of hot-rolled elements during the manufacturing process, were considered in the model. The results of the residual stress measurement for wide-flange hot-rolled shapes show that compression stresses tend to develop at the tips of the flanges, while tension-stresses are produced near the intersections of the web and flanges (Ziemian 2010). Such residual stresses can result in non-uniform yielding in wide-flange sections and cause premature yielding of parts of the cross-section and reduce the stiffness of the section (Ziemian 2010). This effect can be severe when wide-flange member bends in the weak-axis direction since the tips of the flanges have built-in compressive stresses that overlap with the compressive stresses produced by the flexural bending moment. Residual stresses were incorporated into beams and columns of the finite element model based on the pattern proposed by Galambos and Ketter (1958) as illustrated in Figure 4.13. The residual stresses developed in the HSS braces due to the cold-forming process were neglected in the model because they are deemed to have a limited influence on the brace capacities (Izvernari 2007).

4.2.7 Gravity Loading

Seismic evaluation of the CBF prototypes was carried out using two analysis steps. In the first step, the gravity load was applied at the top of the leaning and braced frame columns using the static/general procedure (Dassault Systèmes 2014). A vertical downwards load of 227 kN was applied on the braced frame columns, and a 3 MN load was applied at the top end of the leaning column, as shown in Figure 4.14. The load at the top of the leaning column is based on the dead and live load acting on one-quarter of the tributary area of the building plus the corresponding weight associated with the wall as described in Section 3.3.

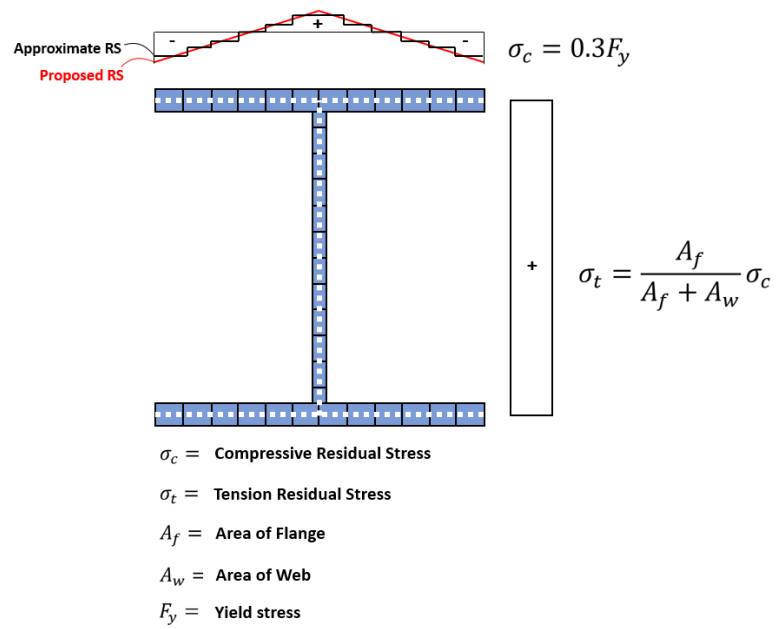


Figure 4.13: Residual stress pattern assigned to Wide-flange sections

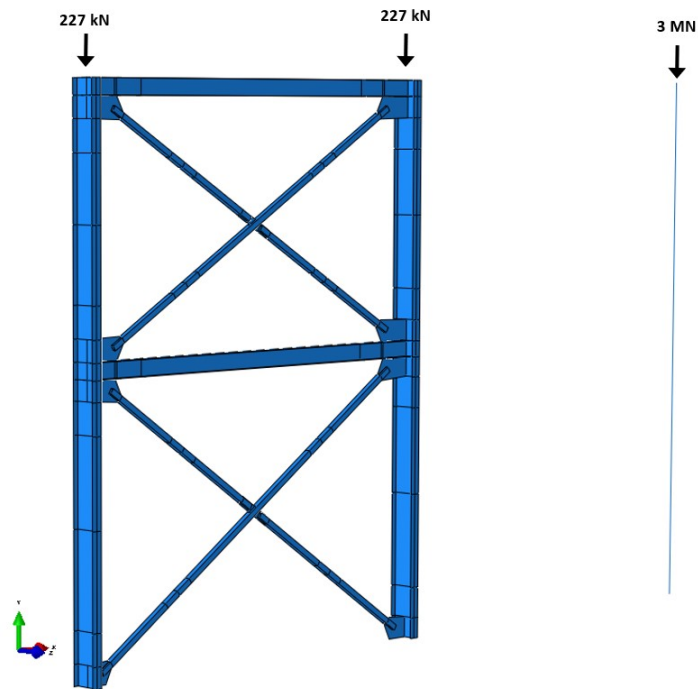


Figure 4.14: Gravity analysis step

4.3 Analysis

4.3.1 Nonlinear Static (Pushover) Analysis

Once the gravity load was applied, a cyclic horizontal displacement history shown in Figure 4.15 was applied at the roof level of the frame to simulate the seismic load effects. In Figure 4.15, Δ_{by} and Δ_{bm} are the ratios of brace yield deformation and the design storey drift, respectively. A static/general step in the Abaqus program was employed using the Full Newton solution technique to perform the pushover analysis. The horizontal displacement applied has 14 cycles based on the loading protocol proposed by Appendix K of the 2016 Seismic Provisions for experimental testing of buckling restraint braces (BRBs). The loading protocol includes two cycles at $1.0\Delta_{by}$, $0.5\Delta_{bm}$, $1.0\Delta_{bm}$, $1.5\Delta_{bm}$, $2.0\Delta_{bm}$, $3.0\Delta_{bm}$, and $4.0\Delta_{bm}$. The last 4 cycles were modified by applying higher displacement demands to ensure that the 2% tier drift limit, as permitted by 2016 AISC Seismic Provisions, was captured during the pushover analysis.

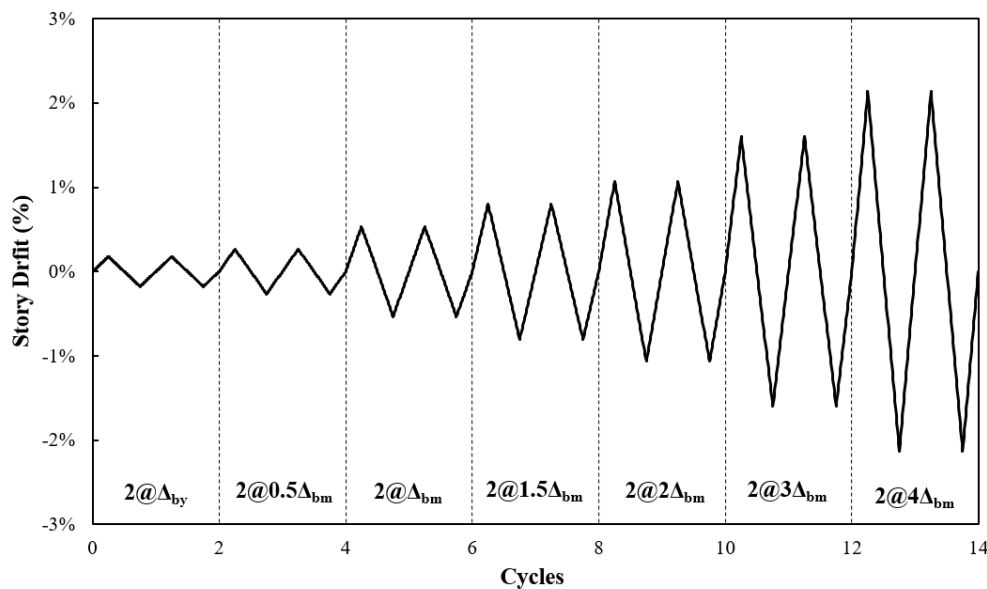


Figure 4.15: Pushover loading protocol

4.3.2 Nonlinear Response History (Dynamic) Analysis

A nonlinear response history (dynamic) analysis was used to examine the seismic response of the selected prototype braced frames. The application of such analysis is essential when evaluating the response parameters including internal forces, reactions, displacements, rotations as it leads to a realistic estimation of such parameters and provides reliable information about the seismic-induced demands used in structural design (ASCE 2017).

4.3.2.1 Ground Motion Records

Ground motion records used as input for the dynamic analysis were applied in the plane of the frame to the base of the frame and leaning column in the horizontal X-direction of the braced frame. The set of ground motions used comprises 40 historical ground motions (Table 4.1) obtained from Dehghani (2016). The ensemble contains 21 records representing interplate earthquakes (70-300 km deep), 14 records representing crustal earthquakes (0-300 km), and 5 records representing in-slab earthquakes (300-700 km). The horizontal component of selected records was selected and scaled using the method proposed by Dehghani and Tremblay (2016) to match, on average, the code-prescribed MCE_R response spectra as given in ASCE 7 at the fundamental period of the braced frame.

4.3.2.2 Analysis method

The 'Dynamic, implicit' procedure was selected to conduct the analysis. This analysis uses the Hilbert-Hughes-Taylor implicit time integration method with parameter $\alpha = -0.05$ to solve the differential equations, where the Full Newton technique is implemented to solve the nonlinear dynamic equilibrium (Dassault Systèmes 2014). The initial step was set to 0.01 and the minimum step increment was set to 2E-15.

Table 4.1: Selected ground motions for dynamic analysis (Dehghani 2016)

Source	ID	Event	Magnitude	Date	Recorded Station
Interface	SCI1	Japan, Tokachi-Oki	8.0	9/26/2003	HKD054
	SCI2	Japan, Tokachi-Oki	8.0	9/26/2003	HKD093
	SCI3	Japan, Tohoku	8.0	3/11/2011	IWTH24
	SCI4	Japan, Tohoku	8.0	3/11/2011	MYGH06
	SCI5	Japan, Tohoku	8.0	3/11/2011	MYGH08
	SCI6	Japan, Tohoku	8.0	3/11/2011	FKS011
	SCI7	Japan, Tohoku	8.0	3/11/2011	MYG009
	SCI8	Japan, Tokachi-Oki	8.0	9/26/2003	TKCH01
	SCI9	Japan, Tokachi-Oki	8.0	9/26/2003	TKCH02
	SCI10	Japan, Tokachi-Oki	8.0	9/26/2003	HKD095
	SCI11	Japan, Tokachi-Oki	8.0	9/26/2003	HKD107
	SCI12	Japan, Tokachi-Oki	8.0	9/26/2003	HKD129
	SCI13	Japan, Tohoku	8.0	3/11/2011	MYGH09
	SCI14	Chile, Iquique	8.1	4/1/2014	PB09
	SCI15	Mexico, Michoacan	8.0	9/19/1985	SUCHC
	SCI16	Southern Peru	8.4	6/23/2001	Arica Cementerio
	SCI17	Peru, Pisco	8.0	8/15/2007	CAL001
	SCI18	Chile, Maule	8.8	2/27/2010	LACHb
	SCI19	Chile, Maule	8.8	2/27/2010	SJCHb
	SCI20	Peru, Pisco	8.0	8/15/2007	LIM003
	SCI21	Southern Peru	8.4	6/23/2001	POCONCHILE
Crustal	SCC1	Irpinia, Italy-01	6.9	11/23/1980	Bagnoli Irpinio
	SCC2	Cape Mendocino	7.0	4/25/1992	Petrolia
	SCC3	Kobe, Japan	6.9	1/16/1995	KJMA
	SCC4	Kobe, Japan	6.9	1/16/1995	Takarazuka
	SCC5	Darfield, New Zealand	7.0	9/3/2010	HORC
	SCC6	Landers	7.3	6/28/1992	Lucerne
	SCC7	El Mayor-Cucapah	7.2	4/4/2010	El Centro Array #12
	SCC8	Northridge-01	6.7	1/17/1994	Sylmar - Converter Sta East
	SCC9	Northridge-01	6.7	1/17/1994	Sylmar - Olive View Med FF
	SCC10	Morgan Hill	6.2	4/24/1984	Coyote Lake Dam - Southwest Abutment
	SCC11	Loma Prieta	6.9	10/18/1989	Gilroy - Historic Bldg.
	SCC12	Loma Prieta	6.9	10/18/1989	Saratoga - W Valley Coll.
	SCC13	Montenegro, Yugo.	7.1	4/15/1979	Bar-Skupstina Opstine
	SCC14	Northridge-01	6.7	1/17/1994	Pacoima Kagel Canyon
Deep	SCD1	Olympia, WA	6.8	4/13/1949	Olympia Hwy Test Lab
	SCD2	Nisqually, WA	6.8	2/28/2001	Shelton Fire Station
	SCD3	Olympia, WA	6.7	4/29/1965	Seattle Federal Building
	SCD4	El Salvador	7.6	1/13/2001	Ciudadela Don Bosco
	SCD5	Nisqually, WA	6.8	2/28/2001	West Seattle Fire Station

4.3.2.3 Inertia Masses

Inertial forces developed at the roof level were reproduced using two point-masses at the top end of the braced frame column as shown in Figure 4.16. The masses represent the weight equal to one-eighth of the total building seismic weight, which equals to 97.13 tonnes (as calculated in section 3.3 of Chapter 3) carried by the braced frame.

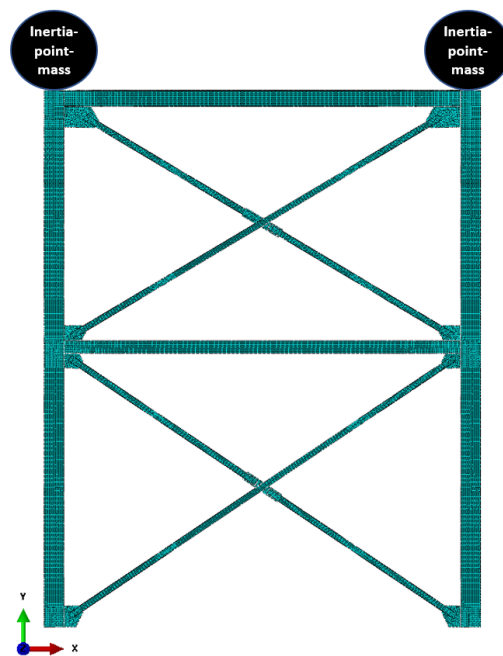


Figure 4.16: Inertia point masses assigned to the braced frame model

The mass corresponding to the self-weight of the braces was modelled using two approaches: 1) mass corresponding to the self-weight was assigned to the brace components; and 2) only 0.1% of the mass corresponding to the self-weight is considered. The results of the dynamic analysis obtained from the first modelling approach showed that the maximum compression capacity of the brace did not appropriately match the expected buckling capacity, C_{exp} . It was found that dynamic

buckling can produce higher buckling load as a result of overshoot effects, which can also delay brace buckling as confirmed by Kazemzadeh Azad et al. (2017). Although this effect may be representative of what a brace might experience during an earthquake, the variation of the dynamic characteristics of ground motions including natural period, input energy, frequency content and duration can substantially change the overshoot effects resulting in a significant variation in the response parameters used to evaluate the frames herein. The overshoot effect was diminished by reducing the density of the braces from its standard value to 0.1% of the regular density. Figure 4.17 shows an example of the hysteretic response of a continuous brace in the 2016 design under a ground motion record with 100% and 0.1% mass assigned to the frame components.

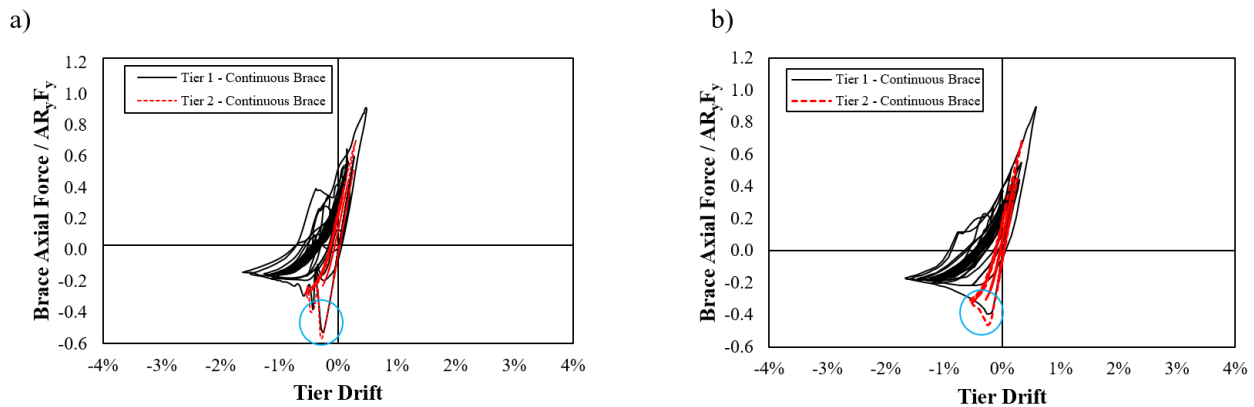


Figure 4.17: HSS 89×89×6.4 brace hysteretic response under 1980 Irpinia, Italy (SCC1) ground motion record using a) full density; and b) 0.1% density

Similarly, the results of NLRH analyses showed that higher mode of vibrations associated with the individual column member with a long-unbraced length could significantly affect the out-of-plane moment demands induced in the columns. The long-unbraced length of the column in the out-of-plane direction can amplify the local dynamic response of the member (e.g. out-of-plane bending moment) under dynamic loading. As discussed earlier, two modelling approaches were

examined to evaluate the effects of the local vibration modes. Figure 4.18 compares the response of the 2016 frame under the 1980 Irpinia, Italy (SCC1) ground motion record when 1) the column mass is fully considered, and 2) when the columns are modelled using only 0.1% of their full density. As shown, the effects of higher vibration modes were minimized when using the smaller density.

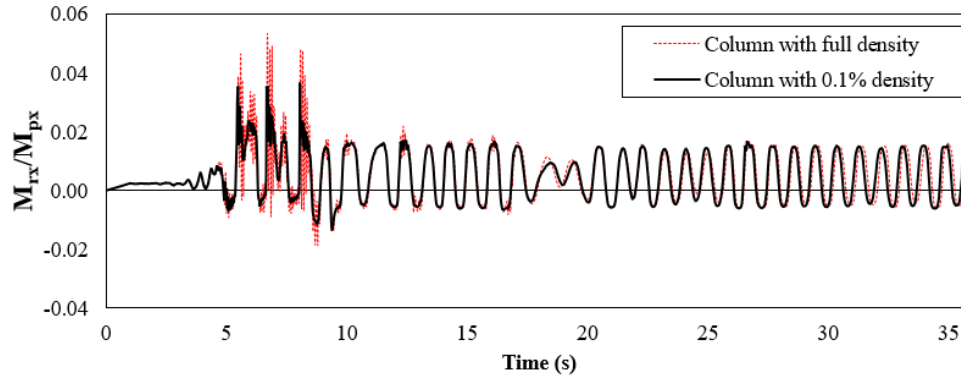


Figure 4.18: Influence of column density on the out-of-plane moment under the 1980 Irpinia, Italy (SCC1) ground motion record

4.3.2.3 Damping

Rayleigh's damping was used to determine the classical damping matrix as defined in the equation of motion to generate the internal damping forces, which cause the attenuation of the frame movement under dynamic loading. Rayleigh's damping is described as $\mathbf{c} = \alpha \mathbf{m} + \beta \mathbf{k}$, where \mathbf{m} and \mathbf{k} are mass and stiffness matrices, respectively. α and β are the mass- and stiffness-proportional damping coefficients, respectively (Chopra 2011). To obtain these coefficients, an Eigen-buckling analysis was performed to calculate the frame natural frequencies. Subsequently, the first two natural frequencies, $\omega_i = 13.4$ rad/s and $\omega_j = 55.04$ rad/s, were used in combination with the critical damping ratio $\zeta = 2\%$, in Equations 4.1 and 4.2 to determine the damping coefficients $\alpha = 0.43$ and $\beta = 0.00058$. These coefficients were finally introduced in the finite element model.

$$\alpha = \zeta \frac{2\omega_i\omega_j}{\omega_i+\omega_j} \quad (4.1)$$

$$\beta = \zeta \frac{2}{\omega_i+\omega_j} \quad (4.2)$$

Chapter 5 – Seismic Response of Two-Tiered Steel Concentrically Braced Frames

5.1 General

The seismic response of the prototype two-tiered concentrically braced frames was evaluated using the pushover and nonlinear response history (NLRH) analyses. The global response of the frames including the lateral force, storey drift and tier drifts is first presented. Then, the seismic-induced demands including the column and brace forces are discussed.

5.2 Pushover Analysis

Pushover analysis is a static analysis with a nonlinear material definition where the roof displacement is incrementally increased up to a target displacement under a given displacement pattern. This analysis was used to simulate the lateral response of the frame and its components. The displacement scheme applied was based on the protocol proposed by Appendix K of the 2016 Seismic Provision (AISC 2016a) for the experimental testing of buckling restraint braces. A full description of the displacement scheme is presented in Section 4.3.1.

The static loading scheme was applied to the frame designed using the 2010 AISC Seismic Provisions, hereafter referred to as 2010 design, and the frame designed in accordance with the 2016 Seismic Provisions, hereafter referred to as the 2016 design.

5.2.1 Frame Global Response

Figure 5.1 shows the lateral response of 2010 and 2016 designs. For the 2010 design, a stable response with an increased lateral load was observed up to a storey drift equal to 2.0%, at which column buckling occurred and analysis was halted because of a convergence issue. As shown in

Figure 5.2a column buckling was observed in the right-hand-side (RHS) column. In contrast, the 2016 design was able to complete the cyclic pushover analysis without column buckling or frame instability. A stable lateral load–lateral displacement response was obtained as shown in Figure 5.1b. The 2016 frame reached a maximum lateral displacement applied corresponding to a storey drift of 2.1%. Figure 5.2 shows the frame deformed shape at 2.1% storey drift.

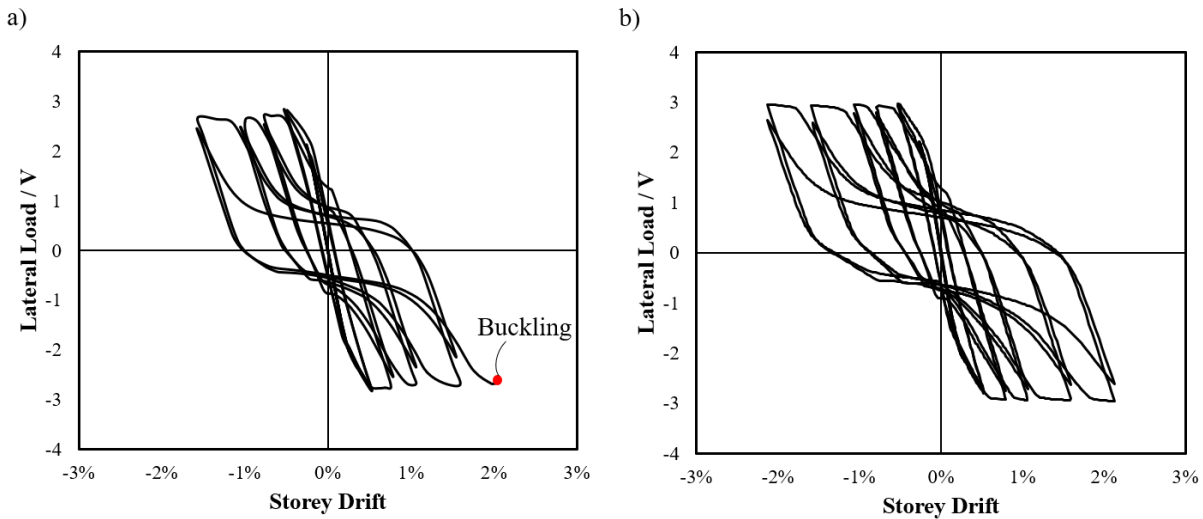


Figure 5.1: Normalized lateral load–lateral displacement response: (a) 2010 design; and (b) 2016 design, (V is the design base shear as defined in Section 3.3)

The tier drift is plotted against the storey drift in Figure 5.3a and 5.3b for the 2010 and 2016 designs, respectively. For both designs, the tier drifts in both tiers were nearly the same in the initial elastic cycles. However, under larger storey drifts, in the 2010 design, lateral frame deformation was concentrated in Tier 1 as brace tensile yielding occurred first in this tier; however, very limited lateral deformations were concentrated in Tier 2 and the braces in this tier remained relatively elastic. As a result of this response, nonlinear lateral deformations of the frame were unevenly distributed along the height of the frame as shown in Figure 5.3a. By further increasing the roof displacement, column instability occurred in the first-tier segment of the RHS column.

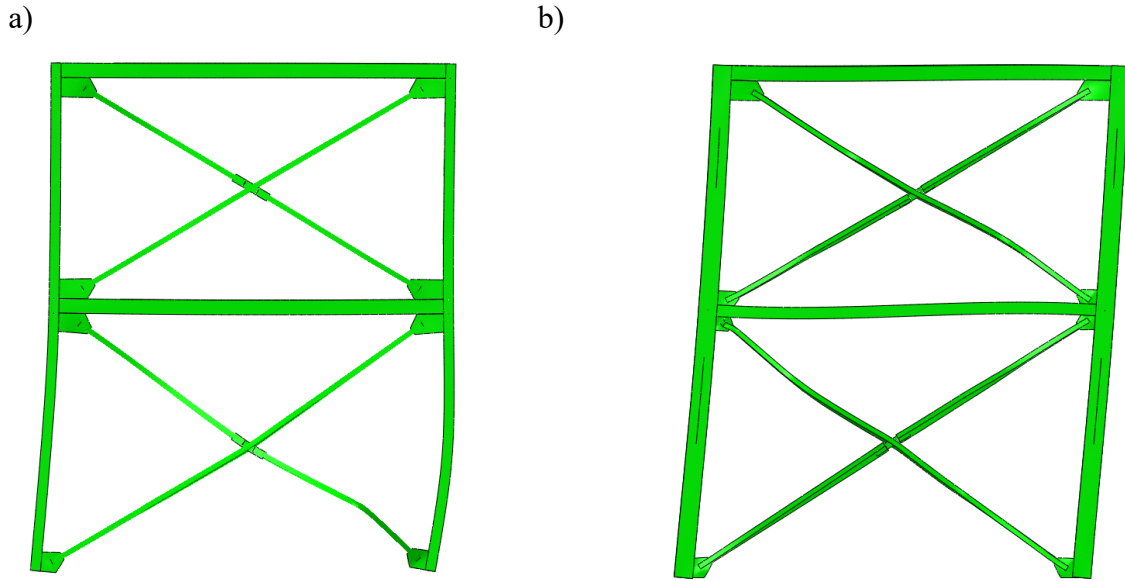


Figure 5.2: Frame deformed shape: (a) 2010 design: column buckling at story drift 2.0%; and (b) 2016 design final deformed shape at story drift 2.1%

The lateral response of the 2016 design was different compared to its 2010 counterpart. Beyond 0.5% storey drift, brace tensile yielding was observed first in Tier 1 and then in Tier 2 (noncritical tier). Although the storey shear in Tier 1 reduced as tension brace yielded and compression brace buckled at 0.5% storey drift, the columns compensated for the storey shear difference between the tiers, which led to brace tensile yielding to take place in Tier 2 at 1.0% storey drift. As a result of this response, frame lateral deformations were more uniformly distributed between the tiers. Table 5.1 compares the tier drifts at of the two designs at 2.0%—the maximum storey drift applied to the 2010 design—which highlights the improvement of the seismic behaviour of the 2016 design.

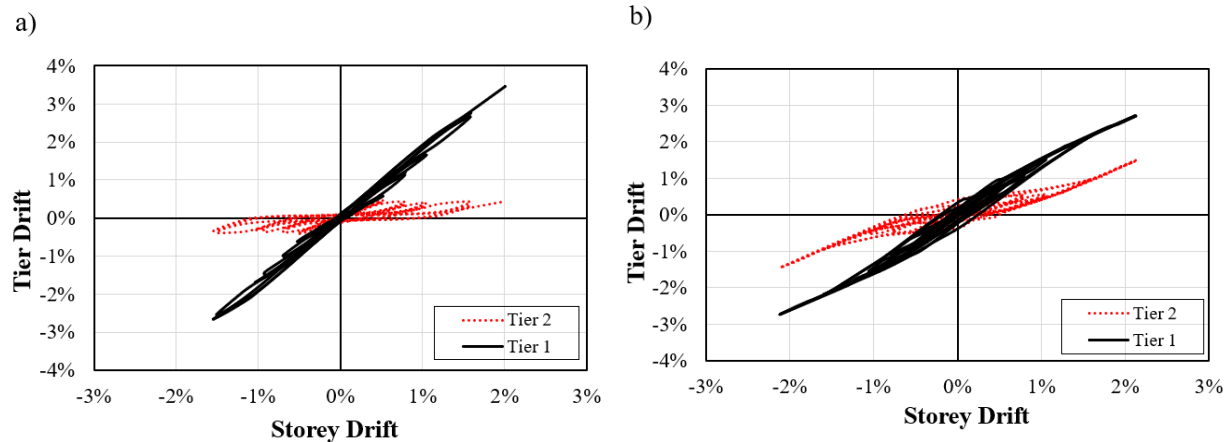


Figure 5.3: Tier drifts: a) 2010 design; and b) 2016 design

Table 5.1: Tier drifts at a storey drift 2.0%

	2010 Design	2016 Design
Tier 2 (Δ_2)	0.5%	1.3%
Tier 1 (Δ_1)	3.5%	2.6%

5.2.2 Brace Behaviour

The brace axial forces (normalized by the maximum expected tensile strength, AR_yF_y) are plotted against the tier drift in Figures 5.4 for continuous and discontinuous braces of both tiers. The buckling and tensile resistances of the braces were appropriately predicted when compared to the values calculated using the Specification (ASIC 2016b). For the 2010 design, both continuous and discontinuous braces in Tier 2 (Figure 5.4a and 5.4b) remain nearly elastic. No tension yielding occurred in Tier 2 and the compression brace force slightly degraded as a result of cyclic loading. However, severe inelastic deformations were induced in Tier 1 due to the buckling and yielding of the braces in this tier as expected. In contrast to the 2010 design, the braces in both tiers of the

2016 design contributed to the inelastic response of the frame and underwent yielding and buckling as shown in Figures 5.4c and 5.4d.

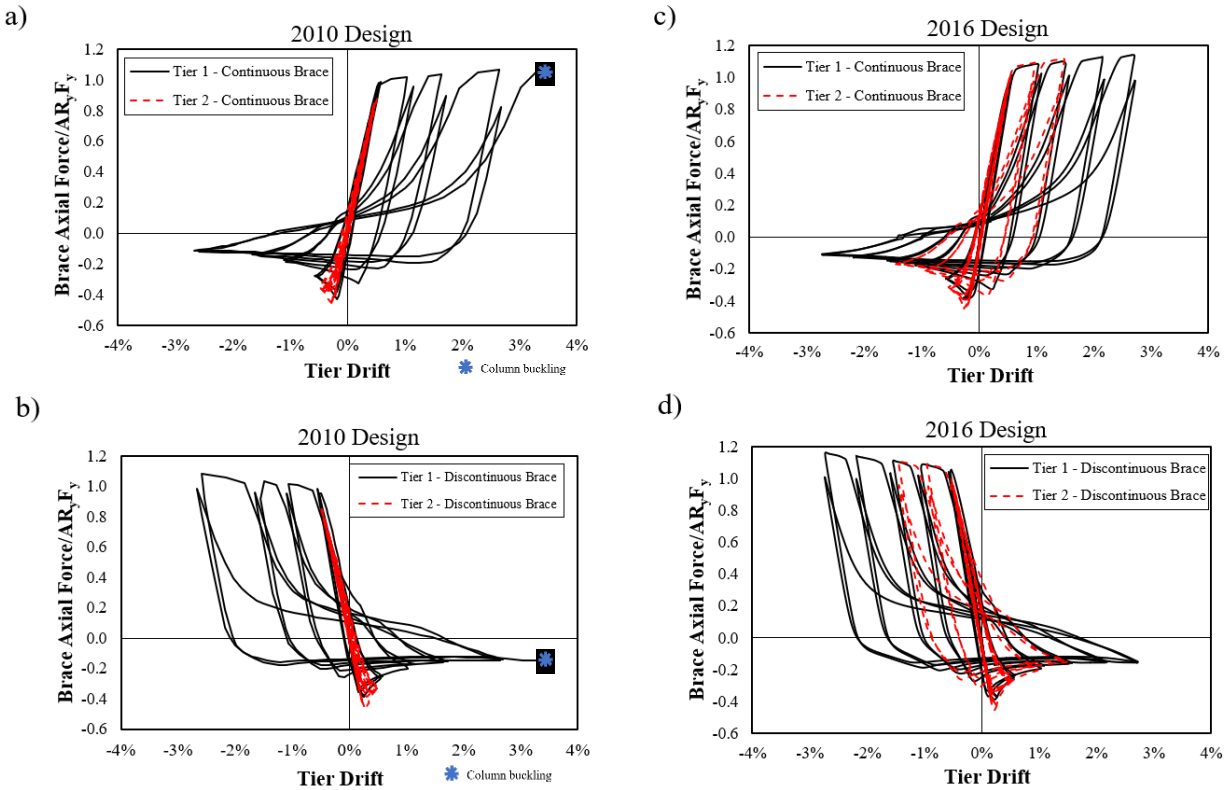


Figure 5.4: Normalized brace axial force: (a) continuous braces of the 2010 design; (b) discontinuous braces of the 2010 design; (c) continuous braces of the 2016 design; (d) discontinuous braces of the 2016 design

5.2.3 Column Behaviour

5.2.3.1 In-Plane Response

In-plane bending moment demand induced in the columns caused by the progressive yielding and buckling of braced panels was used to examine the in-plane response of the prototype frames. The bending moment was measured just below the brace-to-column connection at the strut level where the maximum in-plane moment occurs. The moments were plotted for the 2010 and 2016 designs

in Figures 5.5a and 5.5b, respectively. The moments were normalized by the plastic moment of the corresponding section about its minor axis M_{py} . Note that under positive storey drifts, the right column was axially loaded in compression; similarly, under negative storey drifts the left column was axially loaded in compression. The maximum normalized moment demand in the compression column of the 2010 and 2016 designs were 0.34 and 0.33, respectively. The larger maximum absolute value of the in-plane moment in the columns of the 2016 design, in comparison to that of the 2010 design (126 vs 28 kN-m), is caused by the higher stiffness, which attracts higher moments to compensate for the unbalanced brace storey shear force between the braced panels. Moreover, in the 2010 design, when the columns are in tension, the in-plane moment demand increases linearly; whereas when the columns are in compression, the moment rapidly decreases after the attainment of the maximum in-plane moment that corresponds to the maximum unbalanced brace storey shear force. The column moment degrades beyond the maximum value mainly because of the loss of strength in the compression column caused by the yielding of the member. The first plastic hinge formed within the first-tier segment of the compression column (Figure 5.6), which led to the reversal of the column bending moment sign as shown Figure 5.5a. However, the in-plane moment of the 2016 design columns increased proportionally with the lateral displacement until it reached a plateau (Figure 5.5b). Although the moment arising from the unbalance brace storey shear force decreased, in-plane bending moment resulting from the P- δ effect increased with enlarged storey drift, which prevented a net decrease of the in-plane moment.

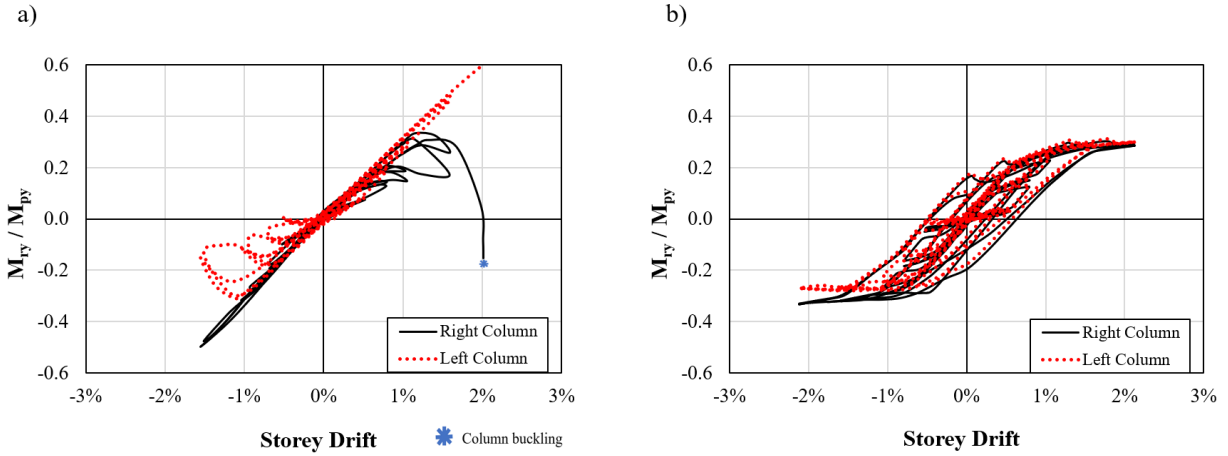


Figure 5.5: Column in-plane bending moments for a) 2010 design; and b) 2016 design

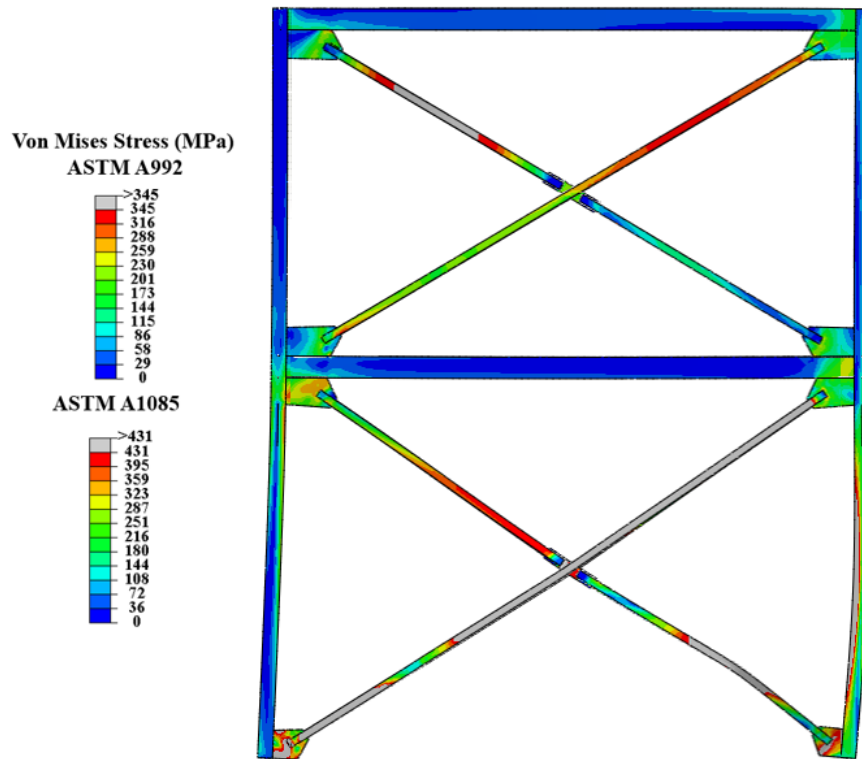


Figure 5.6: Deformed shape with Von-Mises stress contour at the verge of RHS column buckling at 2.0% storey drift

5.2.3.2 Out-of-Plane Response

Column out-of-plane bending moments were used to evaluate the response of the frame in the out-of-plane direction. Figures 5.7a and 5.7b show the column moments for 2010 and 2016 designs, respectively. The moments were measured on the column at strut-to-column connection and were normalized by the corresponding plastic section moment about the section strong axis M_{px} . The columns of the 2010 and 2016 designs experienced a maximum out-of-plane demand of 23 kN-m ($0.05M_{px}$) and 25 kN-m ($0.031M_{px}$), respectively. It was found that the maximum out-of-plane moments do not coincide with the maximum story drifts, which may be attributed to the fact that compression brace forces reduce at higher storey drifts, resulting in lower out-of-plane bending moments imposed on the columns.

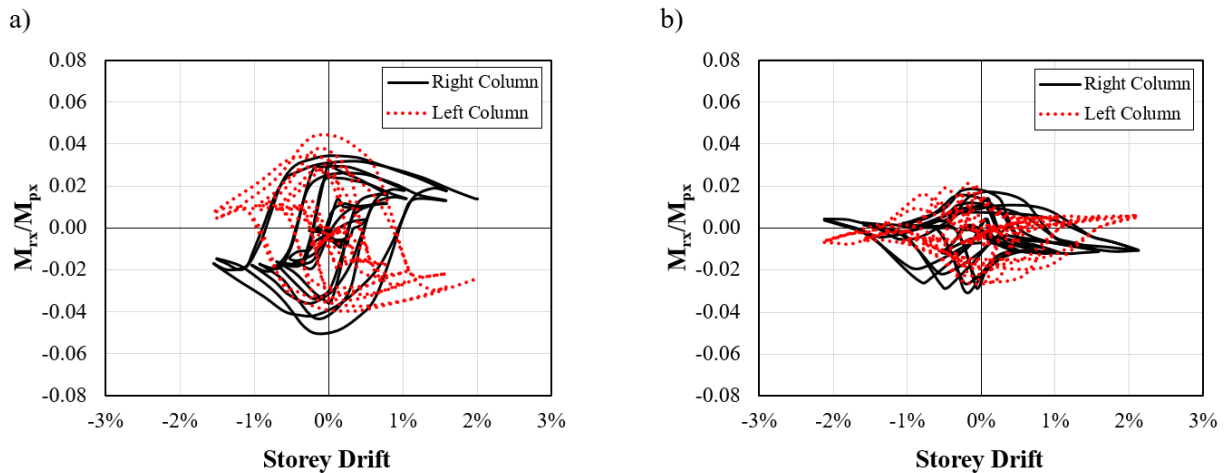


Figure 5.7: Column out-of-plane bending moments for a) the 2010 design; and b) the 2016 design

5.3 Nonlinear Response History Analysis

Nonlinear response history (NLRH) analysis was used to evaluate the dynamic response of the prototype braced frames under earthquake loads. NLRH analysis is a powerful method in

earthquake engineering that considers in detail the dynamic effects of seismic loading. This analysis method is performed by applying an acceleration record to the base of the structure (Filiatrault et al. 2013). The ground motion input used for this study contains 40 ground motions which were scaled by Dehghani (2016) to match, on average, the code-prescribed MCE_R response spectra at the fundamental period of the braced frame. Section 4.3.2 provides further information on the selected ground motions.

5.3.1 Frame Global Response

Column instability was observed for the 2010 design under 13 ground motion records. Column buckling triggered inelastic instability and led to frame collapse in all 13 cases. Figure 5.8 shows an example of the frame collapse under the 1994 Northridge (SCC14) ground motion record. Column buckling occurred under the combination of large in-plane bending moment and axial compression force demands. The in-plane flexural buckling, with a limited twist, was observed first; the instability mode then changed to out-of-plane buckling due to the lack of out-of-plane support, resulting in a flexural-torsional buckling mode.

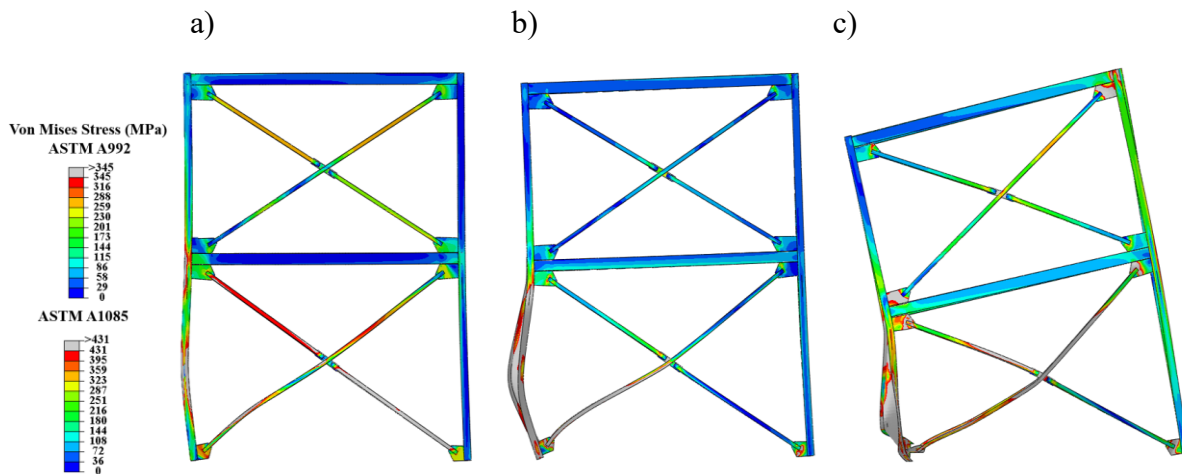


Figure 5.8: 2010 frame deformed shape under 1994 Northridge (SCC14) ground motion record: a) onset of LHS column buckling at $t = 4.70$ s and story drift of 1.7%; b) LHS column buckling at $t = 5.38$ s; and c) frame collapse at $t = 5.49$ s

The statistics of the NLRH analysis results were used to evaluate the seismic response of the prototype frames further. The maximum values of the frame storey drift and tier drifts were recorded under each ground motion. Maximum storey drifts are given in Table 5.2 and plotted in Figure 5.9a for the 2010 design. The ground motions in the horizontal axis of the plot are arranged in the order presented in Table 4.1. The squares highlighted in red are the cases where column instability occurred; additionally, the expected storey drift, $C_d\Delta_e$, as per ASCE 7 is shown. Three indicators were used to identify column buckling in the NLRH analysis:

- stiffness reduction in the axial force–axial displacement response of the column (Figure 5.10a);
- stiffness reduction in the lateral shear force–storey drift response of the frame (Figure 5.10b); and
- curvature reversal due to plastic hinge forming at two locations within the first-tier segment (Figure 5.11).

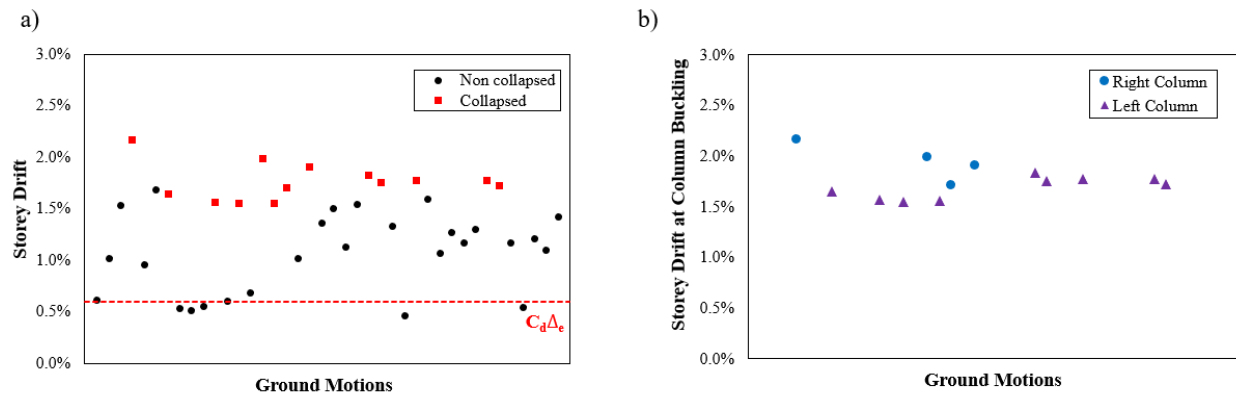


Figure 5.9: 2010 design a) maximum storey drift under 40 ground motion records; and b) storey drifts at buckling under 13 collapsed ground motion records

Table 5.2: Statistics of the global response of the 2010 design

	Ground Motion	Column Buckled / Frame Collapsed	Storey Drift, Δ	$\Delta/C_d\Delta_t$	Tier 1 Drift, Δ_1	Tier 2 Drift, Δ_2	Δ_1/Δ	Δ_2/Δ
Median*			1.1%	1.9	1.7%	0.5%	1.5	0.4
84th Percentile*			1.5%	2.5	2.4%	0.5%	1.6	0.4
Max.			2.2%	3.6	3.6%	0.6%	1.7	1.0
Min.			0.5%	0.8	0.5%	0.5%	1.0	0.2
	SCI 1	No	0.6%	1.0	0.7%	0.5%	1.2	0.9
	SCI 2	No	1.0%	1.7	1.6%	0.5%	1.6	0.5
	SCI 3	No	1.5%	2.6	2.6%	0.5%	1.7	0.3
	SCI 4	Yes	2.2%	3.6	3.6%	0.6%	1.7	0.3
	SCI 5	No	1.0%	1.6	1.5%	0.5%	1.6	0.5
	SCI 6	No	1.7%	2.8	2.9%	0.5%	1.7	0.3
	SCI 7	Yes	1.6%	2.7	2.7%	0.5%	1.6	0.3
	SCI 8	No	0.5%	0.9	0.6%	0.5%	1.1	0.9
	SCI 9	No	0.5%	0.9	0.5%	0.5%	1.0	1.0
	SCI 10	No	0.6%	0.9	0.6%	0.5%	1.1	0.9
	SCI 11	Yes	1.6%	2.6	2.6%	0.5%	1.6	0.3
	SCI 12	No	0.6%	1.0	0.8%	0.5%	1.2	0.8
	SCI 13	Yes	1.6%	2.6	2.5%	0.5%	1.6	0.3
	SCI 14	No	0.7%	1.2	0.9%	0.5%	1.4	0.7
	SCI 15	Yes	2.0%	3.3	3.4%	0.5%	1.7	0.2
	SCI 16	Yes	1.6%	2.6	2.6%	0.5%	1.6	0.3
	SCI 17	Yes	1.7%	2.9	3.0%	0.5%	1.7	0.3
	SCI 18	No	1.0%	1.7	1.6%	0.5%	1.5	0.5
	SCI 19	Yes	1.9%	3.2	3.2%	0.5%	1.7	0.3
	SCI 20	No	1.4%	2.3	2.3%	0.5%	1.7	0.3
	SCI 21	No	1.5%	2.5	2.5%	0.5%	1.6	0.3
	SCC 1	No	1.1%	1.9	1.7%	0.5%	1.5	0.4
	SCC 2	No	1.5%	2.6	2.6%	0.5%	1.7	0.3
	SCC 3	Yes	1.8%	3.1	3.1%	0.5%	1.7	0.3
	SCC 4	Yes	1.8%	2.9	3.0%	0.5%	1.7	0.3
	SCC 5	No	1.3%	2.2	2.2%	0.5%	1.6	0.4
	SCC 6	No	0.5%	0.8	0.5%	0.5%	1.0	1.0
	SCC 7	Yes	1.8%	3.0	2.9%	0.5%	1.7	0.3
	SCC 8	No	1.6%	2.7	2.6%	0.5%	1.6	0.3
	SCC 9	No	1.1%	1.8	1.6%	0.5%	1.5	0.5
	SCC 10	No	1.3%	2.1	2.0%	0.5%	1.6	0.4
	SCC 11	No	1.2%	2.0	1.9%	0.5%	1.6	0.5
	SCC 12	No	1.3%	2.2	2.0%	0.5%	1.6	0.4
	SCC 13	Yes	1.8%	3.0	3.0%	0.5%	1.7	0.3
	SCC 14	Yes	1.7%	2.9	2.8%	0.5%	1.6	0.3
	SCD 1	No	1.2%	1.9	1.9%	0.5%	1.6	0.4
	SCD 2	No	0.5%	0.9	0.6%	0.5%	1.1	0.9
	SCD 3	No	1.2%	2.0	1.9%	0.5%	1.6	0.4
	SCD 4	No	1.1%	1.8	1.7%	0.5%	1.5	0.5
	SCD 5	No	1.4%	2.4	2.3%	0.5%	1.6	0.4

*Note: Ground motions where the frame collapsed were not included in the calculation of the median or 84th percentile.

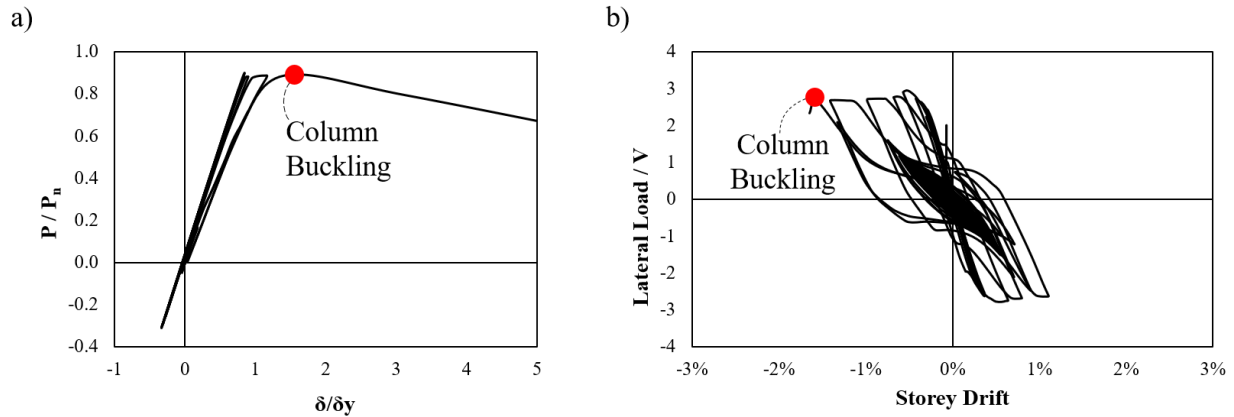


Figure 5.10: 2010 design response under 2007 Pisco, Peru (SCI7) ground motion record: a) axial force–axial displacement response of LHS column; and b) base shear–storey drift response (frame lateral shear force is normalized by the design base shear, V ; and dots represent the instant of column buckling)

The median value of the storey drift obtained from NLRH analyses is 1.1%. Note that the median, as well as the 84th percentile values, were computed based on the ground motion records where the frame did not collapse. For the 13 ground motion records where column buckling was observed, the storey drift at the onset of buckling is plotted in Figure 5.9b. As shown, the storey drifts range between 1.6% and 2.2% with an average of 1.8%. It was found that the LHS column buckled upon reaching lower storey drifts in comparison to the RHS column due to the direction of initial geometric imperfections (see Figure 4.12), which favoured the in-plane buckling of the LHS column.

The results obtained from the NLRH analysis of the 2016 design indicated that no column buckling nor inelastic instability occurred under any of the 40 ground motion records. Table 5.3 present a summary of the frame displacement response for the 2016 designs under the selected ground motion records. Figure 5.12 shows the maximum storey drift under the 40 ground motion records. The median storey drift is 1.4%, and the maximum storey drift of 2.6% occurred under the 1979

Montenegro, Yugo earthquake (SCC13). Note that the median storey drift for the 2016 frame appears higher than that of the 2010 design; however, this is because the collapsed cases are not included in the calculation of median for the 2010 design.

Table 5.3: Statistics of global response of the 2016 design

	Ground Motion	Column Buckled and Frame Collapsed	Storey Drift, Δ	$\Delta/C_d\Delta_e$	Tier 1 Drift, Δ_1	Tier 2 Drift, Δ_2	Δ_1/Δ	Δ_2/Δ
Median			1.4%	2.5	2.0%	0.7%	1.4	0.5
84th Percentile			1.9%	3.5	2.6%	1.3%	1.5	0.7
Max.			2.6%	4.7	3.3%	1.9%	1.6	1.0
Min.			0.5%	0.9	0.5%	0.5%	1.0	0.4
	SCI 1	No	0.6%	1.1	0.7%	0.5%	1.1	0.9
	SCI 2	No	1.0%	1.8	1.5%	0.5%	1.5	0.5
	SCI 3	No	1.6%	2.9	2.5%	0.8%	1.5	0.5
	SCI 4	No	2.2%	4.0	2.8%	1.5%	1.3	0.7
	SCI 5	No	1.2%	2.2	1.9%	0.5%	1.5	0.4
	SCI 6	No	1.7%	3.1	2.3%	1.1%	1.3	0.6
	SCI 7	No	1.7%	3.1	2.5%	0.9%	1.4	0.5
	SCI 8	No	0.5%	1.0	0.6%	0.5%	1.1	0.9
	SCI 9	No	0.5%	0.9	0.5%	0.5%	1.0	1.0
	SCI 10	No	0.6%	1.1	0.7%	0.5%	1.2	0.8
	SCI 11	No	1.7%	3.0	2.3%	1.0%	1.4	0.6
	SCI 12	No	0.7%	1.2	0.8%	0.5%	1.2	0.8
	SCI 13	No	1.7%	3.1	2.5%	1.0%	1.4	0.6
	SCI 14	No	0.7%	1.2	0.9%	0.5%	1.3	0.8
	SCI 15	No	1.9%	3.5	2.5%	1.4%	1.3	0.7
	SCI 16	No	1.8%	3.3	2.6%	1.0%	1.4	0.6
	SCI 17	No	2.1%	3.8	2.7%	1.4%	1.3	0.7
	SCI 18	No	1.0%	1.8	1.5%	0.5%	1.5	0.5
	SCI 19	No	1.8%	3.2	2.5%	1.1%	1.4	0.6
	SCI 20	No	1.5%	2.8	2.4%	0.7%	1.5	0.4
	SCI 21	No	1.6%	2.9	2.2%	1.0%	1.3	0.6
	SCC 1	No	1.1%	2.0	1.7%	0.6%	1.5	0.5
	SCC 2	No	1.5%	2.8	2.1%	0.9%	1.4	0.6
	SCC 3	No	2.5%	4.5	3.2%	1.7%	1.3	0.7
	SCC 4	No	1.6%	3.0	2.2%	1.0%	1.3	0.6
	SCC 5	No	1.4%	2.5	2.1%	0.6%	1.5	0.4
	SCC 6	No	0.5%	1.0	0.6%	0.5%	1.1	0.9
	SCC 7	No	2.4%	4.3	3.1%	1.7%	1.3	0.7
	SCC 8	No	1.5%	2.8	2.0%	1.0%	1.3	0.7
	SCC 9	No	1.1%	2.0	1.6%	0.6%	1.4	0.5
	SCC 10	No	1.3%	2.3	1.9%	0.6%	1.5	0.5
	SCC 11	No	1.2%	2.2	1.9%	0.6%	1.5	0.5
	SCC 12	No	1.2%	2.2	1.8%	0.6%	1.4	0.5
	SCC 13	No	2.6%	4.7	3.3%	1.9%	1.3	0.7
	SCC 14	No	2.3%	4.1	3.0%	1.5%	1.3	0.7
	SCD 1	No	1.3%	2.3	2.0%	0.6%	1.6	0.4
	SCD 2	No	0.6%	1.1	0.7%	0.5%	1.2	0.9
	SCD 3	No	1.3%	2.3	1.9%	0.6%	1.5	0.5
	SCD 4	No	1.0%	1.9	1.5%	0.6%	1.4	0.5
	SCD 5	No	1.4%	2.5	1.9%	0.9%	1.4	0.6

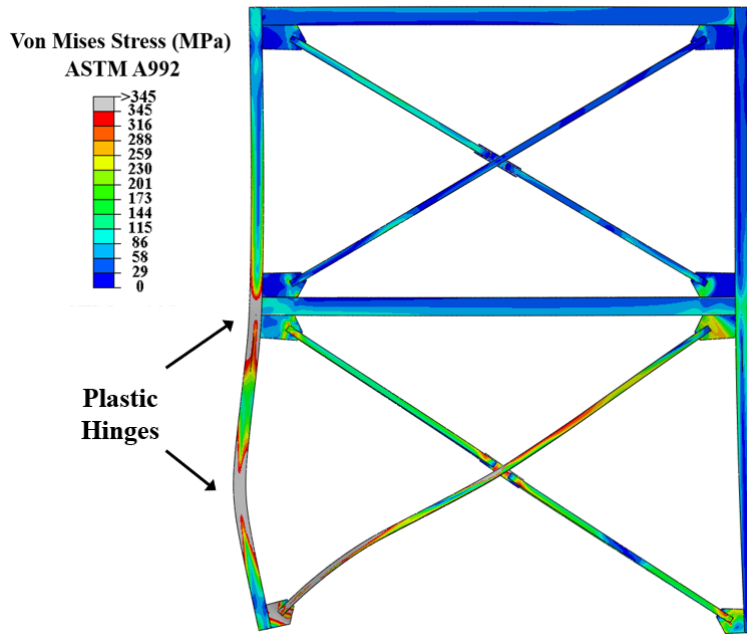


Figure 5.11: 2010 design: LHS column buckling at 34.7 s and 1.6% storey drift under 2007 Pisco, Peru (SCI7) ground motion record

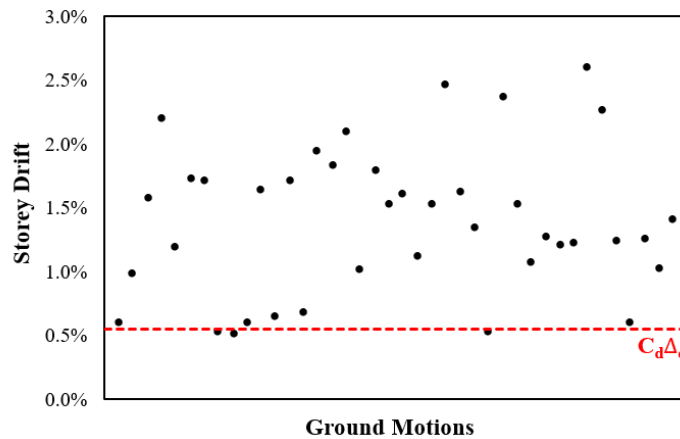


Figure 5.12: 2016 design: maximum storey drifts under the 40 ground motion records

The maximum tier drifts recorded in Tiers 1 and 2 are shown for the 2010 and 2016 designs in Figures 5.13 and 5.14, respectively. As shown in Figure 5.13 for the 2010 design, a larger tier drift was observed in Tier 1 while consistent elastic lateral deformations were obtained in Tier 2

without initiation of brace yielding under any of the ground motion records. The Tier 2 drifts were near a 0.5% tier drift, which corresponds to the lateral semi elastic deformation of the tier. The median tier drifts for the 2010 design were 1.7% and 0.5% for the first and second tier, respectively. The maximum tier drift observed before frame collapse was 3.7%, which was measured under 2011 Tohoku, Japan record (SCI4).

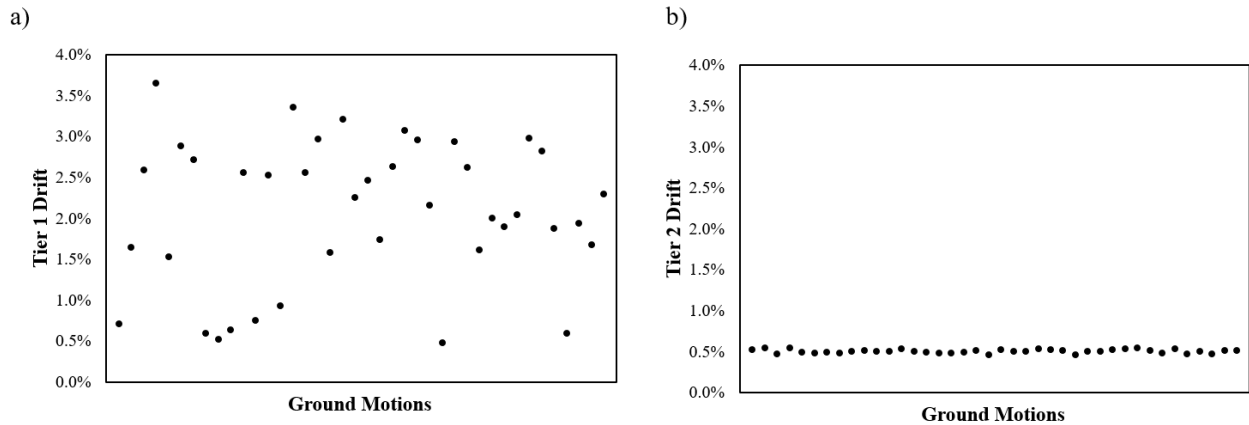


Figure 5.13: 2010 design a) Tier 1 drift; and b) Tier 2 drift

Tier drift results are plotted in Figure 5.14 for the 2016 design. As shown, frame nonlinear deformations are distributed between the tiers, although it is more pronounced in Tier 1 where brace yielding is initiated first. The results suggest that an improved seismic response is expected in the 2016 frame with larger columns compared to the 2010 design. The median tier drifts for the 2016 design were 2.0% and 0.7% for the first and second tier, respectively. The maximum value of the tier drift was observed under the 1979 Montenegro, Yugo record and was equal to 3.3%.

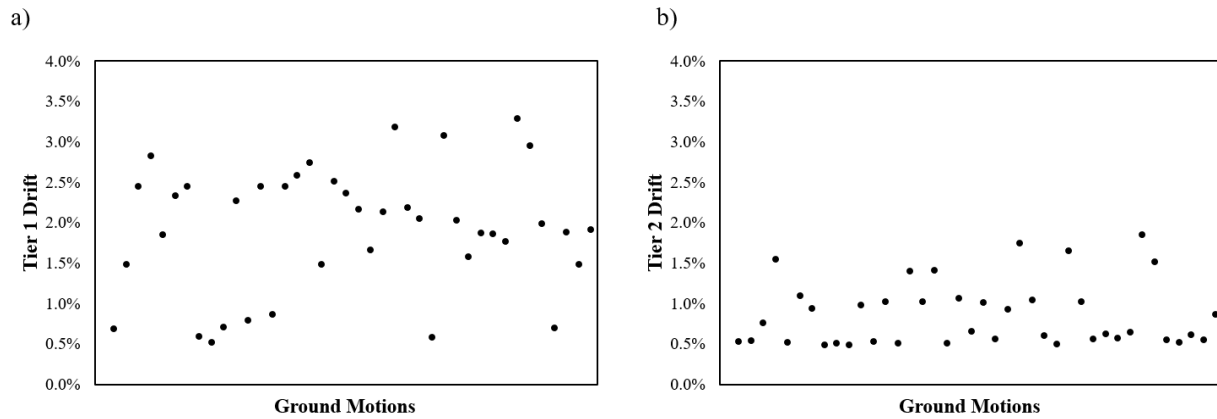


Figure 5.14: 2016 design a) Tier 1 drift; and b) Tier 2 drift

5.3.2 Brace Behaviour

Tension yielding and buckling in the braces of the 2010 design was observed under all the ground motion records. However, braces in the second tier of this frame did not yield in tension and suffered a modest degradation of their buckling strength. An example of the brace axial force–tier drift response is presented in Figure 5.15a. As shown, a larger tier drift was developed for the brace in Tier 1, while in Tier 2 limited nonlinear response was obtained in the compression region.

Braces in the first and second tier of the 2016 design buckled and yielded under the ground motions with a storey drift greater than 1.0%, which confirms the more uniform lateral response expected in the 2016 design. An example of such a response is shown in Figure 5.15b.

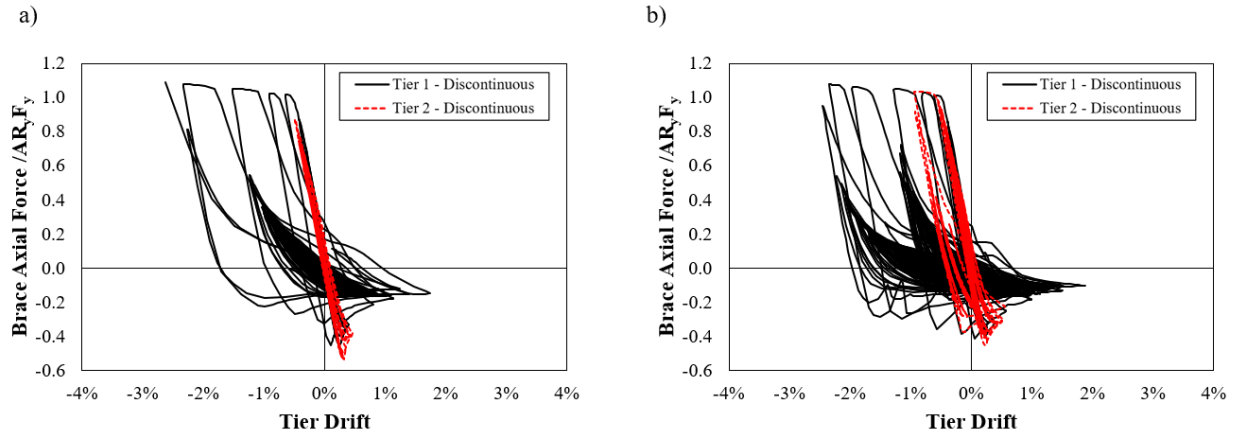


Figure 5.15: Brace axial force response in Tier 1 and Tier 2 under 2007 Pisco, Peru (SCI7) ground motion record: a) 2010 design; and b) 2016 design

Brace local buckling occurred in braces of Tier 1 of the 2010 design in several occasions including the ground motion records under which the frame collapsed (Table 5.2) and in three other ground motions (2011 Tohoku, Japan, SCI3; 2011 Tohoku, Japan, SCI6; and 2007 Pisco, Peru, SCI20) under which the frame did not collapse (Figure 5.16). Although brace fracture was not explicitly simulated in the finite element model, the occurrence of the brace local buckling together with large tier drifts observed (Figure 5.13a) suggests that brace fracture could be a limit state for the 2010 design. The results of past experimental study showed the drift where HSS brace fractures range between 2.0%–3.0% for various slenderness ratios (Tremblay et al. 2003; Yang and Mahin 2005; Uriz and Mahin 2008; Fell et al. 2009; Roeder et al. 2011; Hsiao et al. 2013). Despite the large tier drifts induced in Tier 1 of the 2016 design, local buckling was not observed under any of the ground motions.

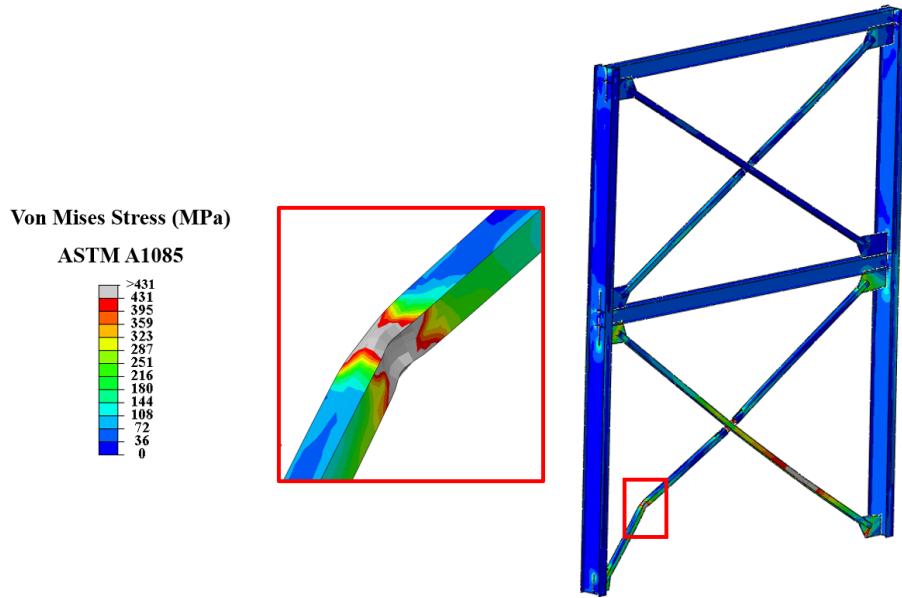


Figure 5.16: Local buckling of the first tier brace in 2010 design under 2011 Tohoku, Japan (SCI3) ground motion record at 9.7 s 1.5% storey drift and 2.6% tier drift

5.3.3 Column Behaviour

The statistics of the maximum column demands obtained from the NLRH analyses for the 2010 and 2016 designs are given in Tables 5.4 and 5.5, respectively. In each table, the bending moment demands and axial forces are presented. For the 2010 design, the axial forces were compared against the design value, and for the 2016 design, both the moment and axial force components were compared against the designed values.

Table 5.4: Statistics of column demands for 2010 design

	Ground Motion	M_{ry}/M_{py}	M_{rx}/M_{px}	P_r/P_n	$P_r/P_{r, design}$
Median		0.18	0.06	0.90	1.04
84th Percentile		0.28	0.08	0.91	1.06
Max.		0.31	0.10	0.92	1.07
Min.		0.04	0.01	0.86	1.00
	SCI 1	8%	2.7%	89%	1.03
	SCI 2	15%	0.07	90%	1.04
	SCI 3	10%	4.8%	89%	1.04
	SCI 4	30%	0.07	91%	1.06
	SCI 5	16%	4.9%	89%	1.03
	SCI 6	31%	5.7%	90%	1.04
	SCI 7	18%	5.3%	90%	1.04
	SCI 8	6%	1.8%	90%	1.04
	SCI 9	7%	1.9%	88%	1.02
	SCI 10	7%	1.7%	90%	1.04
	SCI 11	13%	4.6%	90%	1.04
	SCI 12	8%	3.0%	89%	1.04
	SCI 13	16%	4.3%	89%	1.03
	SCI 14	9%	3.5%	89%	1.04
	SCI 15	23%	9.6%	92%	1.07
	SCI 16	20%	5.7%	90%	1.05
	SCI 17	31%	5.3%	90%	1.04
	SCI 18	12%	4.4%	90%	1.04
	SCI 19	19%	4.8%	92%	1.06
	SCI 20	20%	5.1%	90%	1.04
	SCI 21	27%	8.3%	90%	1.04
	SCC 1	22%	5.7%	90%	1.04
	SCC 2	29%	8.7%	91%	1.05
	SCC 3	27%	7.5%	91%	1.06
	SCC 4	30%	8.3%	91%	1.06
	SCC 5	18%	7.2%	91%	1.06
	SCC 6	7%	2.0%	86%	1.00
	SCC 7	14%	8.2%	91%	1.06
	SCC 8	28%	7.0%	91%	1.05
	SCC 9	14%	6.5%	92%	1.07
	SCC 10	18%	8.2%	90%	1.05
	SCC 11	18%	8.4%	90%	1.05
	SCC 12	22%	6.7%	90%	1.05
	SCC 13	23%	7.5%	92%	1.06
	SCC 14	11%	2.8%	92%	1.07
	SCD 1	19%	5.9%	89%	1.04
	SCD 2	4%	1.4%	89%	1.04
	SCD 3	20%	5.5%	90%	1.04
	SCD 4	29%	4.6%	91%	1.06
	SCD 5	25%	6.9%	90%	1.05

Table 5.5: Statistics of column demands for 2016 design

Ground Motion	M_{ry}/M_{py}	$M_{ry}/M_{ry, design}$	M_{rx}/M_{px}	$M_{rx}/M_{rx, design}$	P_r/P_n	$P_r/P_{r, design}$
Median	0.30	0.46	0.04	1.63	0.26	0.99
84th Percentile	0.35	0.53	0.05	1.96	0.26	1.00
Max.	0.41	0.61	0.06	2.32	0.27	1.02
Min.	0.01	0.01	0.01	0.51	0.25	0.94
SCI 1	4%	0.06	2.4%	0.90	25%	0.95
SCI 2	25%	0.38	5.7%	2.10	25%	0.96
SCI 3	41%	0.61	3.9%	1.45	26%	0.98
SCI 4	38%	0.58	5.7%	2.12	27%	1.01
SCI 5	29%	0.44	4.7%	1.74	26%	0.97
SCI 6	33%	0.49	4.3%	1.59	26%	0.99
SCI 7	35%	0.53	5.2%	1.94	26%	1.00
SCI 8	2%	0.03	1.7%	0.64	25%	0.96
SCI 9	1%	0.01	1.4%	0.51	25%	0.94
SCI 10	5%	0.07	2.1%	0.77	25%	0.96
SCI 11	30%	0.46	5.7%	2.09	26%	1.00
SCI 12	6%	0.10	3.1%	1.16	25%	0.96
SCI 13	36%	0.55	4.7%	1.72	26%	1.00
SCI 14	8%	0.13	3.8%	1.40	25%	0.95
SCI 15	28%	0.43	4.9%	1.81	26%	0.99
SCI 16	37%	0.57	6.0%	2.21	26%	1.00
SCI 17	31%	0.47	4.1%	1.52	26%	0.99
SCI 18	24%	0.37	5.3%	1.96	26%	0.97
SCI 19	37%	0.56	5.3%	1.97	26%	1.00
SCI 20	39%	0.59	3.6%	1.34	26%	1.00
SCI 21	32%	0.49	5.3%	1.95	27%	1.00
SCC 1	26%	0.39	3.6%	1.33	26%	0.99
SCC 2	30%	0.46	4.5%	1.66	26%	1.00
SCC 3	34%	0.51	4.3%	1.60	27%	1.02
SCC 4	30%	0.45	4.7%	1.74	26%	0.99
SCC 5	31%	0.48	4.7%	1.73	26%	1.00
SCC 6	2%	0.03	1.9%	0.70	25%	0.96
SCC 7	33%	0.49	4.0%	1.50	27%	1.02
SCC 8	27%	0.41	4.1%	1.52	26%	1.00
SCC 9	23%	0.35	4.2%	1.57	26%	0.99
SCC 10	30%	0.46	4.8%	1.79	26%	1.00
SCC 11	33%	0.50	4.9%	1.82	26%	0.98
SCC 12	26%	0.39	4.2%	1.55	26%	0.99
SCC 13	34%	0.52	4.3%	1.58	27%	1.02
SCC 14	32%	0.48	5.2%	1.92	27%	1.01
SCD 1	35%	0.53	6.3%	2.32	26%	0.97
SCD 2	4%	0.06	2.8%	1.04	25%	0.96
SCD 3	31%	0.48	5.9%	2.20	26%	0.98
SCD 4	21%	0.32	4.9%	1.81	26%	0.97
SCD 5	26%	0.40	3.3%	1.22	26%	0.99

5.3.3.1 In-Plane Response

Column moment demands were recorded for each ground motion just below the brace-to-column connection. The in-plane bending moments were normalized by the corresponding plastic moment M_{py} and plotted against the storey drift for the 2010 and 2016 designs under 40 ground motions records. Appendix A provides the details of the measured response parameters including column moment demands, tier and storey drift under the ground motion records analyzed.

Figure 5.17 shows the in-plane bending moment of the column for the 2010 and 2016 designs under the 2011 Southern Peru ground motion record. Relatively insignificant moments were induced in the columns before yielding of the tension brace in the critical tier, which corresponds to 0.5% storey drift. Once the tension brace in Tier 1 yielded, the member elongated while the noncritical tier remained elastic. As a result of differential deformation between Tiers 1 and 2, an in-plane moment was imposed on the column.

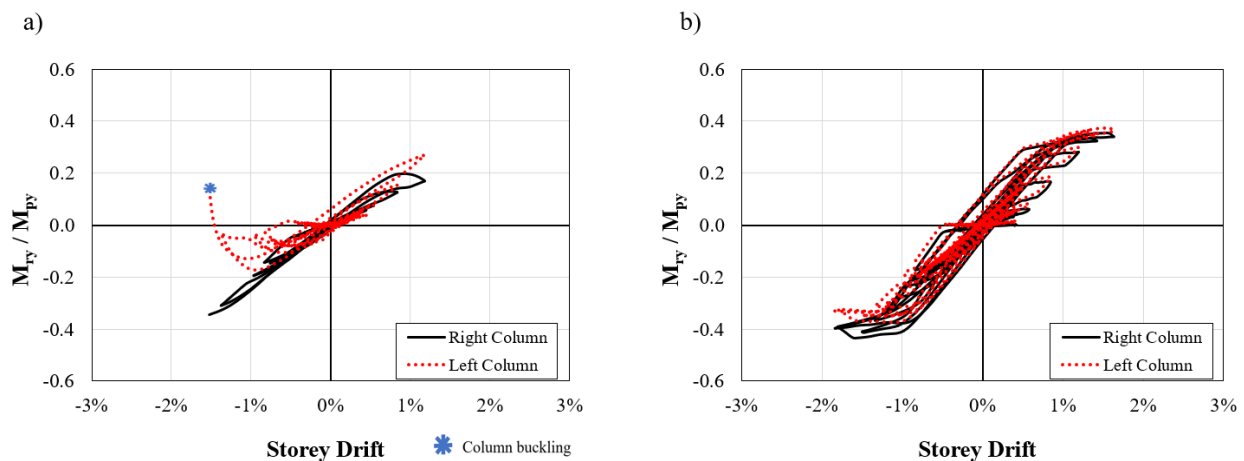


Figure 5.17: Column in-plane bending moment demand under the 2011 Southern Peru (SCI16) ground acceleration record: a) 2010 design; and b) 2016 design

The in-plane moment results for the 2010 design shown in Figure 5.17a indicates that the column loaded in compression reaches its maximum moment value and subsequently decreases as lateral

displacement was increased because the flexural stiffness of the column reduces upon large lateral displacements. The in-plane moment demand in the compression column reduced suddenly and changed sign when a plastic hinge (second plastic hinge) formed at the strut level, which led to column buckling as shown in Figure 5.11. Opposite to the compression column, the in-plane demand of the tension column increased nearly linearly as the frame was moved laterally.

In the 2010 design, the maximum flexural demand of the compression column before buckling was not consistent throughout all the ground motions. For the ground motions with multiple nonlinear cycles, the in-plane bending moment of the compression column reached higher values before column buckling. However, when the column buckled within the first cycle of the ground motion, a lower in-plane demand was observed in the columns. Figure 5.18 compares two column buckling scenarios under the 1994 Northridge and the 2001 Southern Peru ground motion records. The former is presented in Figure 5.18a, and Figure 5.18b shows the latter. Under 1994 Northridge ground motion record, the maximum moment before column buckling was $0.11M_{py}$; however, a higher moment of $0.17M_{py}$ was recorded in the LHS column under 2001 Southern Peru ground motion. This behaviour is due to the degradation of compression force in the bracing members after multiple cycles, which results in lower compression forces in the columns and in turn, allows for higher in-plane moments to develop prior to column buckling.

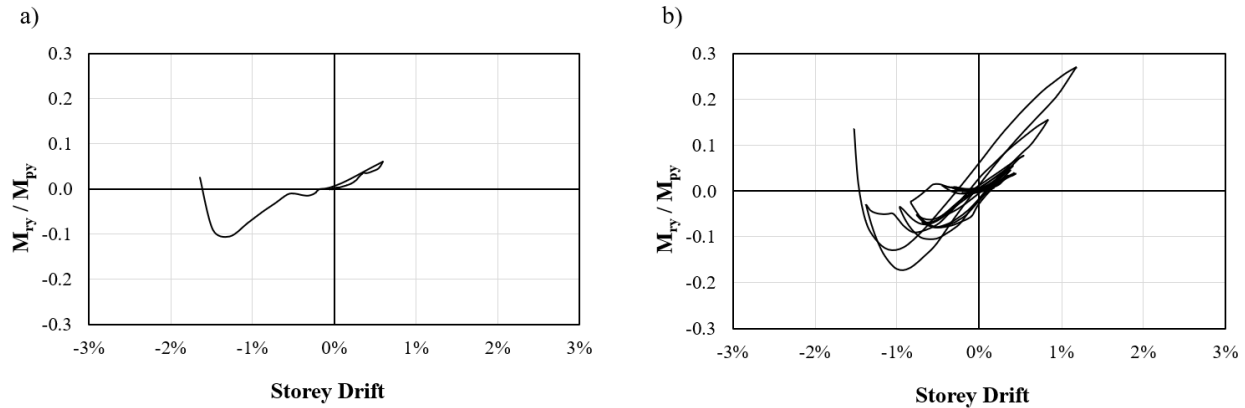


Figure 5.18: Column in-plane bending moments for the LHS column under a) the 1994 Northridge (SCC14) ground motion record; and b) the 2001 Southern Peru (SCI16) ground motion record

In-plane flexural demands on the columns of the 2016 design obtained from the NLRH analysis was consistent with the results obtained from the pushover analysis in Section 5.2. The in-plane moment increases steeply as the unbalanced brace storey shear force develops due to the inelastic brace response (Figure 5.17b). This increase was not pronounced when the frame reached storey drifts greater than 1.0% as the moment caused the unbalance braces storey shear force decreased. The maximum in-plane flexural demands observed under the 40 ground motion records are provided in Figure 5.19. The red-dashed line represents the design in-plane moment M_{ry} in accordance with the 2016 AISC Seismic Provisions. The maximum in-plane moment measured on a braced frame column was $0.41M_{ry}$, and the median was $0.30M_{ry}$.

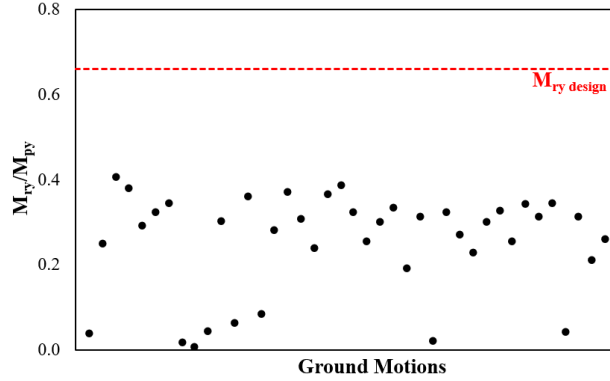


Figure 5.19: Column in-plane bending moments for 2016 design

5.3.3.2 Out-of-Plane Response

The out-of-plane response of the frame was examined using the bending moment demands induced in the columns of the prototype frames obtained from the NLRH analyses. The out-of-plane moments under to the selected ground motion records are shown in Figures 5.20a and 5.20b for the 2010 and 2016 designs, respectively. The median moment was $0.05M_{px}$ and $0.044M_{px}$ for the 2010 and 2016 designs, respectively, where M_{px} is the strong-axis plastic moment of the corresponding column. The out-of-plane moments observed for the 2016 frame exceeded the design out-of-plane moment as per the 2016 AISC Seismic Provisions, $M_{rx} = 0.007M_{px}$, in all 40 cases.

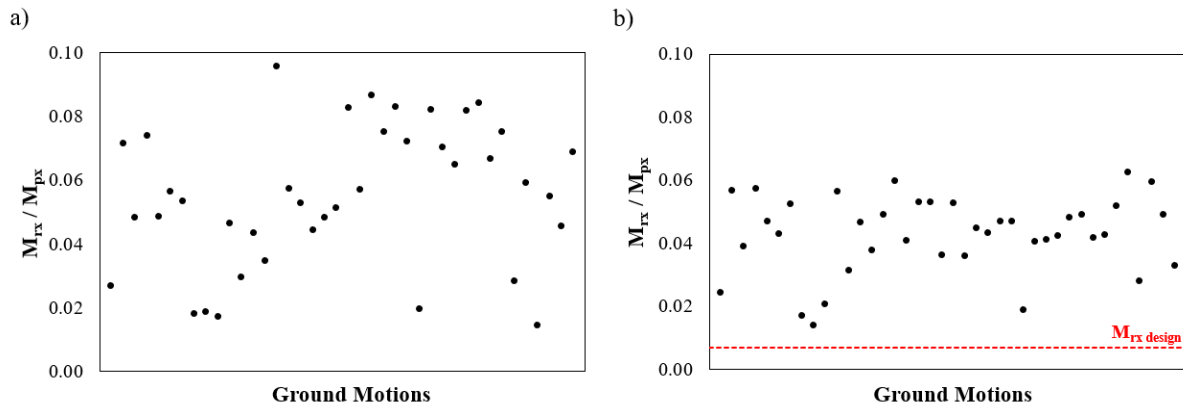


Figure 5.20: Column out-of-plane bending moments for a) 2010 design; and b) 2016 design

The out-of-plane moment was investigated further by differentiating the contributing components including (tension and compression) brace forces, strut forces, gusset plate plastic moments, and $P-\delta$ effects. Once a brace buckles out-of-plane, a portion the compression force was directed out of the plane (Figure 5.21), which produced a moment on the column. The strut force produced insignificant out-of-plane forces due to misalignment of the frame. Also, a portion of the moment was developed by the axial load of the column acting on an imperfect column, known as $P-\delta$ effects. Additionally, as the braces buckled, the connections yielded and produced a moment, which had components in the out-of-plane direction of the column and the strut member as illustrated in Figure 5.22. These components were plotted for the 2016 design under 1980 Irpinia, Italy (SCC1) ground motion record in Figure 5.23. As shown, the out-of-plane moment induced by the out-of-plane component of the brace forces and the $P-\delta$ effects are the key contributors to the out-of-plane bending moment of the compression column.



Figure 5.21: Brace out-of-plane buckling (deformations magnified)

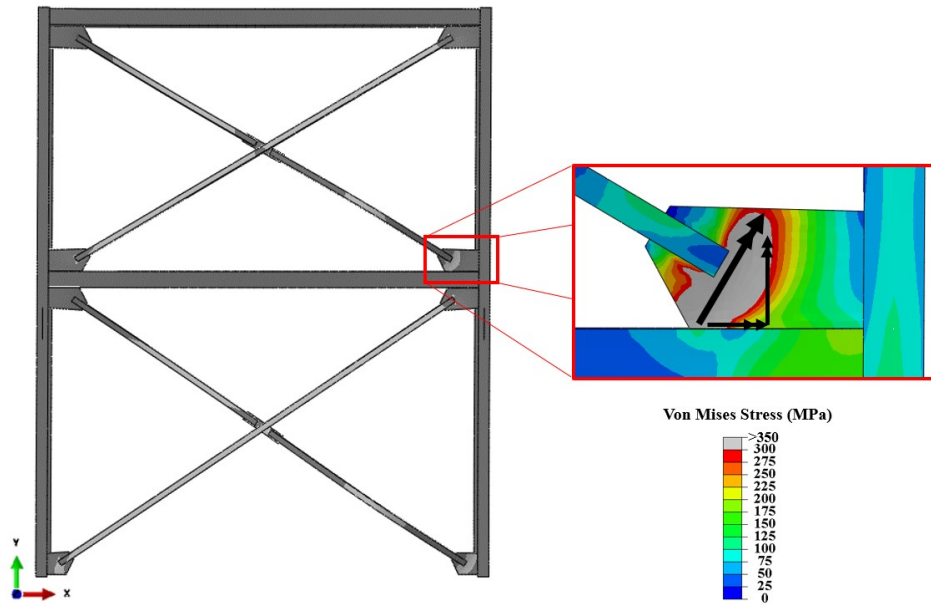


Figure 5.22: Moments in the X- and Y-directions produced by plastic hinging of the brace gusset plate

The contribution from the braces on the out-of-plane moment of the columns was not only limited to the buckled compression braces. It was found that tension braces also contribute to the out-of-plane bending moment imposed on the column. This is because residual plastic deformations developed upon brace out-of-plane buckling results in an elongated brace in the subsequent loading cycle where the brace in tension, which in turn develops out-of-plane forces on the column prior to the development of full tension capacity of the member. However, such out-of-plane deformations in the tension brace were considerably smaller than those in the compression brace, which led to lower out-of-plane bending moments in the columns.

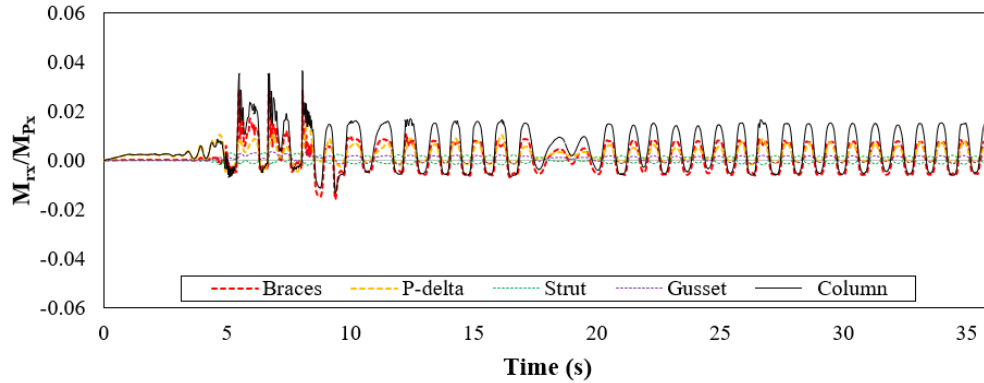


Figure 5.23: History of column out-of-plane bending moment under 1980 Irpinia, Italy (SCC1) ground motion record

The summation of the moments arising from the four individual components was compared to the measured out-of-plane moment on the column in Figure 5.24. A strong correlation was observed between the summation of identified components and the measured demand on the column.

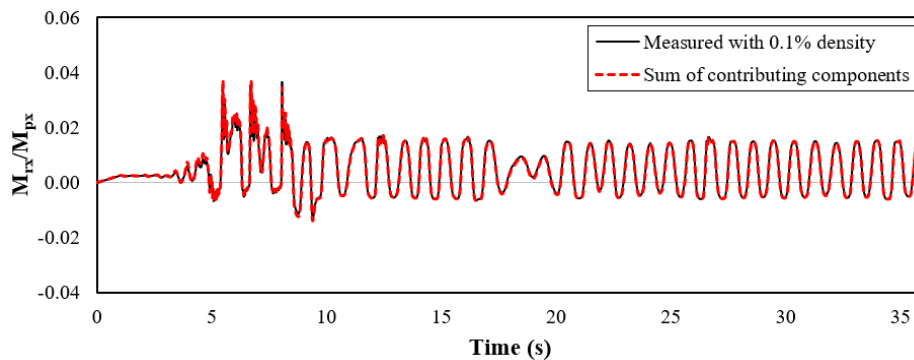


Figure 5.24: Column out-of-plane moment history under the 1980 Irpinia, Italy (SCC1) ground motion record

Since the most significant contribution to the out-of-plane bending moment on the columns is the force produced from braces buckling out-of-plane, which represents a correlation between the compression brace force and the column out-of-plane moments. As the compression brace force degrades in large tier drifts, smaller out-of-plane bending moments are imposed in the columns.

Figure 5.25 shows the out-of-plane moment measured in the columns of the 2016 design under the 2011 Tohoku, Japan (SCI6) ground motion record. As shown, the out-of-plane moment decreases significantly when the frame is pushed to the storey drifts greater than 1% in both columns.

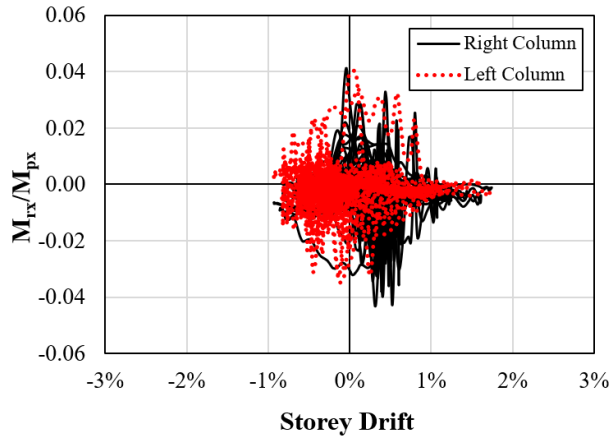


Figure 5.25: Column out-of-plane bending moment for the 2016 design under the 2011 Tohoku, Japan (SCI6) ground motion record

5.3.3.2 Axial Force

The maximum axial forces exerted on the columns of the 2010 and 2016 designs are plotted for all 40 ground motions in Figures 5.26a and 5.26b. In both designs, the axial force on the columns is well estimated in comparison to the design value. The median values for the maximum axial load 2010 and 2016 designs are 1.04 and 0.99, respectively.

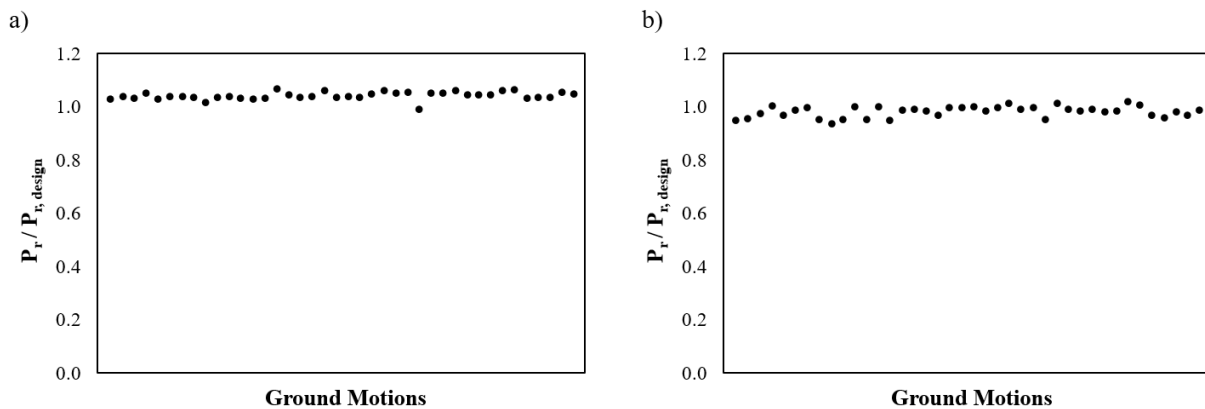


Figure 5.26: Column axial force for a) 2010 design; and b) 2016 design

5.4 Summary

Nonlinear static and dynamic analyses were carried out to evaluate the response of the prototype two-tiered braced frames designed in accordance with the 2010 and 2016 AISC Seismic Provisions. The results show that column stability is compromised in the 2010 design. The results of NLRH confirmed column buckling and subsequent frame instability under 13 ground motion records. Column stiffness was found insufficient in the 2010 design to propagate brace tensile yielding between the tiers, which led to the concentration of drift in the critical tier.

The analysis results indicate that the frame designed in accordance with the 2016 AISC Seismic Provisions remain stable under the applied seismic loads. No column buckling nor frame instability occurred under the ground motion records. The columns possess sufficient strength and stiffness to prevent column buckling and trigger brace tensile yielding in both braced panels. However, the in-plane moment demand was found to be over-estimated and the out-of-plane moment demand be under-estimated. Moreover, the median storey drift was 2.5 times larger than the design storey drift. Consequently, the tier drift was also larger than the expected value.

Chapter 6 – Design Recommendations

6.1 General

In this chapter, improved design recommendations are proposed based on the results obtained in Chapter 5 to achieve an efficient design for MT-SCBF design. The results obtained from the NLRH analyses of the two-tiered concentrically braced frame designed in accordance with the 2016 AISC Seismic Provisions were used to make recommendations on the column force demands and frame drift requirements.

6.2 Strength Requirements

Improved in-plane and out-of-plane bending moment requirements are proposed for columns of MT-CBFs. The column interaction ratio was measured under the axial compression force P_r/P_n and biaxial bending moment demands, weak-axis bending moment M_{ry}/M_{py} and strong-axis bending moment, M_{rx}/M_{px} , at the instant of a ground motion when the interaction ratio resulted in the highest value from the combination of axial compression force and flexural bending moments. Note that only ground motions where the brace tensile yielding occurs in both braced tiers were considered. Table 6.1 presents the results of the column interaction ratios, the ratio between the measured axial force and moment demands and the corresponding design values, and brace axial forces at the instant when the interaction ratio results in the highest value. Interaction ratios represent the column in-plane buckling limit state as per AISC 360 in Chapter H. Design values are obtained from AISC 341-16 as given in Chapter 3 Section 3.5.2.

Table 6.1: Statistics of column axial force and biaxial moment demands plus brace forces at the maximum interaction ratio

Ground Motion*	$\frac{P_r}{P_n} + \frac{8}{9} \left(\frac{M_{rx}}{M_{nx}} + \frac{M_{ry}}{M_{ny}} \right)$	P_r/P_n	M_{ry}/M_{py}	M_{rx}/M_{px}	$P_r/P_{r, design}$	$M_{ry}/M_{ry, design}$	$M_{rx}/M_{rx, design}$	T_1/T_{exp1}	T_2/T_{exp2}	C_1/C'_{exp1}	C_2/C_{exp2}
Median	0.55	0.26	0.31	0.01	0.99	0.47	0.93	1.07	1.02	1.23	0.71
84th Percentile	0.59	0.26	0.36	0.02	1.00	0.55	2.07	1.09	1.03	1.08**	0.79
Max.	0.61	0.27	0.39	0.05	1.01	0.59	5.83	1.11	1.04	1.63	0.81
Min.	0.46	0.23	0.22	0.00	0.29	0.34	0.13	0.88	0.87	0.87	0.50
SCI 3	0.59	0.23	0.39	0.01	0.86	0.59	1.44	0.88	0.87	0.87	0.68
SCI 4	0.61	0.26	0.38	0.01	0.99	0.57	1.16	1.06	1.04	1.38	0.59
SCI 6	0.55	0.26	0.31	0.01	0.99	0.48	0.60	1.07	1.02	1.25	0.75
SCI 7	0.58	0.26	0.35	0.00	1.00	0.53	0.41	1.07	1.02	1.25	0.79
SCI 11	0.54	0.26	0.30	0.01	1.00	0.46	0.81	1.09	1.02	1.23	0.78
SCI 13	0.55	0.26	0.32	0.00	1.00	0.48	0.16	1.09	1.03	1.19	0.74
SCI 15	0.54	0.26	0.28	0.03	0.99	0.43	3.80	1.11	1.03	1.12	0.67
SCI 16	0.59	0.26	0.37	0.01	0.98	0.55	1.04	1.06	1.01	1.07	0.70
SCI 17	0.53	0.26	0.30	0.00	0.98	0.45	0.13	1.08	1.03	1.06	0.71
SCI 19	0.59	0.25	0.36	0.02	0.95	0.55	2.07	0.99	1.02	1.38	0.54
SCI 20	0.61	0.26	0.38	0.02	1.00	0.57	1.88	1.08	1.01	1.16	0.80
SCI 21	0.56	0.26	0.32	0.00	1.00	0.49	0.35	1.09	1.01	1.22	0.78
SCC 2	0.57	0.26	0.30	0.04	1.00	0.45	4.56	1.07	1.01	1.44	0.69
SCC 3	0.58	0.26	0.31	0.05	1.00	0.47	5.83	1.10	1.04	1.08	0.59
SCC 4	0.49	0.25	0.27	0.01	0.29	0.40	0.24	1.04	1.01	1.13	0.58
SCC 5	0.54	0.26	0.31	0.00	1.00	0.47	0.49	1.08	1.01	1.32	0.79
SCC 7	0.56	0.27	0.32	0.01	1.01	0.49	1.45	1.11	1.04	1.17	0.66
SCC 8	0.51	0.26	0.27	0.01	0.99	0.41	1.23	1.08	1.02	1.56	0.70
SCC 9	0.46	0.26	0.22	0.01	0.98	0.34	0.79	1.06	0.97	1.63	0.81
SCC 10	0.51	0.26	0.28	0.00	0.99	0.42	0.37	1.08	1.01	1.43	0.78
SCC 12	0.50	0.26	0.26	0.02	0.99	0.39	1.80	1.07	1.01	1.61	0.71
SCC 13	0.59	0.27	0.32	0.05	1.01	0.48	5.24	1.10	1.02	1.27	0.76
SCC 14	0.51	0.24	0.31	0.00	0.90	0.46	0.33	0.95	0.93	1.15	0.50
SCD 1	0.52	0.23	0.32	0.00	0.89	0.49	0.19	0.93	0.88	1.08	0.81
SCD 3	0.52	0.26	0.29	0.00	0.98	0.44	0.50	1.06	0.98	1.15	0.77
SCD 5	0.50	0.26	0.26	0.01	0.99	0.40	1.07	1.07	1.02	1.58	0.68

*Note: Only ground motions that yielded the non-critical tier are included

**Note: Data arranged in descending order

6.2.1 Column Design Moments: In-plane

In-plane design moment for the MT-CBF columns is estimated based on the progressive yielding and buckling of the braces in two adjacent tiers, which is derived by the unbalanced brace storey shear force. Brace force adjustment factors are proposed to account for the inelastic cyclic response of the bracing members that are in compression when the columns reach their maximum force demands. Brace force adjustment factors for strength, α and α' , are proposed based on the results obtained from the NLRH analyses to estimate a realistic brace axial compression force for multi-tiered concentrically braced frames. The adjustment factor α represents the brace force for the tier where yielding has just been triggered, and α' represents the brace force adjustment factor for the tier where brace tensile yielding has been developed already. The α factor accounts for the limited force degradation of the compression brace in the noncritical tier where yielding has just initiated, and α' accounts for the fact that compression brace force in the critical tier has not reached its post-buckling strength when the combined demand in the column is maximum. Figure 6.1 shows the brace force scenario proposed to calculate the column in-plane bending moment demands using updated compression brace forces. Two yielding scenarios are considered: yielding first takes place in Tier 1 and yielding first occurs in Tier 2.

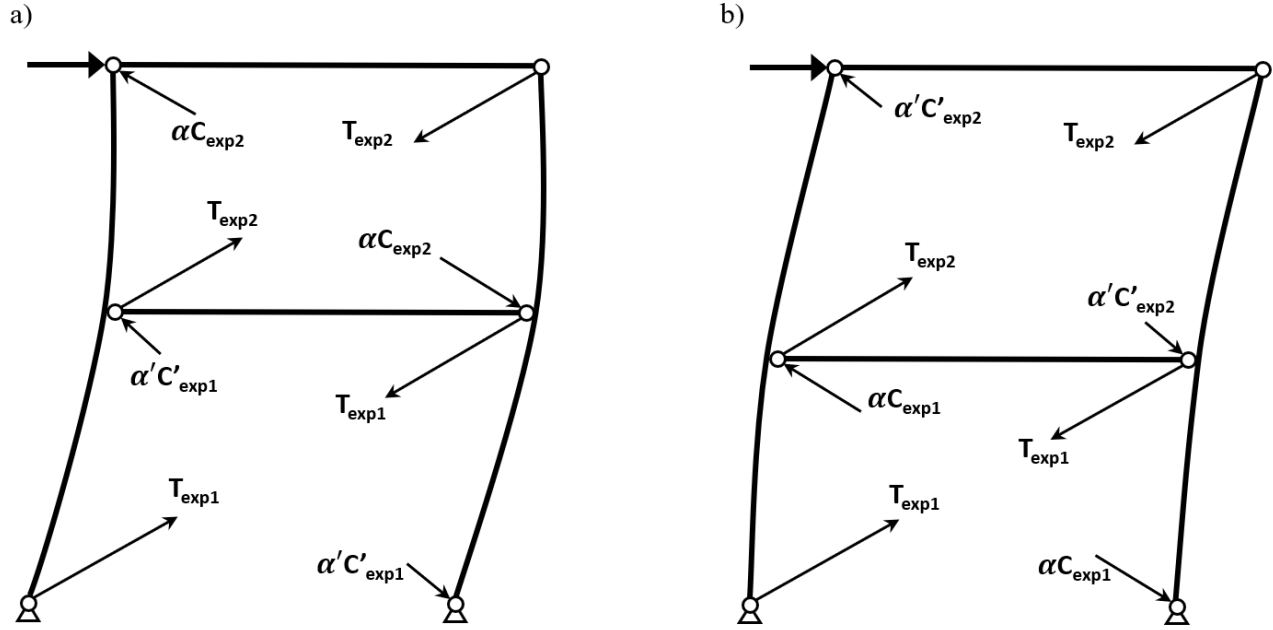


Figure 6.1: Proposed adjusted brace resistances when yielding propagates between tiers: a) brace tensile yielding has just initiated in Tier 2; and b) brace tensile yielding has just initiated in Tier 1

The column in-plane bending moment should be computed by incorporating α and α' in the equation (Equation 3.2 in Chapter 3) representing the unbalance brace storey shear force, ΔV_{br} :

$$\Delta V_{br} = (T_{exp} + \alpha C_{exp})_m \cos\theta_m - (T_{exp} + \alpha' C'_{exp})_n \cos\theta_n \quad (6.1)$$

where m and n correspond to the tier where brace tensile yielding is just initiated and the tier where brace tensile yielding has been developed, respectively.

Based on the results of the NLRH analyses, it is proposed to set the force adjustment factors as $\alpha = 0.80$ and $\alpha' = 1.10$ based on the 84th percentile values from Table 6.1. The 84th percentile values are suggested to account for the possibility of using stockier braces, which could lead to a higher unbalanced brace storey shear force (Figure 6.2). Using the adjustment brace force factors and the brace strengths, ΔV_{br} can then be calculated to obtain the column in-plane moment demand M_{ry} as described in Chapter 3.

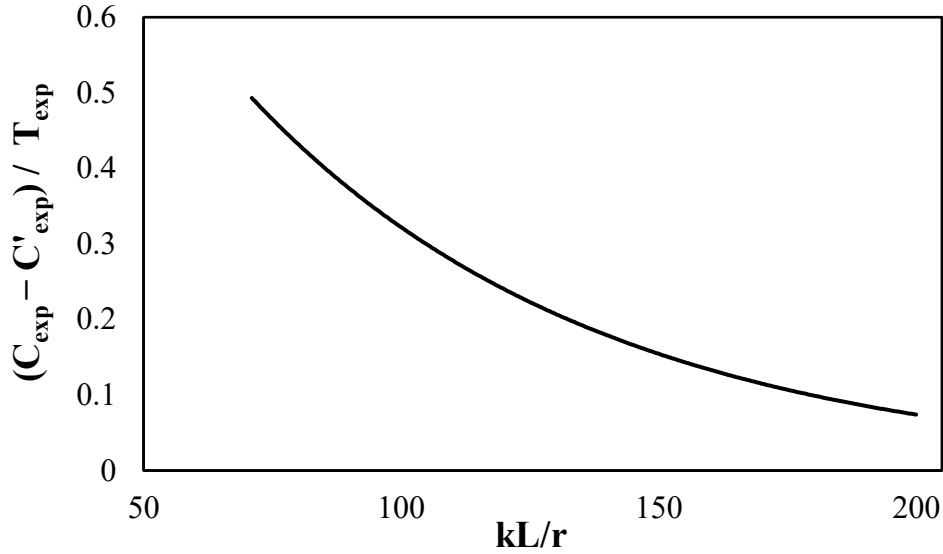


Figure 6.2: Slenderness effect on the difference between C_{exp} and C'_{exp}

6.1.2 Column Design Moments: Out-of-plane

The out-of-plane bending moment induced in the columns of the prototype frame was measured as a fraction of the plastic section modulus about its strong axis M_{px} . This moment, however, can be represented as a horizontal notional load acting at the strut to column connection similar to CSA S16 procedure, which produces the same bending moment demand on the column as shown in Figure 6.3. The 84th percentile value of the out-of-plane moment demand obtained from the NLRH analyses is $0.02 M_{px}$ at the instant when the column interaction ratio results in the most extreme value, which is greater than the design value of $0.007 M_{px}$. However, to further protect the column from potential out-of-plane buckling (Chapter 5, Figure 5.8), the 84th percentile value of the absolute maximum out-of-plane moment is proposed to be used as the design column out-of-plane moment demand. This value, as shown in Table 5.5, is equal to $0.05M_{px}$, which corresponds to a horizontal notional load equal to 0.1 times the vertical component of the compression brace acting at each tier level as per the 2016 AISC Seismic Provisions, or 0.014 times the load in the

compression force acting in the column below the brace-to-column connection as per the CSA S16. Although individual components of the out-of-plane moment (Figure 5.23) including brace forces, $P-\delta$ effects, and out-of-plane buckling and yielding of the brace connection contribute to the total out-of-plane moment on the column, it is proposed here to use a single notional load that represents the contribution from all sources as described in Section 5.3.3.2 to facilitate the design process.

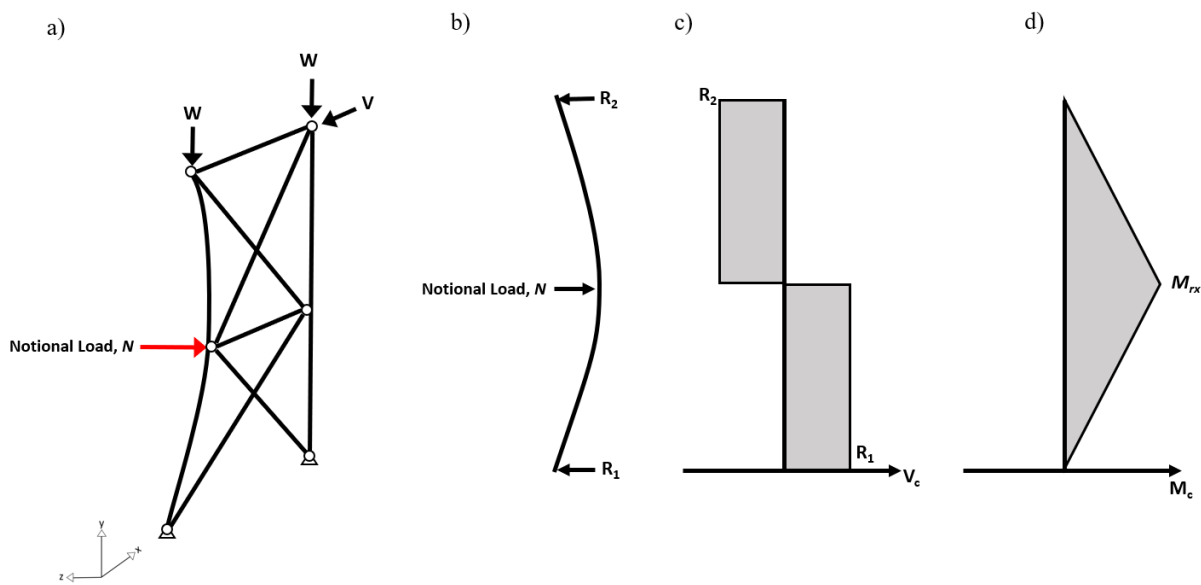


Figure 6.3: a) Deformed shape of MT-CBF; b) deformed shape of compression column caused by the notional out-of-plane load; c) column out-of-plane shear diagram; and d) column out-of-plane moment diagram

6.2 Drift Requirement

A new drift requirement is proposed for two-tiered concentrically braced frame based on the results obtained from the NLRH analyses. Total storey drift and individual tier drift should be verified to ensure the frame satisfies the stiffness requirement and brace deformation demands do not exceed the demands corresponding to brace premature low-cycle fatigue fracture. Tier drift is obtained

from the summation of the overall frame drift and distortion due to column bending when the frame roof displacement reaches the displacement corresponding to the design storey drift. To obtain drift due to column distortion, one can use the unbalance brace storey shear force similar to the in-plane bending moment calculations in Section 6.2.1. The NLRH analysis results suggest that the maximum storey drift experienced under the selected ground motions is significantly higher than the design value prescribed by ASCE 7-16. This finding from this research agrees with the findings by Imanpour et al. (2016a) and Imanpour and Tremblay (2016b).

Table 6.2 presents the storey drift values and brace forces at the maximum storey drift for the analysis where yielding is triggered in both tiers and corresponding brace forces. The results of the NLRH analyses for all the selected ground motion records are given in Table 5.3. Design storey drift prescribed by ASCE 7 for the frame designed using the 2016 AISC Seismic Provisions is $C_d\Delta_e = 0.55\%$, which is 2.5 times lower than the median values obtained from the NLRH analyses as shown in Table 5.3. Such large expected storey drift can result in large ductility demands in braced tiers, which poses concerns regarding the adequacy of the current drift requirements. An amplified design storey drift corresponding to 2.5 times the design storey drift is proposed for two-tiered concentrically braced frames when verifying the storey and tier drifts based on the median value from Table 5.3.

New brace force adjustment factors are proposed to verify the tier drift limitation that include β and β' for the noncritical tier and the critical tier, respectively. This brace force scenario is illustrated in Figure 6.4. According to the results obtained from the NLRH analyses, the brace force adjustment factors for drift $\beta = 0.60$ and $\beta' = 1.15$ are proposed based on the median (statistically neutral) brace force values as given in Table 6.2, where the β factor accounts for the

strength degradation of strength the compression brace in the noncritical tier, and β' amplifies the strength of the compression brace in the critical tier.

Table 6.2: Statistics of brace forces at the maximum storey drift

Ground Motion*	Storey Drift, Δ	T_1 / T_{exp1}	T_2 / T_{exp2}	C_1 / C'_{exp1}	C_2 / C_{exp2}
Median	1.6%	1.07	1.02	1.15	0.58
84th Percentile	2.2%	1.09	1.05	1.01**	0.78
Max.	2.6%	1.13	1.08	1.63	0.81
Min.	1.1%	0.88	0.87	0.67	0.39
SCI 3	1.6%	0.88	0.87	0.87	0.68
SCI 4	2.2%	1.09	1.07	1.38	0.46
SCI 6	1.7%	1.08	1.05	1.19	0.55
SCI 7	1.7%	0.95	0.92	1.07	0.63
SCI 11	1.6%	1.10	1.04	1.18	0.63
SCI 13	1.7%	1.09	1.04	1.16	0.62
SCI 15	1.9%	1.11	1.05	1.04	0.47
SCI 16	1.8%	0.95	0.91	1.00	0.56
SCI 17	2.1%	1.08	1.05	0.67	0.39
SCI 19	1.8%	1.08	1.03	1.05	0.60
SCI 20	1.5%	1.06	1.01	1.15	0.77
SCI 21	1.6%	1.07	1.04	1.44	0.53
SCC 2	1.5%	1.03	1.00	1.42	0.56
SCC 3	2.5%	1.12	1.07	0.98	0.43
SCC 4	1.6%	1.06	1.03	1.09	0.52
SCC 5	1.3%	1.08	1.01	1.32	0.79
SCC 7	2.3%	1.02	0.97	1.01	0.48
SCC 8	1.5%	1.08	1.04	1.53	0.56
SCC 9	1.1%	1.06	0.97	1.63	0.81
SCC 10	1.3%	1.08	1.01	1.43	0.78
SCC 12	1.2%	1.05	1.01	1.59	0.70
SCC 13	2.6%	1.13	1.08	1.03	0.46
SCC 14	2.3%	0.94	0.92	1.15	0.50
SCD 1	1.2%	0.93	0.88	1.08	0.81
SCD 3	1.3%	1.07	0.99	1.15	0.78
SCD 5	1.4%	1.07	1.03	1.57	0.61

*Note: Only ground motions that led to brace tensile yielding in both braced tiers are listed.

**Note: Data arranged in descending order.

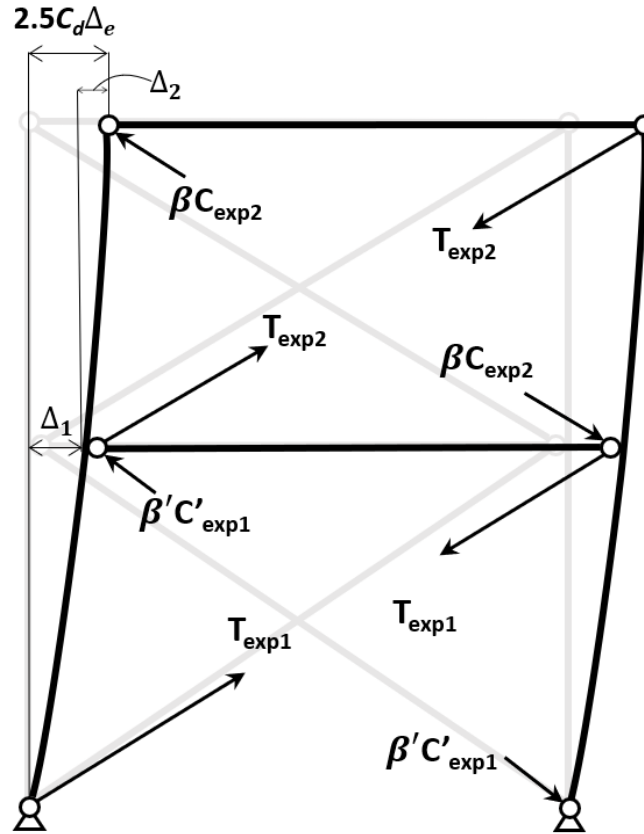


Figure 6.4: Proposed adjusted brace force scenario to verify tier drifts

6.3 Case Study

A case study is presented here to illustrate how the proposed strength and drift requirements would be applied to the prototype frame designed in Chapter 3.

6.3.1 Column In-plane Moment

Maximum column in-plane moment is calculated using the maximum expected brace strengths in the analysis representative of the progressive yielding and buckling of the braces plus the brace force adjusted factor as shown in Figure 6.5.

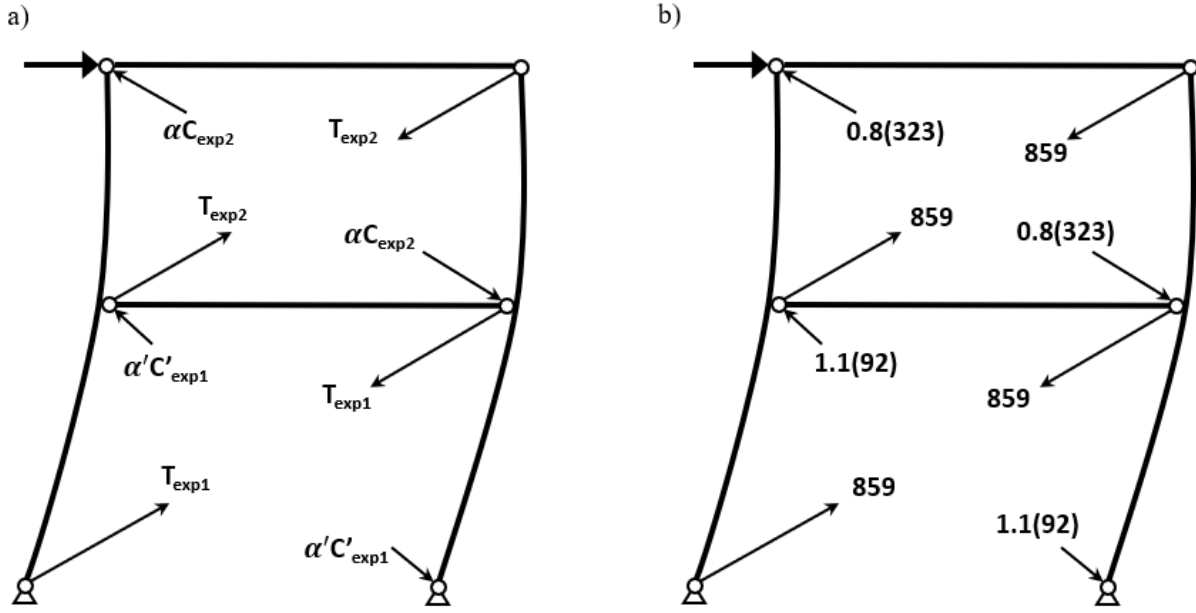


Figure 6.5: Proposed analysis case C for the moment calculation including

The unbalance brace storey shear force ΔV_{br} is calculated as follows:

$$\Delta V_{br} = (T_{exp} + \alpha C_{exp})_m \cos \theta_m - (T_{exp} + \alpha' C'_{exp})_n \cos \theta_n \quad (6.1)$$

$$\Delta V_{br} = (859 + 0.8(323))_2 \cos(31.6^\circ)_2 - (859 + 1.1(92))_1 \cos(33.9^\circ)_1$$

$$\Delta V_{br} = 155 \text{ kN}$$

substituting ΔV_{br} into Equation 3.1, M_{ry} can be calculated for each column:

$$M_{ry} = \frac{\Delta V_{br}}{2} \frac{h_1 h_2}{h} \quad (3.1)$$

$$M_{ry} = \frac{155}{2} \frac{(4.7)(4.3)}{9}$$

$$M_{ry} = 174 \text{ kN-m (originally calculated as 254 kN-m)}$$

6.3.2 Column Out-of-plane Moment

The proposed method to calculate the out-of-plane moment consist on calculating the notional load and then determining the corresponding the out-of-plane moment. The notional load is first calculated using Equation 6.2.

$$N = 0.1C_{exp} P_r \sin(\theta_2) \quad (6.2)$$

$$N = 0.1 (323 \text{ kN}) \sin(33.9^\circ) = 18 \text{ kN}$$

The moment induced in the column due to the notional load is equal to:

$$M_{rx} = N \frac{h_1 h_2}{h} = 18 \text{ kN} \frac{(4.7)(4.3)}{9} = 40 \text{ kN-m} \quad (6.3)$$

To compare the design value to the one prescribed by the CSA S16, the notional load is calculated using the CSA S16 procedure:

$$N = 0.02P_r = 0.02 (1331 \text{ kN}) = 26.6 \text{ kN} \quad (6.4)$$

$$M_{rx} = N \frac{h_1 h_2}{h} = 26.6 \text{ kN} \frac{(4.7)(4.3)}{9} = 60 \text{ kN-m} \text{ (50\% larger than the value in Equation 6.3)}$$

The column strength is verified for a W310×129 section using the interaction equation H1-1a of the AISC Specification as follows:

$$\frac{P_r}{P_c} + \frac{8}{9} \left(\frac{M_{rx}}{M_{cx}} + \frac{M_{ry}}{M_{cy}} \right) \leq 1.0 \quad (6.5)$$

$$0.32 + \frac{8}{9} (0.06 + 0.57) = 0.88 < 1.0 \quad \mathbf{OK}$$

The selected W310×129 section satisfies the strength requirement.

6.3.3 Tier Drift Limit Verification

The tier drift in the critical tier is calculated for the column using Equation 6.6, where $\Delta_{F,1}$ is the drift in Tier 1 corresponding to the linear drift of the frame, and $\Delta_{C,1}$ is the drift in Tier 1 caused by the column distortion under the unbalanced brace storey shear force:

For W310×129

$$\Delta_1 = \Delta_{F,1} + \Delta_{C,1} \leq 0.02 \quad (6.6)$$

where

$$\Delta_{F,1} = 2.5C_d\Delta_e \quad (6.7)$$

$$\Delta_{F,1} = \frac{2.5(5)(10.1 \text{ mm})}{9000 \text{ mm}} = 0.014$$

and

$$\Delta_{C,1} = \frac{\Delta V_{br}}{2} \frac{h_1 h_2^2}{3EI_y h} \quad (6.8)$$

Thus,

$$\Delta V_{br} = \Delta V_{br} = (T_{exp} + \beta C_{exp})_m \cos \theta_m - (T_{exp} + \beta' C'_{exp})_n \cos \theta_n \quad (6.9)$$

$$\Delta V_{br} = (859 + 0.60(323))_2 \cos(31.6^\circ)_2 - (859 + 1.15(92))_1 \cos(33.9^\circ)_1$$

$$\Delta V_{br} = 95.9 \text{ kN}$$

Substituting the $\Delta_{C,1}$ value in Equation 6.8:

$$\Delta_{C,1} = \frac{95.9 \text{ kN}}{2} \frac{(4700)(4300 \text{ mm})^2}{3(200,000 \text{ MPa})(100 \times 10^6 \text{ mm}^4)(9000)}$$

$$\Delta_{C,1} = 0.0077$$

The tier drift is the calculated by summing the values from equations 6.7 and 6.8 as follows:

$$\therefore \Delta_1 = 0.014 + 0.0077 = 0.022 > 0.02 \quad \text{NOT OK}$$

The selected W310X129 does not satisfy the proposed drift requirement.

A larger W310×143 section is verified to meet the the tier drift using Equation 6.6, where $\Delta_{F,1}$ and $\Delta_{C,1}$ are calculated using Equations 6.7 and 6.8, respectively.

$$\Delta_{F,1} = \frac{2.5(5)(9.95 \text{ mm})}{9000 \text{ mm}} = 0.014 \quad (6.7)$$

$$\Delta_{C,1} = \frac{\Delta V_{br}}{2} \frac{h_1 h_2^2}{3EI_y h} \quad (6.8)$$

Thus, the tier drift is equal to:

$$\Delta_{C,1} = \frac{95.900 \text{ kN}}{2} \frac{(4700)(4300 \text{ mm})^2}{3(200,000 \text{ MPa})(113 \times 10^6 \text{ mm}^4)(9000)}$$

$$\Delta_{C,1} = 0.0064$$

$$\therefore \Delta_1 = 0.014 + 0.0064 = 0.02 = 0.02 \quad \mathbf{OK}$$

The W310×143 section satisfies the proposed tier drift check. Since, this new section has been selected based on the drift check only, its strength should be verified using Equation. 6.5 :

$$0.29 + \frac{8}{9}(0.05 + 0.50) = 0.79 < 1.0 \quad \mathbf{OK}$$

The selected W310×143 section satisfies the strength requirement.

In this case study, the column section did not change from the original desing in Chapter 3 by implemnting the recommendations proposed in this chapter; however, the proposed recommendations represent a realistic estimation of the force and drift demands on MT-CBFs under seismic loads. The key difference between the design presented here and the one shown in Chapter 3 is that the column design was originally governed by the strength and not stiffness limit; in constrast, the design of the column when implementing the proposed design recommendations is

dominated by the required stiffness to meet the tier drift limit. Although, if the tier-heights were modified, such that $h_1 = 4.6$ m and $h_2 = 4.4$ m to reduced the stiffness demand caused by the unbalanced braced storey shear force, the column size could be decreased from W310×143 to a W310×129 and result in a more efficient design by implementing the design recomedations.

The proposed design recommnedations to determine the bending moment demads can also be considered in the design of frames with lower ductility levels such as moderatly ductile frames in Canada.

For MT-CBFs with more than two tiers, the design recommendations can be applied in the cases where brace tensile yielding propagates progressively from the bottom tier or the top tier following the method proposed by Imanpour et al. (2016a).

Chapter 7 – Conclusions and Recommendations

7.1 Summary

Steel multi-tiered concentrically braced frames (MT-CBFs) are commonly used in North America to resist lateral loads in tall single-storey buildings. Multi-tiered configurations involve multiple bracing panels stacked along the height of the storey that divide the height of a storey into several bracing panels. The primary advantage of using this configuration is to avoid using a single bracing panel between the ground and roof levels, which is not practical in most of cases. This configuration reduces the buckling length of the columns in the plane of the frame. Furthermore, the length of the bracing members is reduced, which results in smaller brace sizes that can easily satisfy the stringent width-to-thickness ratio and slenderness limits in high seismic areas. If the capacity design is required, lower capacity-induced forces are imposed on the adjacent members and connections of the braced frame.

Past studies confirmed unfavourable limit states under seismic load effects when the columns are designed under the axial load only. Moreover, under lateral seismic load brace tensile yielding is not distributed along the height of the frame and rather takes place in one of the tiers. As a result of this response, large in-plane flexural bending moment is induced in the column, which in some cases leads to plastic hinging and subsequent buckling of columns, and in some extreme cases frame collapse. Additionally, nonuniform brace yielding develops large inelastic deformations in one of the tiers, which may cause brace fracture. Improved design guidelines were introduced in the Canadian Steel Design Standard (CSA S16) and the AISC Seismic Provisions (AISC 341-16) to address these concerns and protect the columns of multi-tiered braced frames. The special

seismic provisions in Canada are limited to limit ductility CBFs (Type LD) and moderately ductile (Type MD) CBFs. The U.S. seismic provisions address ordinary CBFs, special CBFs, and Buckling Restrained Brace Frames (BRBFs) with multi-tiered configurations. The recent provisions require designers to design columns under the combined effects of the axial force, the in-plane bending moment due to progressive yielding of the braced panels, and out-of-plane bending moment due to brace out-of-plane buckling and column initial imperfections. Tier drift must also be verified to ensure that columns have enough flexural stiffness to prevent large tier drift that can cause premature brace fracture. Finally, the provisions require that the multi-tiered braced frames have intermediate struts to avoid unsatisfactory K-braced frame response.

Although significant improvement has been achieved in the design methodology of MT-CBFs, there is very limited detail numerical models and no experimental test data available to understand the stability response of the columns in such frames, verify the column moment demands, validate and improve the current design guidelines. The objective of this M.Sc. thesis is to evaluate the seismic behaviour of and the design methods for multi-tiered special concentrically braced frames.

A survey of the existing literature was conducted. Furthermore, a prototype frame consisting of a two-tiered special concentrically braced frame was designed using the 2010 and 2016 AISC Seismic Provisions. The seismic behaviour of the prototype frames was then evaluated in detail with the Abaqus finite element software (Dassault Systèmes 2014) using two nonlinear analysis methods: static (pushover) and nonlinear response history (dynamic) analyses. The global response of the selected prototype braced frames was examined and the force demands induced in the columns including the in-plane and out-of-plane bending moment demands were investigated. The results obtained from NLRH analyses were finally used to propose seismic design recommendations to improve the design of multi-tiered concentrically braced frames.

7.2 Limitations

This study only examined a single braced frame geometry and applied the AISC Seismic Provisions to design the braced frame. The geometrical properties including the frame height, number of tiers, tier height ratio was not examined in this study. Although extensive efforts were made to develop the detailed finite element model, certain assumptions were used in cases where enough information was not available. Specifically, the hardening properties used for the definition of the inelastic material behaviour for the bracing members are similar to those used for wide-flange sections. Furthermore, the base condition of the braced frame was assumed to be pinned to create a severe inelastic instability condition by reducing the frame redundancy.

7.3 Conclusions

The main findings of this M.Sc. research project are summarized as follows:

Numerical model of the braced frame:

- Detailed three-dimensional finite element model was developed, which is capable of predicting the seismic response of MT-CBFs and provides a good understanding of the column stability condition.
- Numerical analysis results produced in this study offers valuable input data for future experimental studies, in particular, the displacement history obtained from the NLRH analyses can be used to performed seismic testing of the full-scale two-tiered braced frame.

Two-tiered SCBF designed in accordance with the 2010 AISC Seismic Provisions:

- Non-uniform distribution of inelastic frame deformations was observed due to brace tensile yielding in one of the tiers only.

- Non-uniform distribution of lateral displacement induced large in-plane flexural demands on the columns.
- Excessive tier lateral deformations occurred in the tier where brace yielded initiated. Tier drifts ranged between 0.5% and 3.6%, where larger tier deformations combined with local buckling observed can lead to brace premature fracture.
- Strength and stiffness of the columns were not sufficient to propagate yielding along the height of the frame.
- Column buckling occurred in the cyclic pushover analysis because of the combined high axial compression force and in-plane flexural demand at 2.0% storey drifts.
- High strength degradation was observed in the lateral force–lateral displacement response obtained from the pushover analysis, which confirmed column instability.
- Pushover analysis was able to predict well the seismic behaviour of the frame plus force and deformation demands in the members compared to the NLRH analysis.
- Column buckling was observed under 13 ground motions record out of 40 records studied using the NLRH analysis method. In-plane buckling dominated the instability of the column that changed to bi-axial buckling as a result of the large out-of-plane displacement and lack of out-of-plane lateral bracing. Column buckling occurred in the storey drift range from 1.6% to 2.2%. Variability of storey drifts is attributed to the properties of the ground motion record and in part to the direction of initial geometric imperfections assigned to the column.

- Brace local buckling was observed under several ground motions records. Local buckling was observed in tier drifts ranging from 2.3% to 3.6%.

Two-tiered SCBF designed in accordance with the 2016 AISC Seismic Provisions:

- Frame exhibited a more uniform lateral deformation response under lateral seismic load. Brace tensile yielding was triggered in both braced tiers along the height of the frame in the pushover analysis and under most of the ground motion records.
- Progressive yielding of braces resulted in in-plane moment demands on the columns.
- Strength and stiffness of the columns were sufficient to propagate yielding along the height of the frame.
- A stable and satisfactory response was obtained using both pushover and dynamic analysis methods. No column instability nor frame collapse was observed.
- Maximum axial force induced in the columns from NLRH analyses agreed with the design value prescribed by 2016 AISC Seismic Provisions.
- Results obtained from NLRH analyses found that in-plane bending moment induced in the columns due to progressive yielding of braces is over-estimated by the 2016 AISC Seismic Provisions. The median value of the moments is 46% of the design demand.
- Results obtained from NLRH analyses found that out-of-plane bending moment induced in the columns due to brace out-of-plane buckling, $P-\delta$ effects, plastic hinging of the brace connection, and strut forces is under-estimated by the 2016 AISC Seismic Provisions. The median value of the moments is 163% of the design demand.
- Pushover analysis results compare well with the results obtained from the NLRH analysis.

Proposed design recommendations for two-tiered CBFs:

- Brace force adjustment factors were proposed to amplify the compression brace resistance in the tier which yields first by $\alpha' = 1.10$ and de-amplify the compressive brace resistance in the other tier by $\alpha = 0.80$ when calculating the unbalance brace storey shear force on the column, which then is used to obtain the column in-plane bending moment.
- An out-of-plane horizontal notional load applied at the tier level on the column was proposed to be equal to 0.1 times the vertical component of the compression brace force meeting the column at the same level.
- An amplified design storey drift of 2.5 times the code specified design storey drift is proposed for MT-SCBFs. Brace force adjustment factors were proposed to amplify the compression brace resistance in the tier which yield first by $\beta' = 1.15$ and to de-amplify the compressive brace resistance in the other tier by $\beta = 0.60$. Such adjusted brace forces should be used to calculate the unbalance brace storey shear force on the column when verifying the tier drift under the proposed design storey drift.
- For MT-CBFs with three or more tiers, the proposed design recommendations can be applied in the cases where brace tensile yielding propagates progressively from the bottom tier or the top tier following the method proposed by Imanpour et al. (2016a).

7.4 Recommendations for Further Research

This research has contributed to understanding the seismic stability response of MT-CBFs using the detailed finite element simulation. This research has also made recommendations to improve the current seismic design provisions implicit in North American design standards. However,

further investigation will be beneficial in understanding the complex stability response of such frames and further improve the design guidelines. Proposals for future studies are as follows:

- An experimental evaluation of full-scale two-tiered SCBF specimens is needed to verify column buckling, validate the numerical models used in this study and further validate the current design guidelines.
- A parametric numerical study should be performed to examine the effect of frame geometries such as frame height, tier height ratios, the number of tiers, bracing configurations such as chevron, diagonal and split-X, braced frame system such as eccentrically braced frames and buckling-restraint braced frames.
- The effects of the column base connection on the seismic behaviour of MT-CBFs should be examined.
- Further research is recommended into the effects of dynamic brace response such as the brace overshoot phenomenon at buckling.
- Given the concerns raised regarding the dynamic stability of MT-SCBFs designed excluding the special seismic design provisions, research studies to assess the performance of, identify deficiencies of and propose retrofit strategies for existing MT-SCBFs are recommended.

Bibliography

- AISC. (2010a). *ANSI/AISC 341-10, Seismic Provisions for Structural Steel Buildings*, American Institute of Steel Construction, Chicago, IL.
- AISC. (2010b). *ANSI/AISC 360-10, Specifications for Structural Steel Buildings*, American Institute of Steel Construction, Chicago, IL.
- AISC. (2016a). *ANSI/AISC 341-16, Seismic Provisions for Structural Steel Buildings*, American Institute of Steel Construction, Chicago, IL.
- AISC. (2016b). *ANSI/AISC 360-16, Specifications for Structural Steel Buildings*, American Institute of Steel Construction, Chicago, IL.
- AISC. (2016c). *Code of Standard Practice for Steel Buildings and Bridges*. American Institute of Steel Construction, Chicago, IL.
- Archambault, M.H. (1995). “Étude du comportement séismique des contreventements ductiles en X avec profils tubulaires en acier.” EPM/GCS-1995-09, Department of Civil Engineering, École Polytechnique, Montréal, QC.
- ASCE. (2016). *SEI/ASCE 7-16, Minimum Design Loads for Buildings and Other Structures*, American Society of Civil Engineers.
- ASCE. (2017). *SEI/ASCE 7-41, Seismic Evaluation and Retrofit of Existing Buildings*, American Society of Civil Engineers.
- Astaneh-Asl, A., Goel, S.C. (1984). “Cyclic in-plane buckling of double-angle bracing.” J Struct Eng., ASCE;109:2036–55.
- Astaneh-Asl, A., Goel, S.C., Hanson, R.D. (1985) “Cyclic out-of-plane buckling of double-angle bracing.” J Struct Eng., ASCE;111:1135–53.

- Astaneh-Asl, A., Goel, S.C., and Hanson, R.D (1986). “Earthquake design of double-angle bracing,” *AISC Engineering Journal*, Vol. 23, No. 4, 4th Quarter, 1986, pp. 133-147.
- ASTM. (2015a). *A1085/A1085M-15 Standard Specification for Cold-Formed Welded Carbon Steel Hollow Structural Sections (HSS)*. ASTM International, West Conshohocken, PA.
- ASTM. (2015b). *A992/A992M-11 Standard Specification for Structural Steel Shapes*. ASTM International, West Conshohocken, PA.
- CSA. (2009, 2014). *CSA S16-09, CSA S16-14, Design of Steel Structures*, Canadian Standards Association, Mississauga, ON.
- Bertero, V. V., Uang, C.-M., Llopiz, C. R., and Igarashi, K. (1989). “Earthquake simulator testing of concentric braced dual system.” *J. Struct. Eng.*, 115(8), 1877–1894.
- Black, R. Gary, W. A. Wenger, and E. P. Popov. (1980). “Inelastic Buckling of Steel Struts Under Cyclic Load Reversals.” Berkeley, Calif: Earthquake Engineering Research Center, University of California.
- Carter, C.J., Muir, L.S., Dowswell, B. (2016) “Establishing and developing the weak-axis strength of plates subjected to applied loads.” *8th International Workshop Connections in Steel Structures*, Boston, MA, May 24-26, 2016.
- Chopra, A.K. (2011). *Dynamics of Structures: Theory and Applications to Earthquake Engineering*, 4th Edition, Prentice Hall, Englewood Cliffs, New Jersey, 2011.
- Dalal, S.T. (1969). “Some non-conventional cases of column design.” *Eng. J. AISC*, 6(1), 28–39.
- Dassault Systèmes. (2012;2014). "Abaqus Analysis User's Guide" *Version 6.14*, Dassault Systèmes Simulia Corp, Providence, RI.
- Dehghani, M. (2016). Seismic design and qualification of all-steel buckling-restrained braced frames for Canadian applications. (Order No. 10806518, Ecole Polytechnique, Montreal (Canada)).

ProQuest Dissertations and Theses, 440. Retrieved from <http://login.ezproxy.library.ualberta.ca/login?url=https://search.proquest.com/docview/2024162852?accountid=14474>

Dehghani M., and Tremblay, R. (2016) “Robust Period-Independent Ground Motion Selection and Scaling for Effective Seismic Design and Assessment,” *Journal of Earthquake Engineering*, 20:2, 185-218, DOI: [10.1080/13632469.2015.1051635](https://doi.org/10.1080/13632469.2015.1051635)

Elkady, A., & Lignos, D. G. (2018). “Full-scale testing of deep wide-flange steel columns under multiaxis cyclic loading: Loading sequence, boundary effects, and lateral stability bracing force demands.” *Journal of Structural Engineering*, 144(2), 04017189.

El-Tayem, A. A., and Goel, S. C (1985). “Cyclic behavior of angle X-bracing with welded connections.” *Research Rep. No. UMCE 85-4*, Univ. of Michigan, Ann Arbor, Mich.

El-Tayem, A. A., and Goel, S. C. (1986). “Effective length factor for the design of X-bracing systems.” *AISC Eng. J.*, 24(1), 41–45.

Fell, B.V., Kanvinde, A.M., Deierlein, G.G., and Myers, A.T. (2009). “Experimental Investigation of Inelastic Cyclic Buckling and Fracture of Steel Braces.” *J. Struct. Eng.*, ASCE, 135(1), 19–32.

Foutch, D. A., Goel, S. C., and Roeder, C. W. (1987). “Seismic testing of full-scale steel building—Part I.” *J. Struct. Eng.*, 113(11), 2111–2129.

Galambos, T.V., and Ketter, R.L. (1958). *Columns Under Combined Bending and Thrust*, Fritz Engineering Laboratory Report 205A.21, Bethlehem, Pennsylvania.

Gugerli, H. (1982). “Inelastic cyclic behavior of steel bracing members.” PhD thesis, Univ. of Michigan, Ann Arbor, Mich.

Haddad, M., Brown, T., & Shrive, N. (2011). “Experimental cyclic loading of concentric HSS braces.” *Canadian Journal of Civil Engineering*, 38(1), 110-123.

- Hassan, O. F., and Goel, S. C. (1991). “Modeling of bracing members and seismic behavior of concentrically braced steel structures.” *Research Rep. No. UMCE 91-1*, Univ. of Michigan, Ann Arbor, Mich.
- Hsiao, P-C., Lehman, D.E., and Roeder, C.W. (2013). “A model to simulate special concentrically braced frames beyond brace fracture”, *Earthquake Engineering and Structural Dynamics*, 42, 183-200.
- Imanpour, A., Tremblay, R., and Davaran, A. (2012a). “Seismic performance of steel concentrically braced frames with bracing members intersecting columns between floors.” *Proc., 7th STESSA Conference*, Santiago, Chile, 447–453.
- Imanpour, A., Tremblay, R., and Davaran, A. (2012b). “Seismic Evaluation of Multi-Panel Steel Concentrically Braced Frames.” *15WCEE*, Lisbon, Portugal, Paper No. 2996.
- Imanpour, A., and Tremblay, R. (2012). “Analytical Assessment of Stability of Unbraced Column in Two Panel Concentrically Braced Frames.” *3rd International Structural Specialty Conference*, Edmonton, Alberta, Canada, Paper No. 1218.
- Imanpour, A., Stoakes, C., Tremblay, R., Fahnestock, L., and Davaran, A. (2013). “Seismic Stability Response of Columns in Multi-Tiered Braced Steel Frames for Industrial Applications.” *ASCE Structures Congress*, Pittsburgh, PA, 2650–2661.
- Imanpour, A., and Tremblay, R. (2014a). “Seismic performance evaluation and design of multitiered steel concentrically braced frames.” *Proc., 10th National Earthquake Engineering Conf.*, Anchorage, AK, Paper No. 1347.
- Imanpour, A., Tremblay, R., Davaran, A., Stoakes, C., and Fahnestock, L. (2016a). “Seismic performance assessment of multi-tiered steel concentrically braced frames designed in accordance with 2010 AISC seismic provisions.” *Journal of Structural Engineering*. ASCE.

- Imanpour, A., Tremblay, Fahnestock, L., and A., Stoakes, C. (2016b). "Analysis and Design of Two-Tiered Steel Braced Frames under In-Plane Seismic Demand." *Journal of Structural Engineering*. ASCE.
- Imanpour, A., Tremblay, R., and Auger, K. (2016c). "Seismic design and performance of multitiered steel braced frames including the contribution from gravity column under in-plane seismic demand." *Advanced in Engineering Software*.
- Imanpour, A. and Tremblay, R. (2016a). "Analysis Methods for the Design of Special Concentrically Braced Frames with Three or More Tiers for In-Plane Seismic Demand." *Journal of Structural Engineering*. ASCE.
- Imanpour, A., & Tremblay, R. (2016b). "Seismic design and response of steel multi-tiered concentrically braced frames in Canada." *Canadian Journal of Civil Engineering*, 43(10), 908-919.
- Imanpour, A., Tremblay, R., Leclerc, M., & Siguier, R. (2018). "Development of a Hybrid Simulation Computational Model for Steel Braced Frames." In *Key Engineering Materials* (Vol. 763, pp. 609-618). Trans Tech Publications.
- Izvernari, C. (2007). *The Seismic Behavior of Steel Braces with Large Sections*, Doctoral Dissertation, Department of Civil, Geological, and Mining Engineering, Ecole Polytechnique, Montreal, Quebec, Canada.
- Jain, A. K., Goel, S. C., and Hanson, R. D. (1980). "Hysteretic cycles of axially loaded steel members." *J. Struct. Div. ASCE*, 106(8), 1777–1795.
- Jiang, Y. (2013). Numerical and experimental seismic assessment and retrofit of steel tension-only double angle braced frames designed before the implementation of detailing provisions for ductile seismic response. (Order No. 1528147, Ecole Polytechnique, Montreal (Canada)). *ProQuest Dissertations and Theses*, 253. Retrieved from

<http://login.ezproxy.library.ualberta.ca/login?url=https://search.proquest.com/docview/1556108729?accountid=14474>

- Kazemzadeh Azad, S., Topkaya, C., and Bybordiani, M. (2018) “Dynamic buckling of braces in concentrically braced frames”. *Earthquake Engng Struct Dyn.*;47: 613–633. <https://doi.org/10.1002/eqe.2982>
- Lee, S., and Goel, S. C. (1987). “Seismic behavior of hollow and concrete-filled square tubular bracing members.” *Research Rep. No. UMCE 87-11*, Univ. of Michigan, Ann Arbor, Mich.
- Lee, S. 1988. Seismic behaviour of hollow and concrete-filled square tubular bracing members. Ph.D. thesis, Department of Civil Engineering, The University of Michigan, Ann Arbor, Michigan.
- Liu, Z. (1987). “Investigation of concrete-filled steel tubes under cyclic bending and buckling.” PhD thesis, Univ. of Michigan, Ann Arbor, Mich.
- McKenna, F., and Fenves, G.L. (2004). “*Open System for Earthquake Engineering Simulation (OpenSees)*.” Pacific Earthquake Engineering Research Center (PEER), University of California, Berkeley, CA. <http://opensees.berkeley.edu/>.
- Nakashima, M., and Wakabayashi, M. (1992). “Analysis and design of steel braces and braced frames in building structures.” *Stability and ductility of steel structures under cyclic loading*, Y. Fukumoto and G. C. Lee, eds., CRC Press, Boca Raton, Fla., 309–321.
- Ozkula, G., Harris, J., & Uang, C. M. (2017). “Classifying Cyclic Buckling Modes of Steel Wide-Flange Columns under Cyclic Loading.” In *Structures Congress 2017* (pp. 155-167).
- Popov, E.P., and Black, R.G. (1981). “Steel struts under severe cyclic loadings.” *J. Struct. Eng.*, 107(9), 1857–1881.

- Roeder, C.W., Lehman, D.E., Clark, K, Powell, J., Yoo, J-H, Tsai, K-C, Lin, C-H, and Wei, C-Y (2011). "Influence of Gusset Plate Connection and Braces on the Seismic Performance of X-Braced Frames." *Earthquake Engineering and Structural Dynamics*, 40(4), 355-374.
- Sabelli, R., Roeder, C.W., and Hajjar, J.F. (2013). "Seismic design of steel special concentrically braced frame systems: A guide for practicing engineers," NEHRP Seismic Design Technical Brief No. 8, produced by the NEHRP Consultants Joint Venture, a partnership of the Applied Technology Council and the Consortium of Universities for Research in Earthquake Engineering, for the National Institute of Standards and Technology, Gaithersburg, MD, NIST GCR 13-917-24.
- S-Frame Software. (2017). Structural analysis software.
- Shaback, J. B. (2001). "Behaviour of square HSS braces with end connections under reversed cyclic axial loading." Master's thesis, Univ. of Calgary, Calgary, Alta., Canada.
- Schmidt, B.J., and Bartlett, F.M. (2002). "Review of resistance factor for steel: data collection," *Can. J. Civ. Eng.* 29: 109–118.
- Stoakes, C.D., and Fahnestock, L.A. (2012). "Influence of weak-axis flexural yielding on strong axis buckling strength of wide flange columns." *Proc., Annual Stability Conference, SSRC*, Grapevine, Texas, April 17–20.
- Stoakes, C. D., and Fahnestock, L. A. (2014). "Three-dimensional Finite Element Simulation of the Seismic Behavior of Multitier Concentrically Braced Frames" *ASCE Structures Congress*, Boston, MA, 3-5 April.
- Stoakes, C. D., and Fahnestock, L. A. (2016). "Strong-axis stability of wide flange steel columns in the presence of weak-axis flexure." *Journal of Structural Engineering.*, 10.1061/(ASCE)ST.1943-541X.00001448, 04016004.

- Suzuki Y, Lignos DG (2015). “Large scale collapse experiments of wide flange steel beam-columns.” *Proceedings of the 8th International Conference on Behavior of Steel Structures in Seismic Areas (STESSA)*, Shanghai, China, July 1-3, 2015.
- Tang, X., and Goel, S. C. (1987). “Seismic analysis and design considerations of braced steel structures.” *Research Rep. No. UMCE 87-4*, Univ. of Michigan, Ann Arbor, Mich.
- Tremblay, R. (2001). “Seismic Behavior and Design of Concentrically Braced Steel Frames.” *Eng. J. AISC*, 38(3), 148–166.
- Tremblay, R. (2002). “Inelastic seismic response of steel bracing members.” *J. Constr. Steel Res.*, 58(5-8), 665–701.
- Tremblay, R. (2003). “Achieving a stable inelastic seismic response for multi-story concentrically braced steel frames.” *Eng. J. AISC*, 40(2), 111–129.
- Tremblay, R., Archambault, M.H., and Filiatrault, A. (2003). “Seismic response of concentrically braced steel frames made with rectangular hollow bracing members.” *J. Struct. Eng., ASCE*, 129(12), 1626–1636.
- Uriz, P., Filippou, F.C., Mahin, S.A. (2008). “Model for cyclic inelastic buckling for steel member.” *J. Struct. Eng., ASCE*, 134(4), 619–28.
- Newell, J. D., & Uang, C. M. (2008). “Cyclic behavior of steel wide-flange columns subjected to large drift.” *Journal of structural engineering*, 134(8), 1334-1342.
- Walpole, W. R. (1996). “Behaviour of cold-formed steel RHS members under cyclic loading.” *Research Rep. No. 96-4*, Univ. of Canterbury, Christchurch, New Zealand.
- Wakabayashi, M., Matsui, C., Minami, K., and Mitani, I. (1974). “Inelastic behavior of full-scale steel frames with and without bracings.” *Bull. Disaster Prevention Research Institute, Kyoto Univ.*, 24(216), 1–23.

Yang, F., and Mahin, S.A. (2008). "Limiting Net Section Fracture in Slotted Tube Braces." *Steel Tips Series, Structural Steel Education Council, Moraga, CA.*

Ziemian, R. D. (Ed.). (2010). *Guide to stability design criteria for metal structures.* John Wiley & Sons.

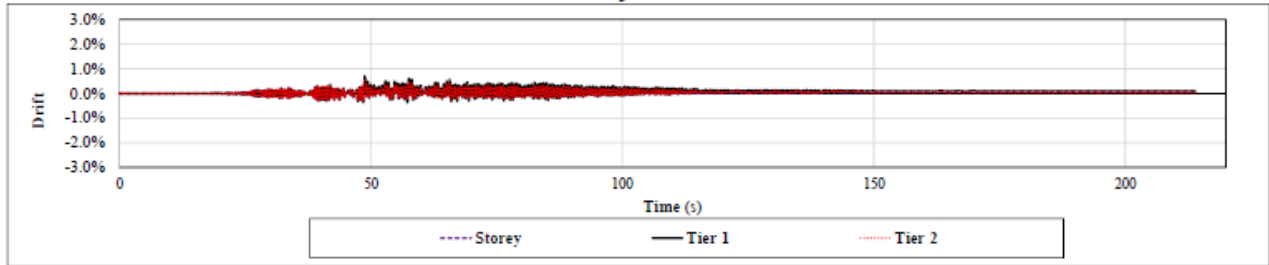
APPENDIX A

Nonlinear response history analyses

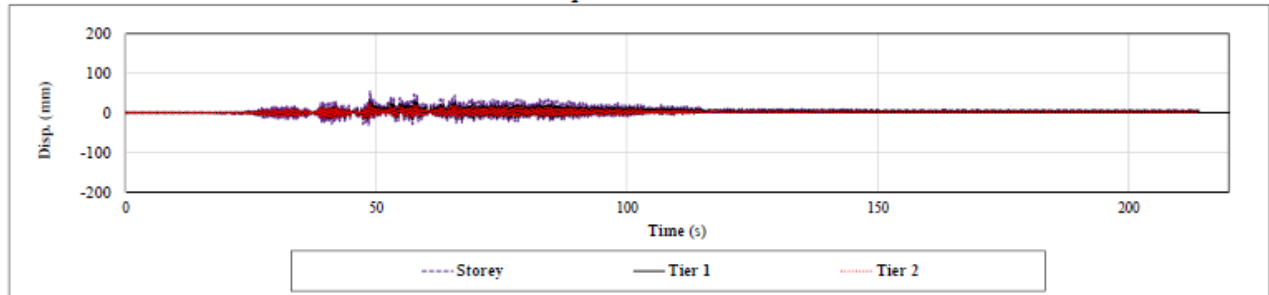
Ground Motion: SCI 1

Two-Tiered SCBF: AISC 341-10 Design

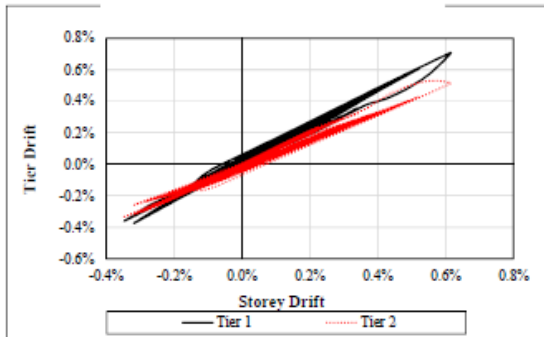
Drift vs. Time



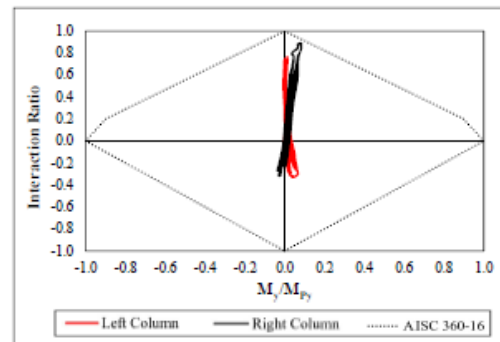
Displacement vs. Time



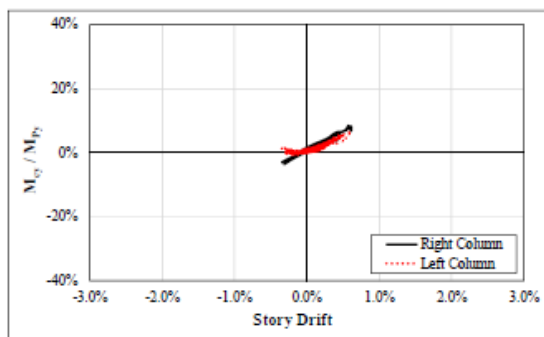
Tier Drift vs. Storey Drift



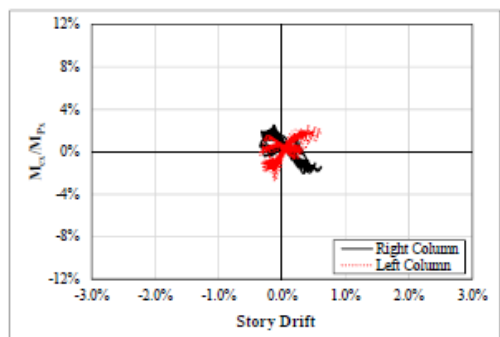
Column P-M Interaction Diagram



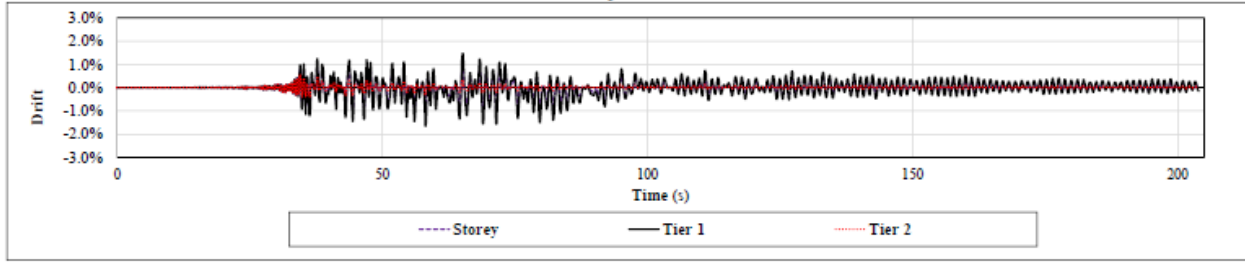
Column In-plane Bending Demand



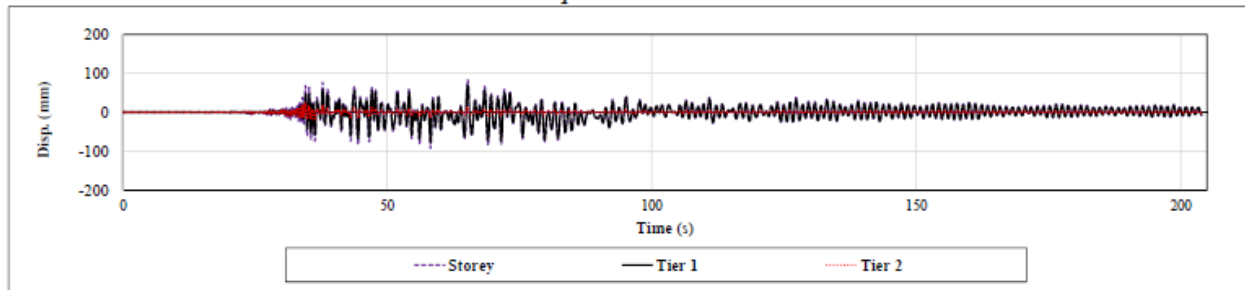
Column Out-of-plane Bending Demand



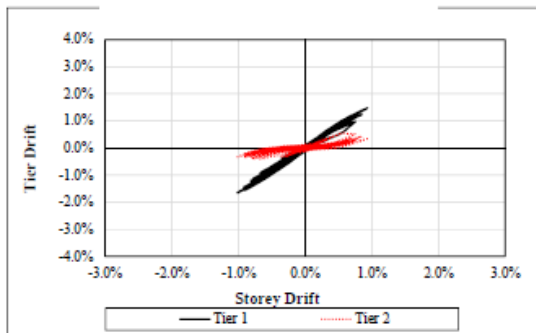
Drift vs. Time



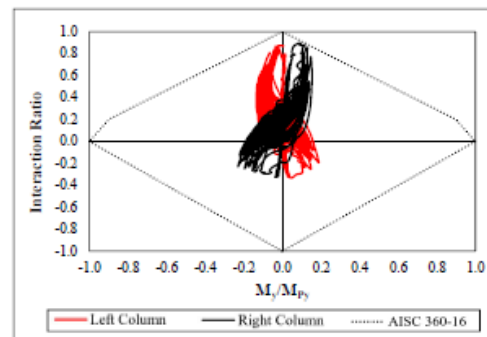
Displacement vs. Time



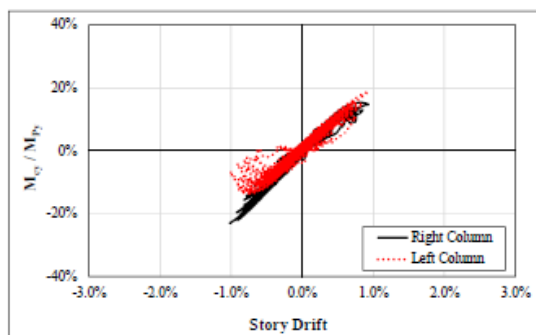
Tier Drift vs. Storey Drift



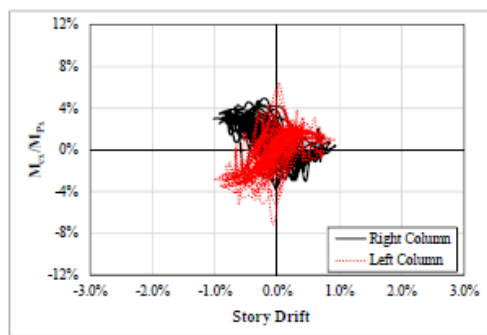
Column P-M Interaction Diagram



Column In-plane Bending Demand



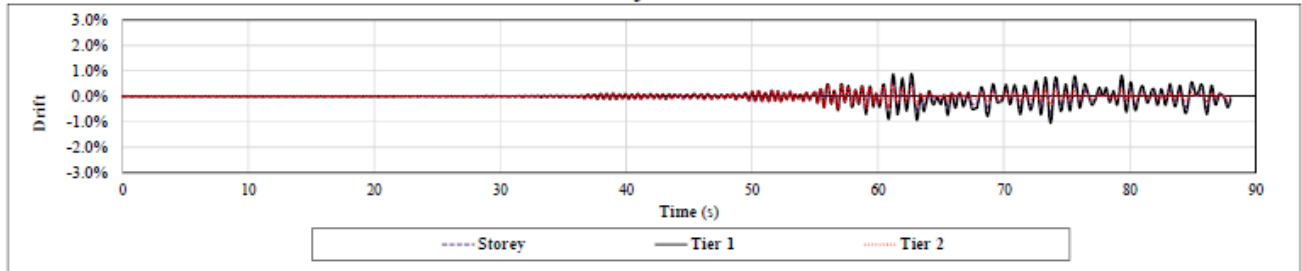
Column Out-of-plane Bending Demand



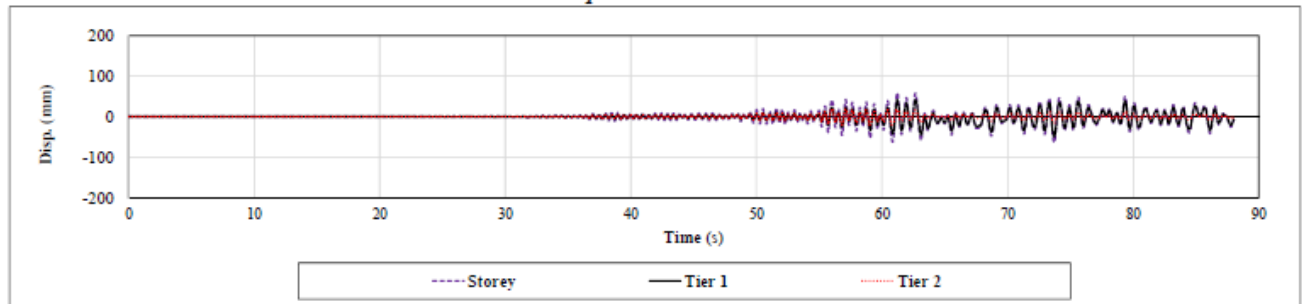
Ground Motion: SCI 3

Two-Tiered SCBF: AISC 341-10 Design

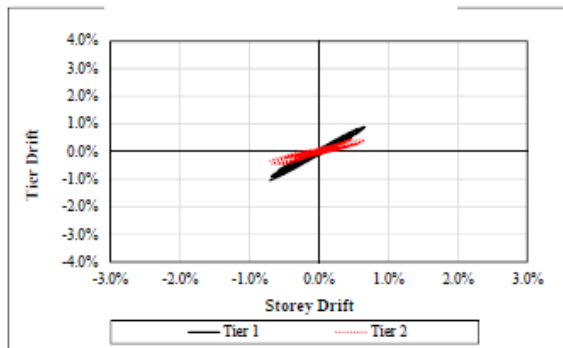
Drift vs. Time



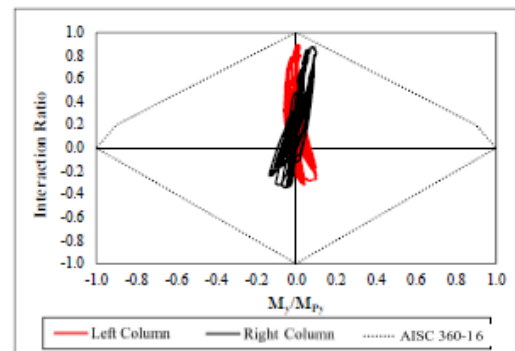
Displacement vs. Time



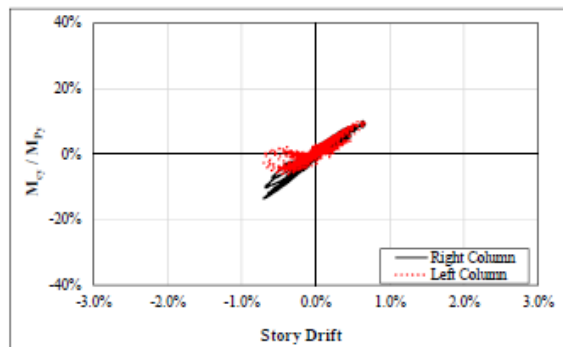
Tier Drift vs. Storey Drift



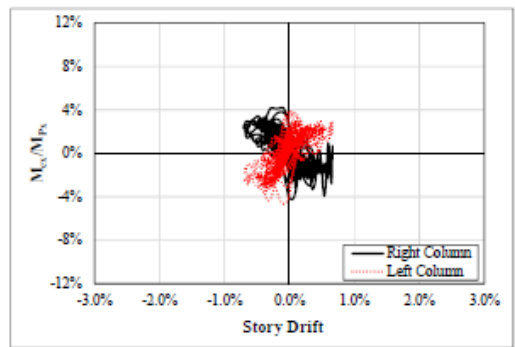
Column P-M Interaction Diagram



Column In-plane Bending Demand



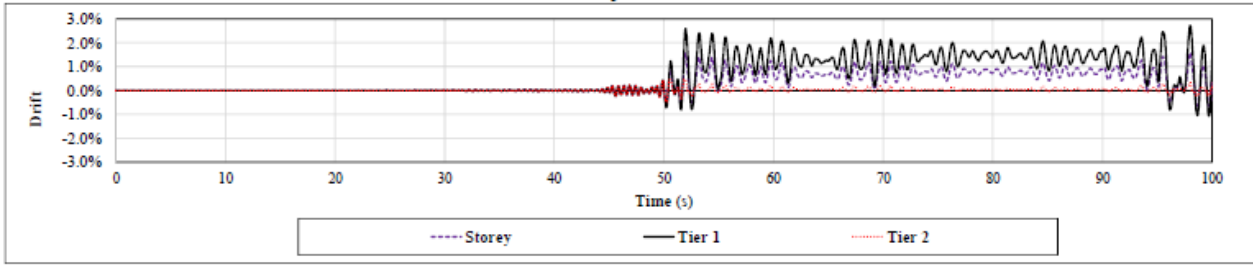
Columns Out-of-plane Bending Demand



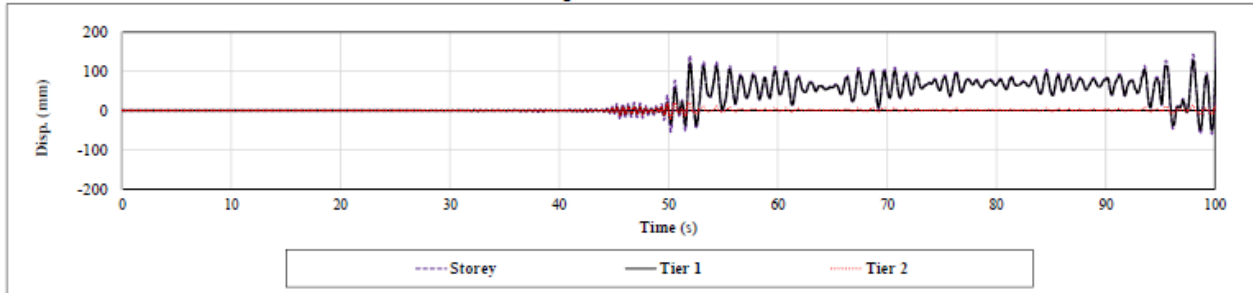
Ground Motion: SCI 4

Two-Tiered SCBF: AISC 341-10 Design

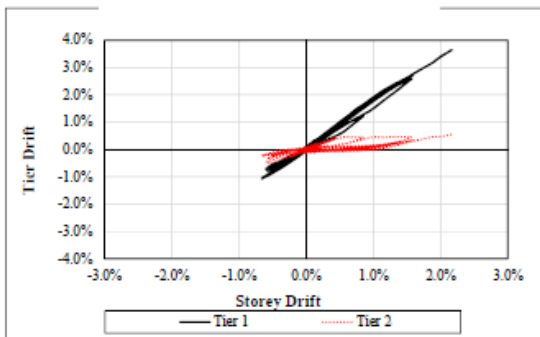
Drift vs. Time



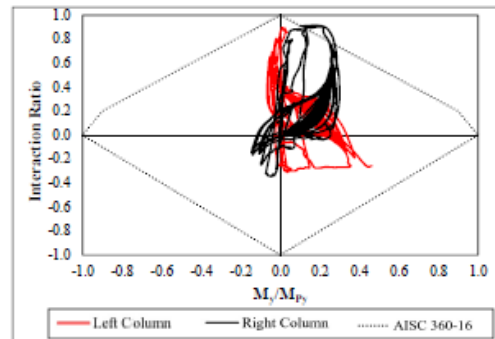
Displacement vs. Time



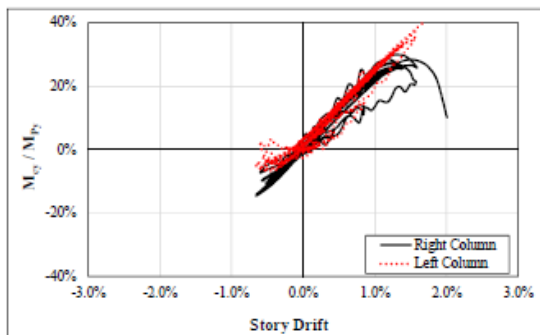
Tier Drift vs. Storey Drift



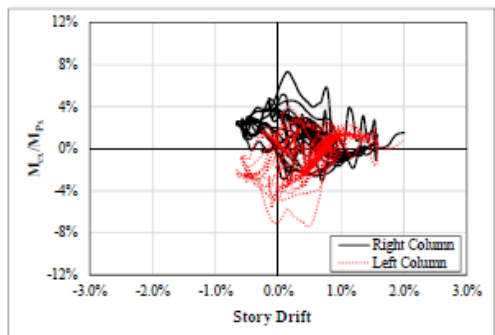
Column P-M Interaction Diagram



Column In-plane Bending Demand



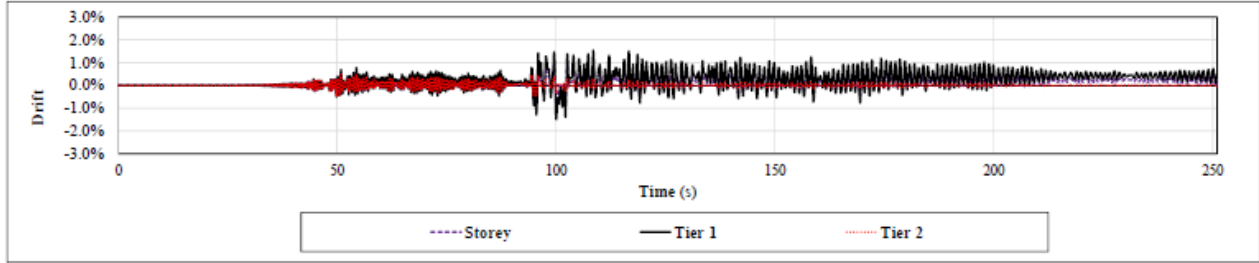
Column Out-of-plane Bending Demand



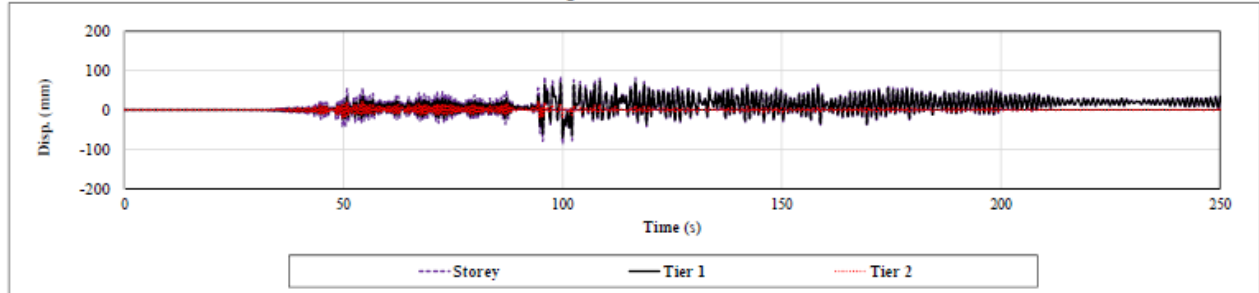
Ground Motion: SCI 5

Two-Tiered SCBF: AISC 341-10 Design

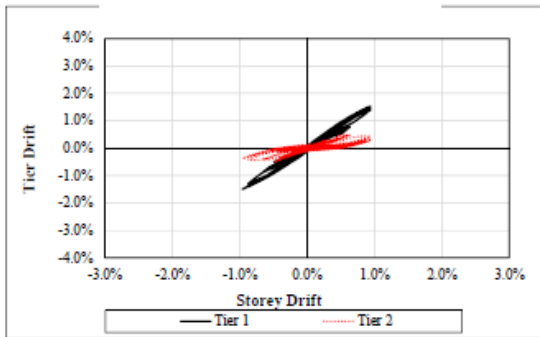
Drift vs. Time



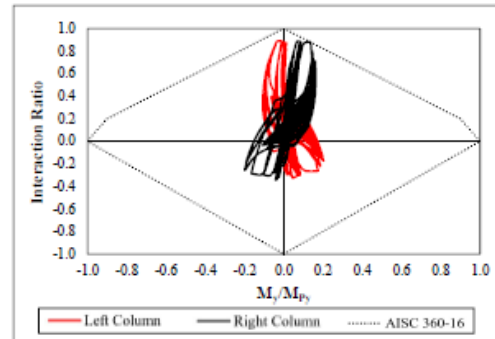
Displacement vs. Time



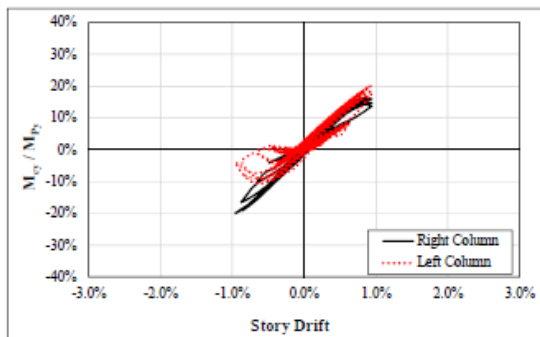
Tier Drift vs. Storey Drift



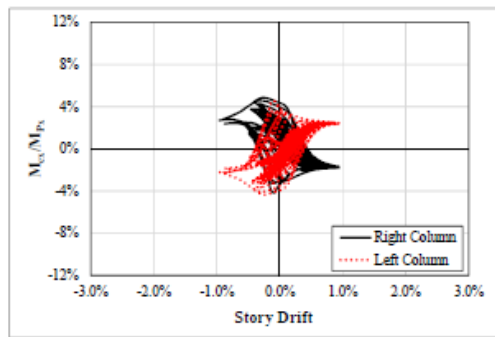
Column P-M Interaction Diagram



Column In-plane Bending Demand



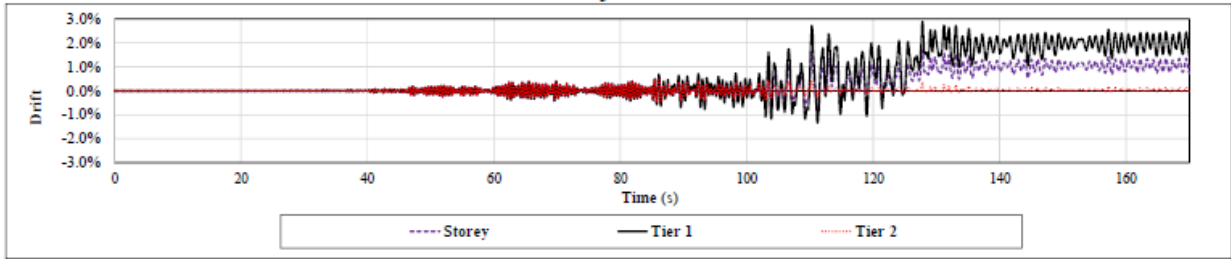
Column Out-of-plane Bending Demand



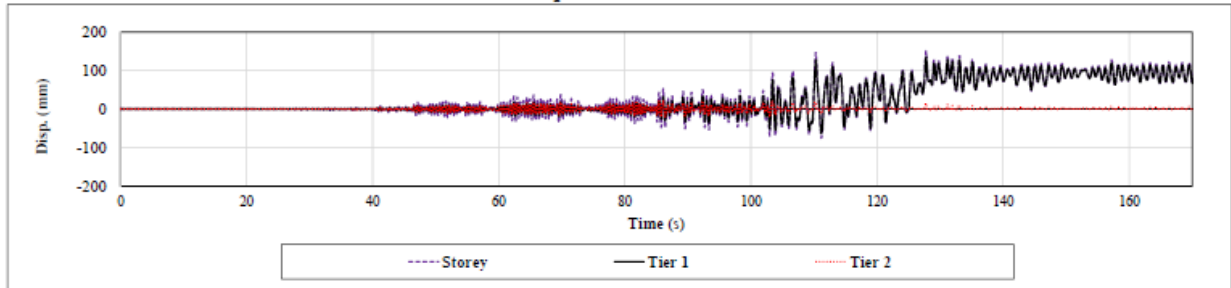
Ground Motion: SCI 6

Two-Tiered SCBF: AISC 341-10 Design

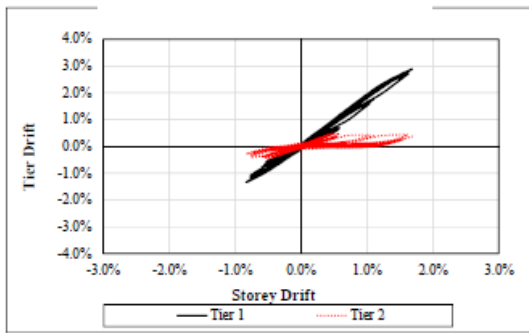
Drift vs. Time



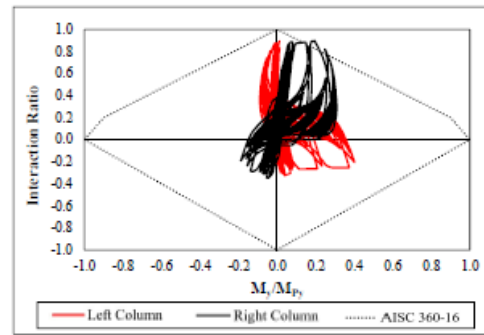
Displacement vs. Time



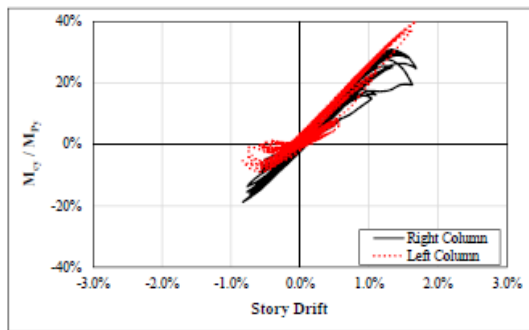
Tier Drift vs. Storey Drift



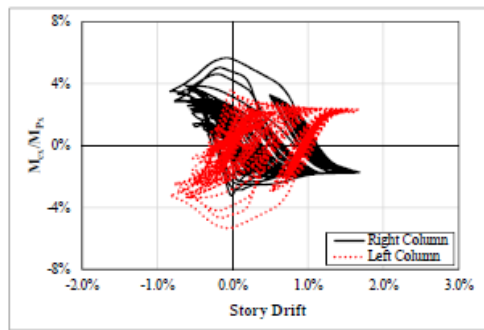
Column P-M Interaction Diagram



Column In-plane Bending Demand



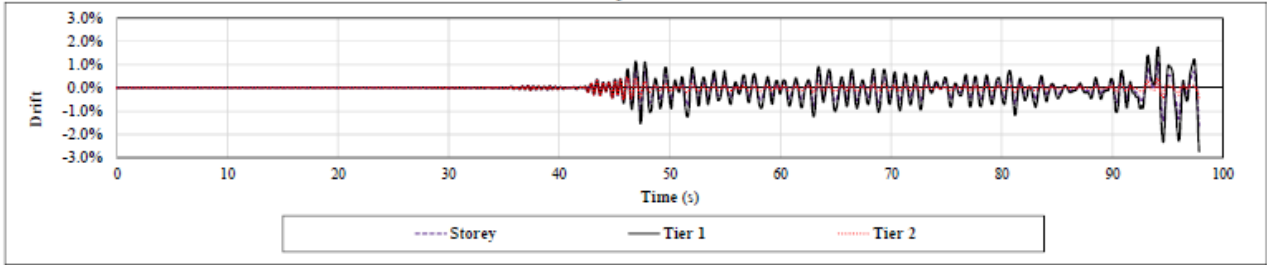
Column Out-of-plane Bending Demand



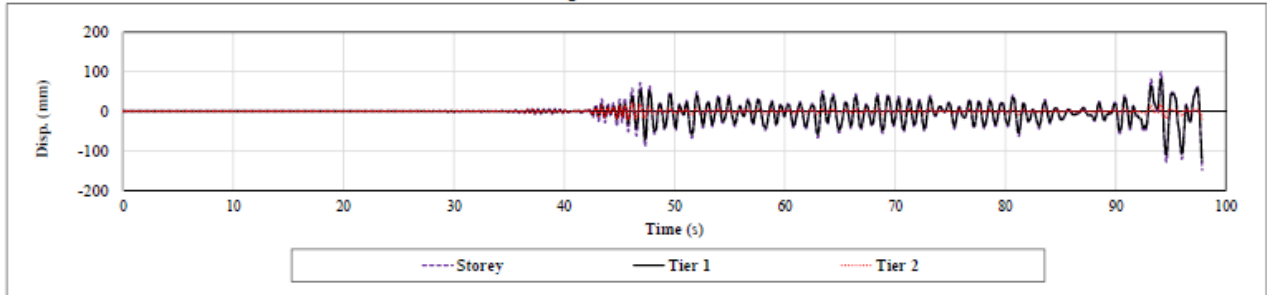
Ground Motion: SCI 7

Two-Tiered SCBF: AISC 341-10 Design

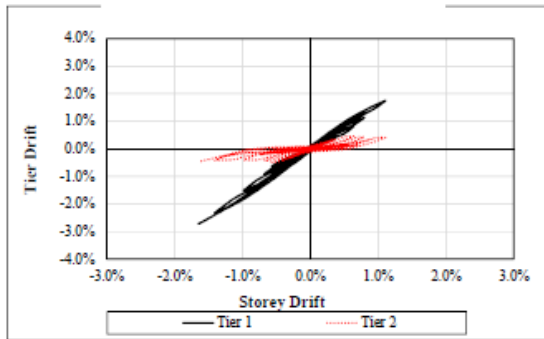
Drift vs. Time



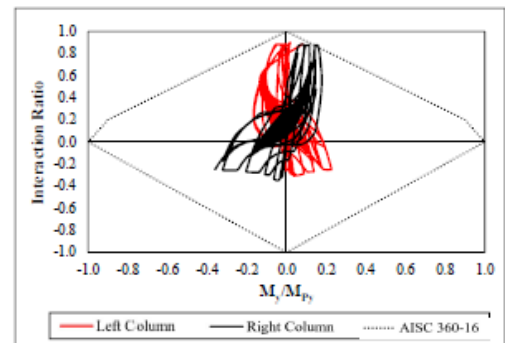
Displacement vs. Time



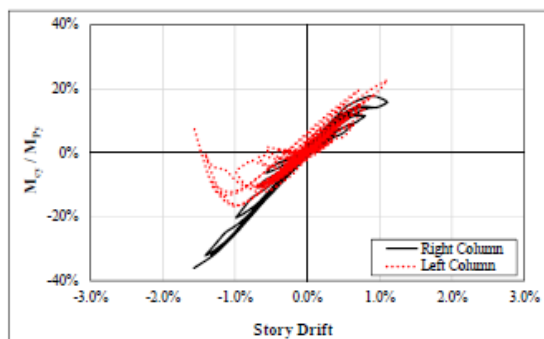
Tier Drift vs. Storey Drift



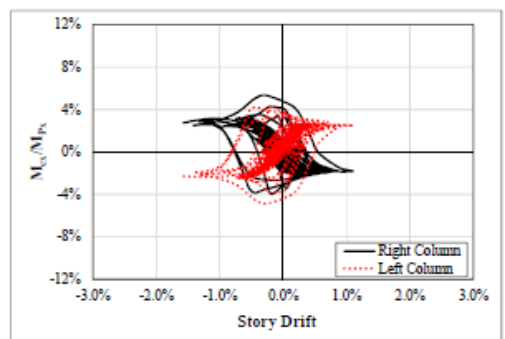
Column P-M Interaction Diagram



Column In-plane Bending Demand



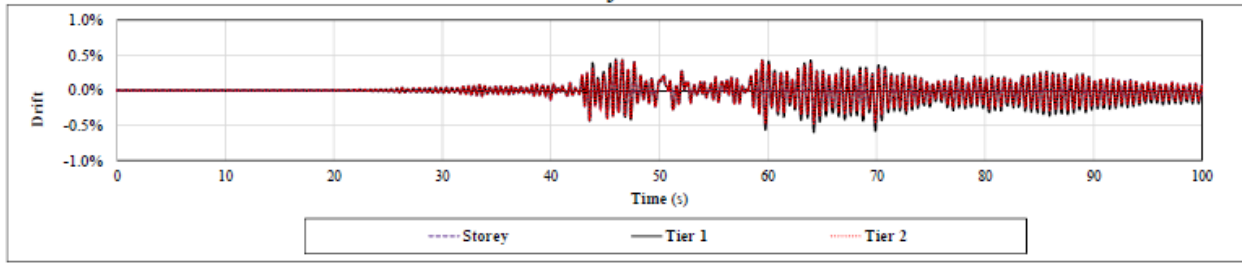
Column Out-of-plane Bending Demand



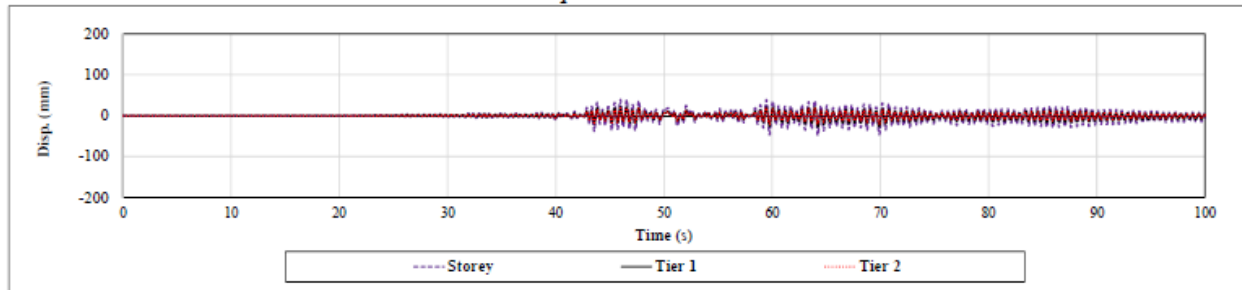
Ground Motion: SCI 8

Two-Tiered SCBF: AISC 341-10 Design

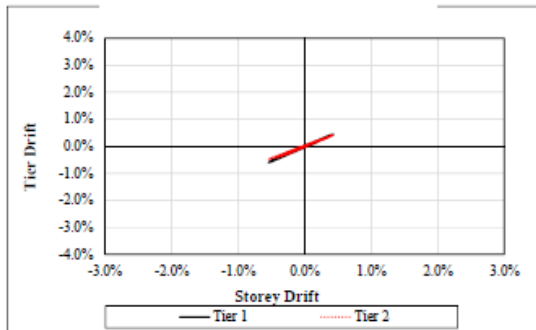
Drift vs. Time



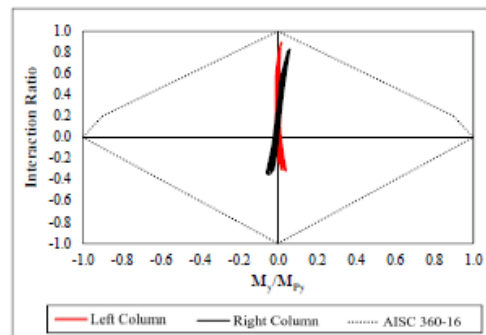
Displacement vs. Time



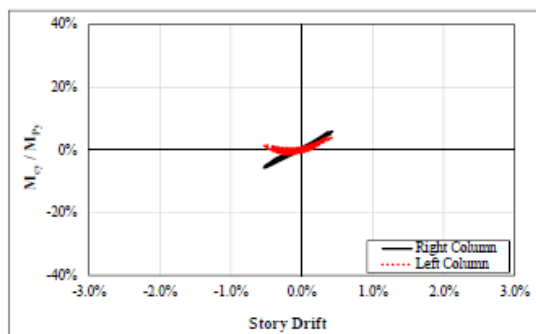
Tier Drift vs. Storey Drift



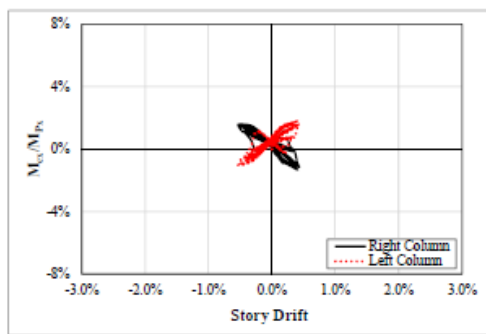
Column P-M Interaction Diagram



Column In-plane Bending Demand



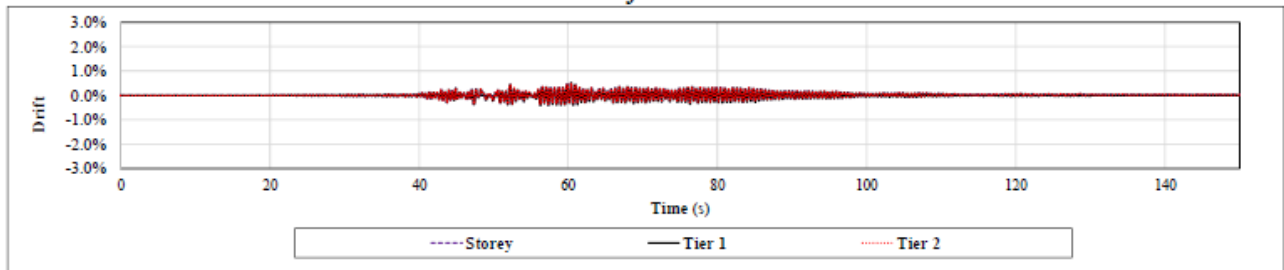
Column Out-of-plane Bending Demand



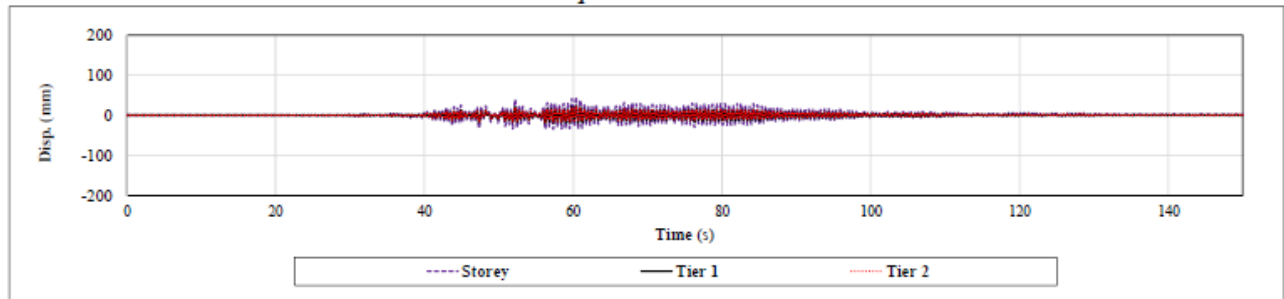
Ground Motion: SCI 9

Two-Tiered SCBF: AISC 341-10 Design

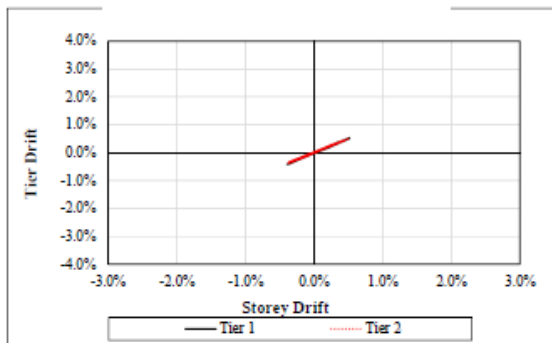
Drift vs. Time



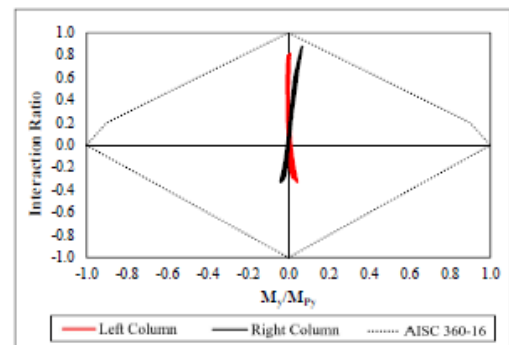
Displacement vs. Time



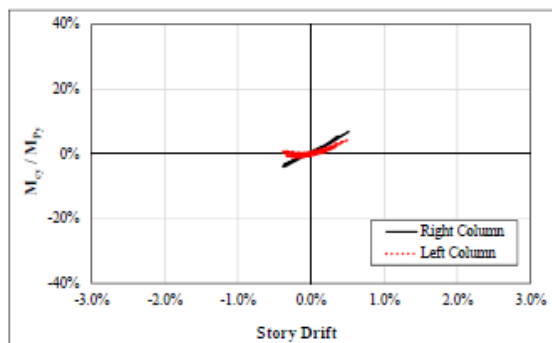
Tier Drift vs. Storey Drift



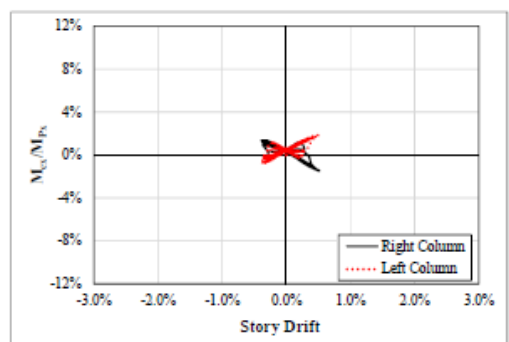
Column P-M Interaction Diagram



Column In-plane Bending Demand



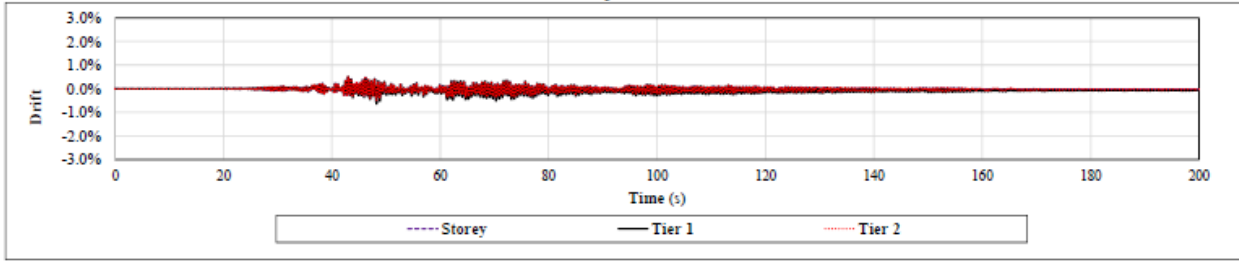
Column Out-of-plane Bending Demand



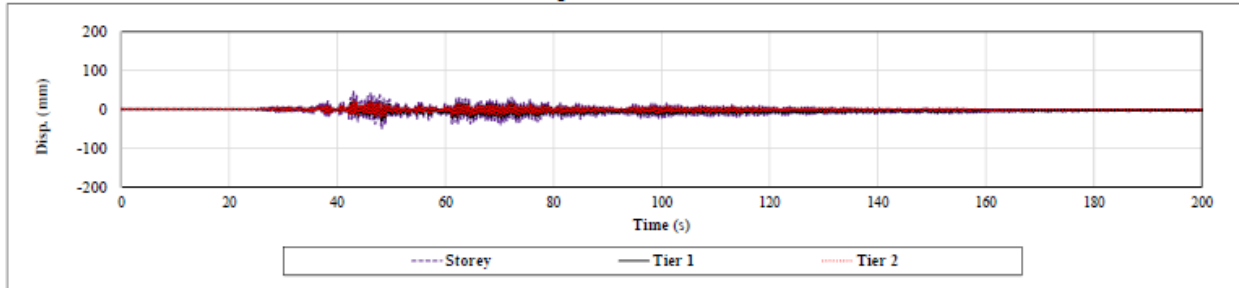
Ground Motion: SCI 10

Two-Tiered SCBF: AISC 341-10 Design

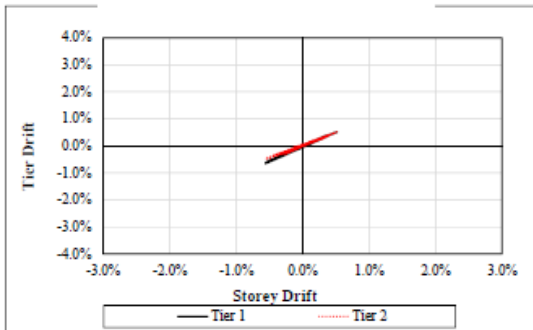
Drift vs. Time



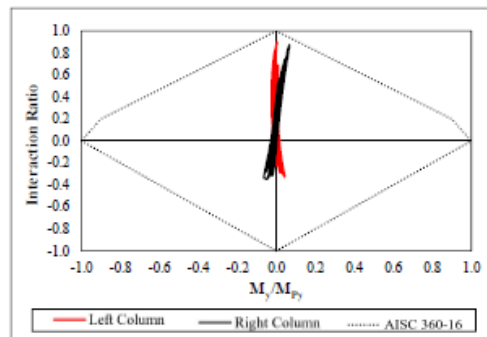
Displacement vs. Time



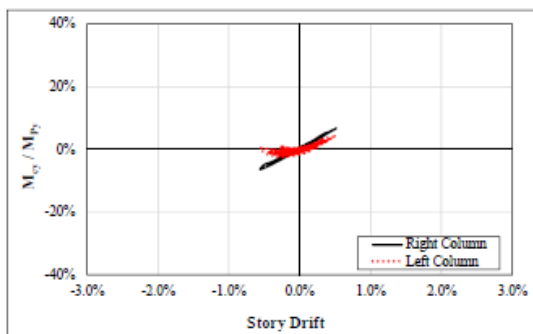
Tier Drift vs. Storey Drift



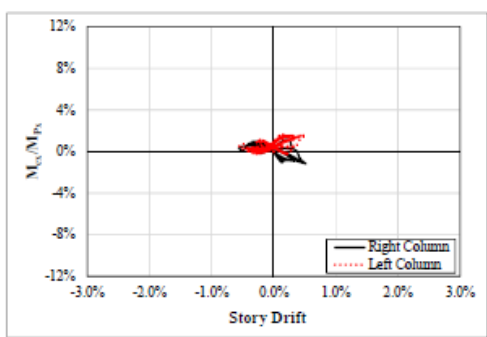
Column P-M Interaction Diagram



Column In-plane Flexure Demand



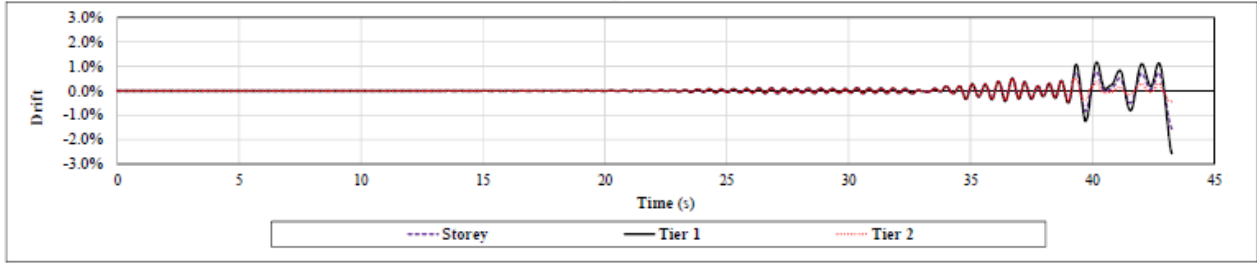
Column Out-of-plane Flexure Demand



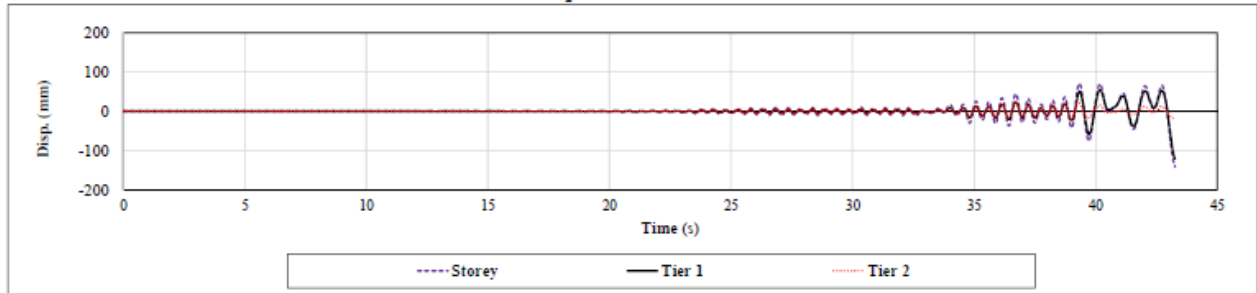
Ground Motion: SCI 11

Two-Tiered SCBF: AISC 341-10 Design

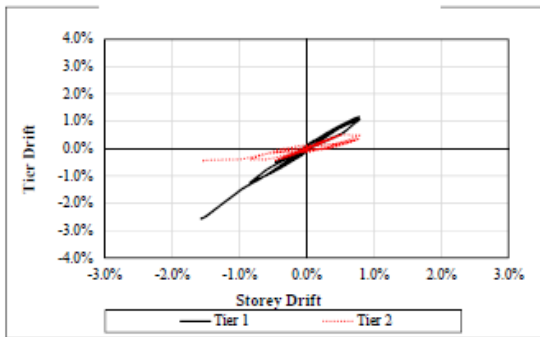
Drift vs. Time



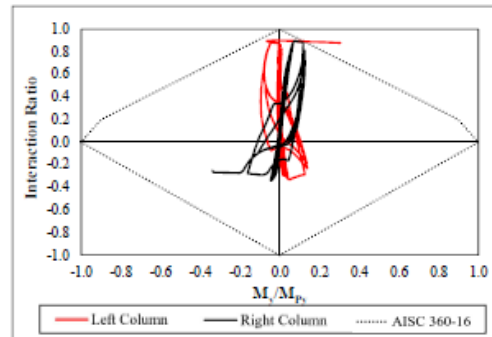
Displacement vs. Time



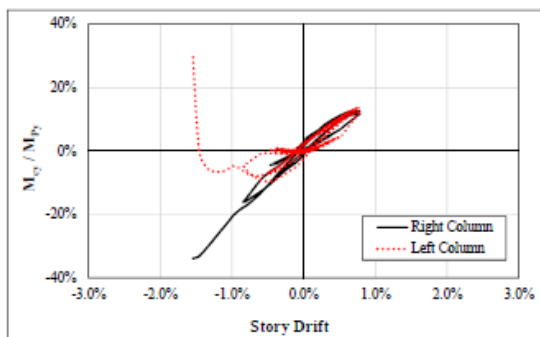
Tier Drift vs. Storey Drift



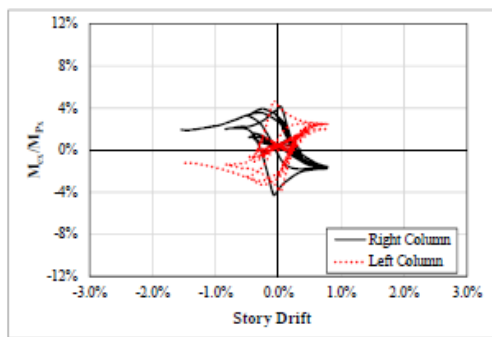
Column P-M Interaction Diagram



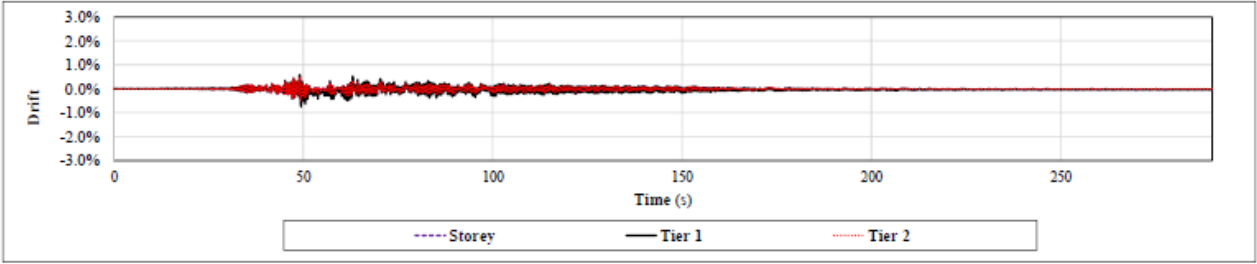
Column In-plane Flexure Demand



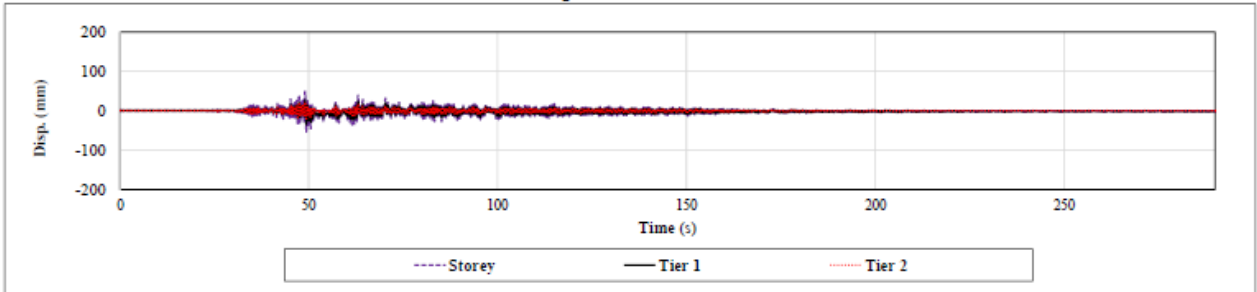
Column Out-of-plane Flexure Demand



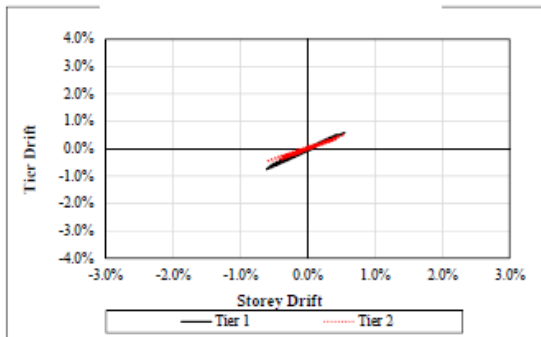
Drift vs. Time



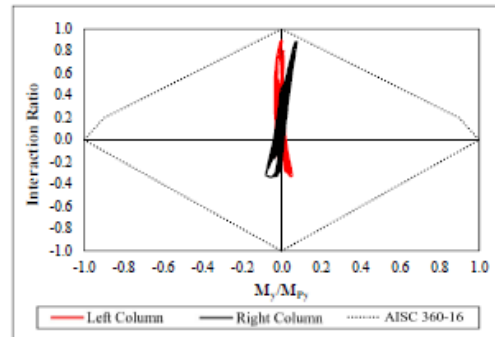
Displacement vs. Time



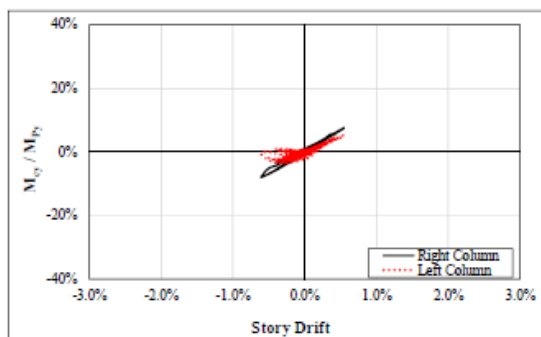
Tier Drift vs. Storey Drift



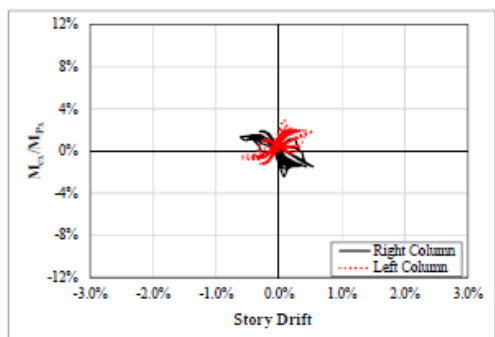
Column P-M Interaction Diagram



Column In-plane Bending Demand



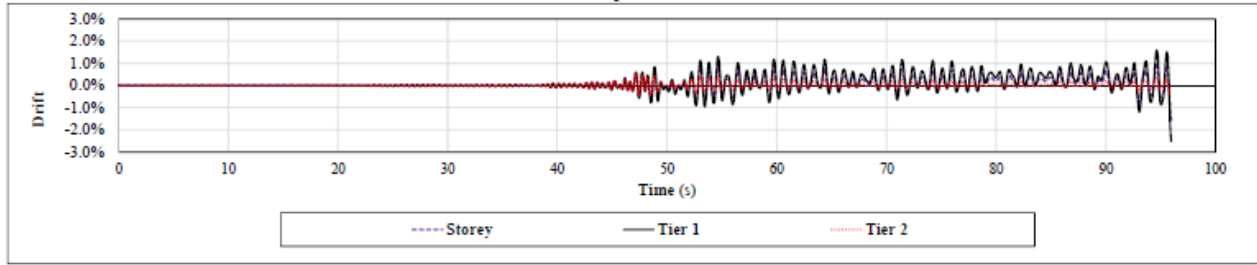
Column Out-of-plane Bending Demand



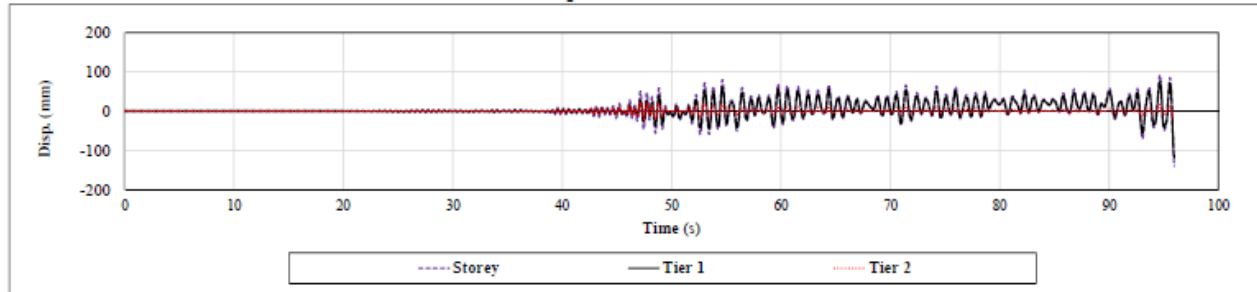
Ground Motion: SCI 13

Two-Tiered SCBF: AISC 341-10 Design

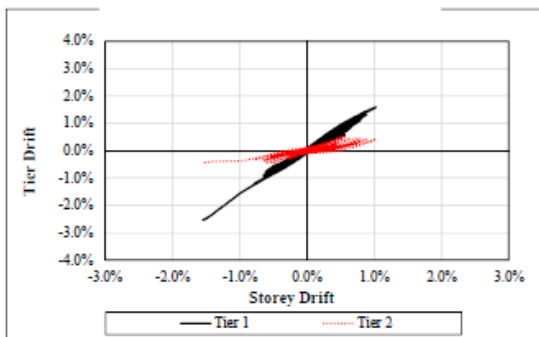
Drift vs. Time



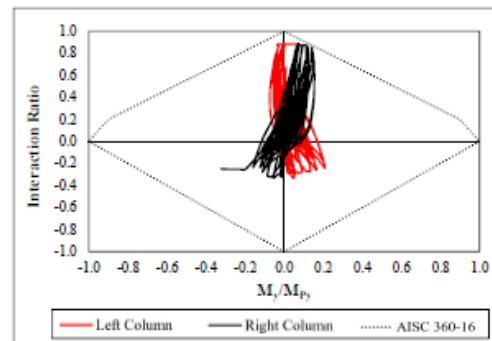
Displacement vs. Time



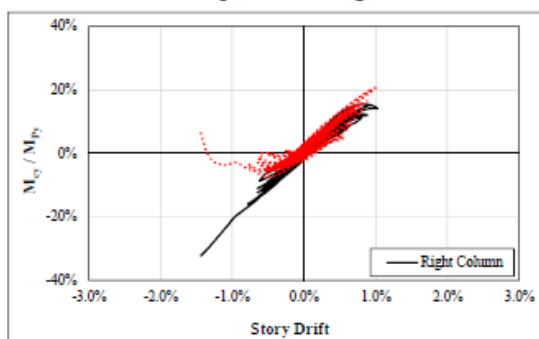
Tier Drift vs. Storey Drift



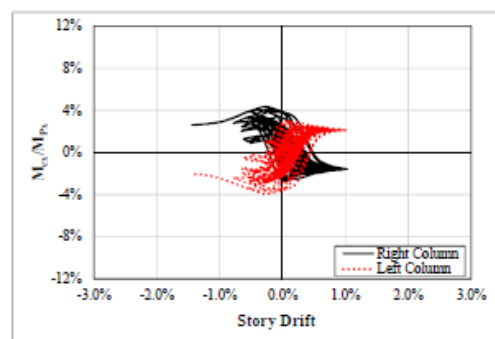
Column P-M Interaction Diagram



Column In-plane Bending Demand



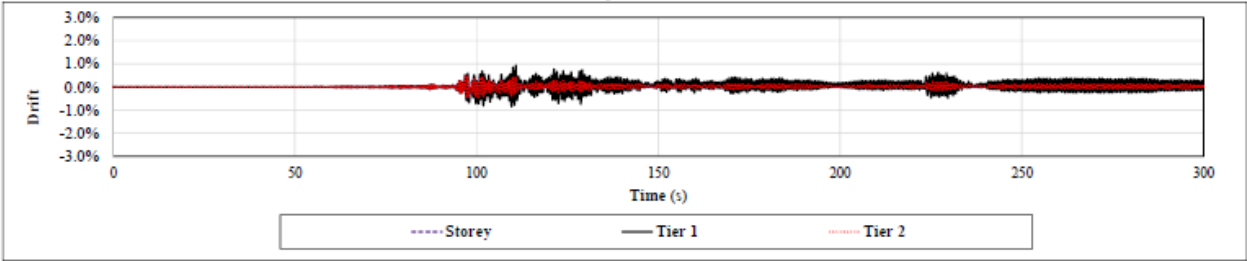
Column Out-of-plane Bending Demand



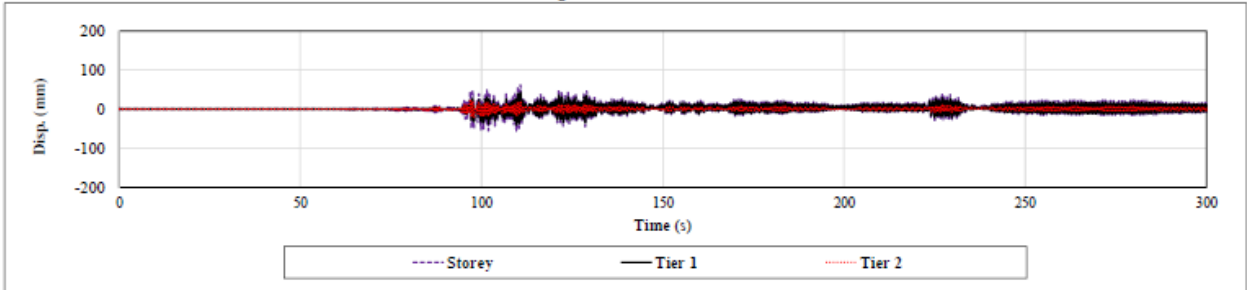
Ground Motion: SCI 14

Two-Tiered SCBF: AISC 341-10 Design

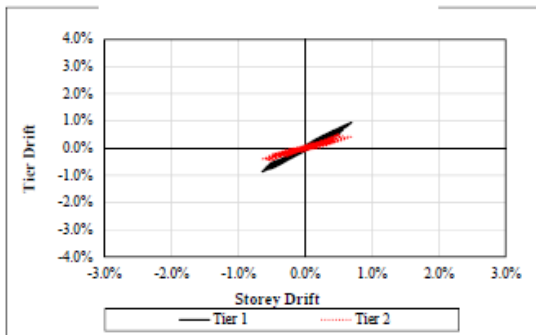
Drift vs. Time



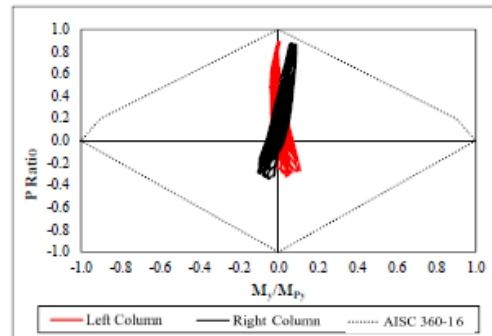
Displacement vs. Time



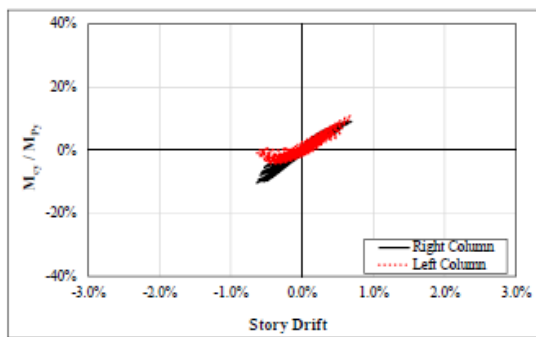
Tier Drift vs. Storey Drift



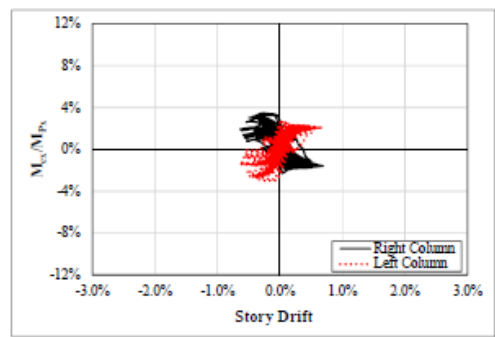
Column P-M Interaction Diagram



Column In-plane Bending Demand



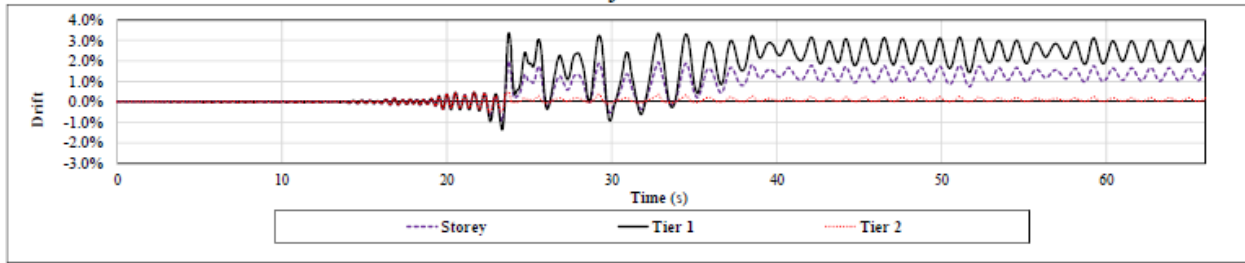
Column Out-of-plane Bending Demand



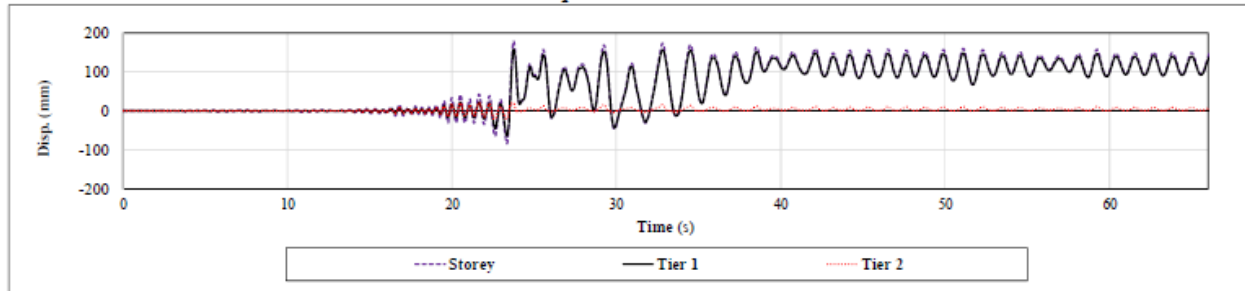
Ground Motion: SCI 15

Tow-Tiered SCBF: AISC 341-10 Design

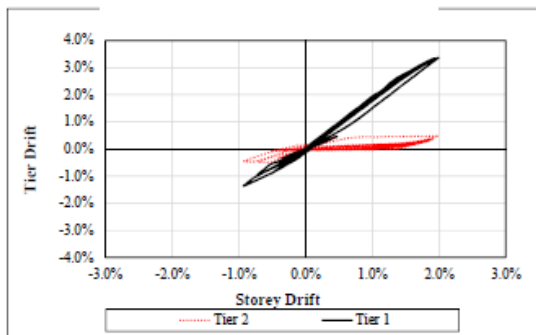
Drift vs. Time



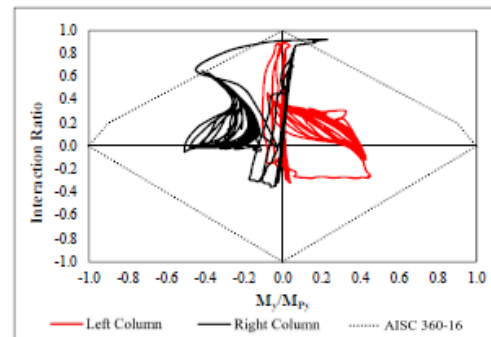
Displacement vs. Time



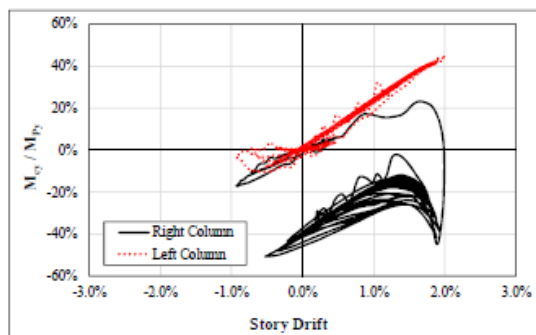
Tier Drift vs. Storey Drift



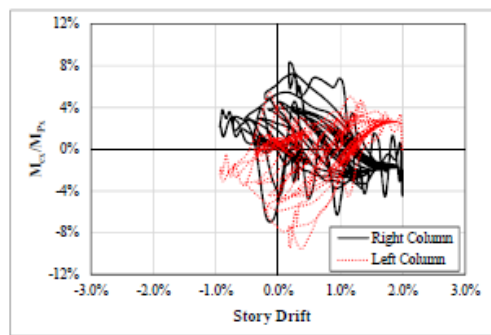
Column P-M Interaction Diagram



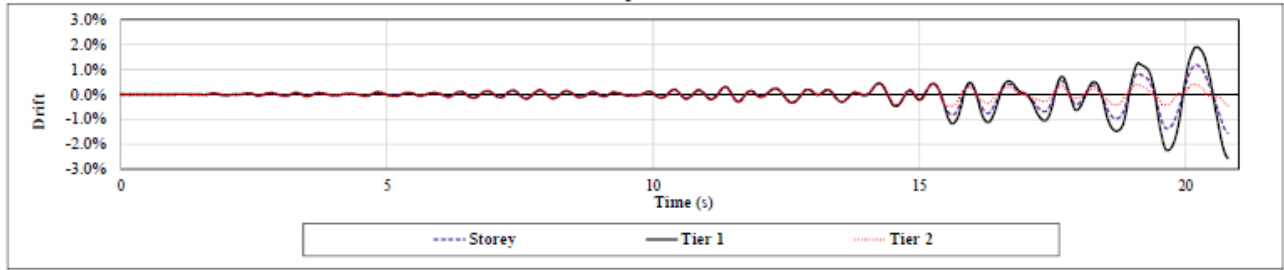
Column In-plane Bending Demand



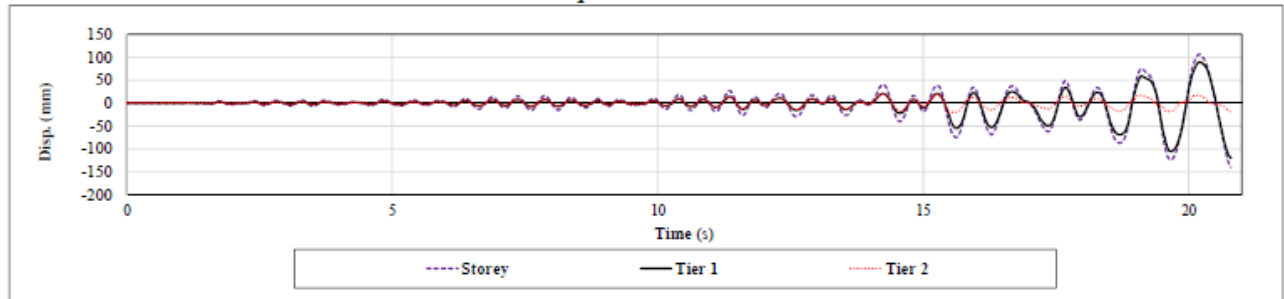
Column Out-of-plane Bending Demand



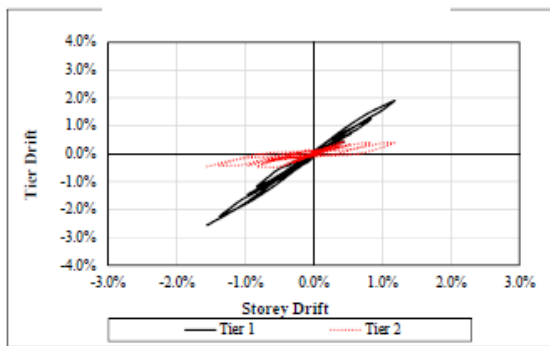
Drift vs. Time



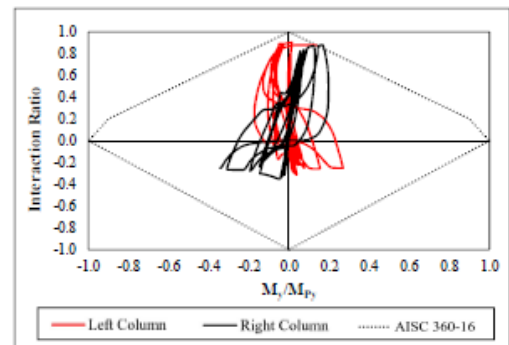
Displacement vs. Time



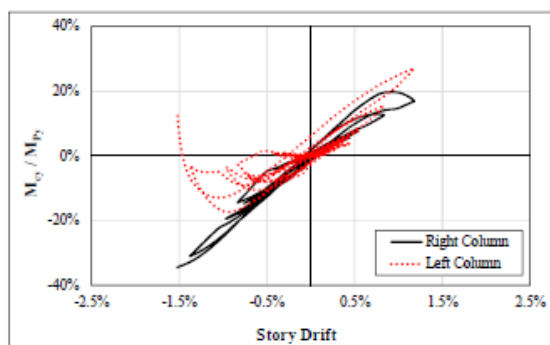
Tier Drift vs. Storey Drift



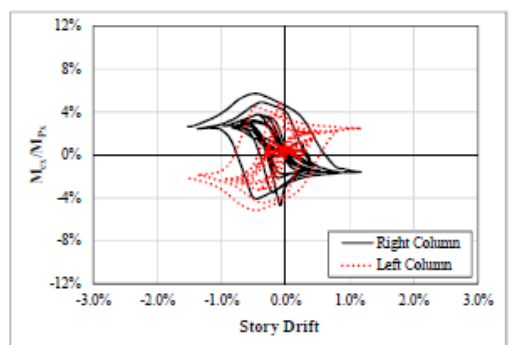
Column P-M Interaction Diagram



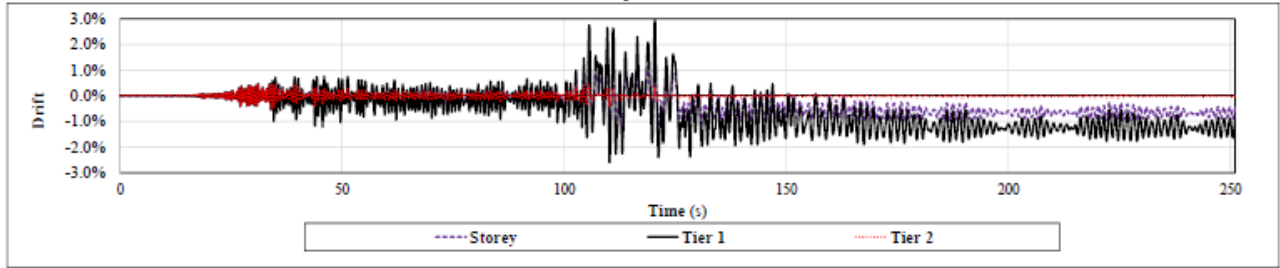
Column In-plane Bending Demand



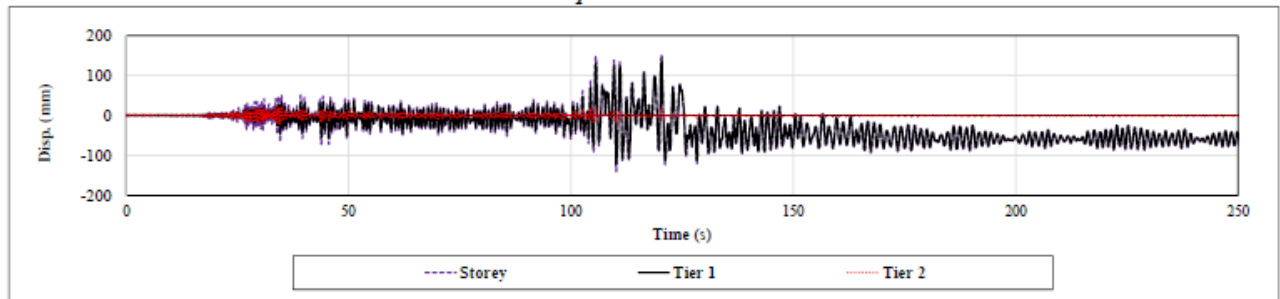
Column Out-of-plane Bending Demand



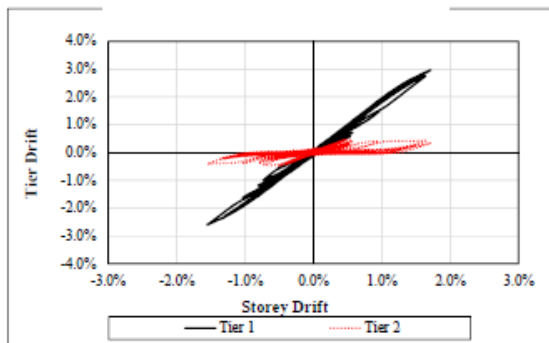
Drift vs. Time



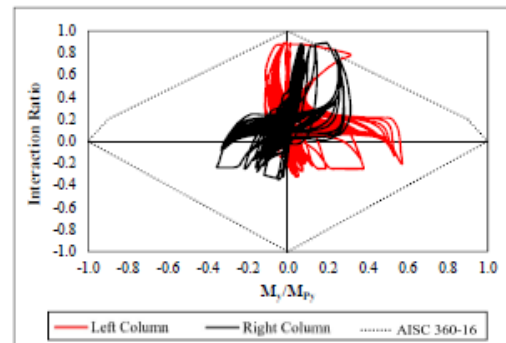
Displacement vs. Time



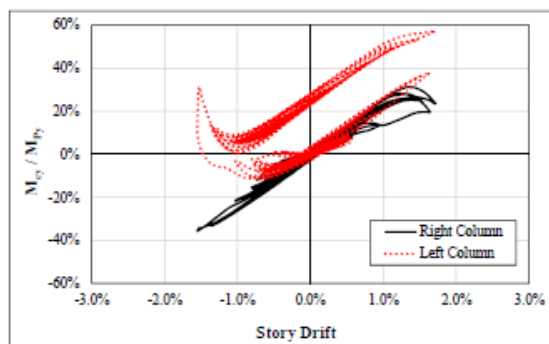
Tier Drift vs. Storey Drift



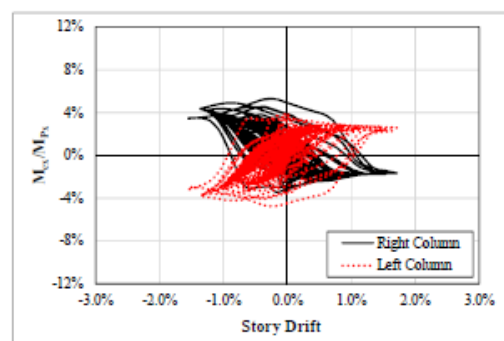
Column P-M Interaction Diagram



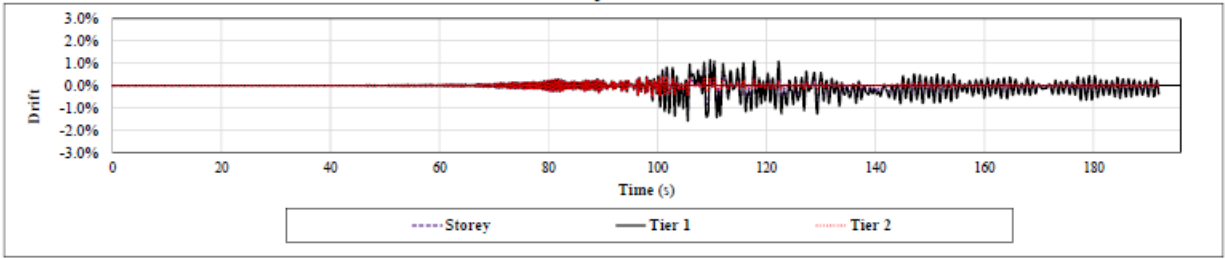
Column In-plane Bending Demand



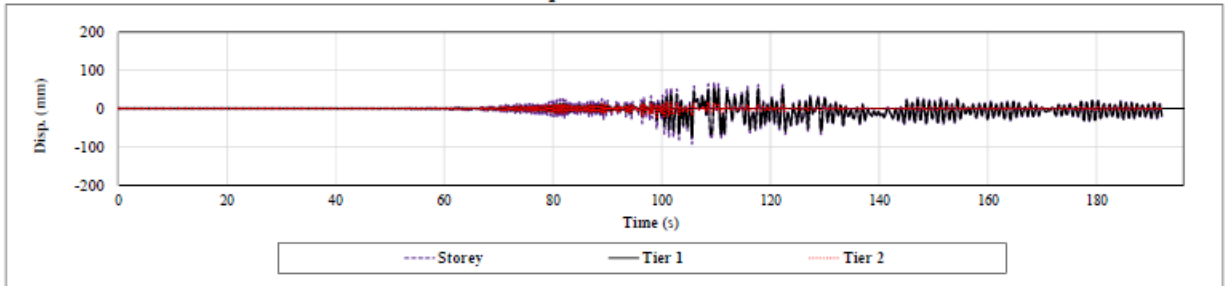
Column Out-of-plane Bending Demand



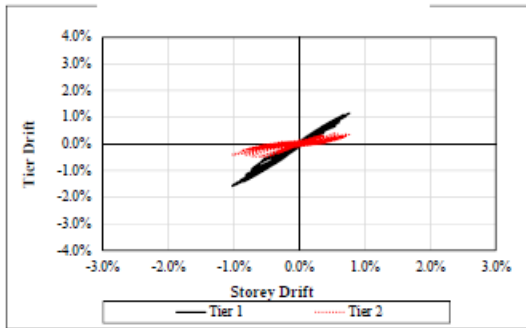
Drift vs. Time



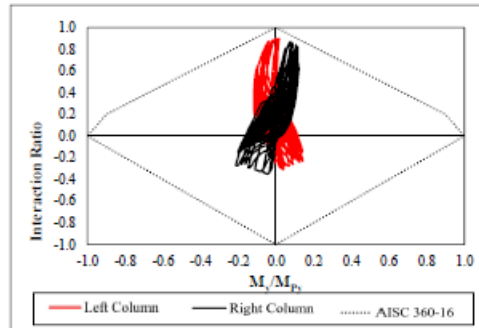
Displacement vs. Time



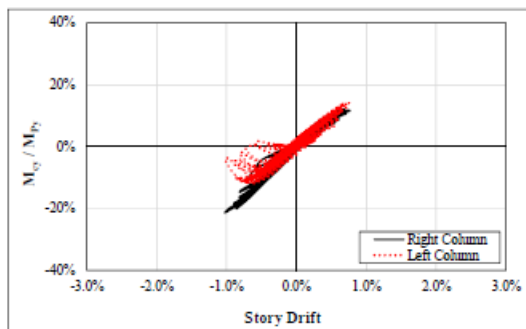
Tier Drift vs. Storey Drift



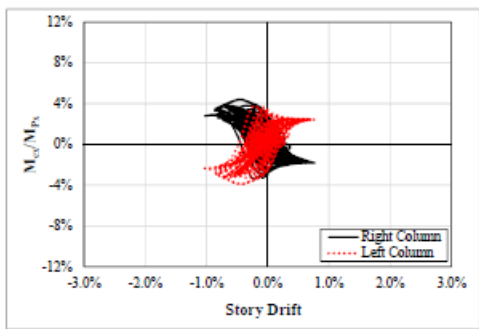
Column P-M Interaction Diagram



Column In-plane Bending Demand



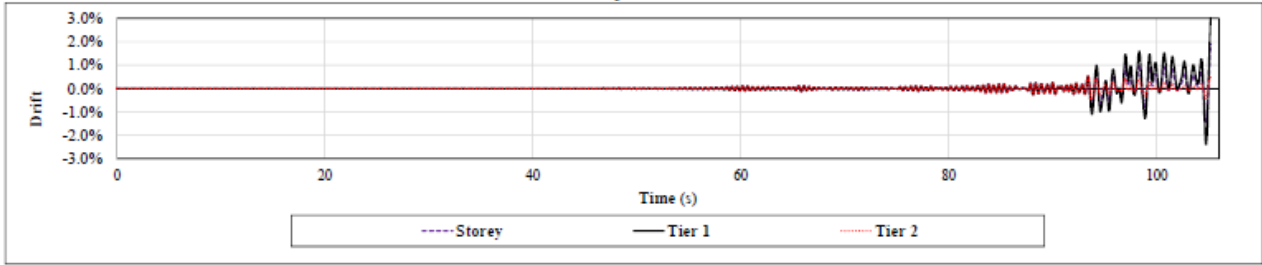
Column Out-of-plane Bending Demand



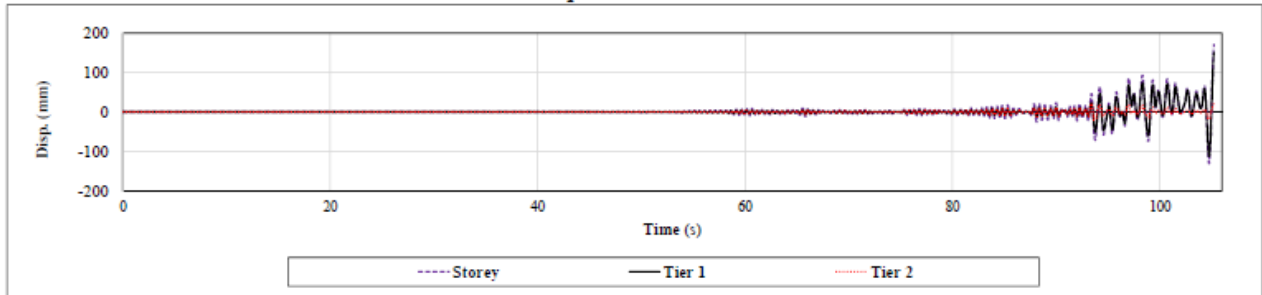
Ground Motion: SCI 19

Two-Tiered SCBF: AISC 341-10 Design

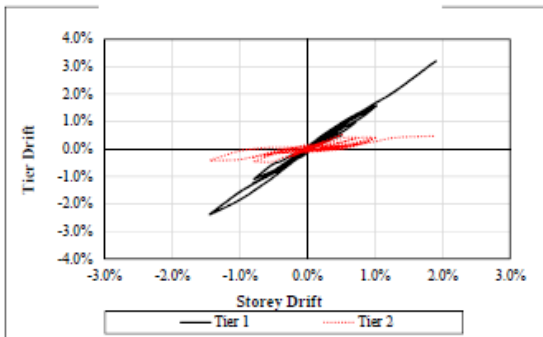
Drift vs. Time



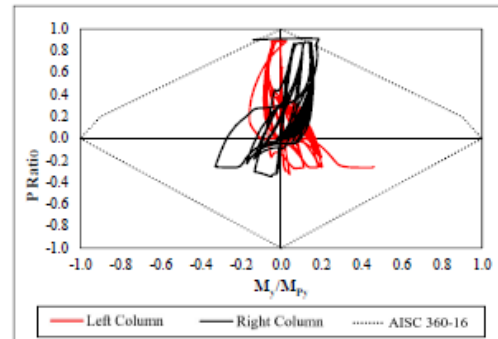
Displacement vs. Time



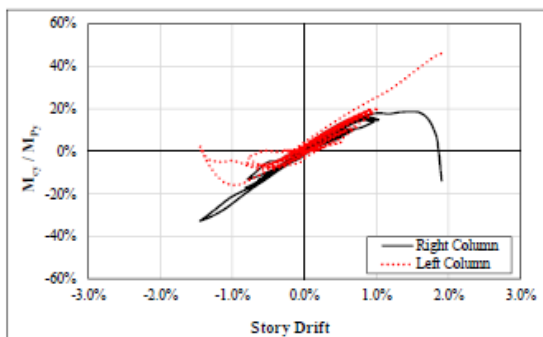
Tier Drift vs. Storey Drift



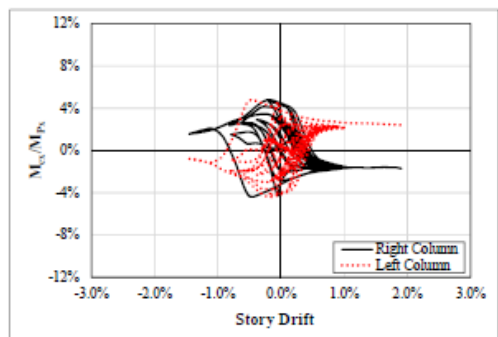
Column P-M Interaction Diagram



Column In-plane Bending Demand



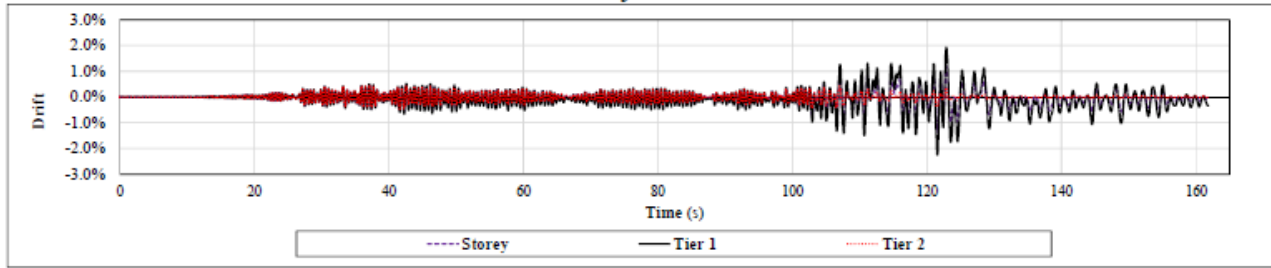
Column Out-of-plane Bending Demand



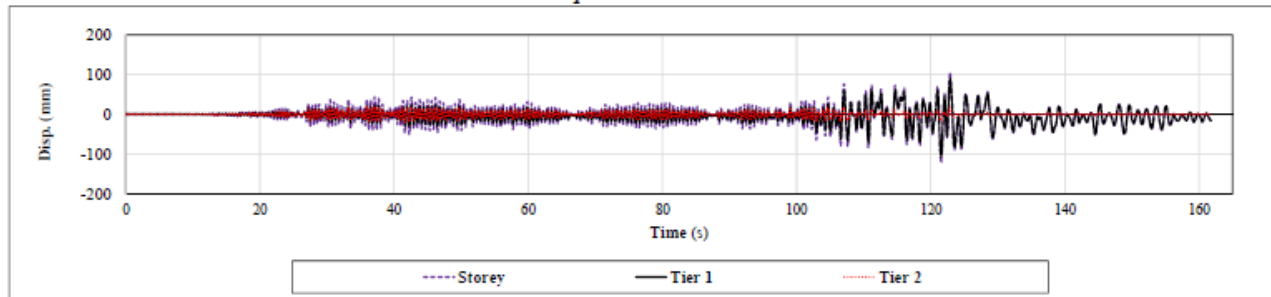
Ground Motion: SCI 20

Two-Tiered SCBF: AISC 341-10 Design

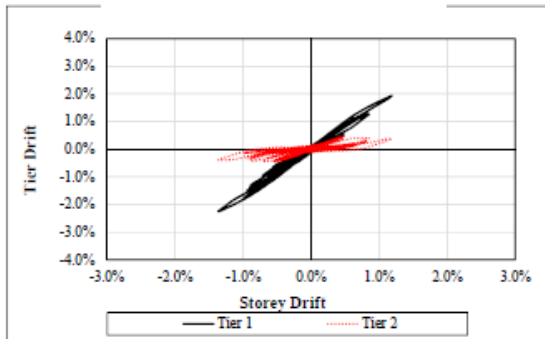
Drift vs. Time



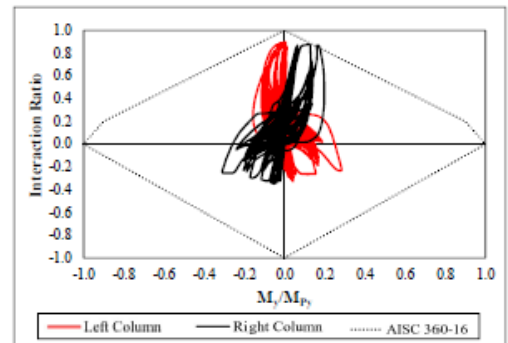
Displacement vs. Time



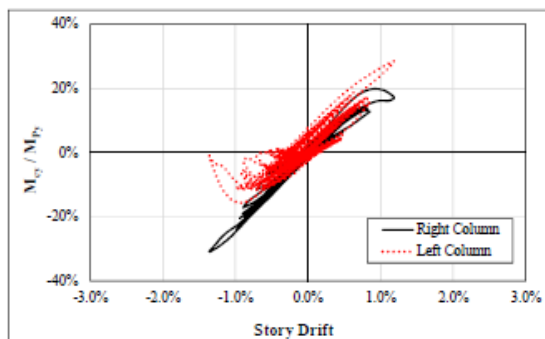
Tier Drift vs. Storey Drift



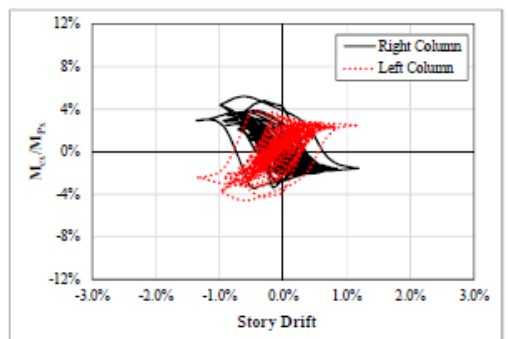
Column P-M Interaction Diagram



Column In-plane Bending Demand



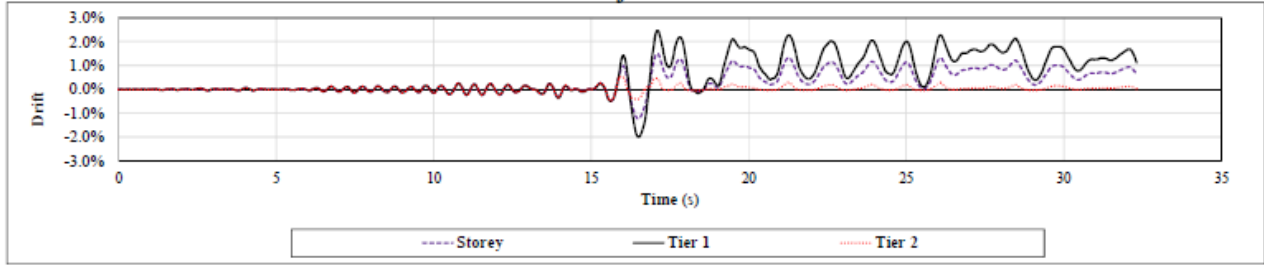
Column Out-of-plane Bending Demand



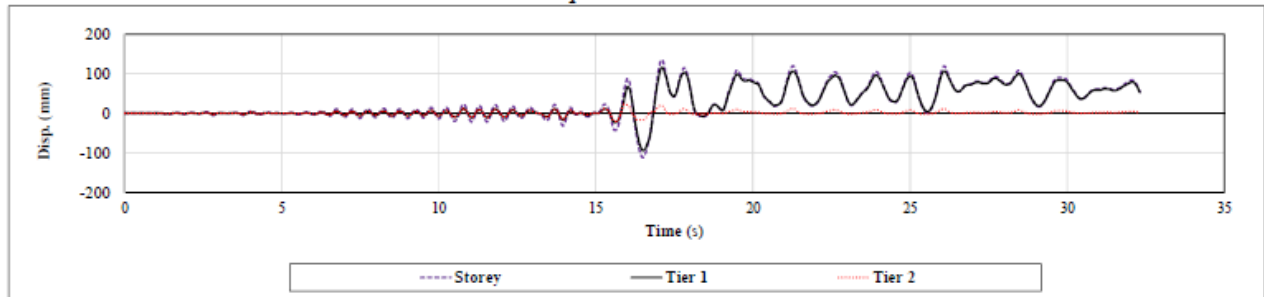
Ground Motion: SCI 21

Two-Tiered SCBF: AISC 341-10 Design

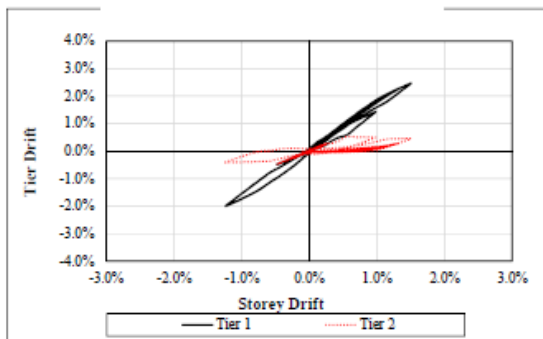
Drift vs. Time



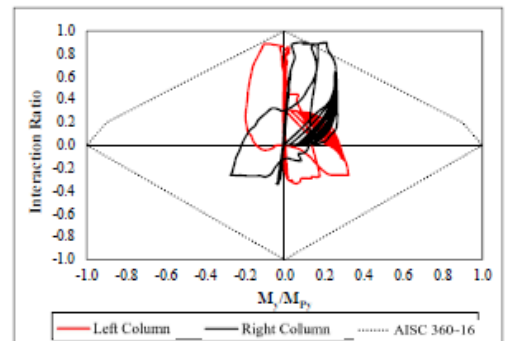
Displacement vs. Time



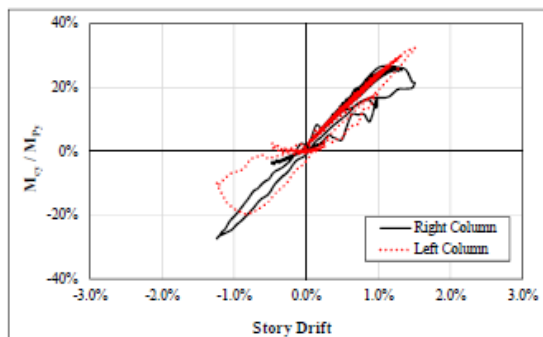
Tier Drift vs. Storey Drift



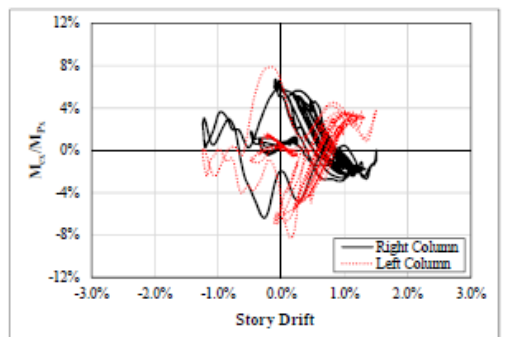
Column P-M Interaction Diagram



Column In-plane Bending Demand



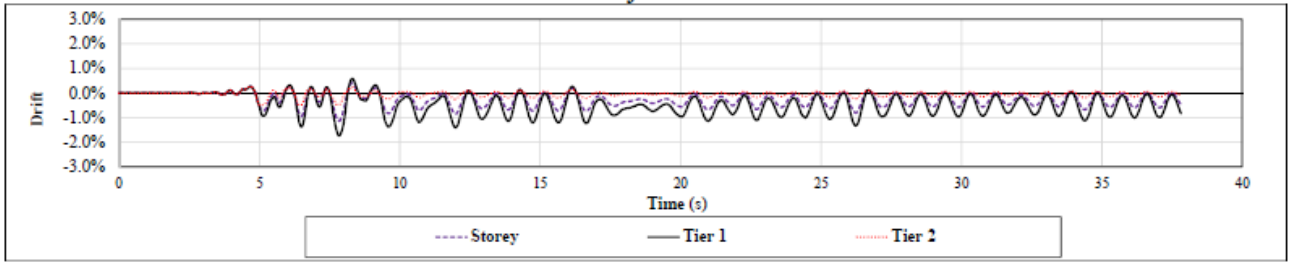
Column Out-of-plane Bending Demand



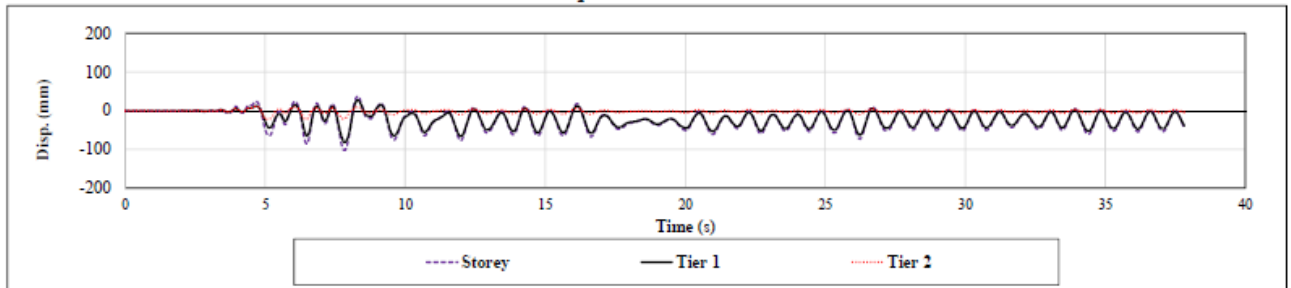
Ground Motion: SCC 1

Two-Tiered SCBF: AISC 341-10 Design

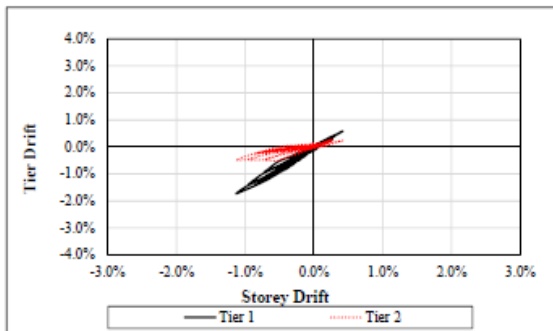
Drift vs. Time



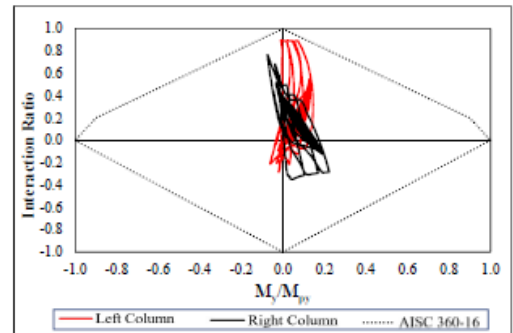
Displacement vs. Time



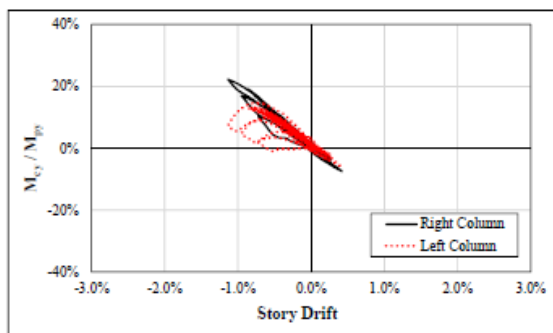
Tier Drift vs. Storey Drift



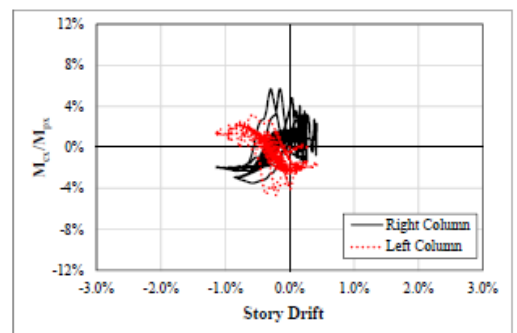
Column P-M Interaction Diagram



Column In-plane Bending Demand



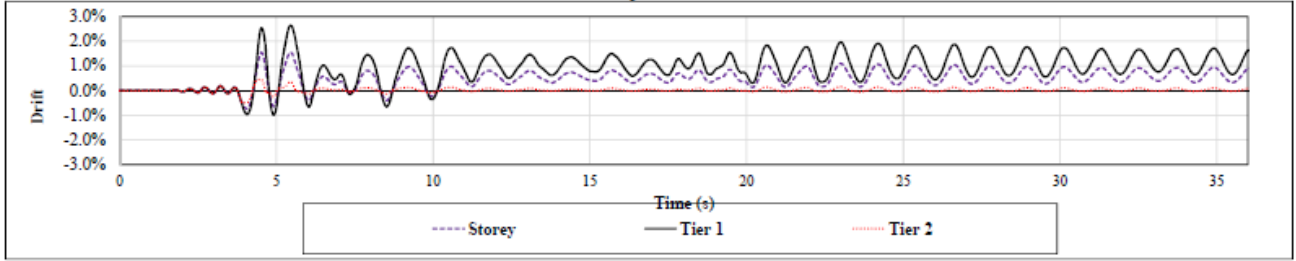
Column Out-of-plane Bending Demand



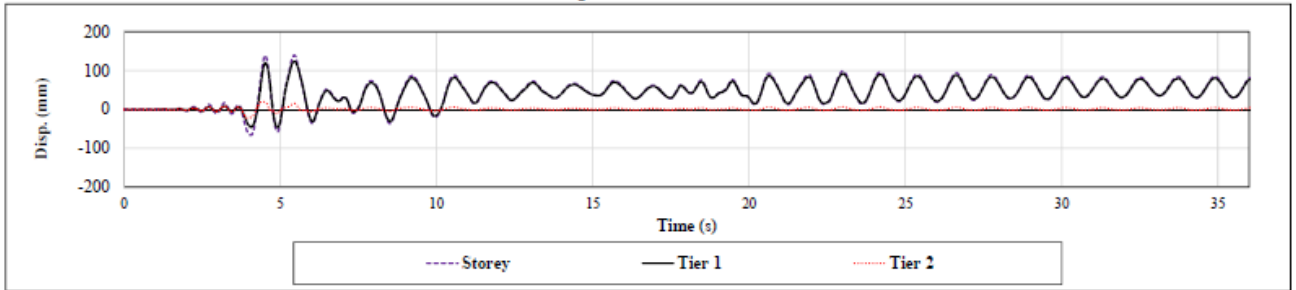
Ground Motion: SCC 2

Two-Tiered SCBF: AISC 341-10 Design

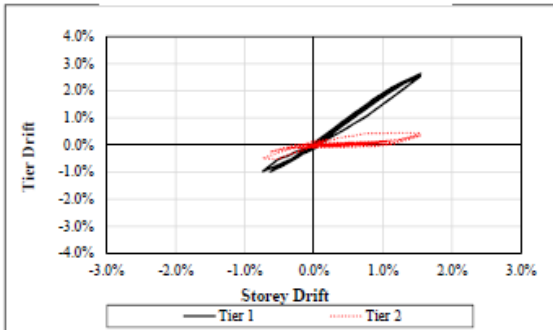
Drift vs. Time



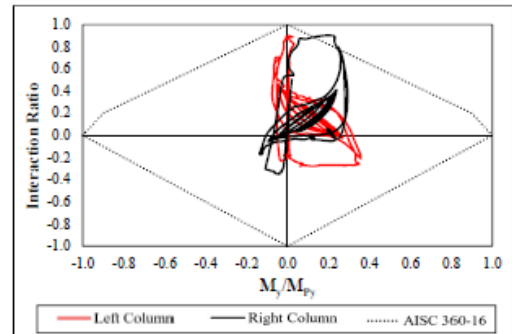
Displacement vs. Time



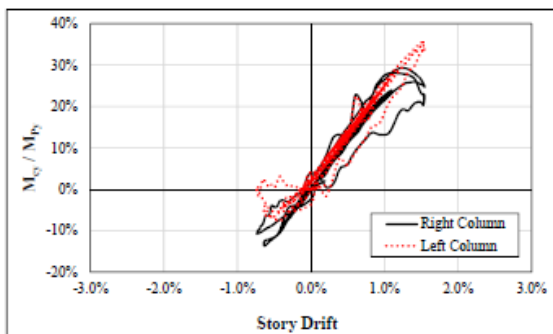
Tier Drift vs. Storey Drift



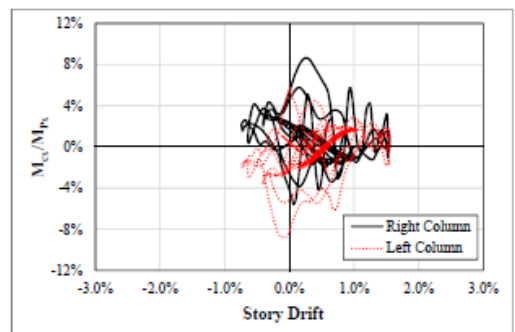
Column P-M Interaction Diagram



Column In-plane Bending Demand



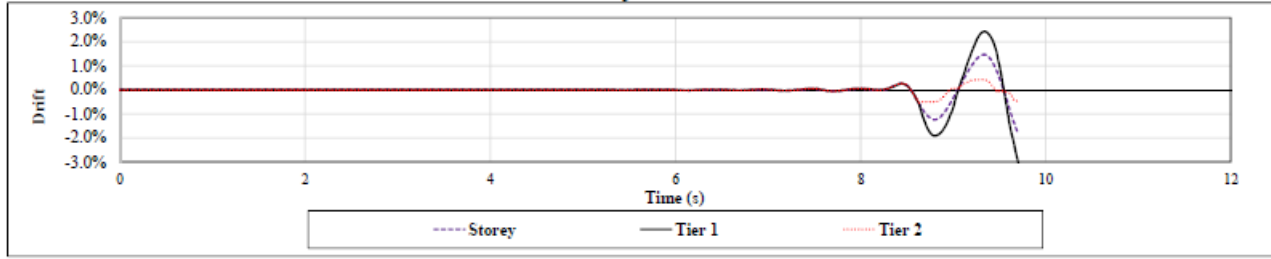
Column Out-of-plane Bending Demand



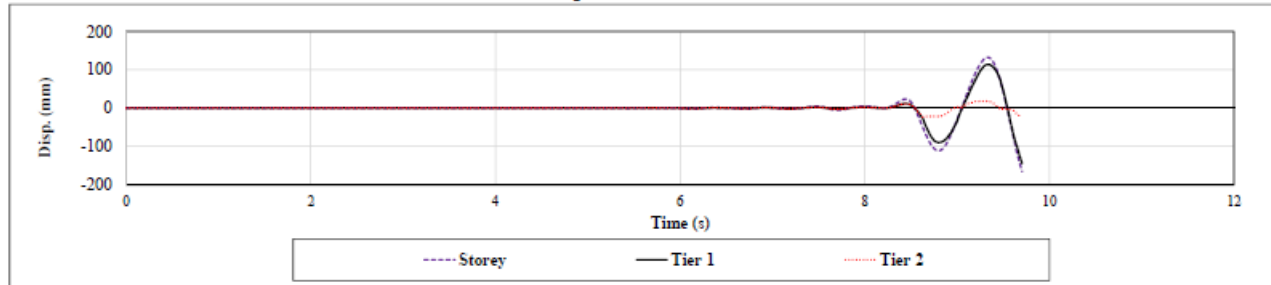
Ground Motion: SCC 3

Two-Tiered SCBF: AISC 341-10 Design

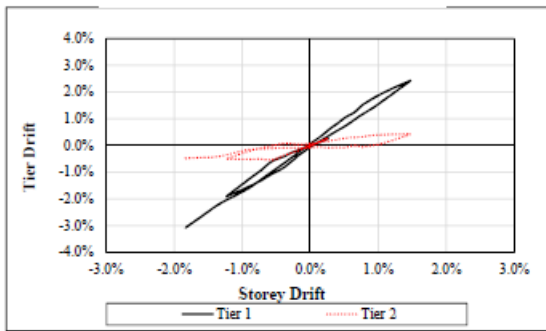
Drift vs. Time



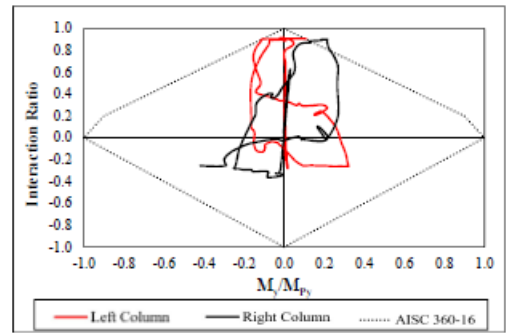
Displacement vs. Time



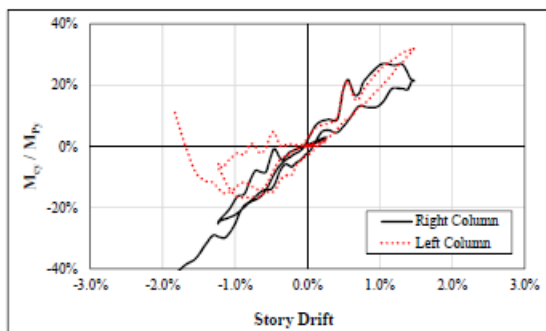
Tier Drift vs. Storey Drift



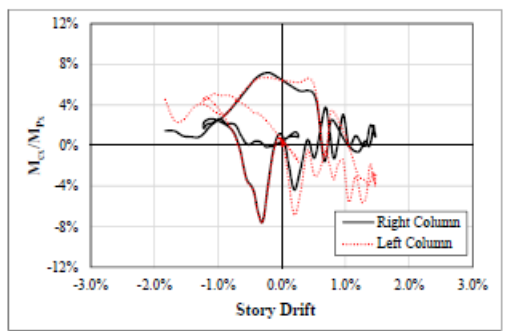
Column P-M Interaction Diagram



Column In-plane Bending Demand



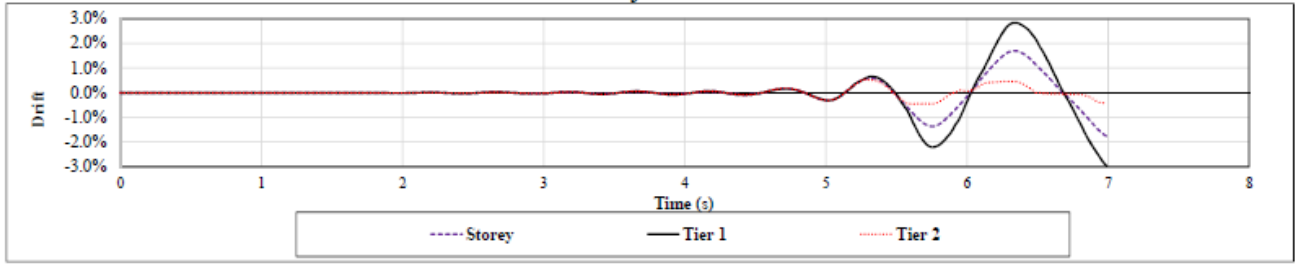
Column Out-of-plane Bending Demand



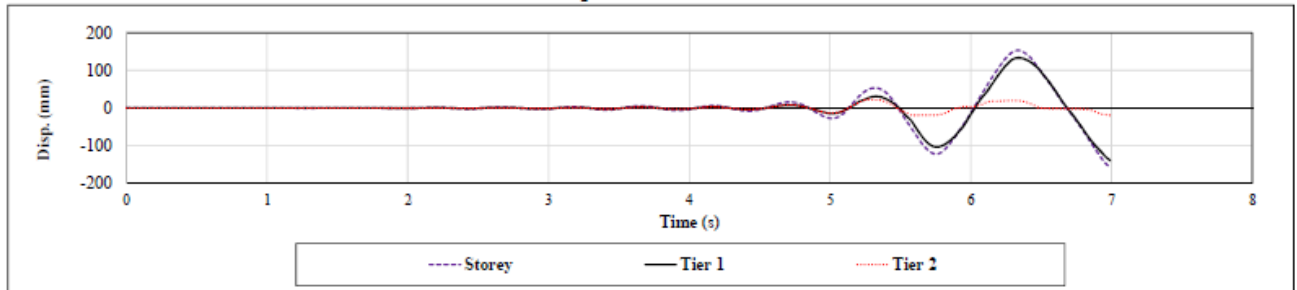
Ground Motion: SCC 4

Two-Tiered SCBF: AISC 341-10 Design

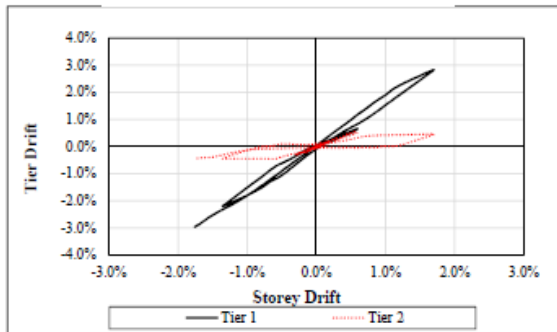
Drift vs. Time



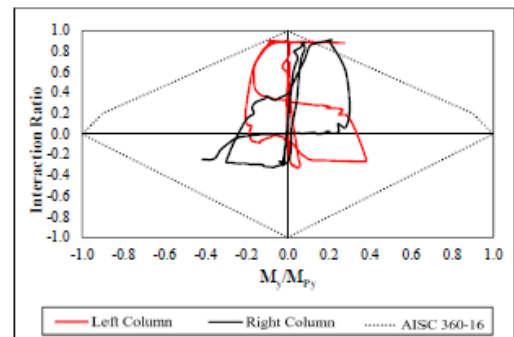
Displacement vs. Time



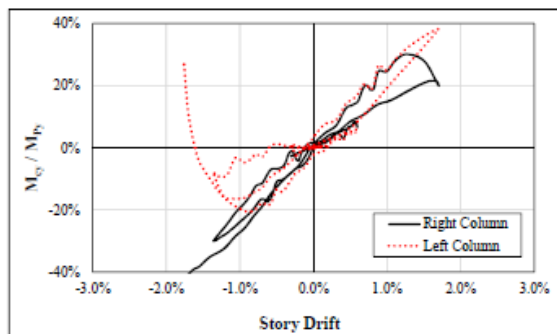
Tier Drift vs. Storey Drift



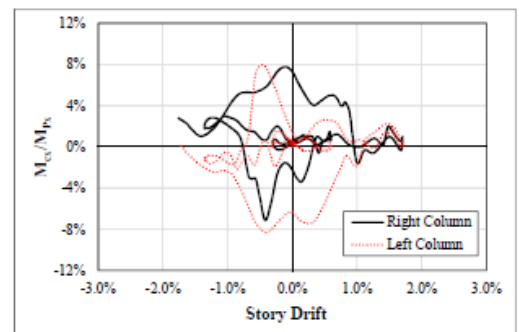
Column P-M Interaction Diagram



Column In-plane Bending Demand



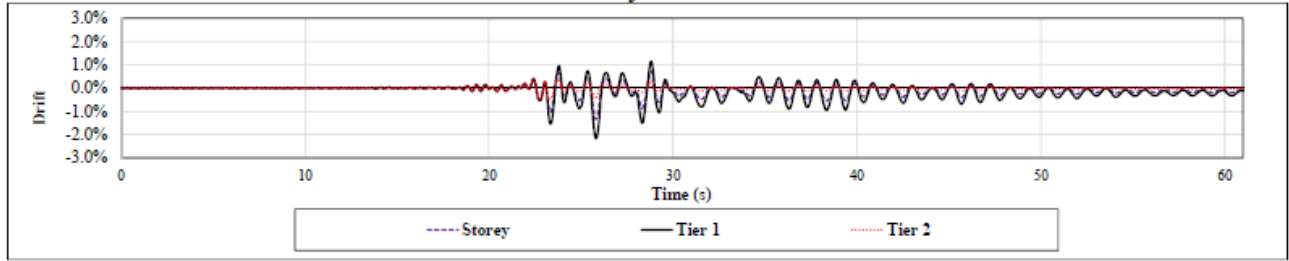
Column Out-of-plane Bending Demand



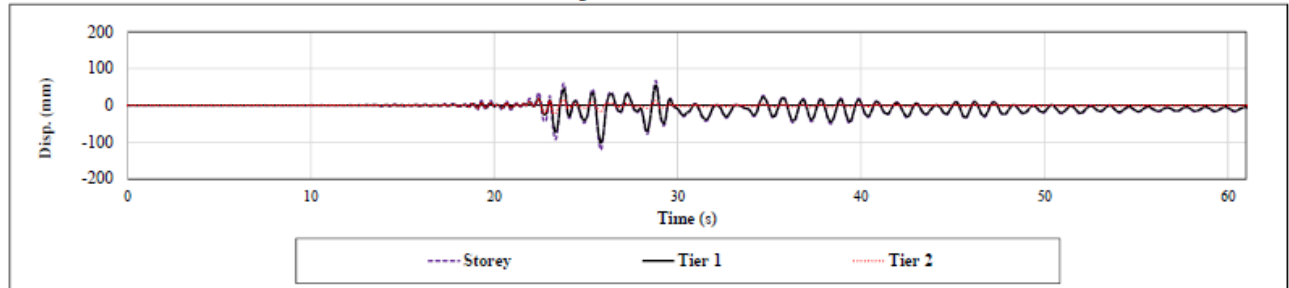
Ground Motion: SCC 5

Two-Tiered SCBF: AISC 341-10 Design

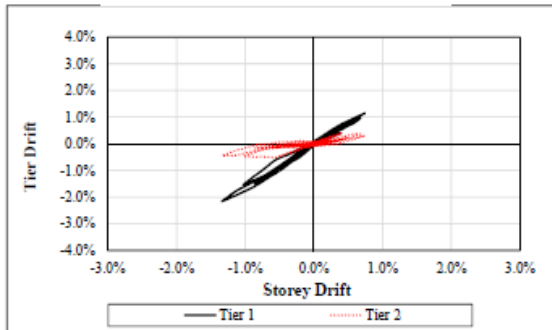
Drift vs. Time



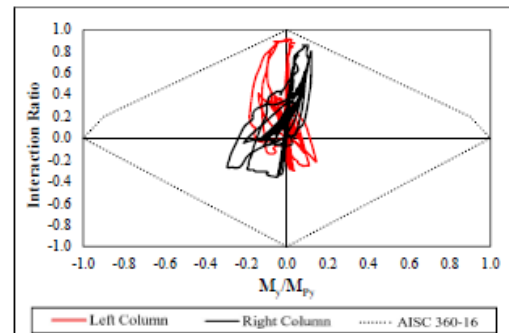
Displacement vs. Time



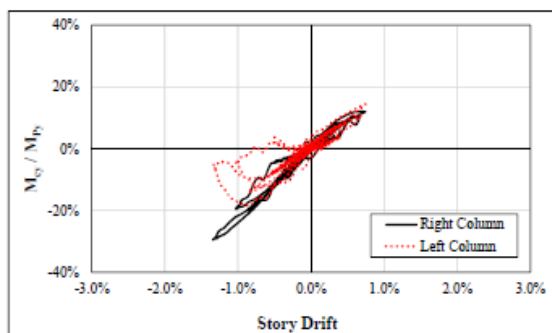
Tier Drift vs. Storey Drift



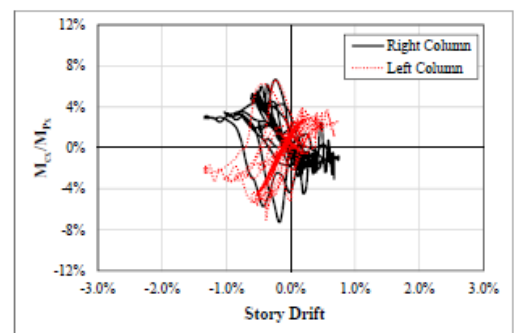
Column P-M Interaction Diagram



Columns In-plane Bending Demand



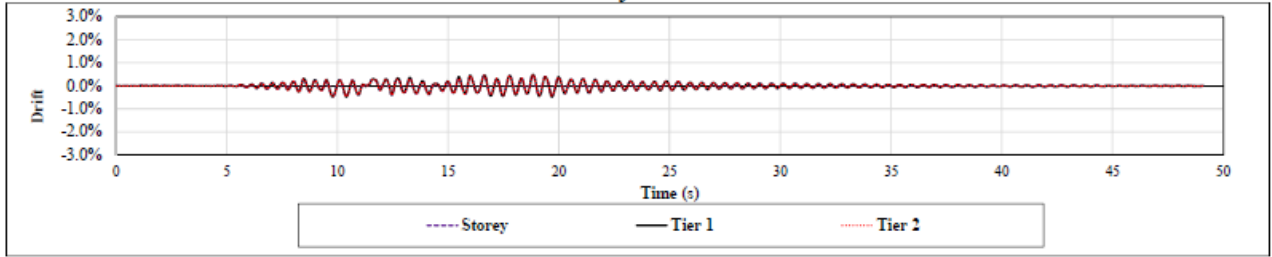
Column Out-of-plane Bending Demand



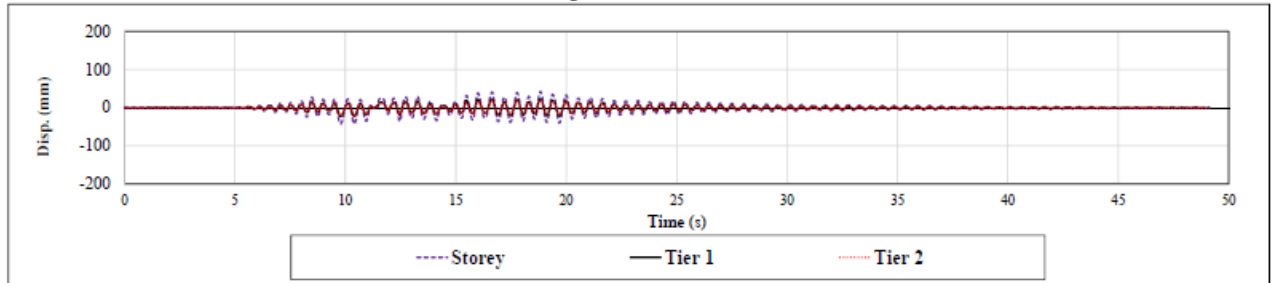
Ground Motion: SCC 6

Two-Tiered SCBF: AISC 341-10 Design

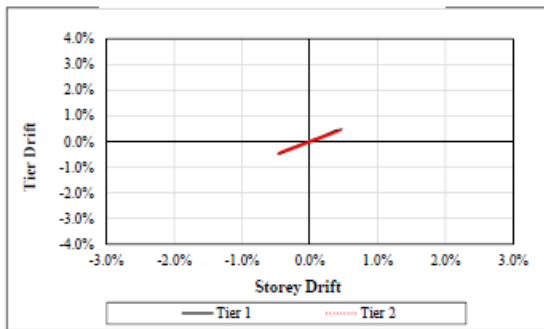
Drift vs. Time



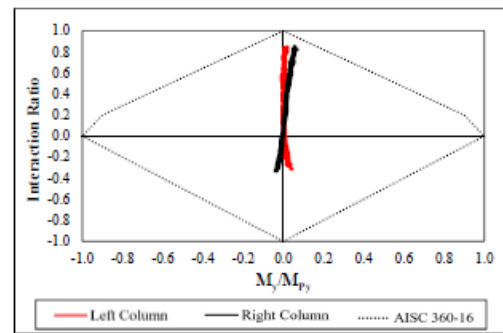
Displacement vs. Time



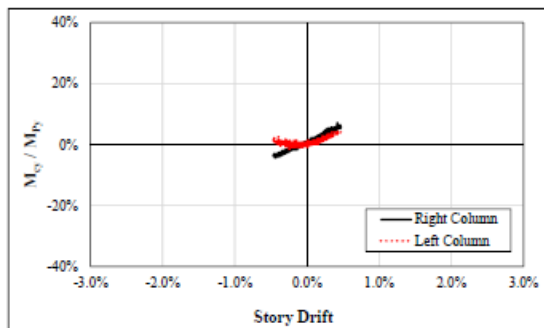
Tier Drift vs. Storey Drift



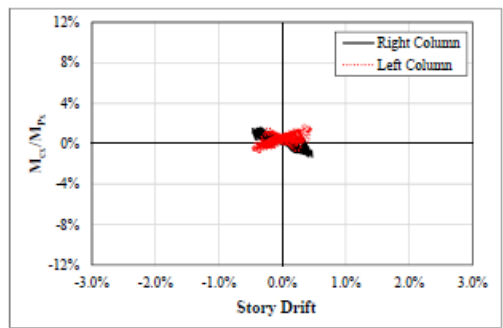
Column P-M Interaction Diagram



Column In-plane Bending Demand



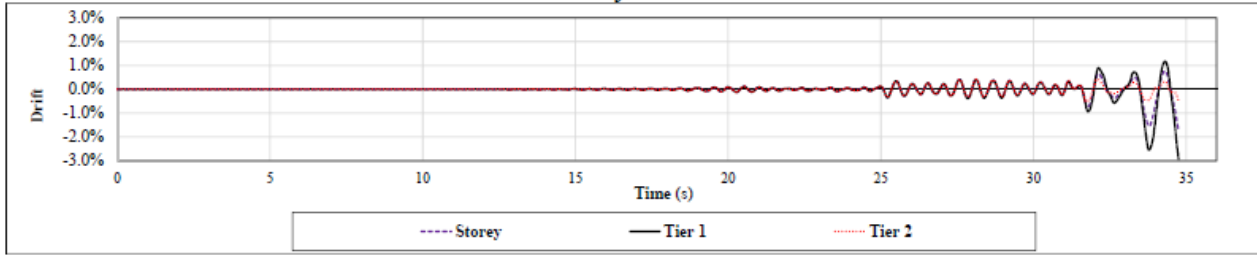
Column Out-of-plane Bending Demand



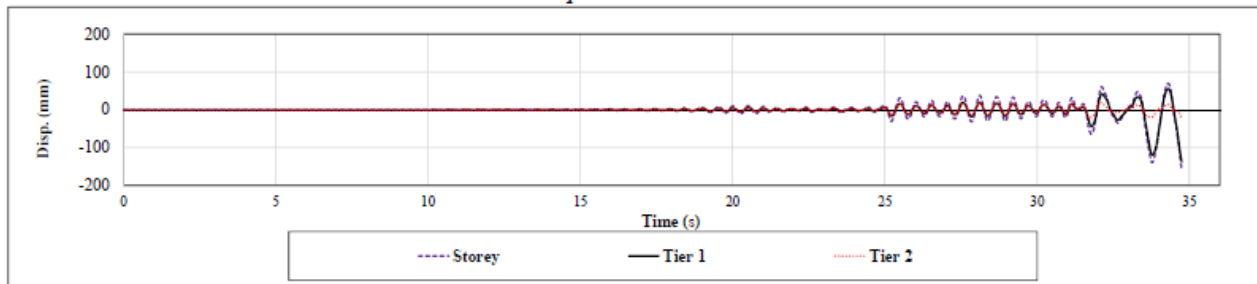
Ground Motion: SCC 7

Two-Tiered SCBF: AISC 341-10 Design

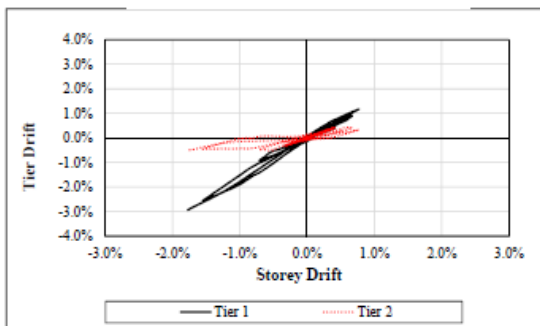
Drift vs. Time



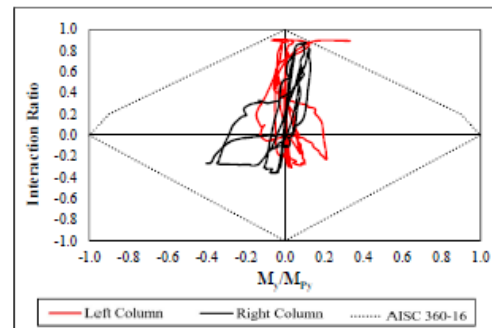
Displacement vs. Time



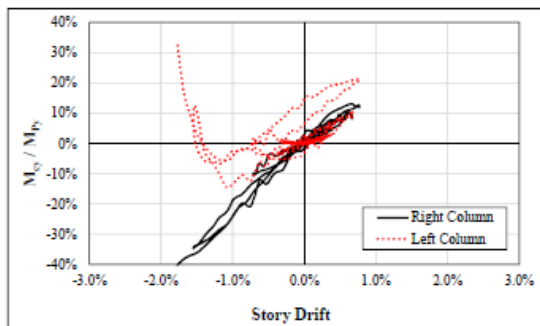
Tier Drift vs. Storey Drift



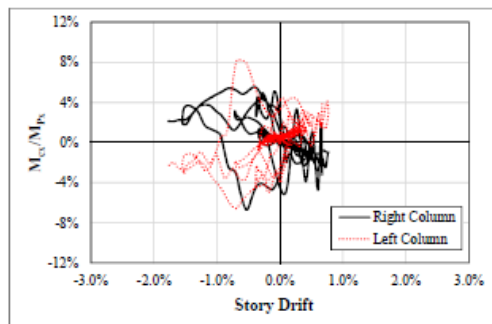
Column P-M Interaction Diagram



Column In-plane Bending Demand



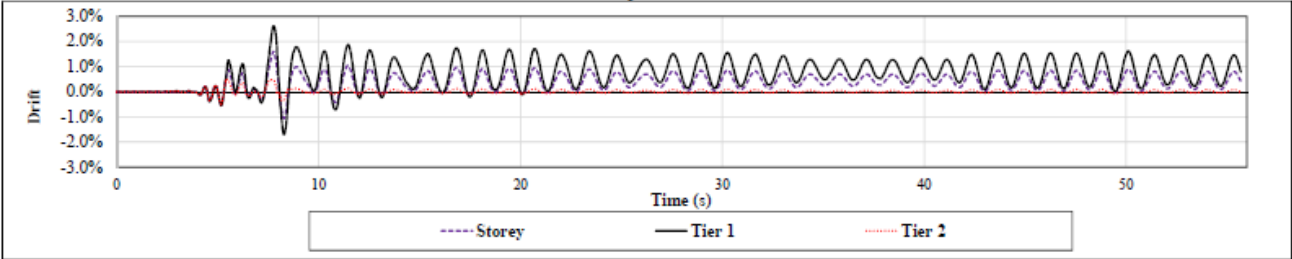
Column Out-of-plane Bending Demand



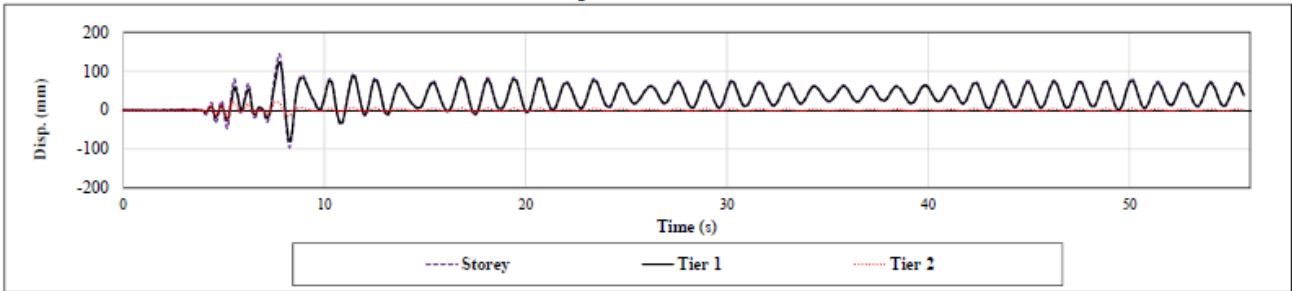
Ground Motion: SCC 8

Two-tiered: AISC 341-10 Design

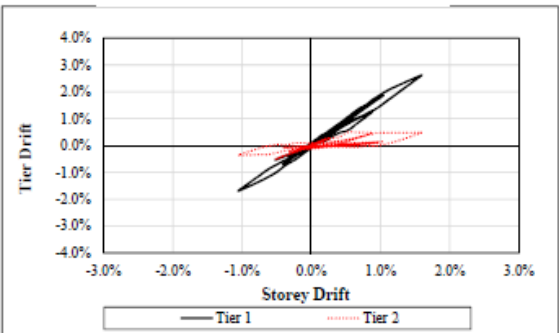
Drift vs. Time



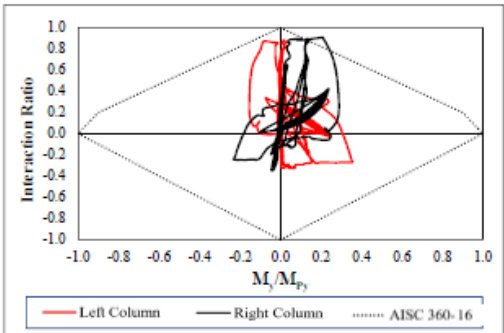
Displacement vs. Time



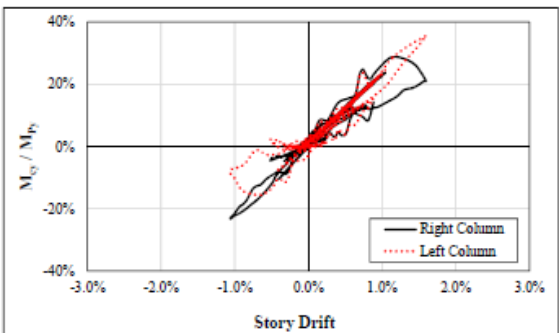
Tier Drift vs. Storey Drift



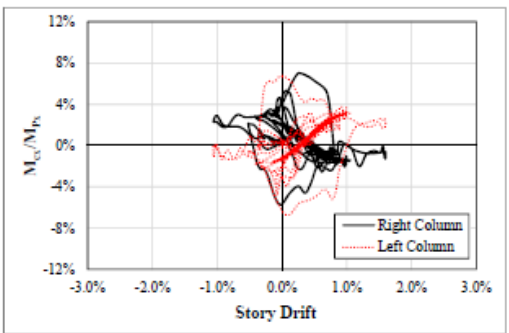
Column P-M Interaction Diagram



Column In-plane Bending Demand



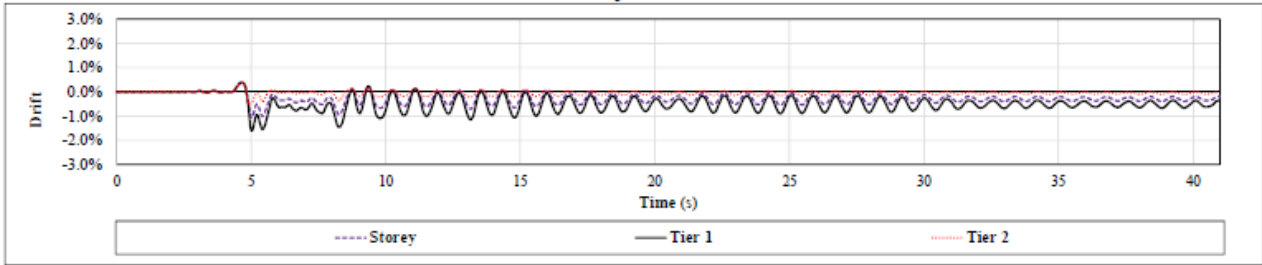
Column Out-of-plane Bending Demand



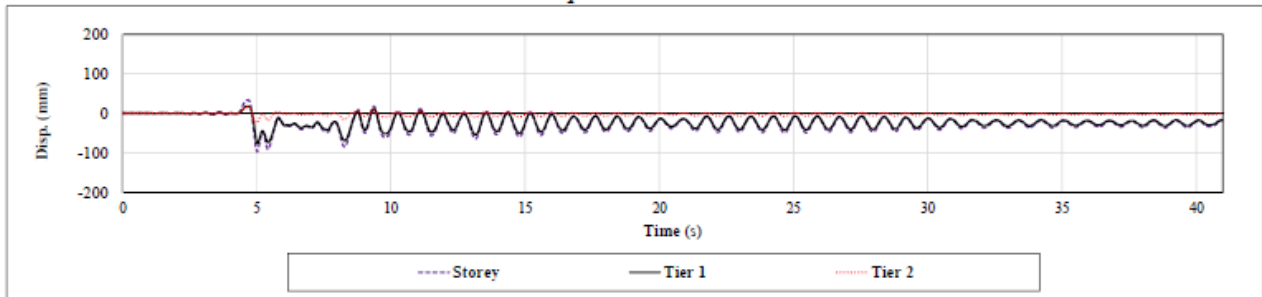
Ground Motion: SCC 9

Two-Tiered SCBF: AISC 341-10 Design

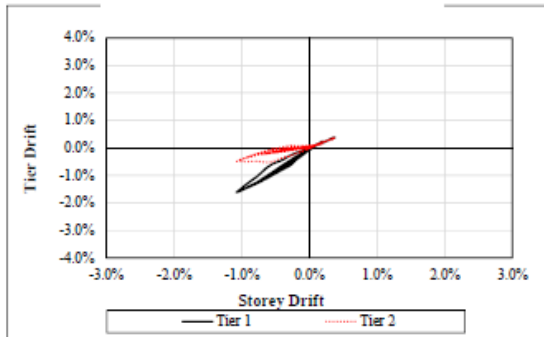
Drift vs. Time



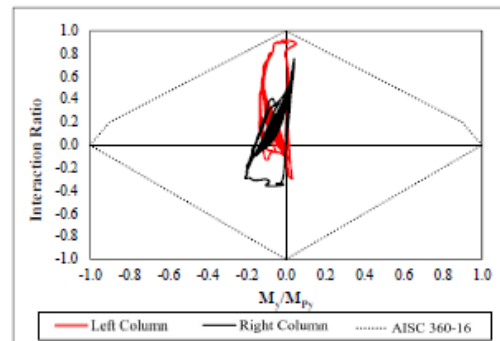
Displacement vs. Time



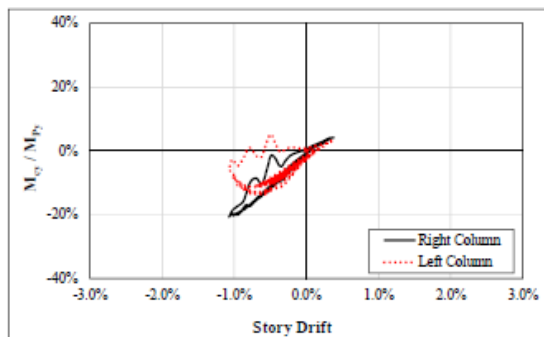
Tier Drift vs. Storey Drift



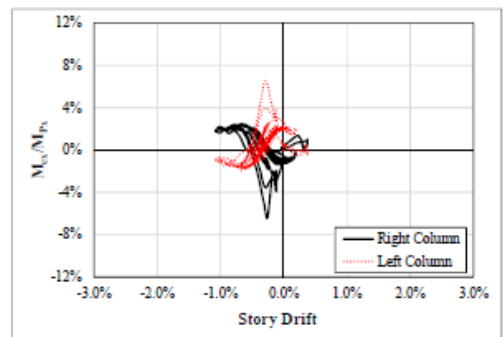
Column P-M Interaction Diagram



Column In-plane Bending Demand



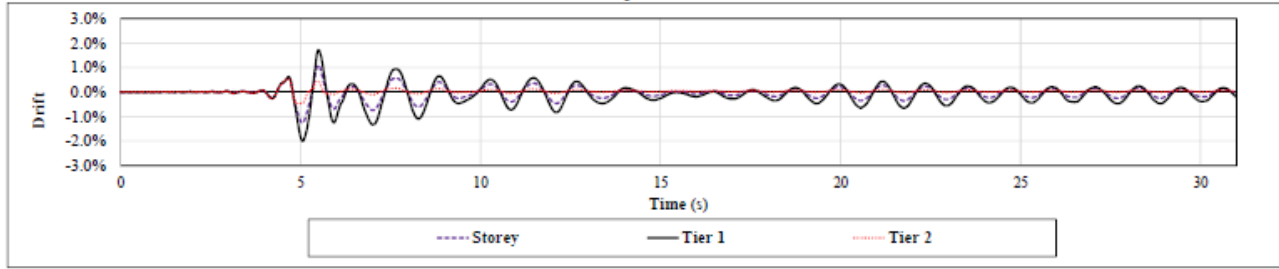
Column Out-of-plane Bending Demand



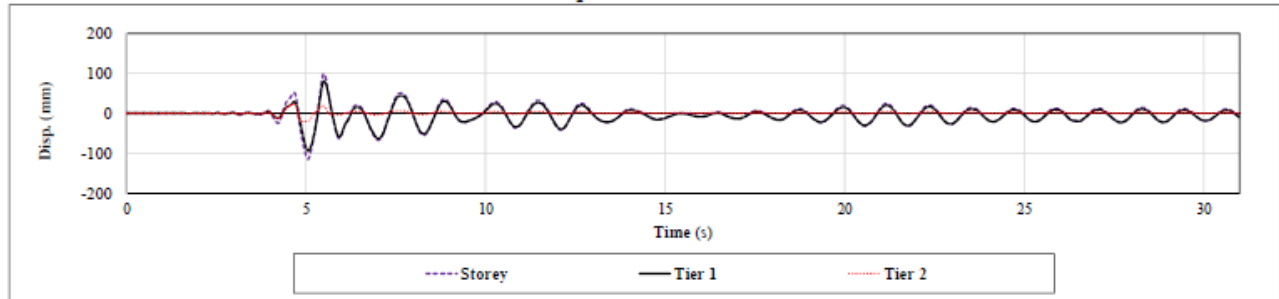
Ground Motion: SCC 10

Two-Tiered SCBF: AISC 341-10 Design

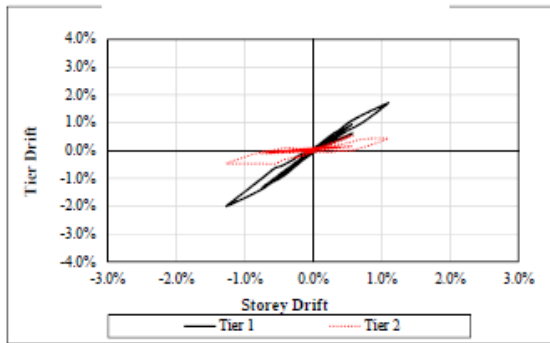
Drift vs. Time



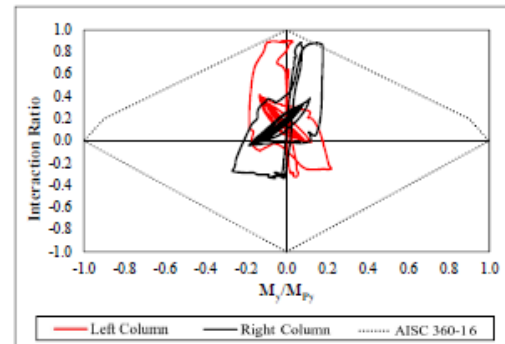
Displacement vs. Time



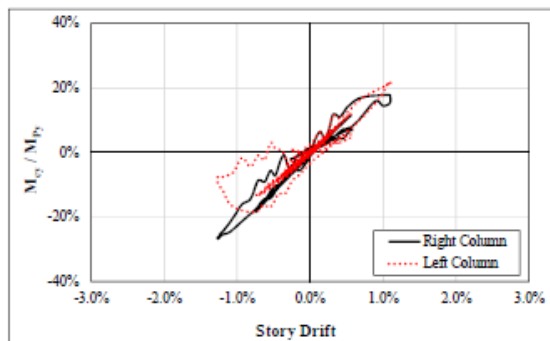
Tier Drift vs. Storey Drift



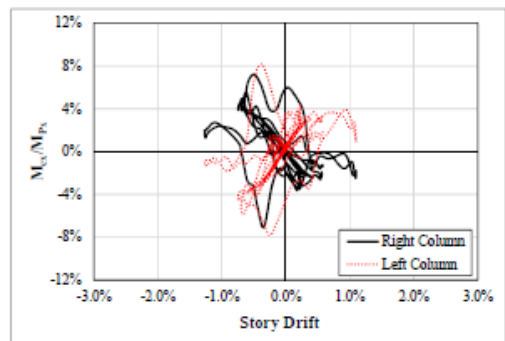
Column P-M Interaction Diagram



Column In-plane Flexure Demand



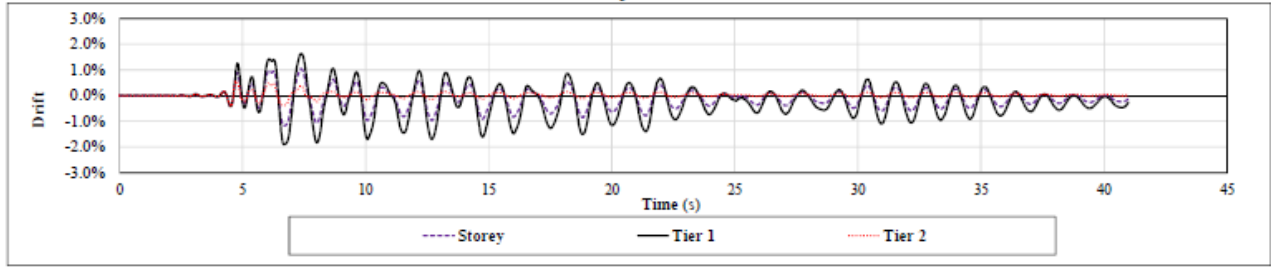
Column Out-of-plane Flexure Demand



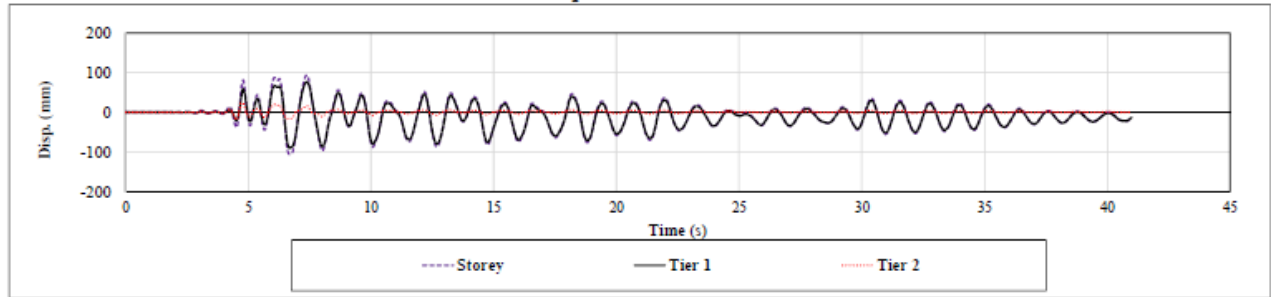
Ground Motion: SCC 11

Two SCBF: AISC 341-10 Design

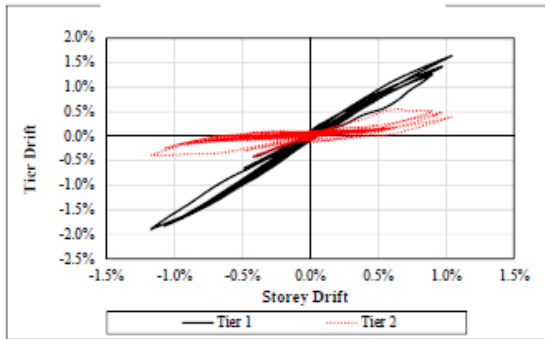
Drift vs. Time



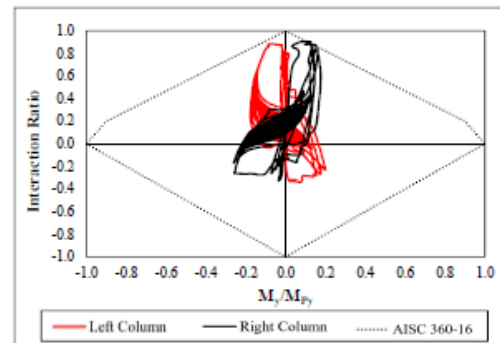
Displacement vs. Time



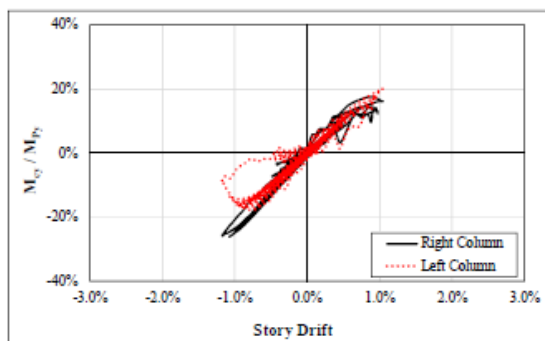
Tier Drift vs. Storey Drift



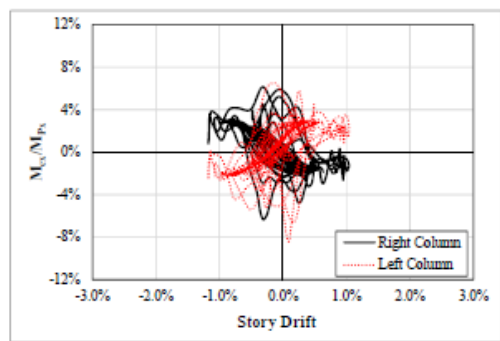
Column P-M Interaction Diagram



Column In-plane Flexure Demand



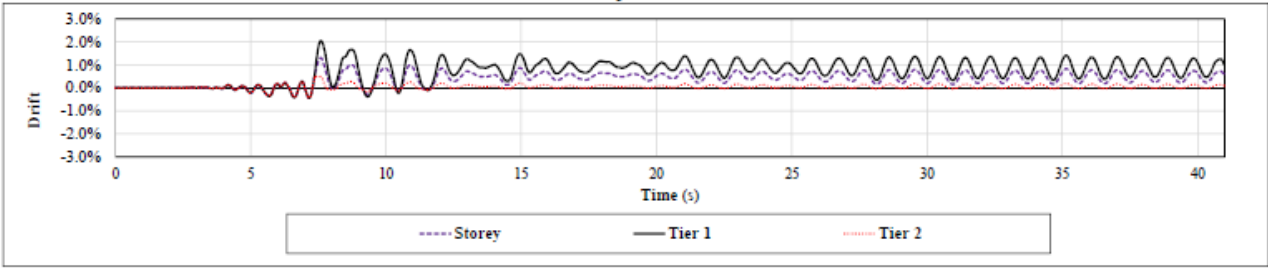
Column Out-of-plane Flexure Demand



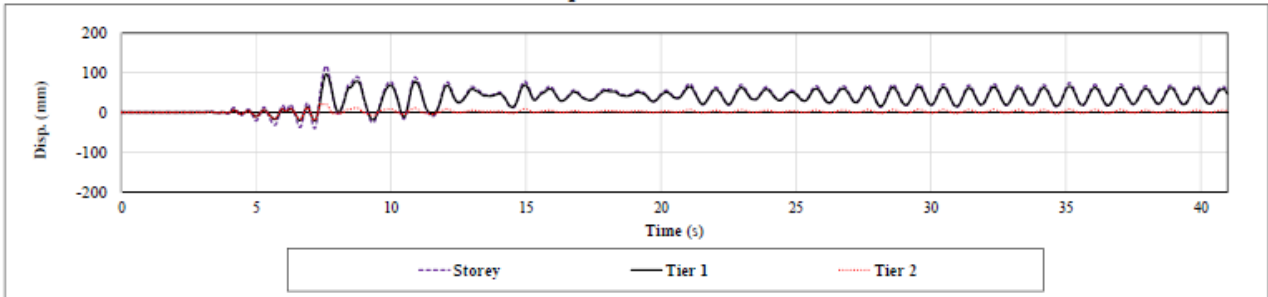
Ground Motion: SCC 12

Two-Tiered SCBF: AISC 341-10 Design

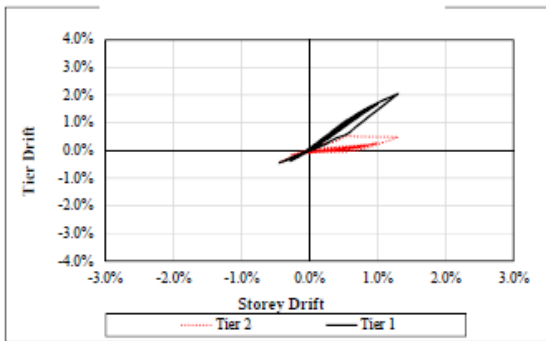
Drift vs. Time



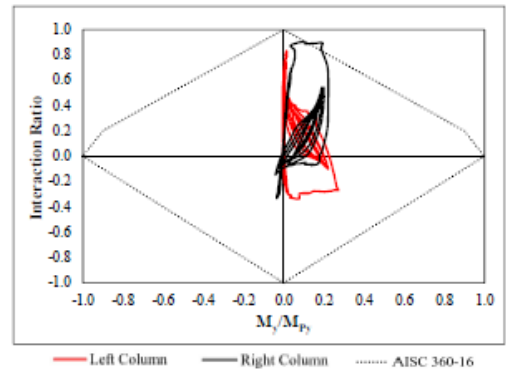
Displacement vs. Time



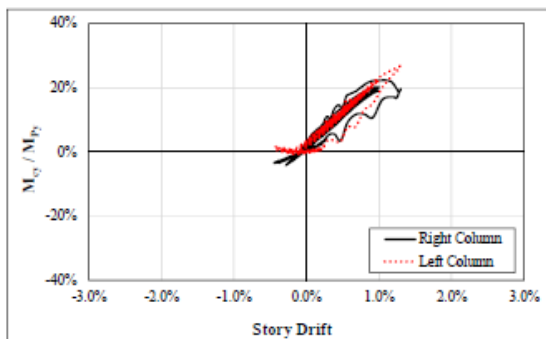
Tier Drift vs. Storey Drift



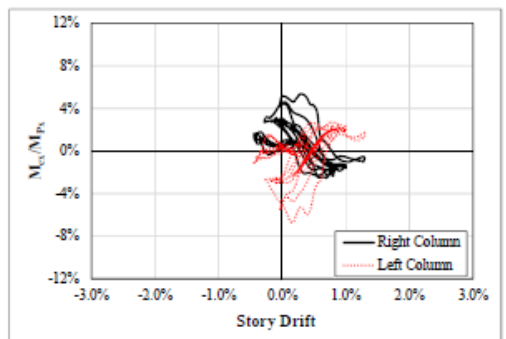
Column P-M Interaction Diagram



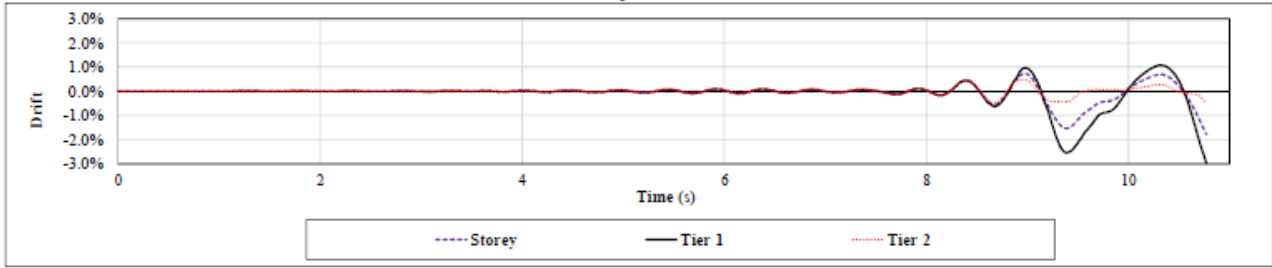
Column In-plane Bending Demand



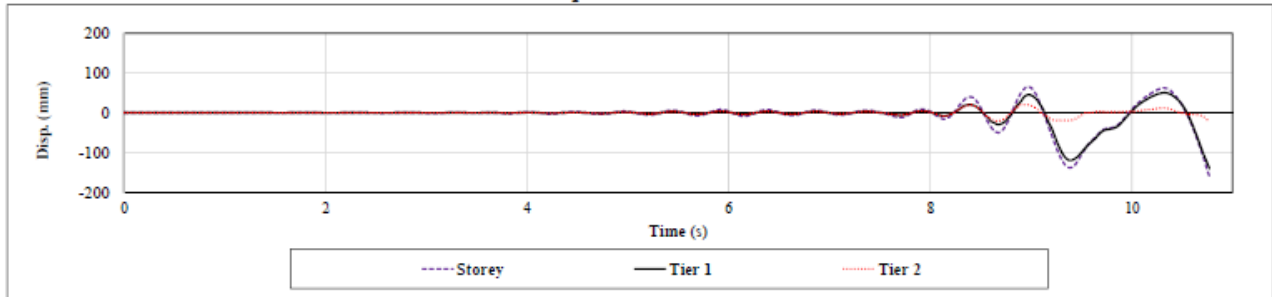
Column Out-of-plane Bending Demand



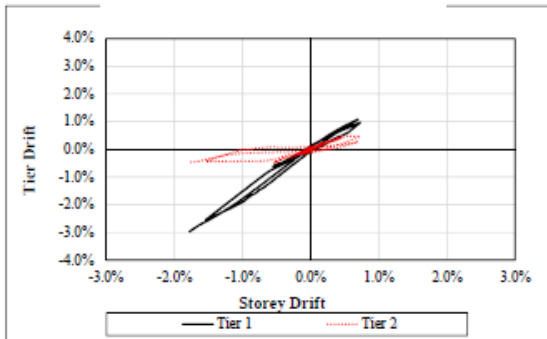
Drift vs. Time



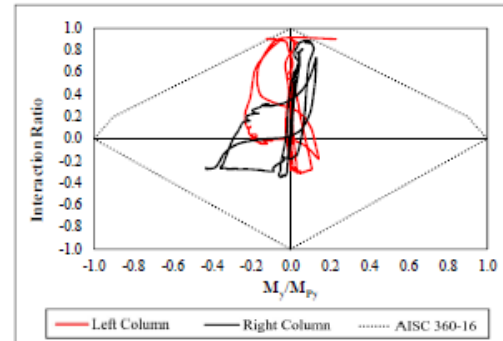
Displacement vs. Time



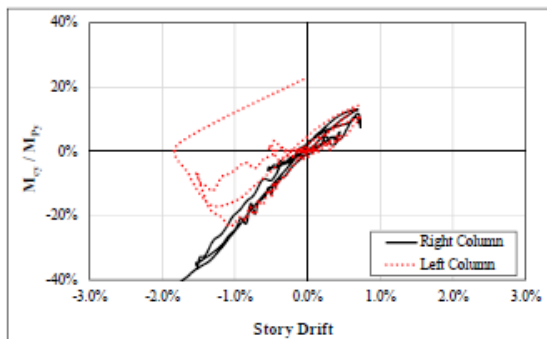
Tier Drift vs. Storey Drift



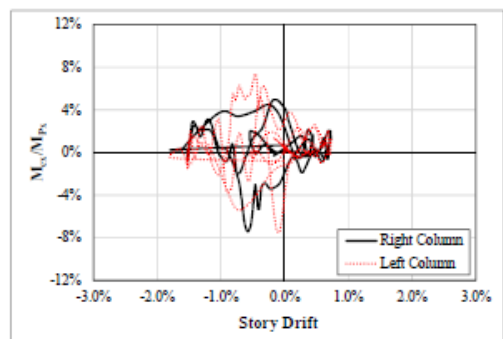
Column P-M Interaction Diagram



Columns In-plane Bending Demand



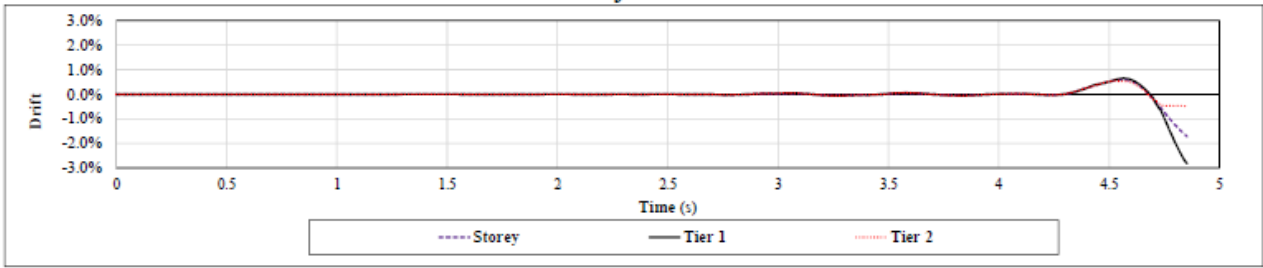
Columns Out-of-plane Bending Demand



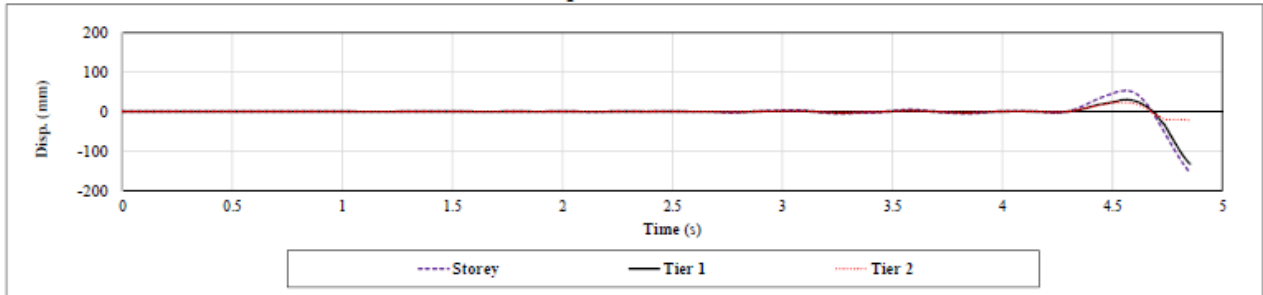
Ground Motion: SCC 14

Two-Tiered SCFB: AISC 341-10 Design

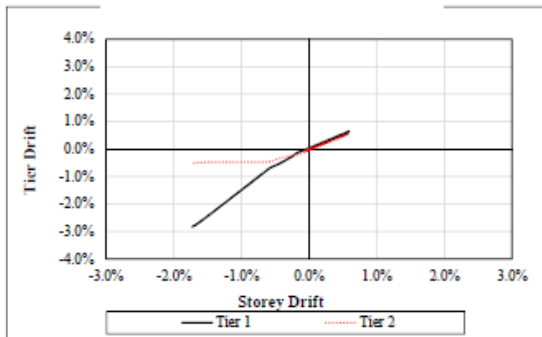
Drift vs. Time



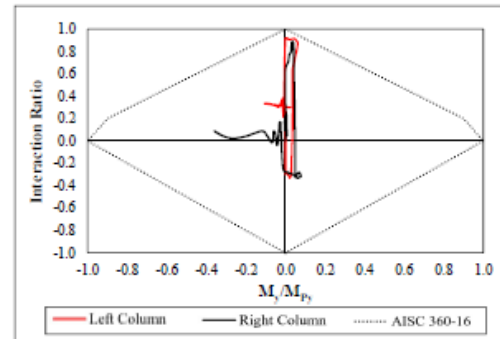
Displacement vs. Time



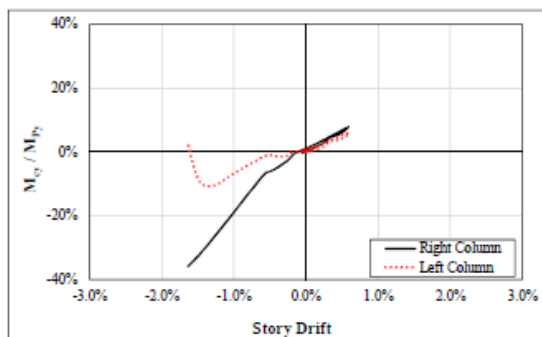
Tier Drift vs. Storey Drift



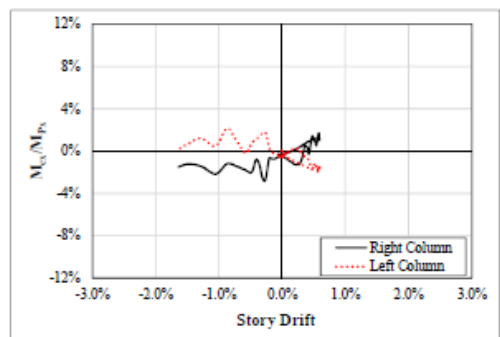
Column P-M Interaction Diagram



Column In-plane Bending Demand



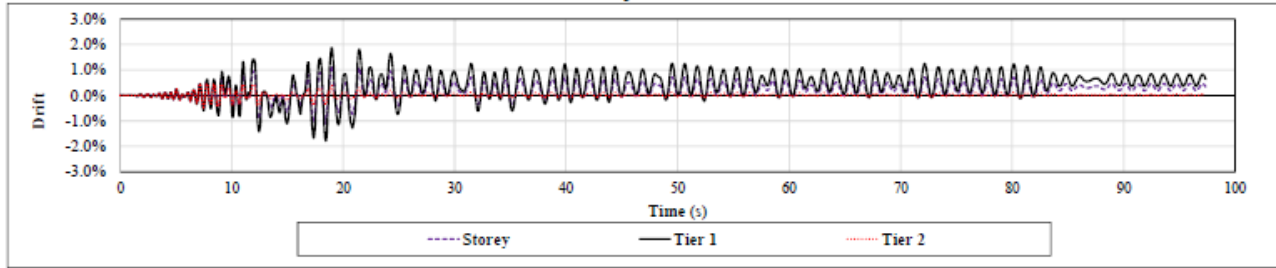
Column Out-of-plane Bending Demand



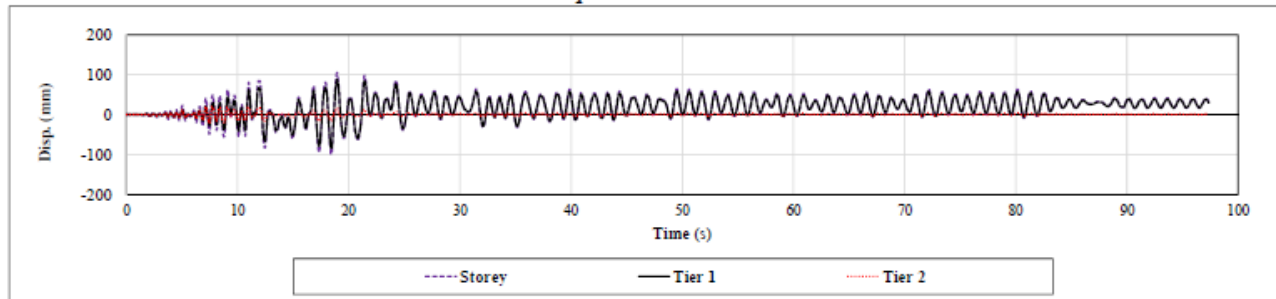
Ground Motion: SCD 1

Two-Tiered SCBF: AISC 341-10 Design

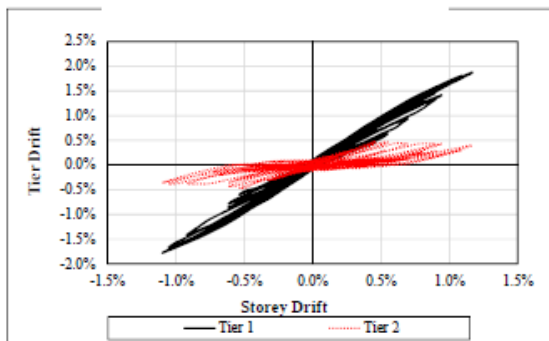
Drift vs. Time



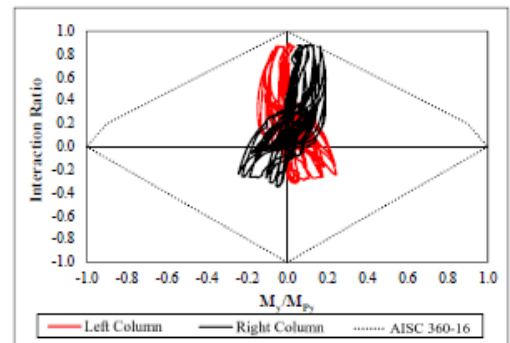
Displacement vs. Time



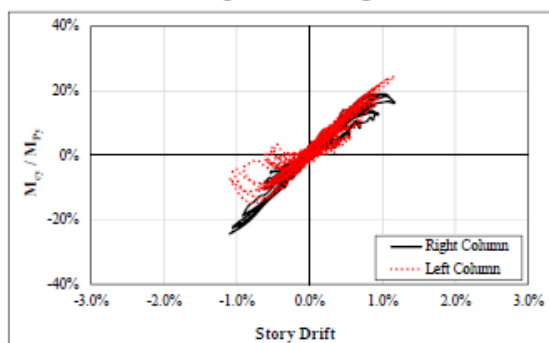
Tier Drift vs. Storey Drift



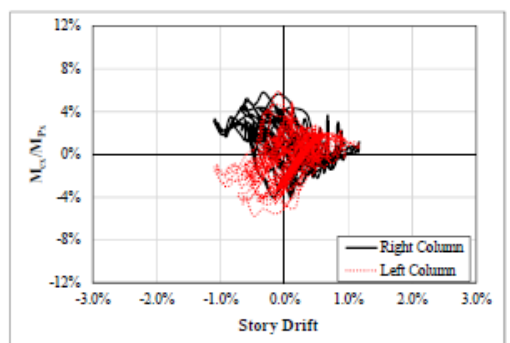
Column P-M Interaction Diagram



Column In-plane Bending Demand



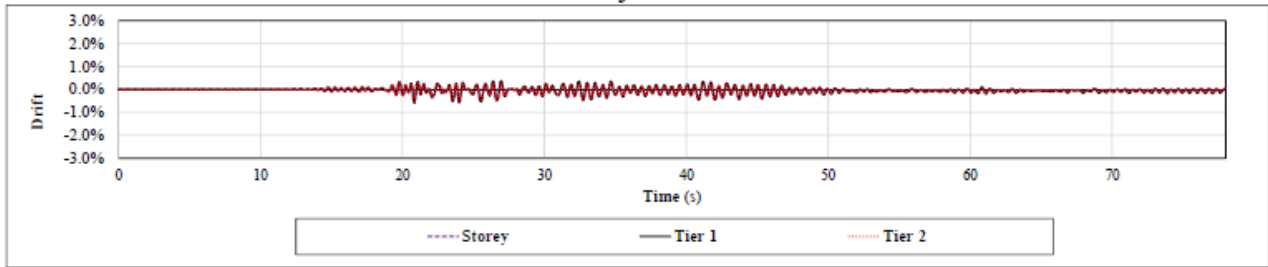
Column Out-of-plane Bending Demand



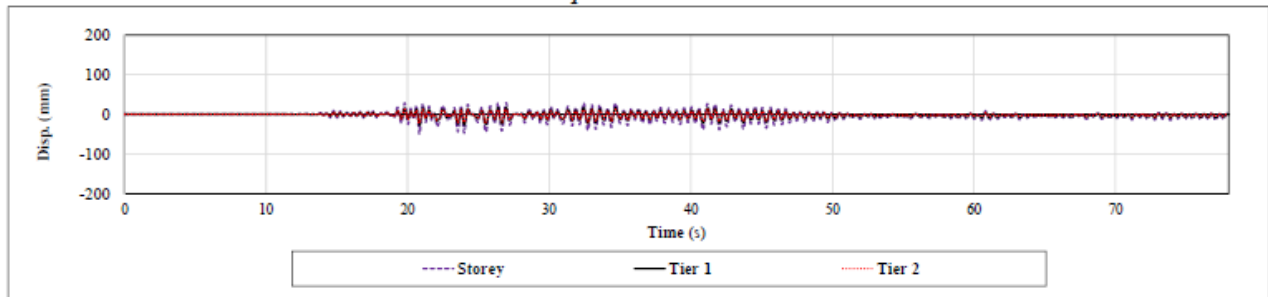
Ground Motion: SCD 2

Two-Tiered SCBF: AISC 341-10 Design

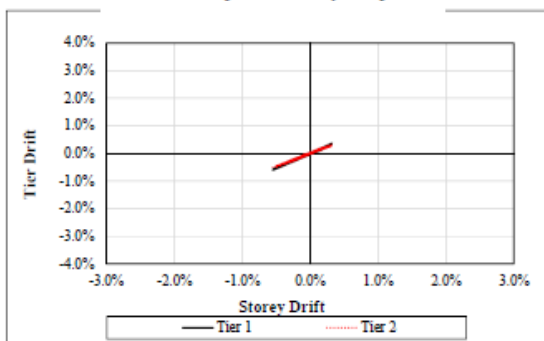
Drift vs. Time



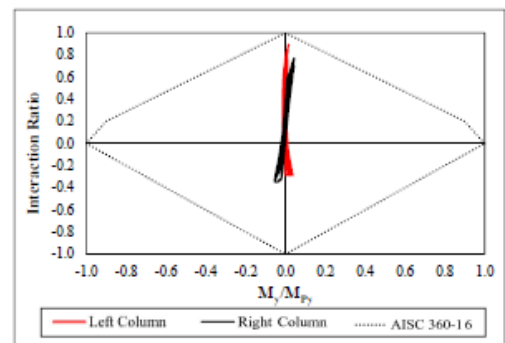
Displacement vs. Time



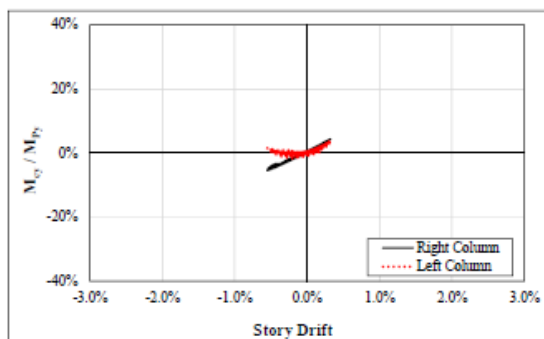
Tier Drift vs. Storey Drift



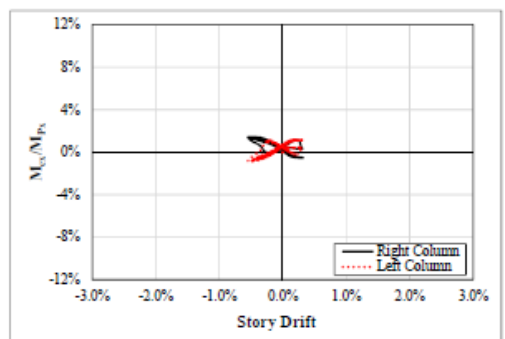
Column P-M Interaction Diagram



Column In-plane Bending Demand



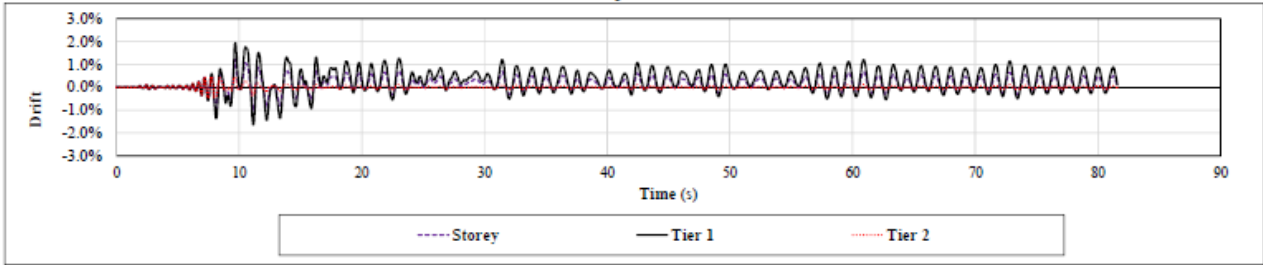
Column Out-of-plane Bending Demand



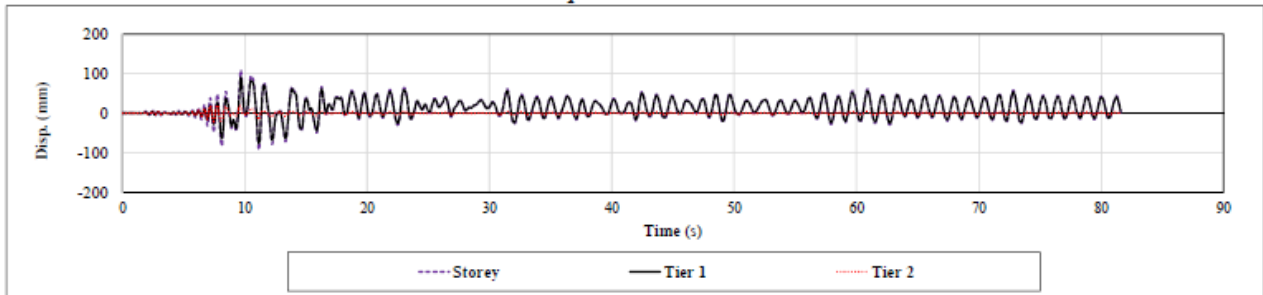
Ground Motion: SCD 3

Two-Tiered SCBF: AISC 341-10 Design

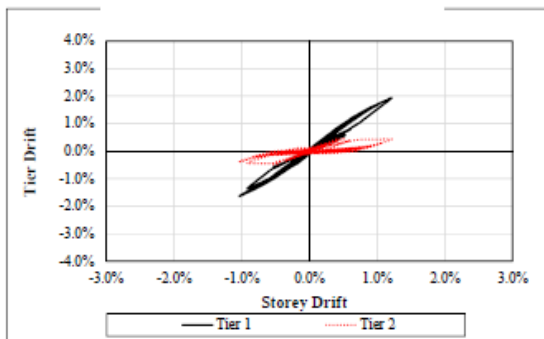
Drift vs. Time



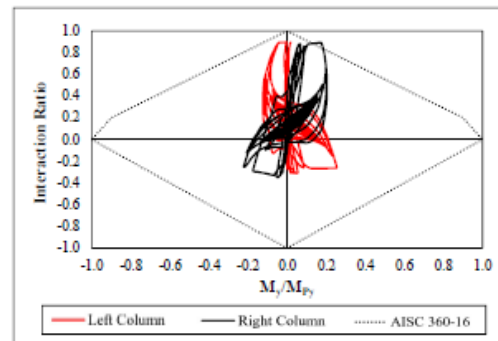
Displacement vs. Time



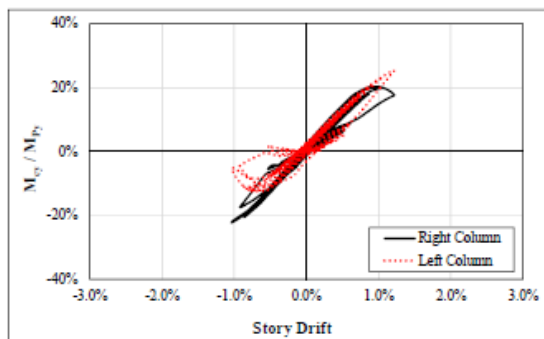
Tier Drift vs. Storey Drift



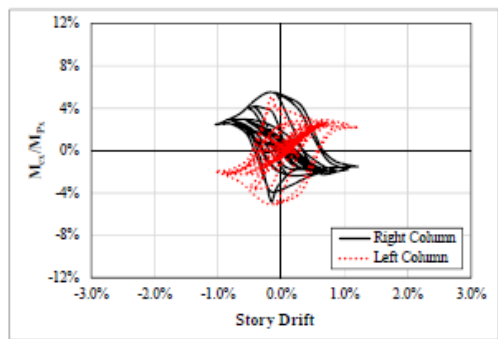
Column P-M Interaction Diagram



Column In-plane Bending Demand



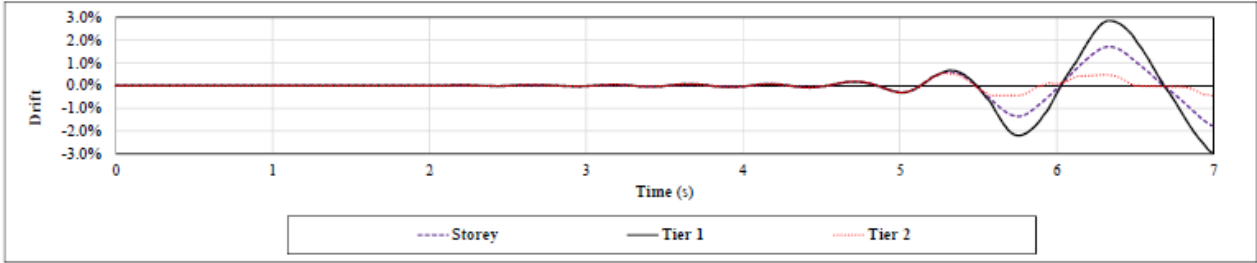
Column Out-of-plane Bending Demand



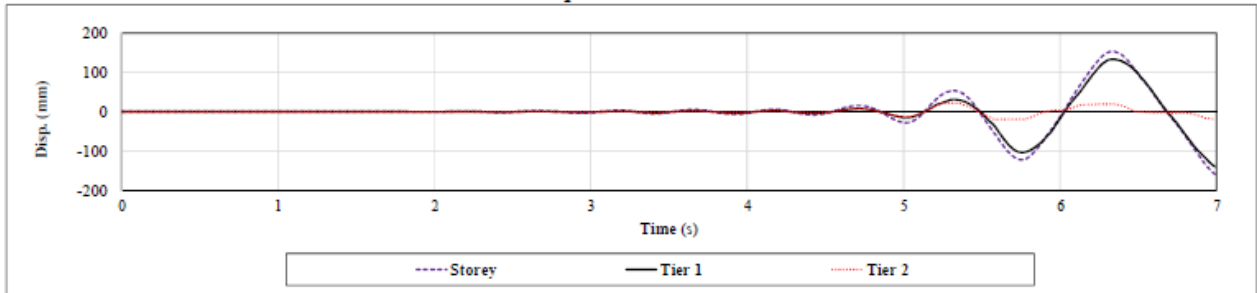
Ground Motion: SCD 4

Two-Tiered SCBF: AISC 341-10 Design

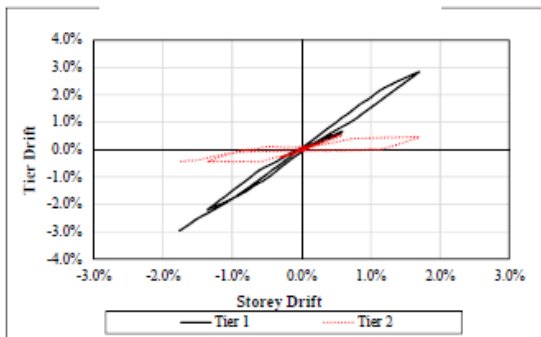
Drift vs. Time



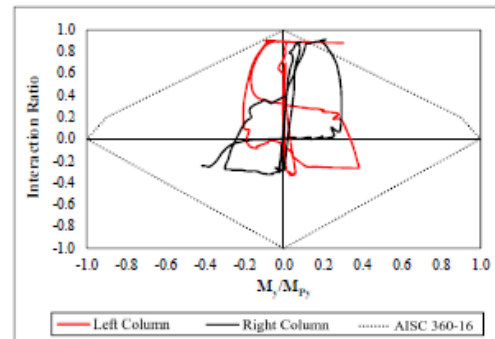
Displacement vs. Time



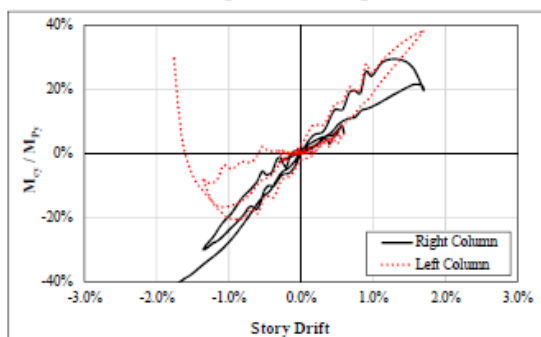
Tier Drift vs. Storey Drift



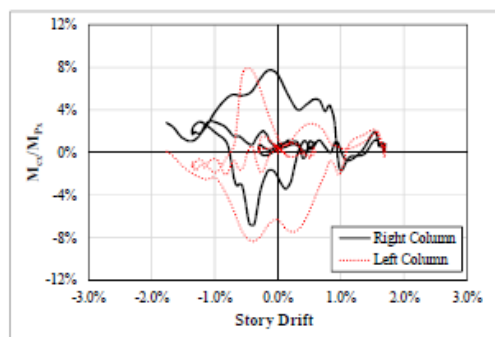
Column P-M Interaction Diagram



Columns In-plane Bending Demand



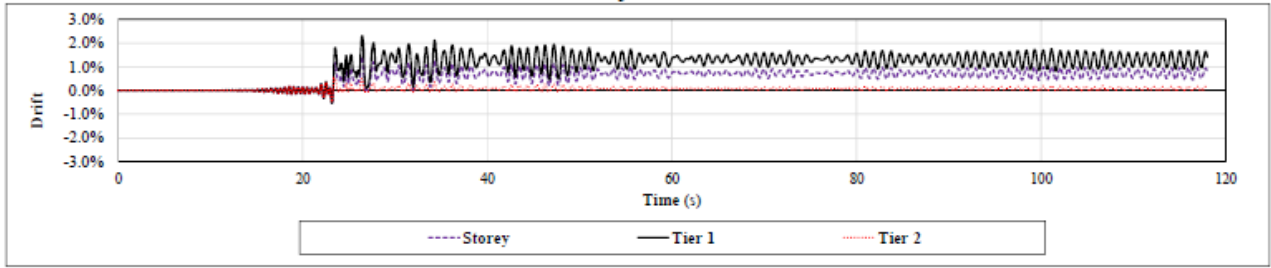
Columns Out-of-plane Bending Demand



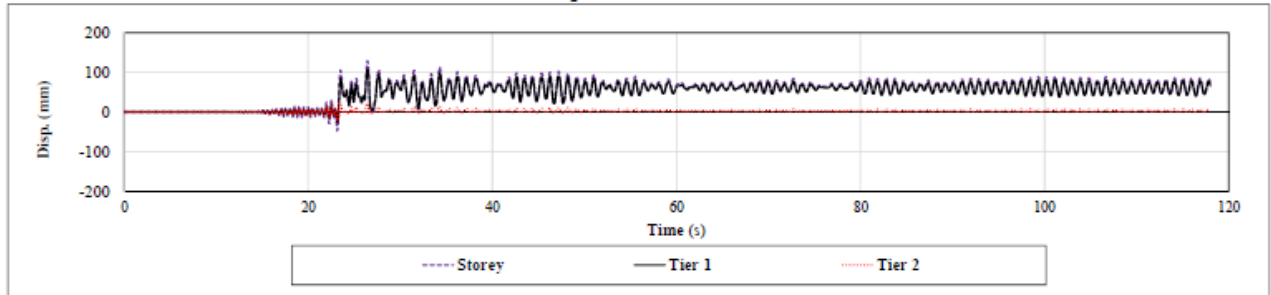
Ground Motion: SCD 5

Two-Tiered SCBF: AISC 341-10 Design

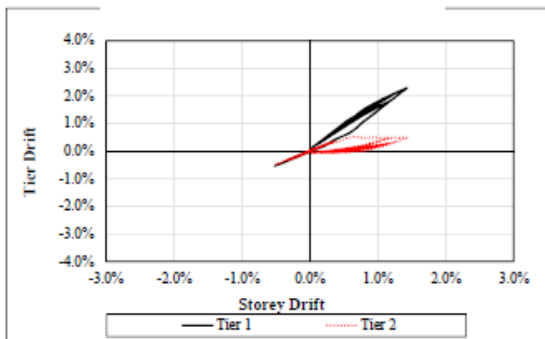
Drift vs. Time



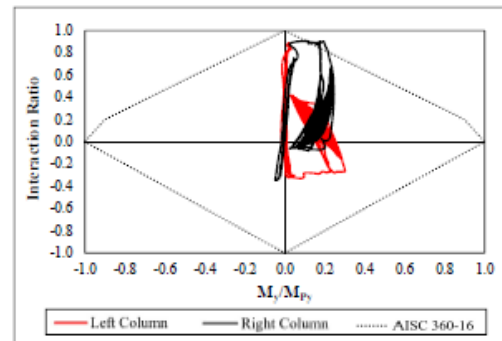
Displacement vs. Time



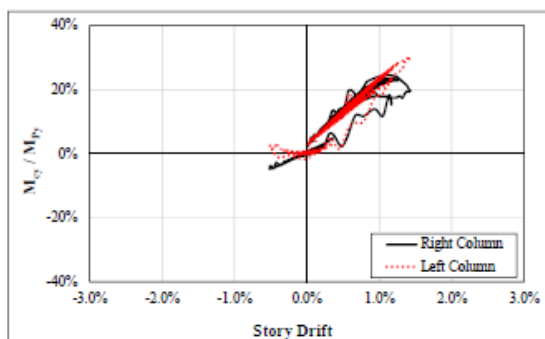
Tier Drift vs. Storey Drift



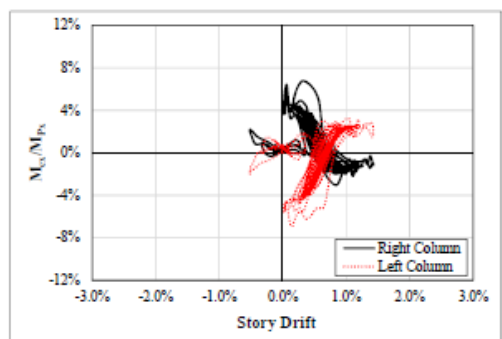
Column P-M Interaction Diagram



Column In-plane Bending Demand



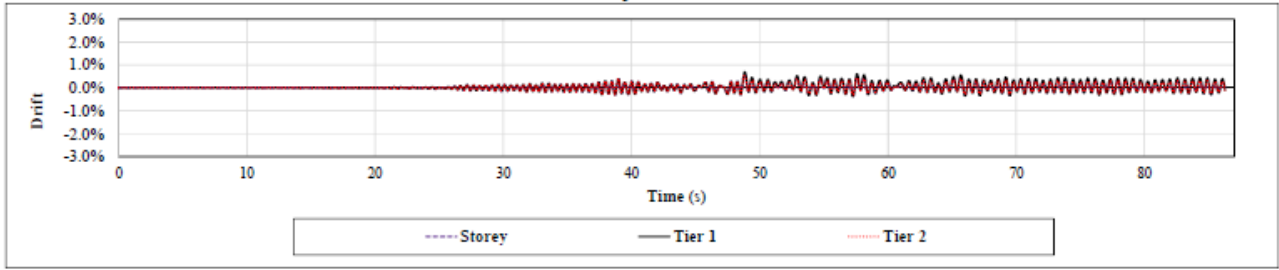
Column Out-of-plane Bending Demand



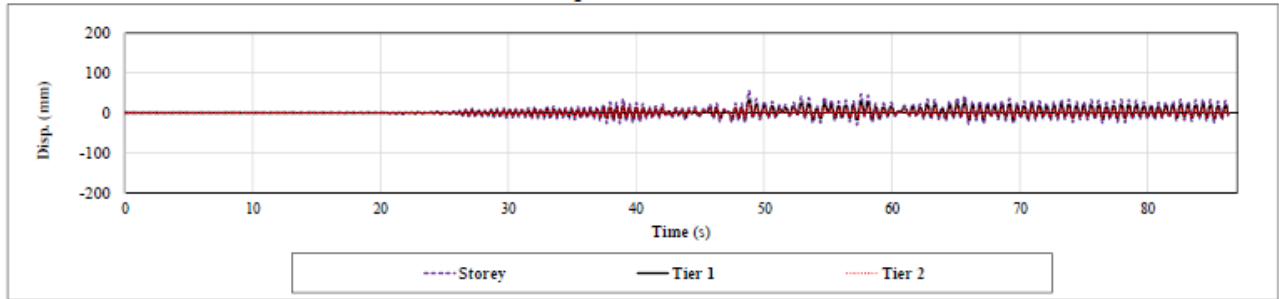
Ground Motion: SCI 1

Two-Tiered SCBF: AISC 341-16 Design

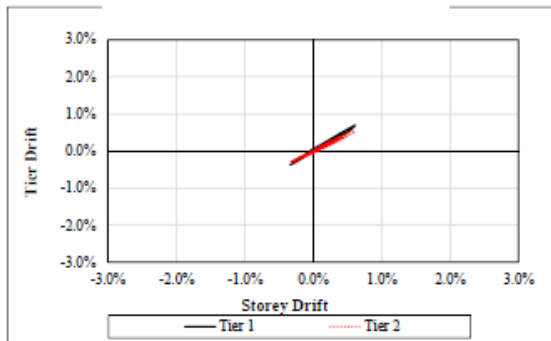
Drift vs. Time



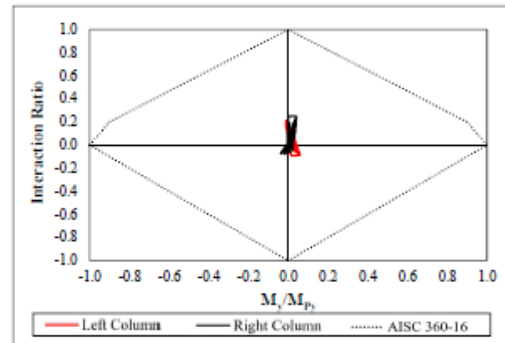
Displacement vs. Time



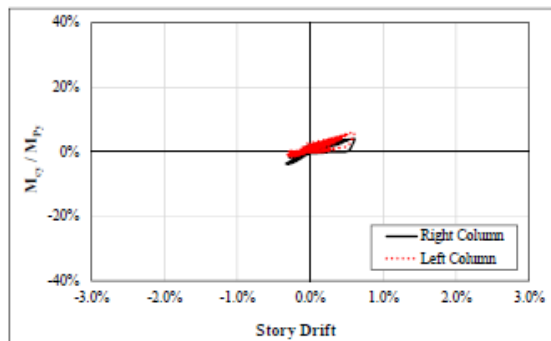
Tier Drift vs. Storey Drift



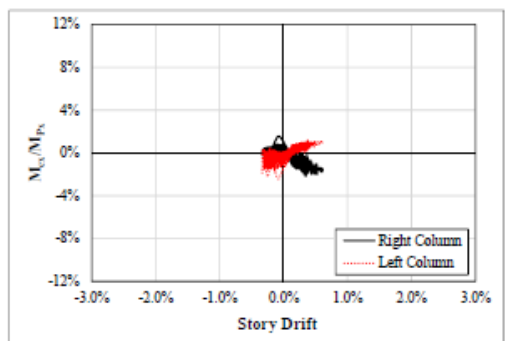
Column P-M Interaction Diagram



Column In-plane Bending Demand



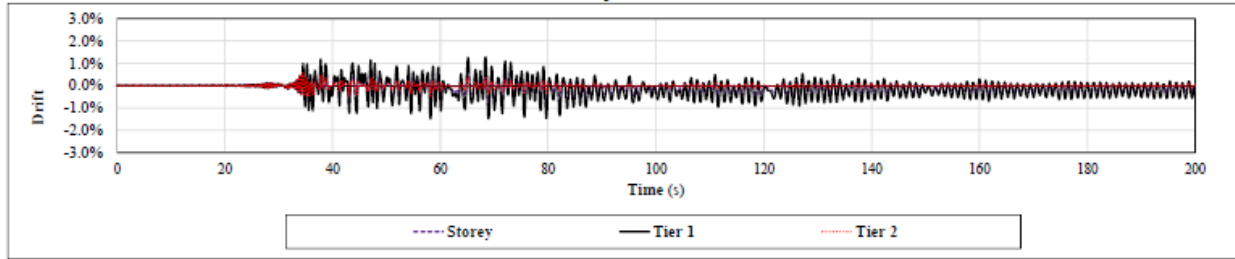
Column Out-of-plane Bending Demand



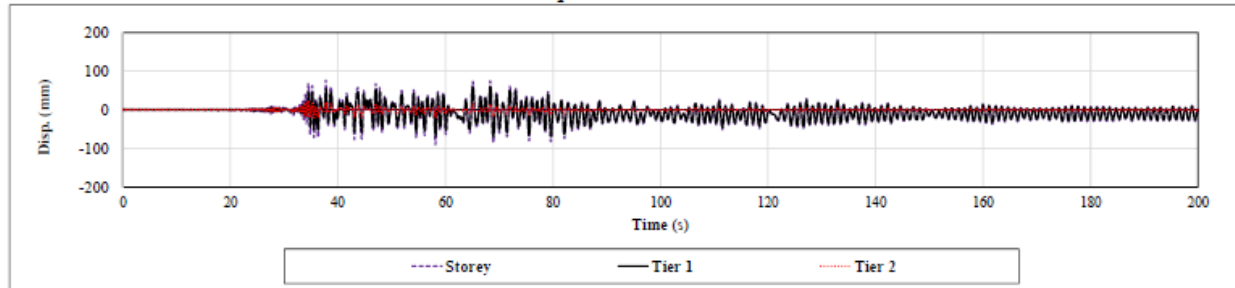
Ground Motion: SCI 2

Two-Tiered SCBF: AISC 341-16 Design

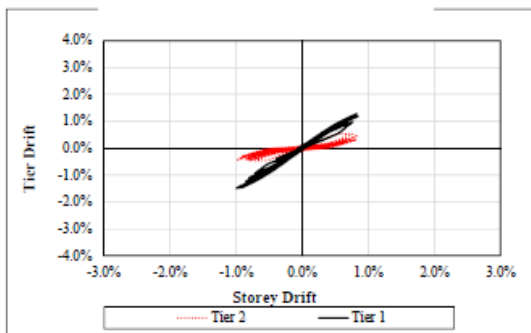
Drift vs. Time



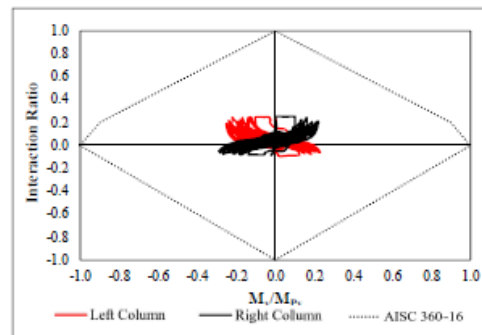
Displacement vs. Time



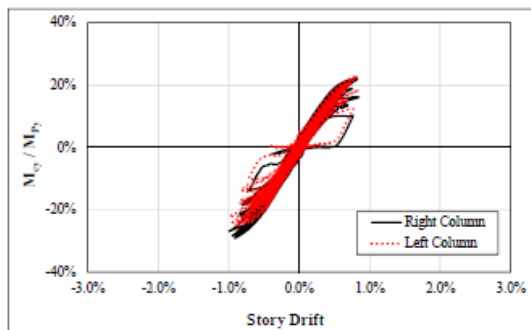
Tier Drift vs. Storey Drift



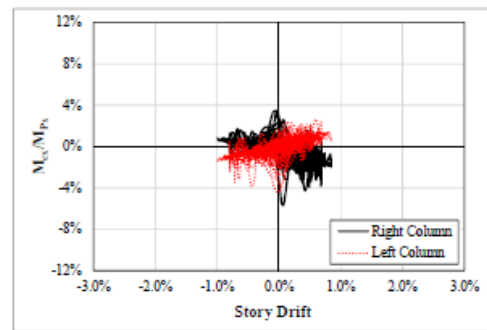
Column P-M Interaction Diagram



Column In-plane Bending Demand



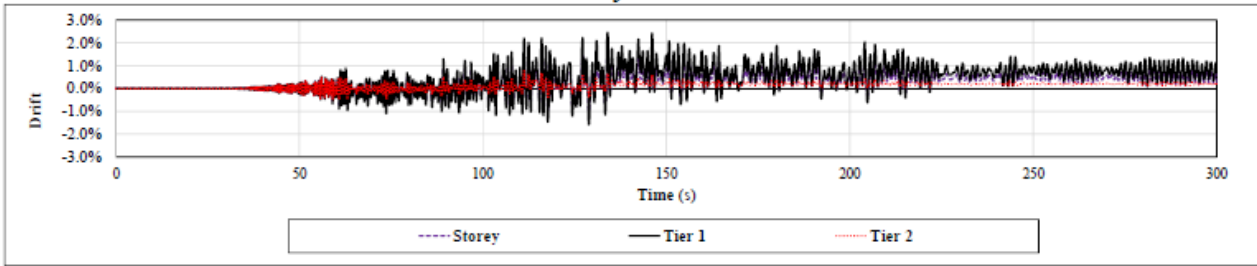
Column Out-of-plane Bending Demand



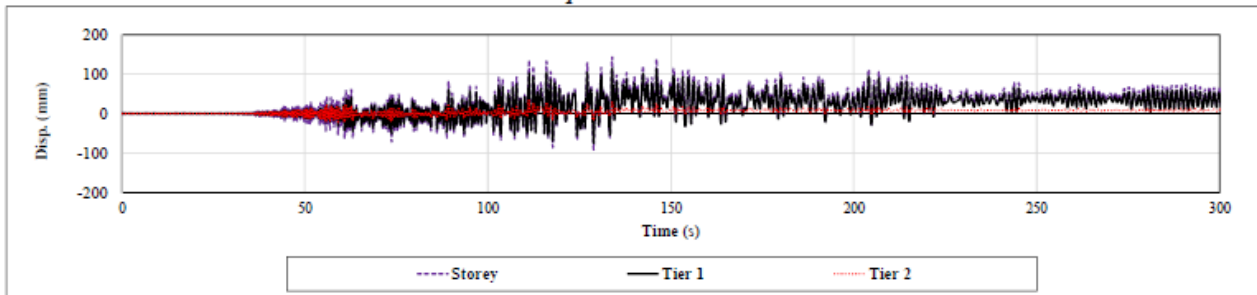
Ground Motion: SCI 3

Two-Tiered SCBF: AISC 341-16 Design

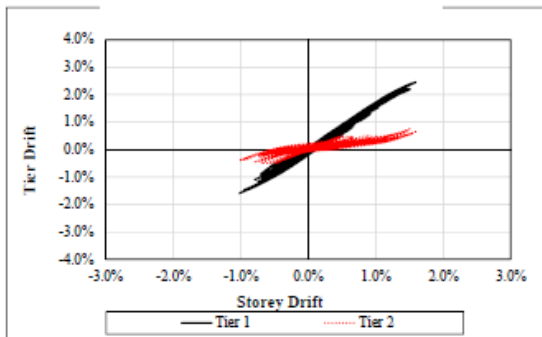
Drift vs. Time



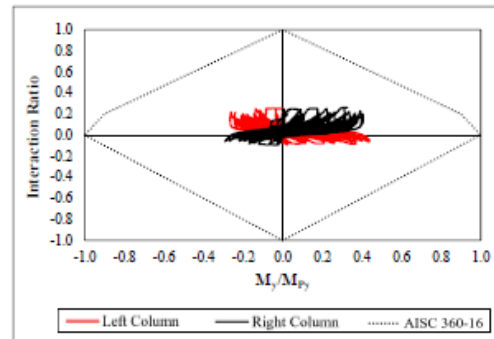
Displacement vs. Time



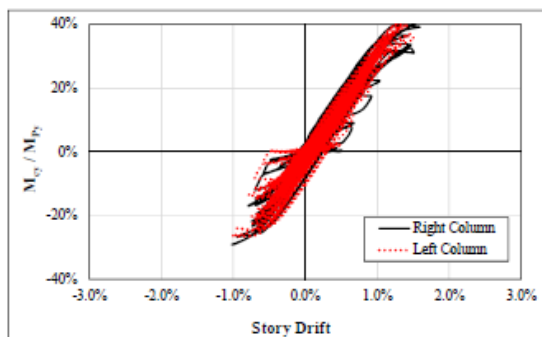
Tier Drift vs. Storey Drift



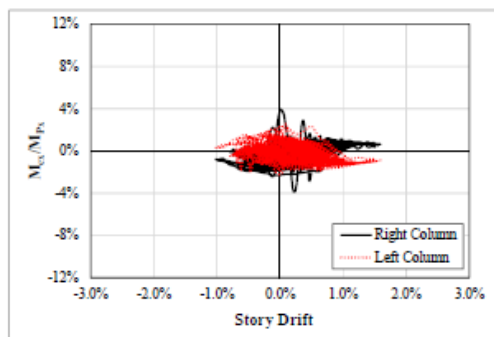
Column P-M Interaction Diagram



Column In-plane Bending Demand



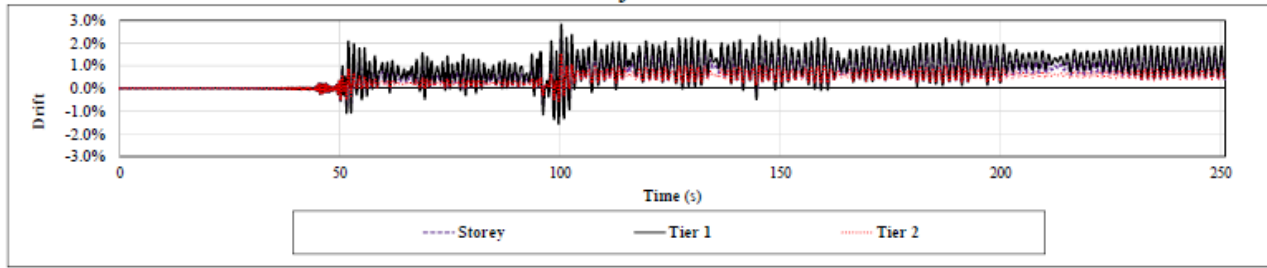
Column Out-of-plane Bending Demand



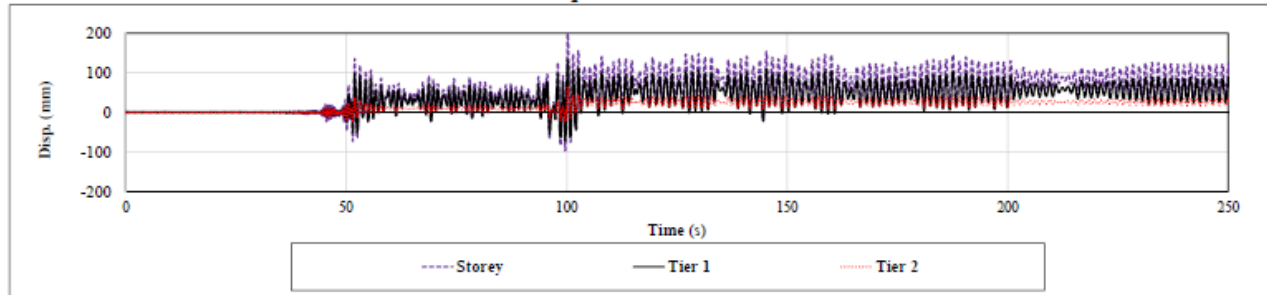
Ground Motion: SCI 4

Two-Tiered SCBF: AISC 341-16 Design

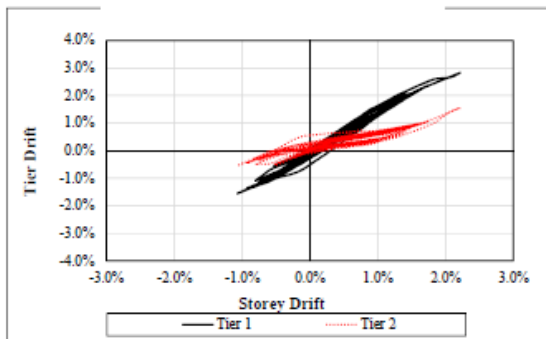
Drift vs. Time



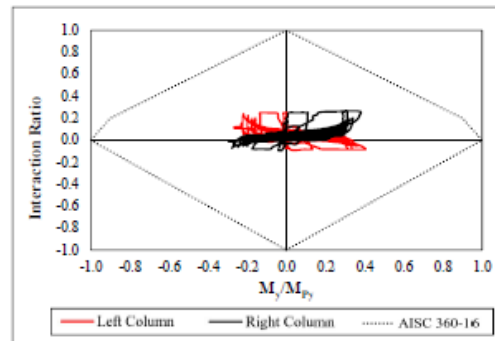
Displacement vs. Time



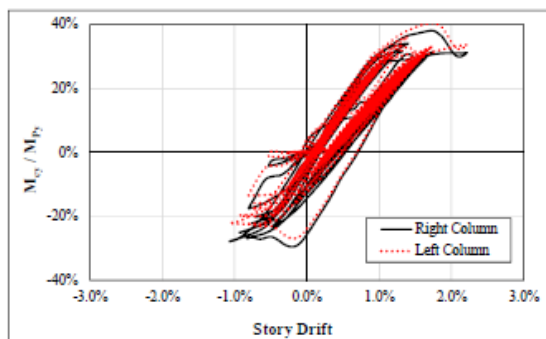
Tier Drift vs. Storey Drift



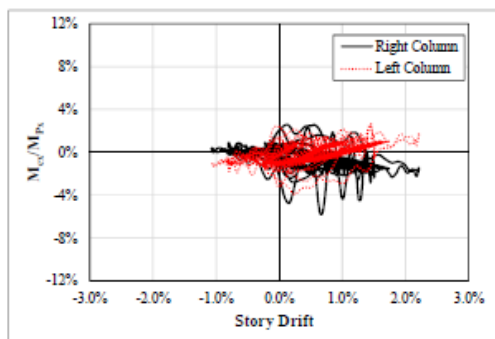
Column P-M Interaction Diagram



Column In-plane Bending Demand



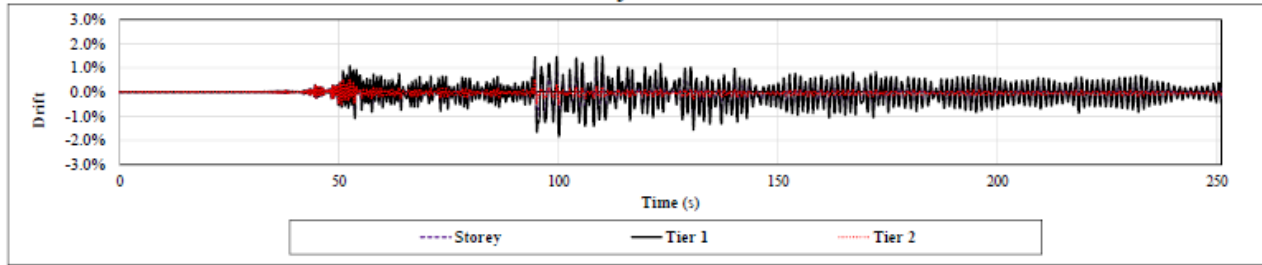
Column Out-of-plane Bending Demand



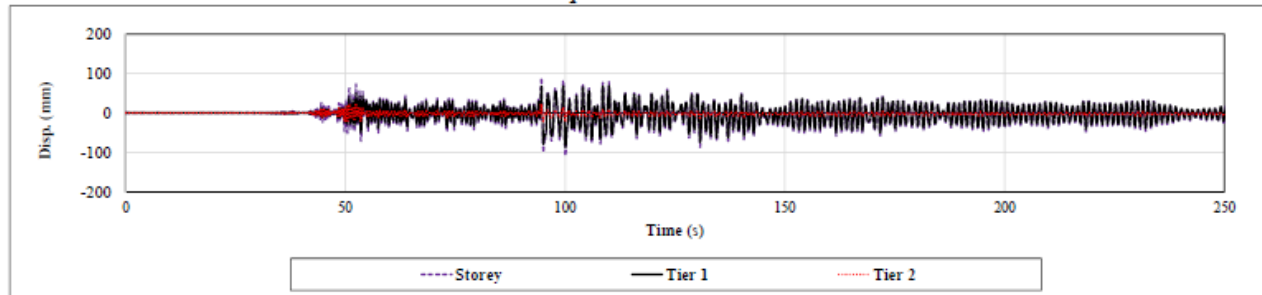
Ground Motion: SCI 5

Two-Tiered SCBF: AISC 341-16 Design

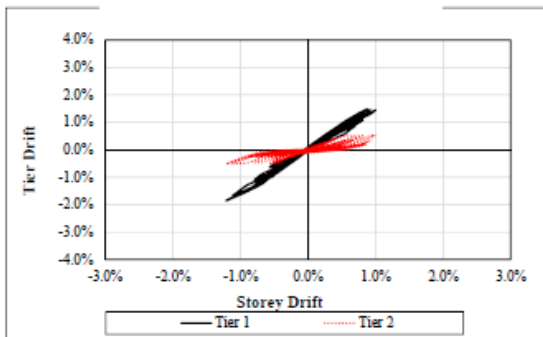
Drift vs. Time



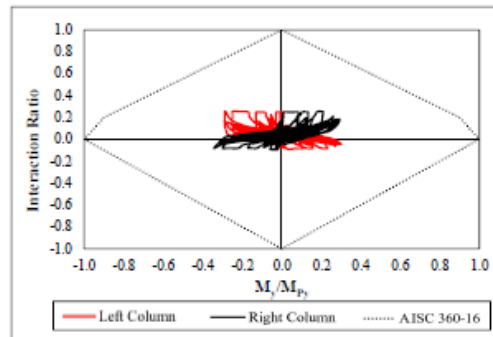
Displacement vs. Time



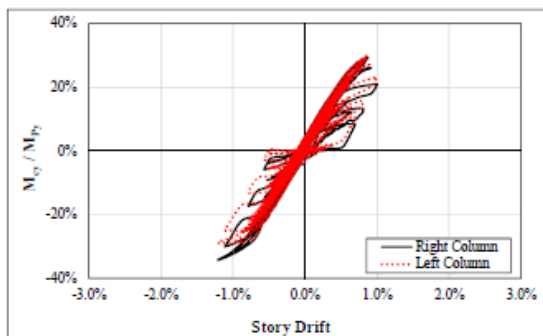
Tier Drift vs. Storey Drift



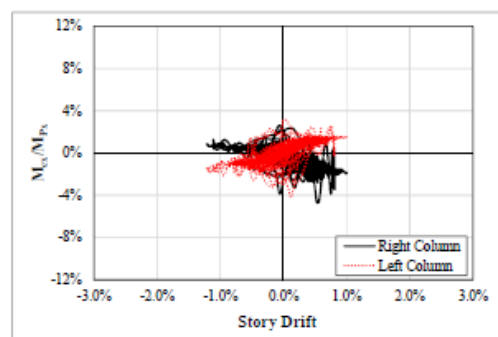
Column P-M Bending Diagram



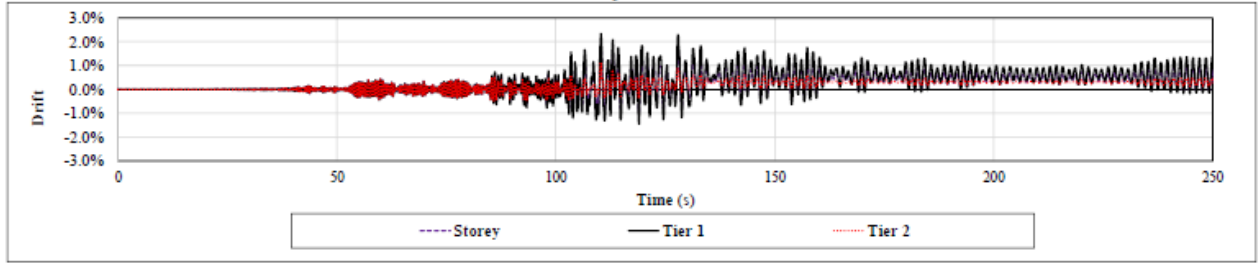
Column In-plane Bending Demand



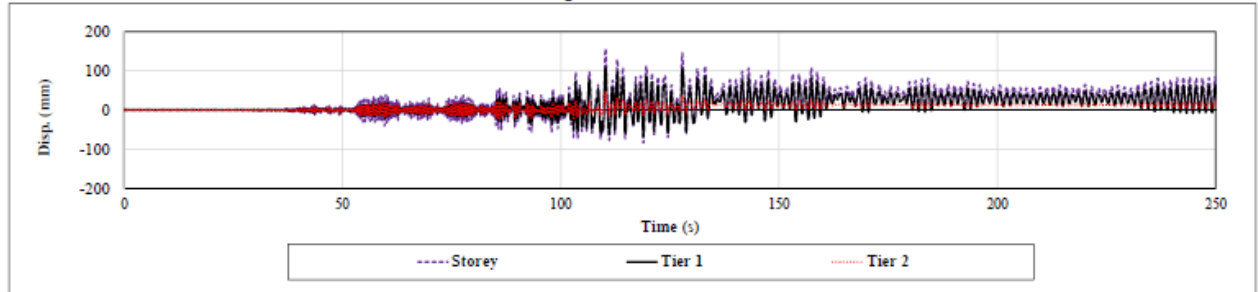
Column Out-of-plane Bending Demand



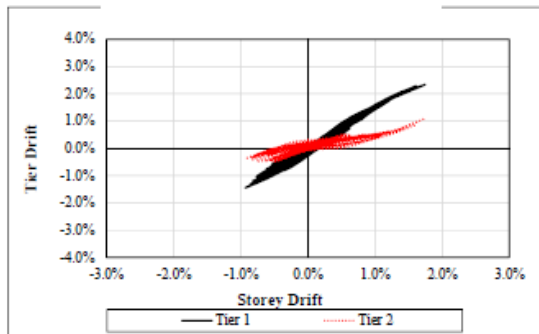
Drift vs. Time



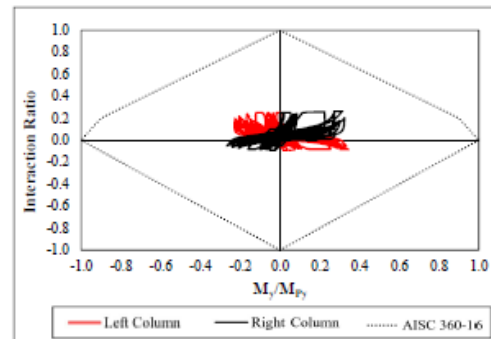
Displacement vs. Time



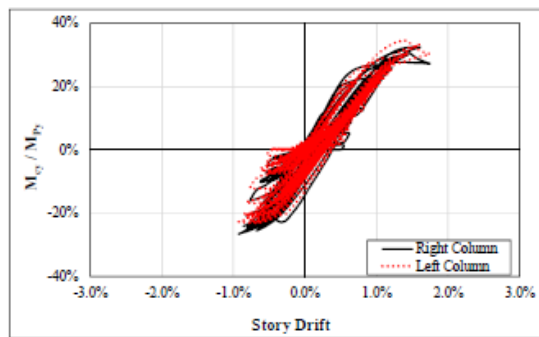
Tier Drift vs. Storey Drift



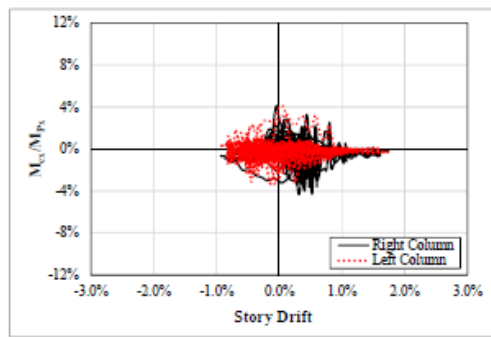
Column P-M Interaction Diagram



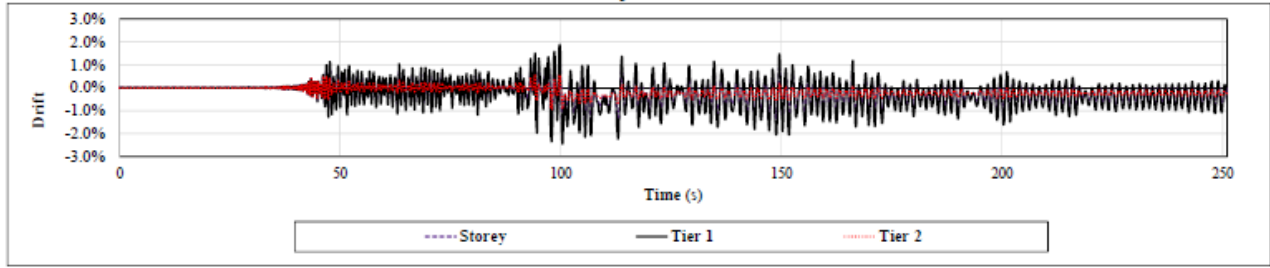
Column In-plane Bending Demand



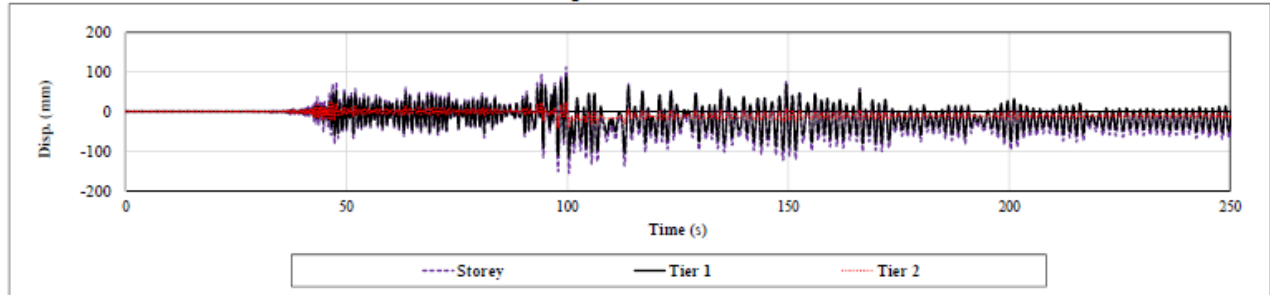
Column Out-of-plane Bending Demand



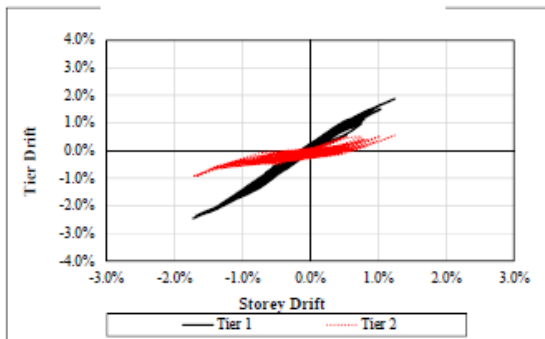
Drift vs. Time



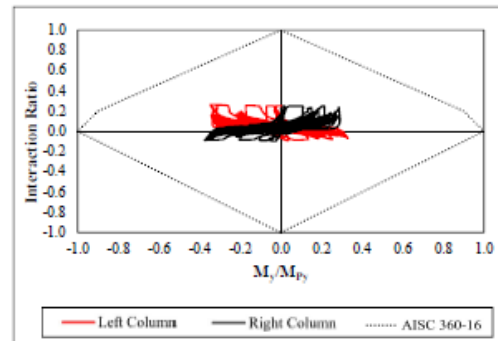
Displacement vs. Time



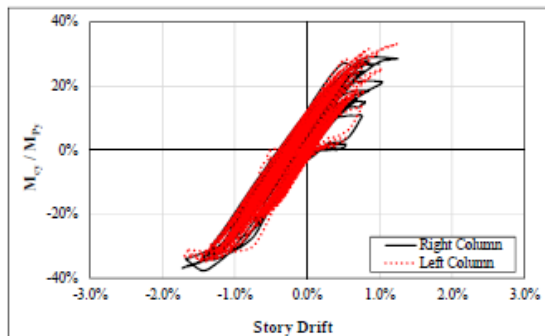
Tier Drift vs. Storey Drift



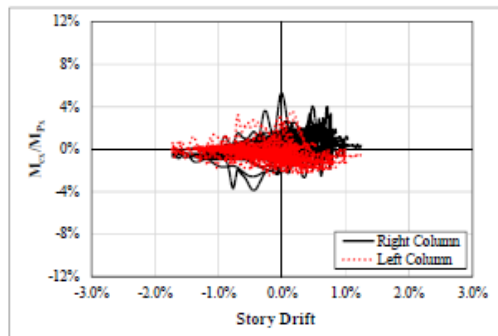
Column P-M Interaction Diagram



Column In-plane Bending Demand



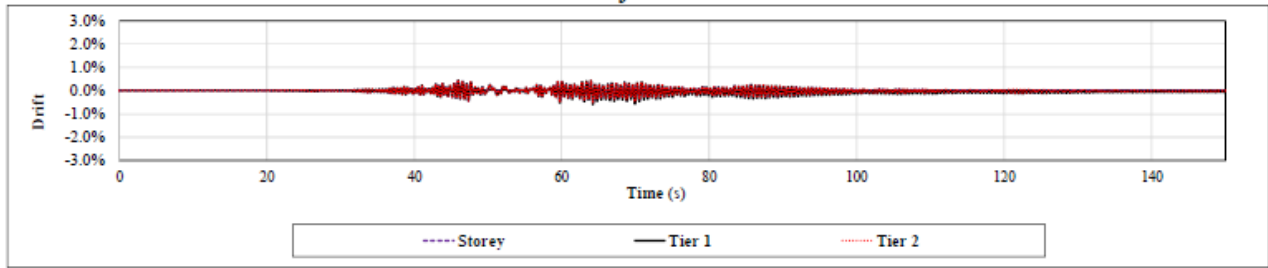
Column Out-of-plane Bending Demand



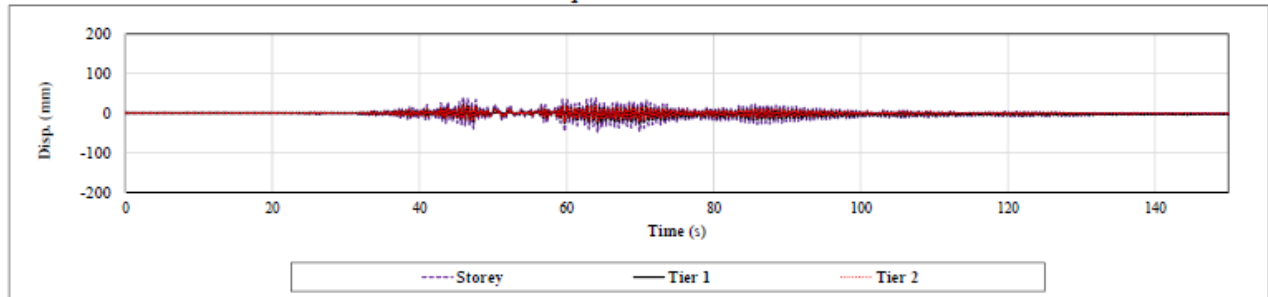
Ground Motion: SCI 8

Two-Tiered SCBF: AISC 341-16 Design

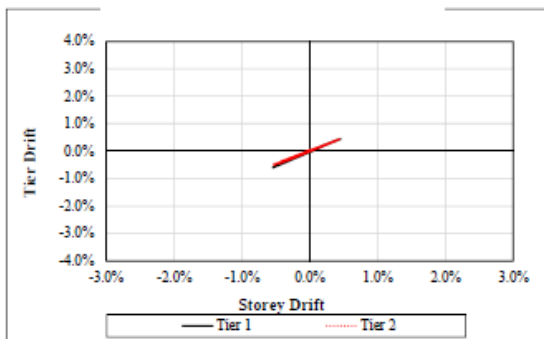
Drift vs. Time



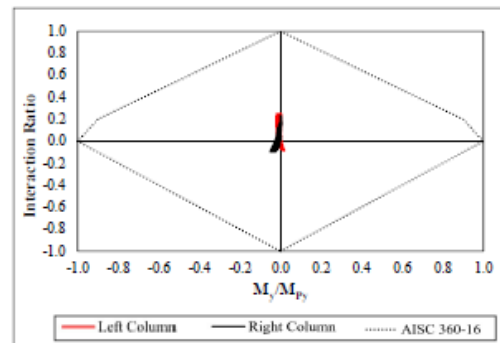
Displacement vs. Time



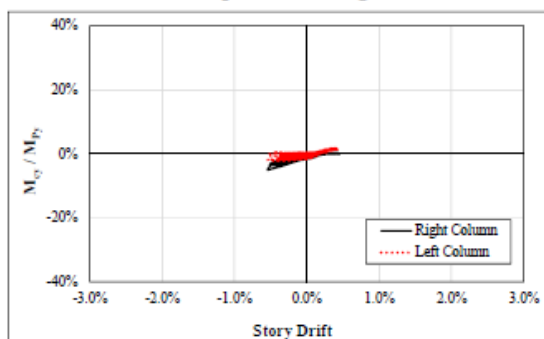
Tier Drift vs. Storey Drift



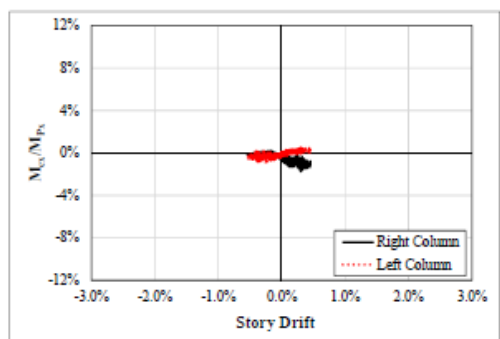
Column P-M Interaction Diagram



Column In-plane Bending Demand



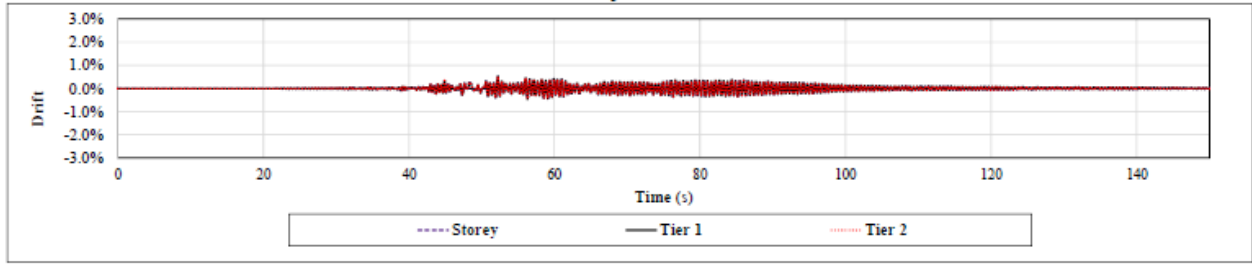
Column Out-of-plane Bending Demand



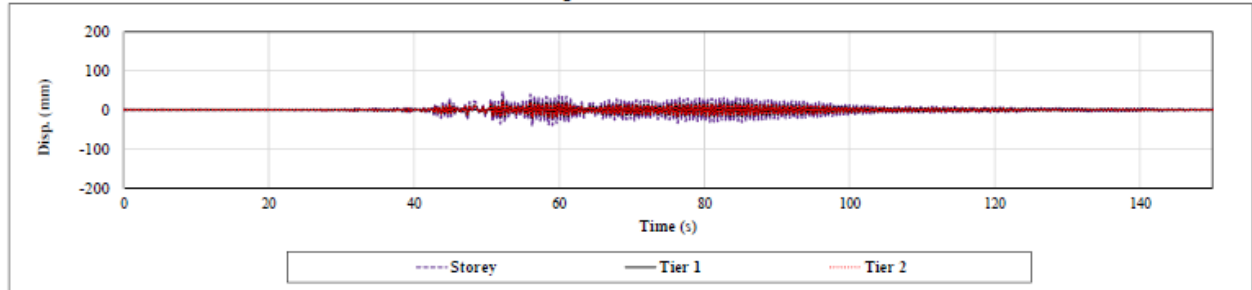
Ground Motion: SCI 9

Two-Tiered SCBF: AISC 341-16 Design

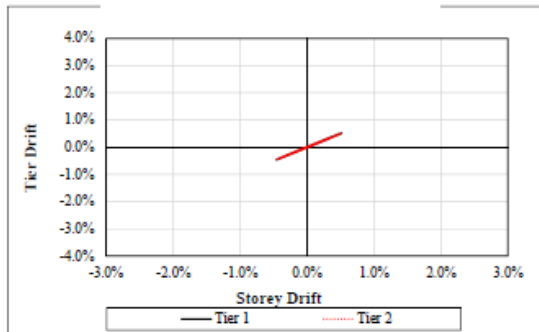
Drift vs. Time



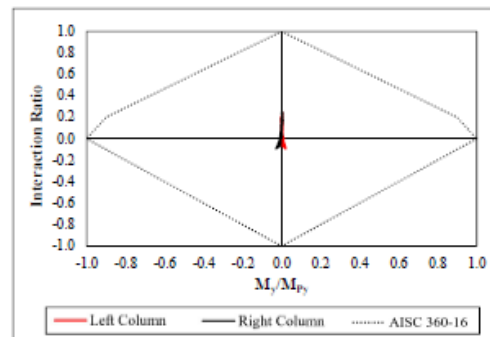
Displacement vs. Time



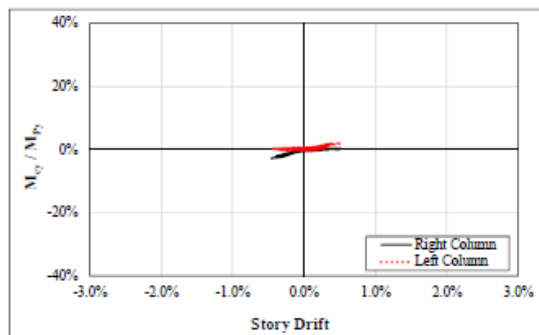
Tier Drift vs. Storey Drift



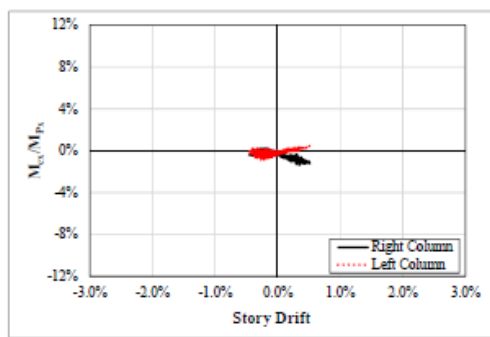
Column P-M Interaction Diagram



Column In-plane Bending Demand



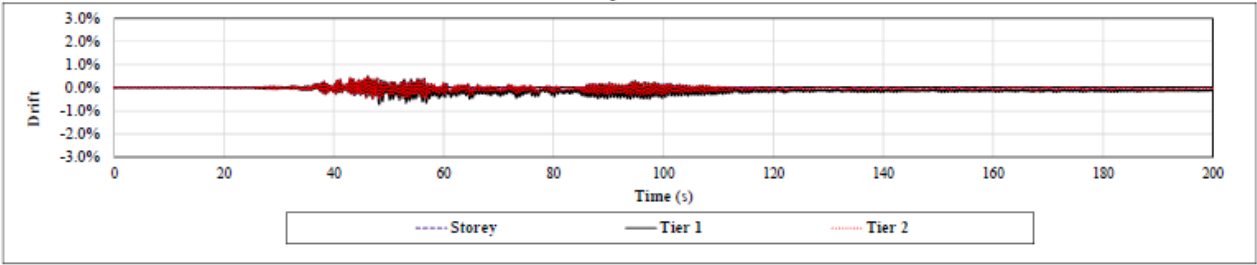
Column Out-of-plane Bending Demand



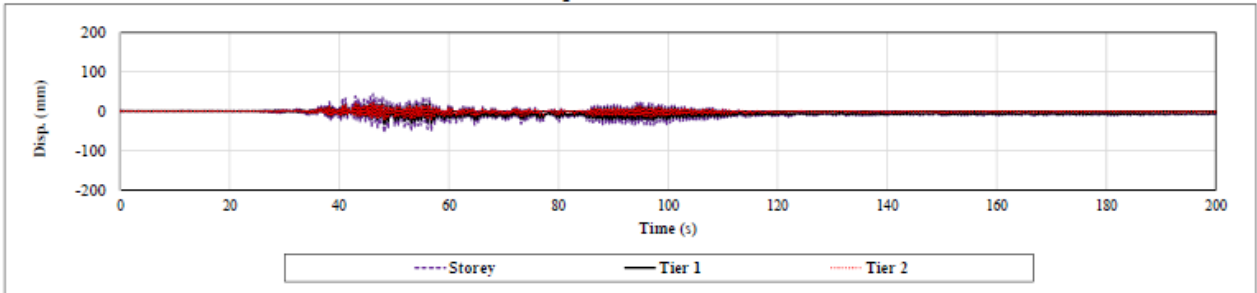
Ground Motion: SCI 10

Two-Tiered SCBF: AISC 341-16 Design

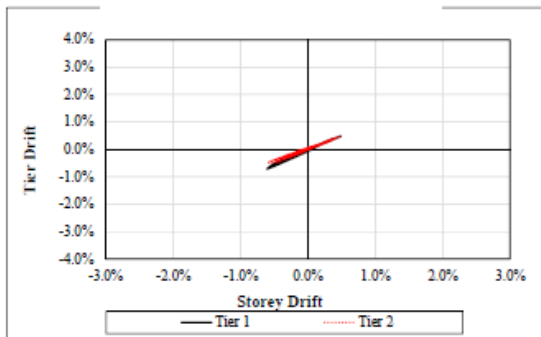
Drift vs. Time



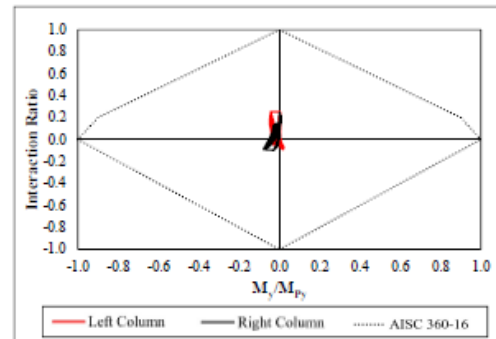
Displacement vs. Time



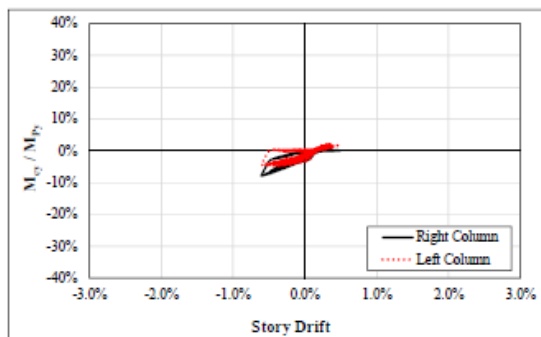
Tier Drift vs. Storey Drift



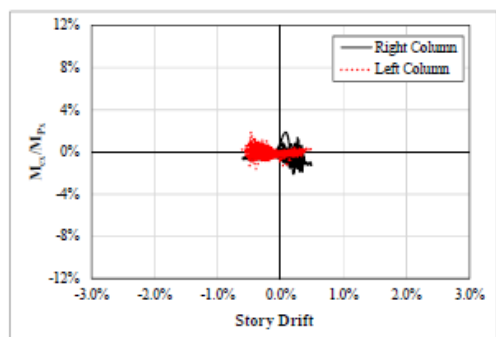
Column P-M Interaction Diagram



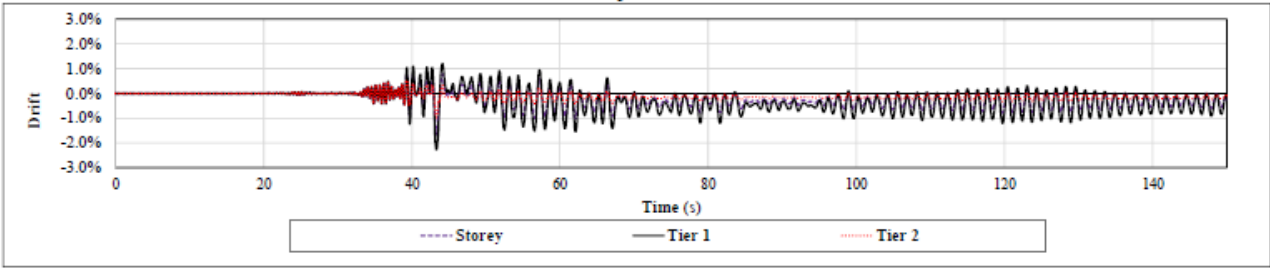
Column In-plane Bending Demand



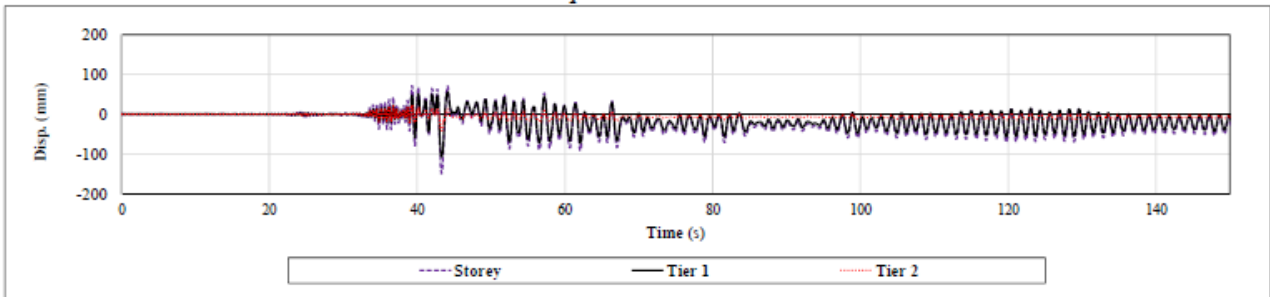
Column Out-of-plane Bending Demand



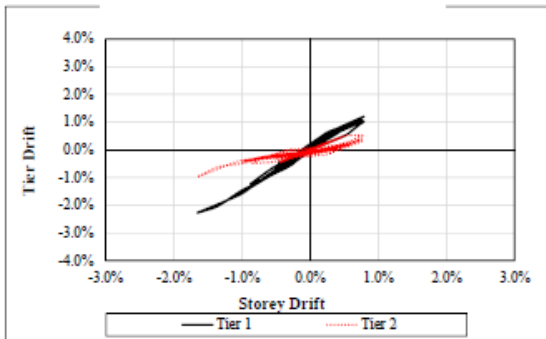
Drift vs. Time



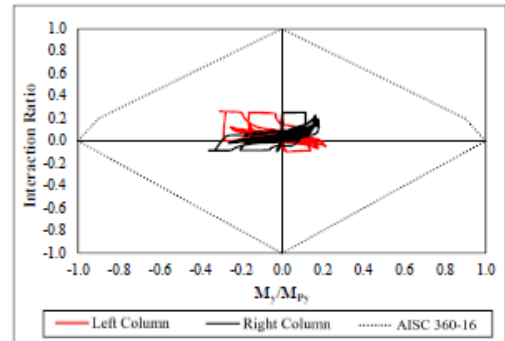
Displacement vs. Time



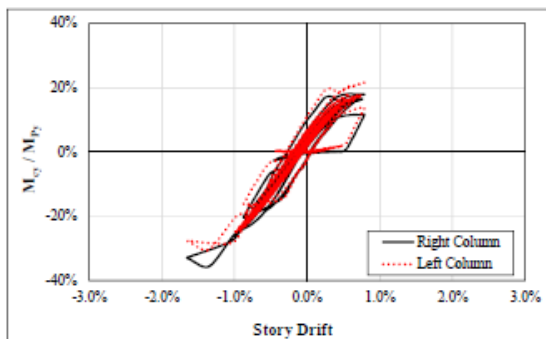
Tier Drift vs. Storey Drift



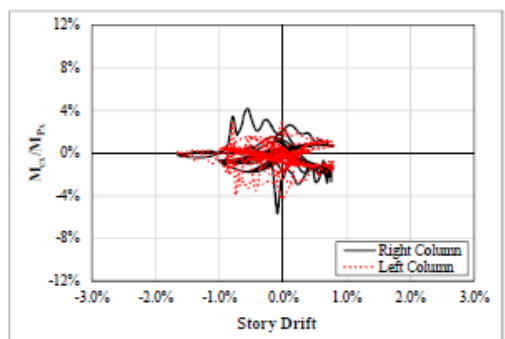
Column P-M Interaction Diagram



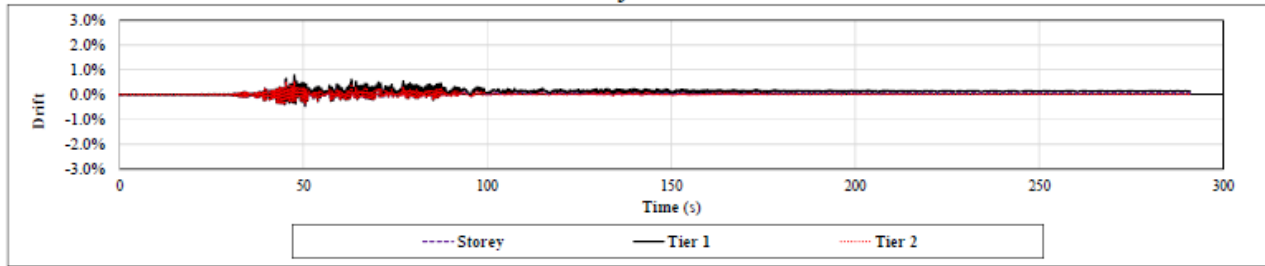
Column In-plane Bending Demand



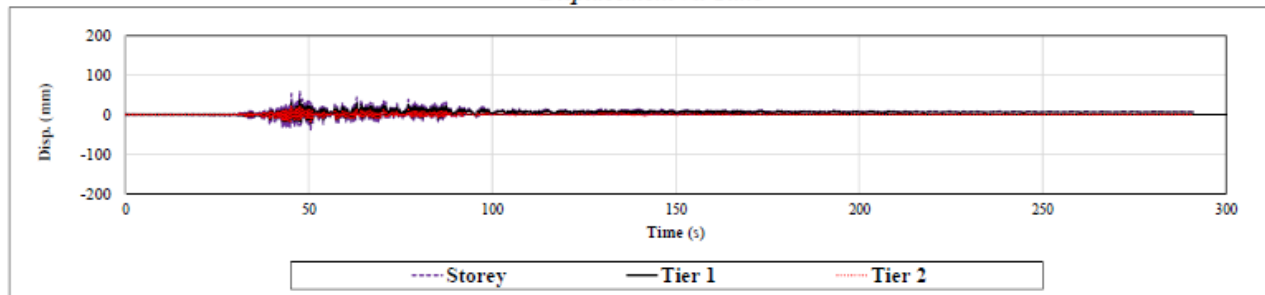
Column Out-of-plane Bending Demand



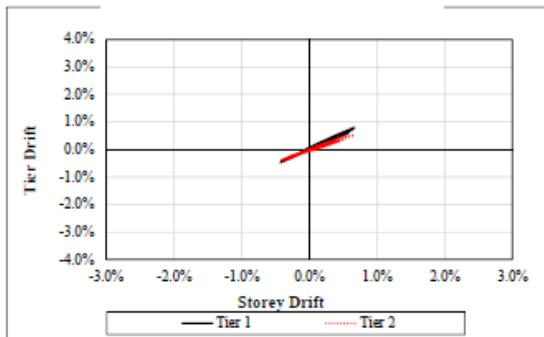
Drift vs. Time



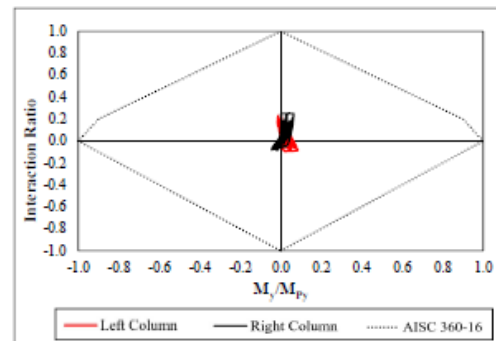
Displacement vs. Time



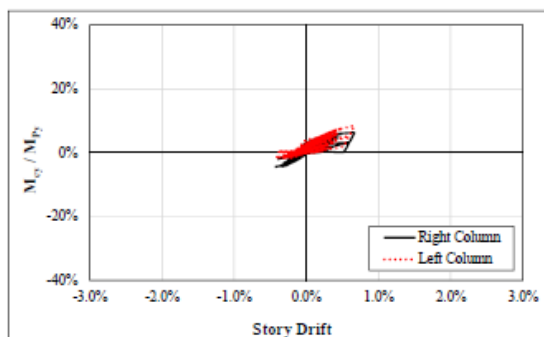
Tier Drift vs. Storey Drift



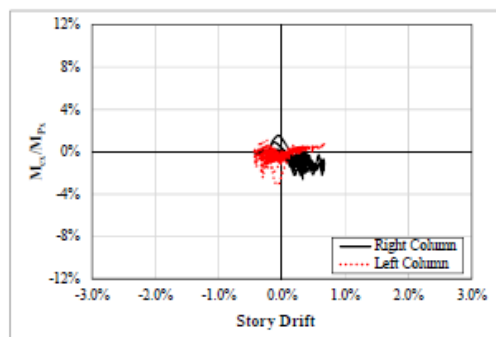
Column P-M Interaction Diagram



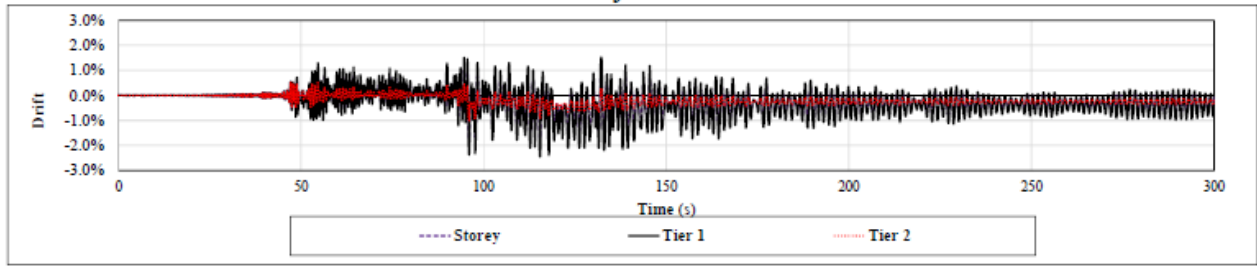
Column In-plane Bending Demand



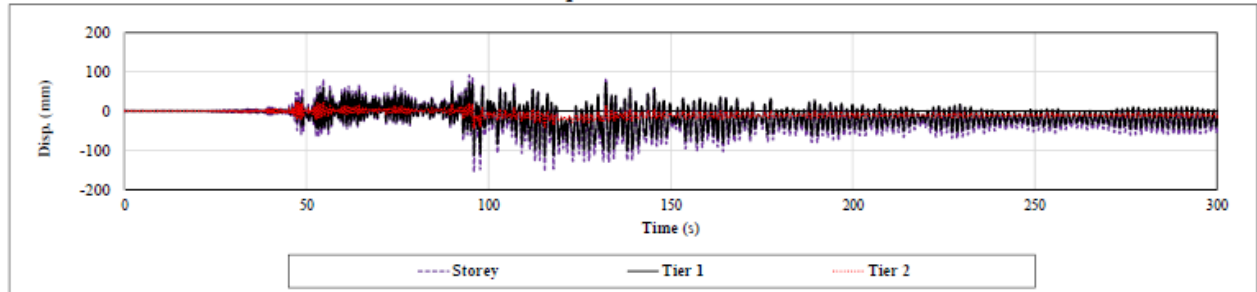
Column Out-of-plane Bending Demand



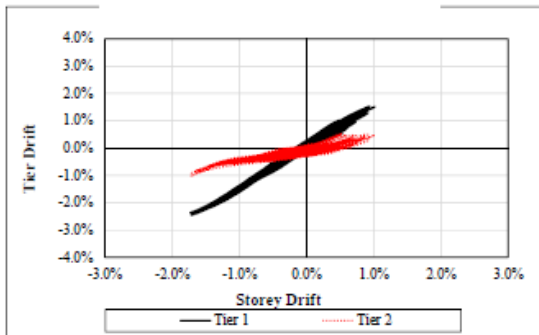
Drift vs. Time



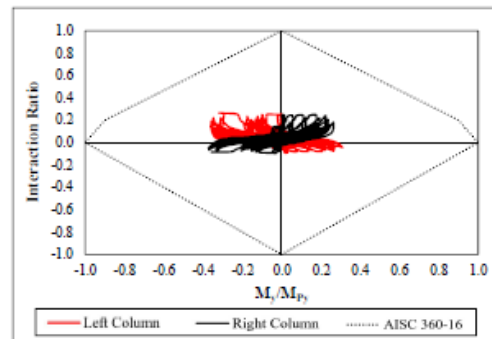
Displacement vs. Time



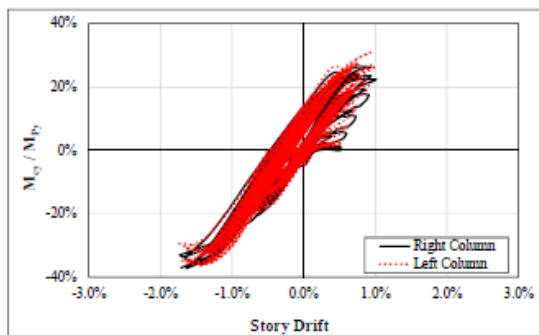
Tier Drift vs. Storey Drift



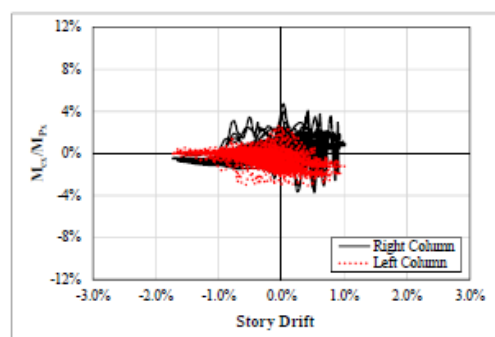
Column P-M Interaction Diagram



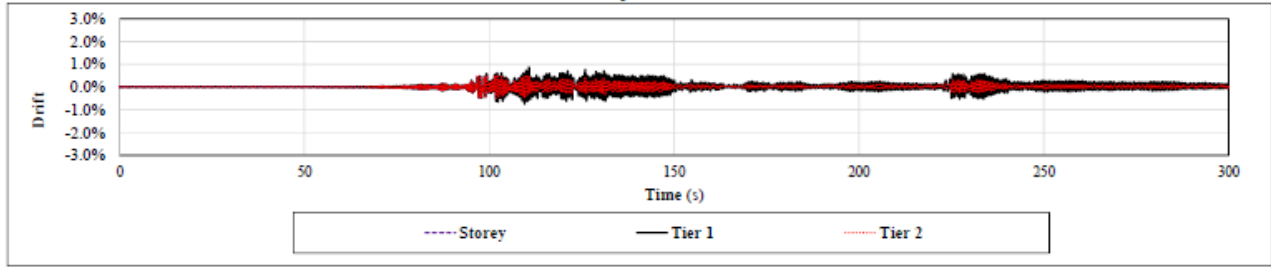
Column In-plane Bending Demand



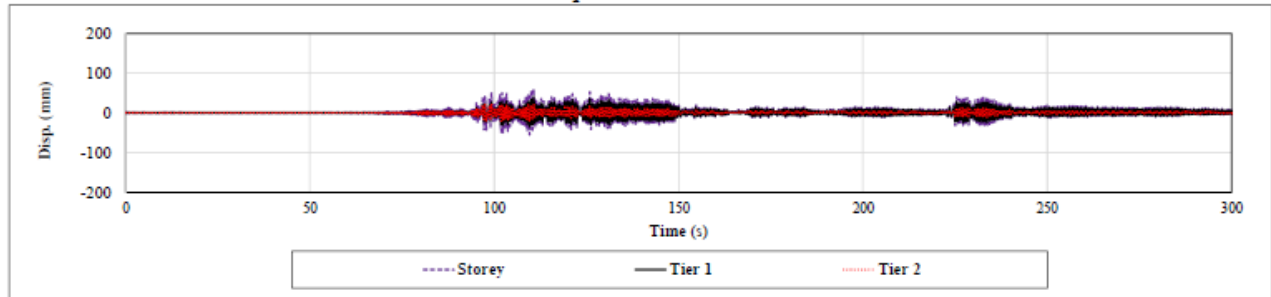
Column Out-of-plane Bending Demand



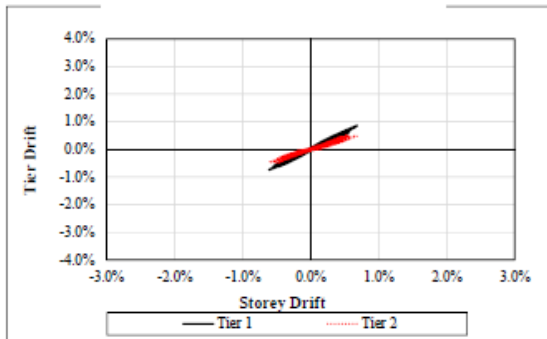
Drift vs. Time



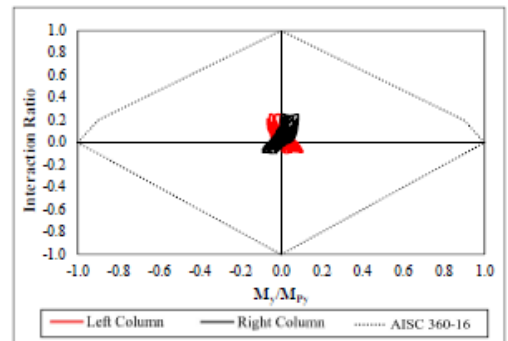
Displacement vs. Time



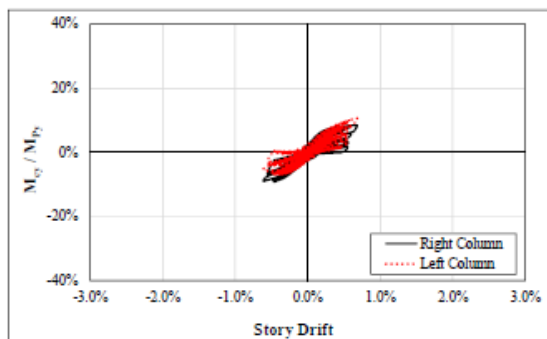
Tier Drift vs. Storey Drift



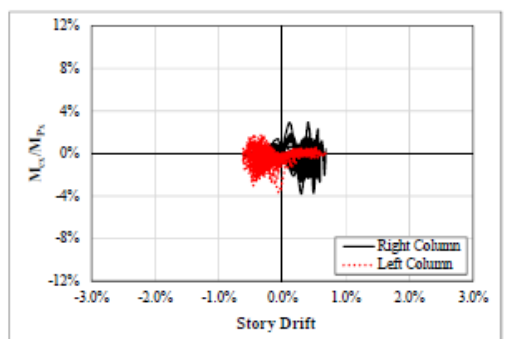
Column P-M Interaction Diagram



Column In-plane Bending Demand



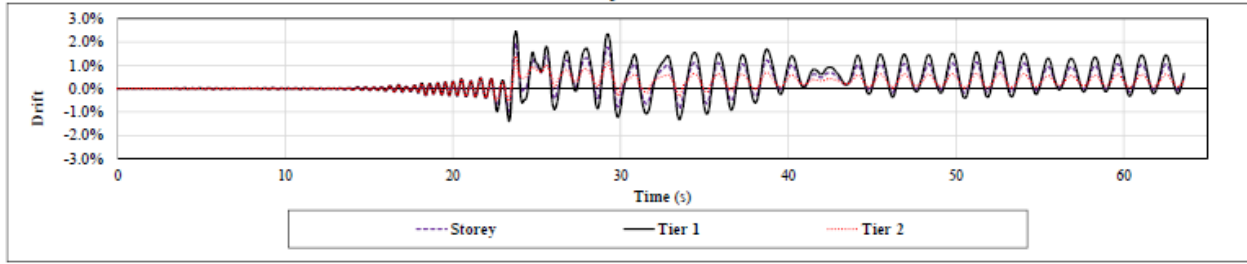
Column Out-of-plane Bending Demand



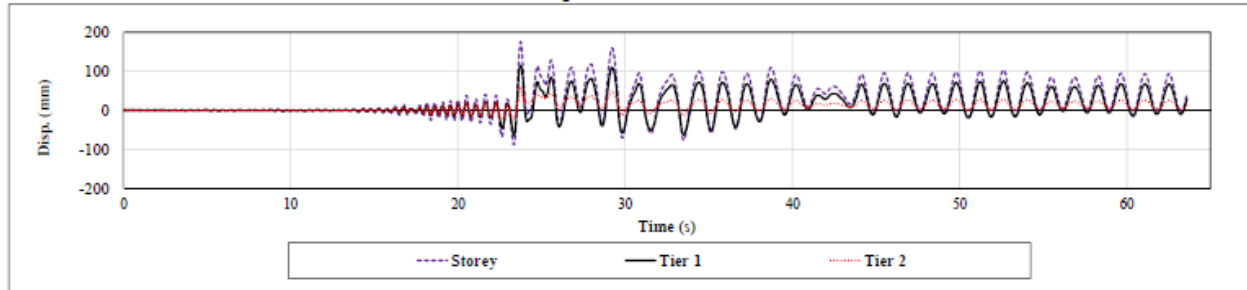
Ground Motion: SCI 15

Two-Tiered SCBF: AISC 341-16 Design

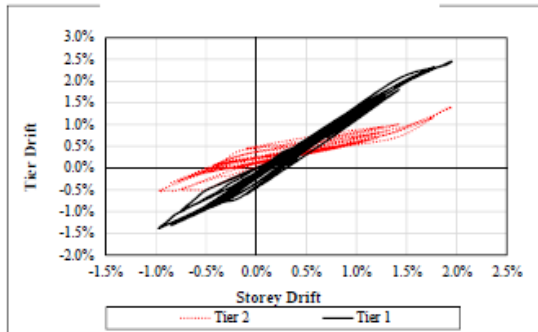
Drift vs. Time



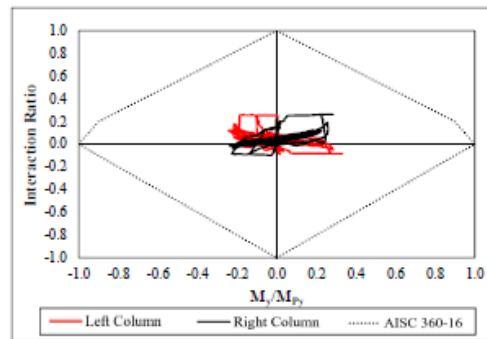
Displacement vs. Time



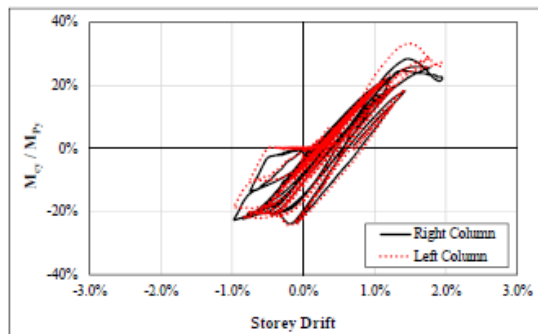
Tier Drift vs. Storey Drift



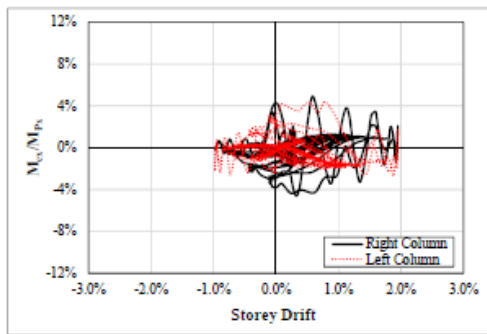
Column P-M Interaction Diagram



Column In-plane Bending Demand



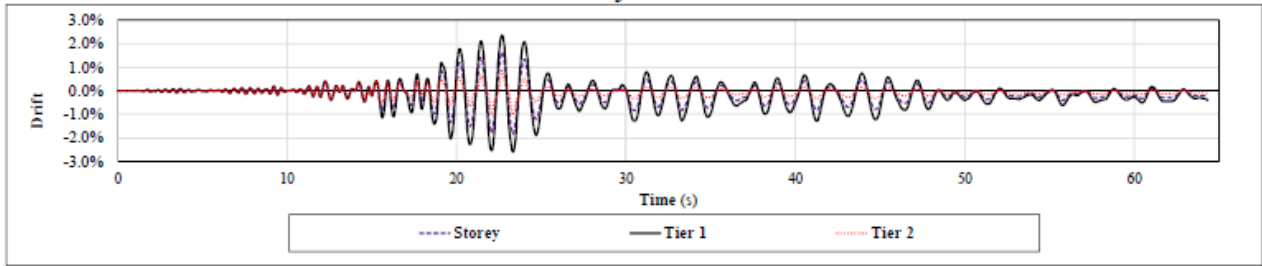
Column Out-of-plane Bending Demand



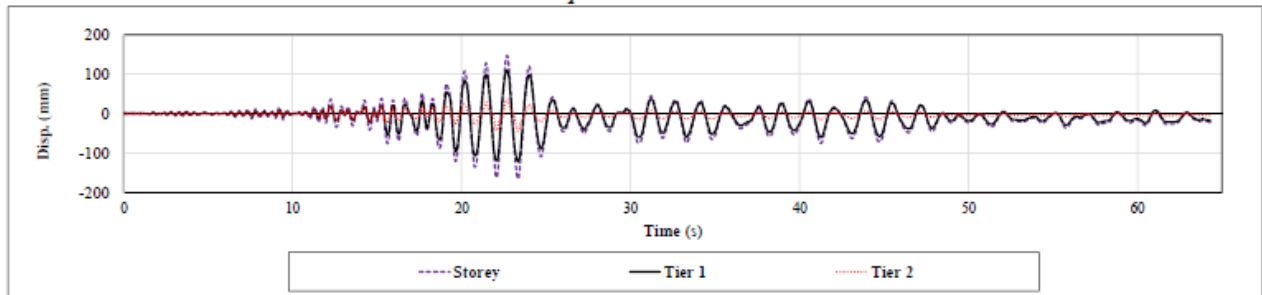
Ground Motion: SCI 16

Two-Tiered SCBF: AISC 341-16 Design

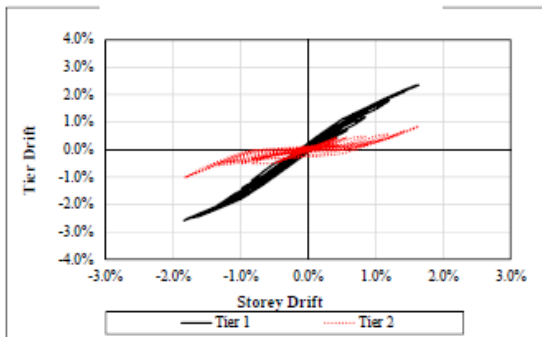
Drift vs. Time



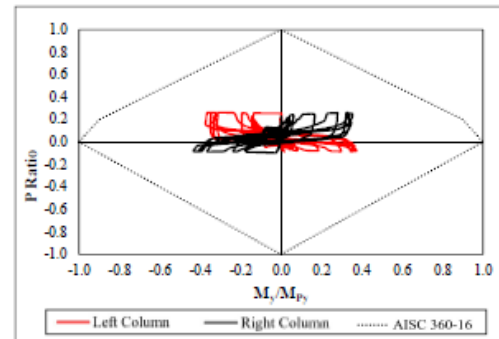
Displacement vs. Time



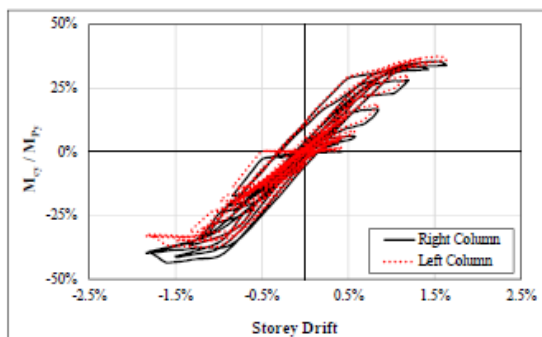
Tier Drift vs. Storey Drift



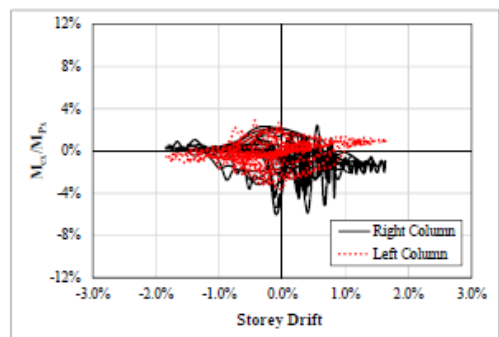
Column P-M Interaction Diagram



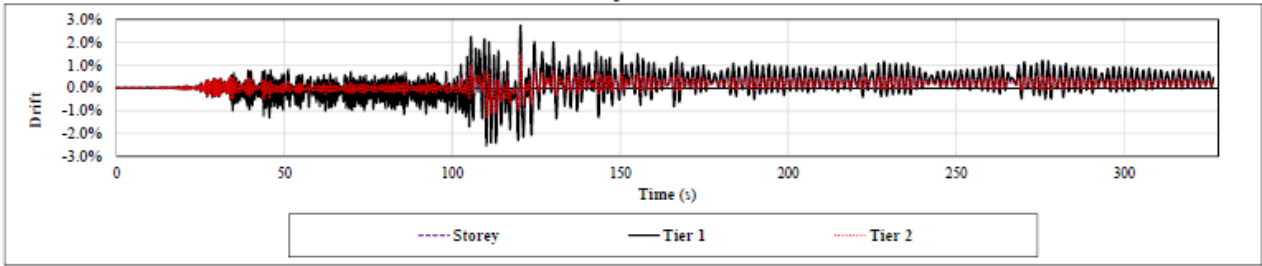
Column In-plane Bending Demand



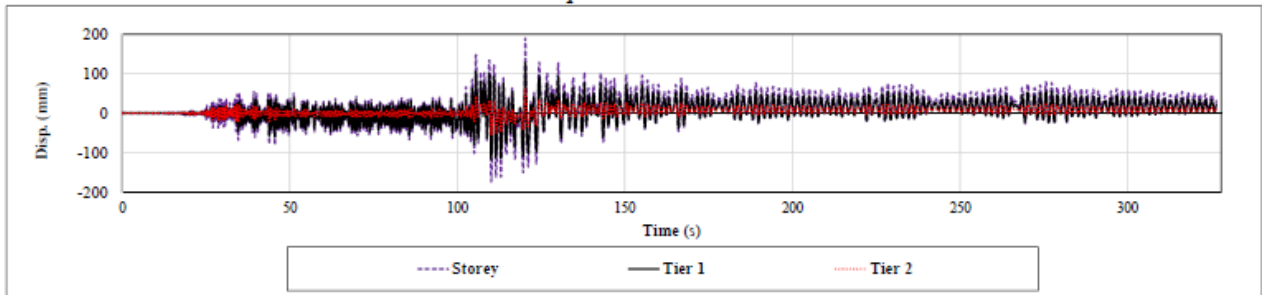
Column Out-of-plane Bending Demand



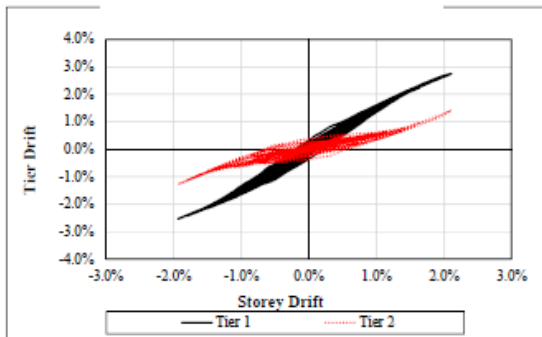
Drift vs. Time



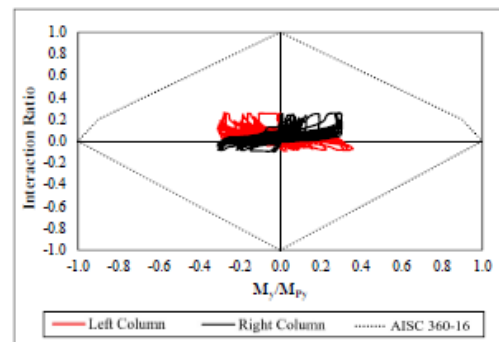
Displacement vs. Time



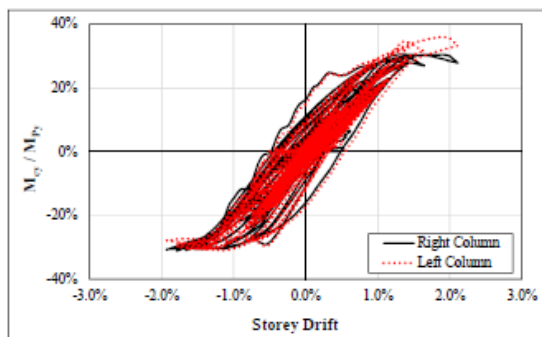
Tier Drift vs. Storey Drift



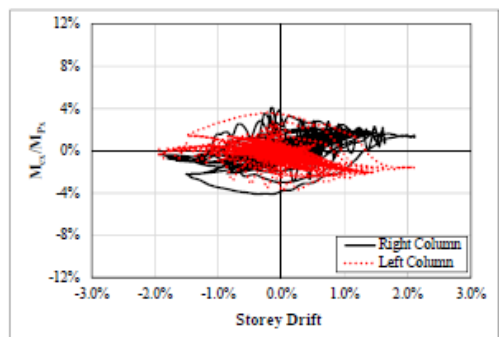
Column P-M Interaction Diagram



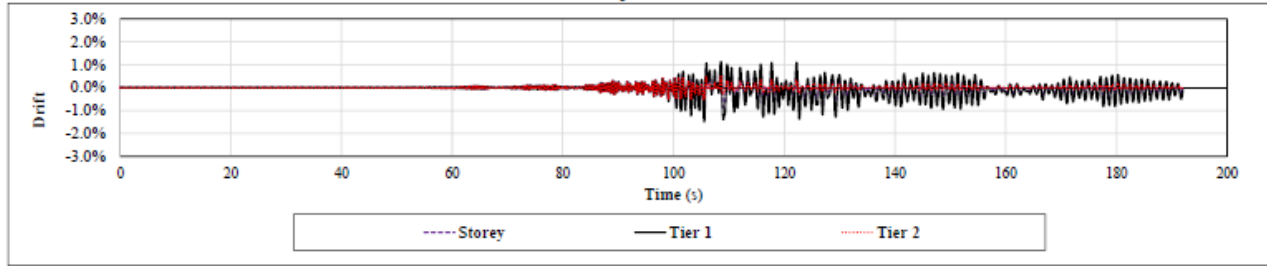
Column In-plane Bending Demand



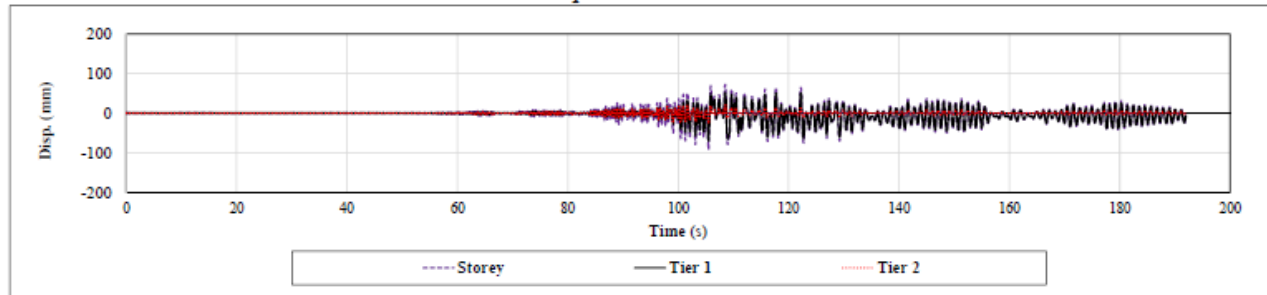
Column Out-of-plane Bending Demand



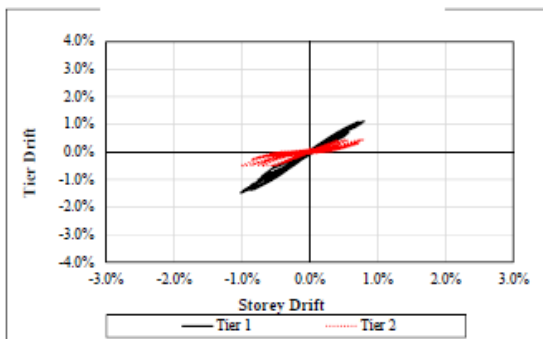
Drift vs. Time



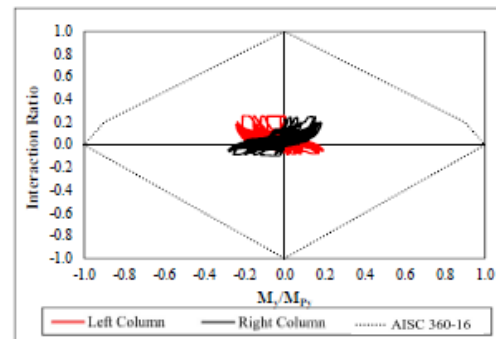
Displacement vs. Time



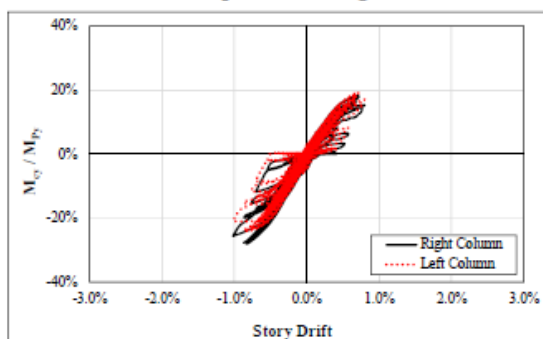
Tier Drift vs. Storey Drift



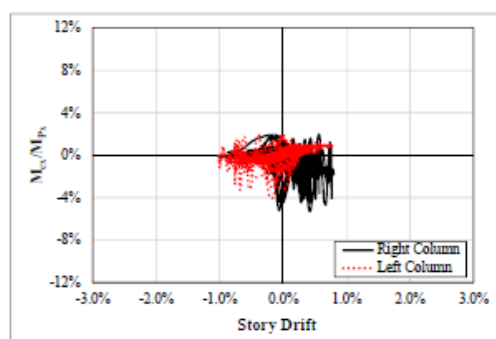
Column P-M Interaction Diagram



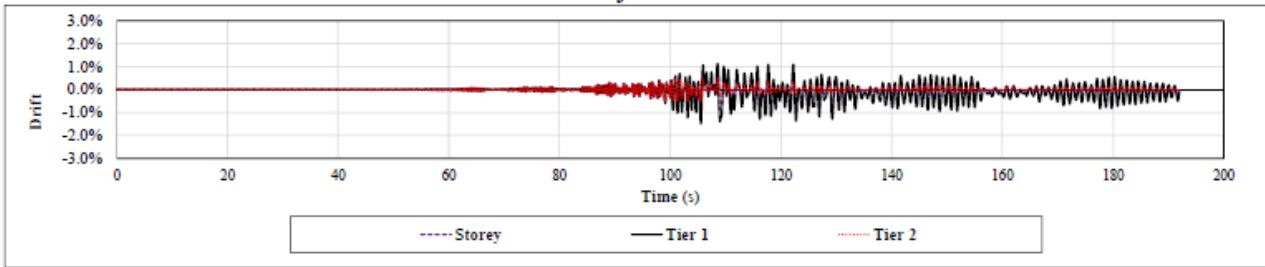
Column In-plane Bending Demand



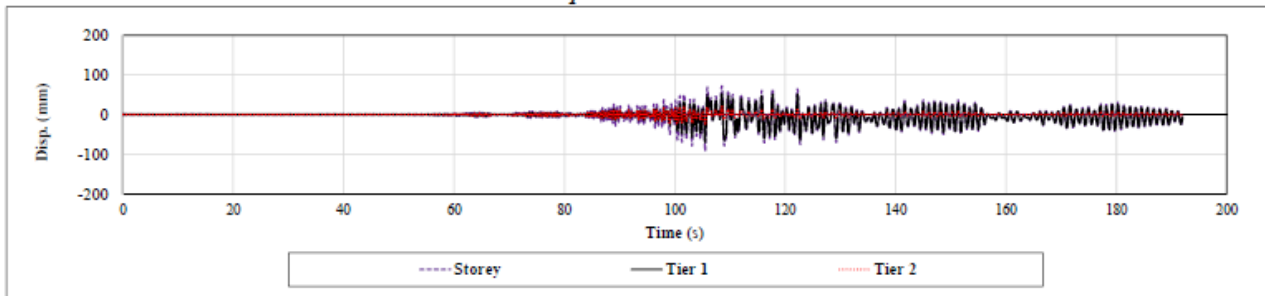
Column Out-of-plane Bending Demand



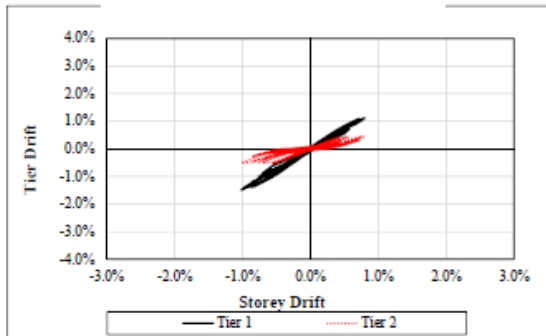
Drift vs. Time



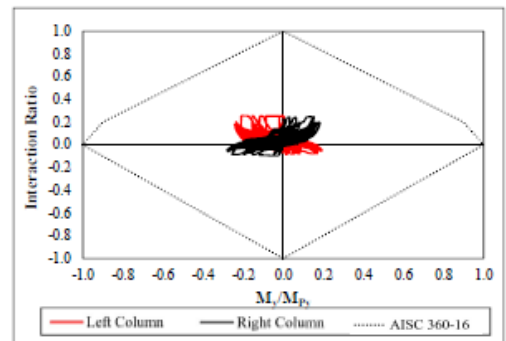
Displacement vs. Time



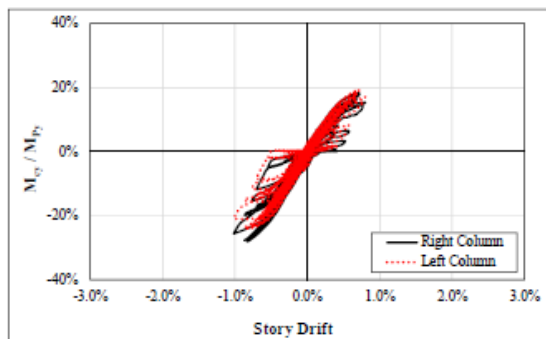
Tier Drift vs. Storey Drift



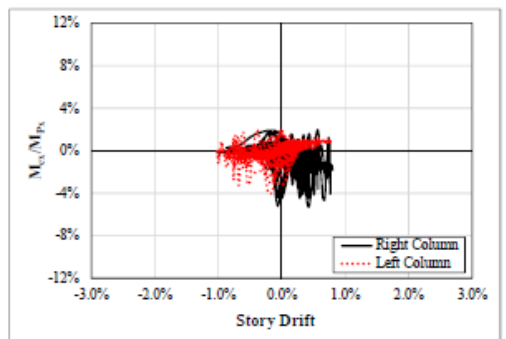
Column P-M Interaction Diagram



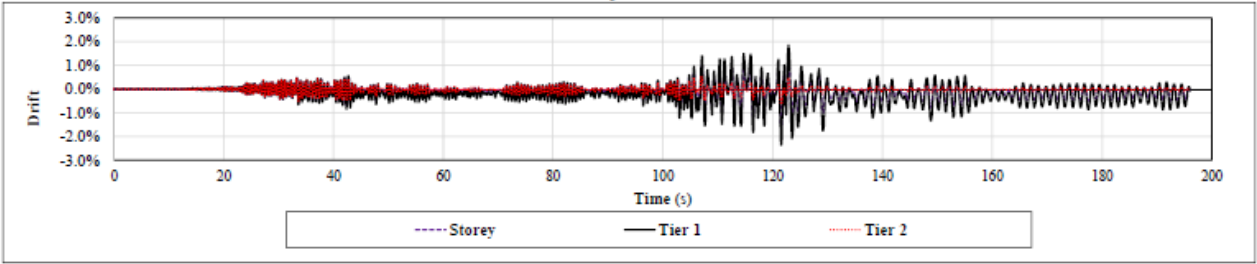
Column In-plane Bending Demand



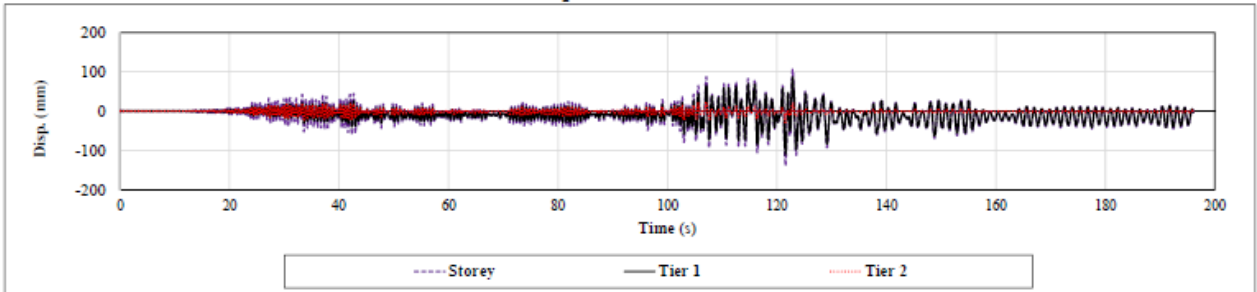
Column Out-of-plane Bending Demand



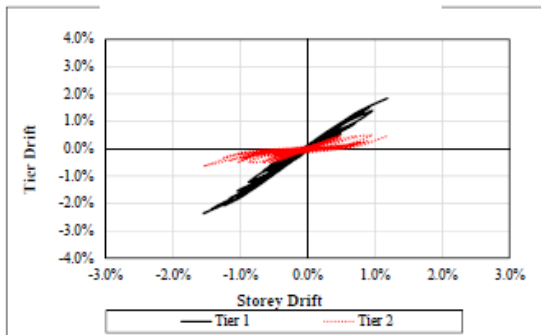
Drift vs. Time



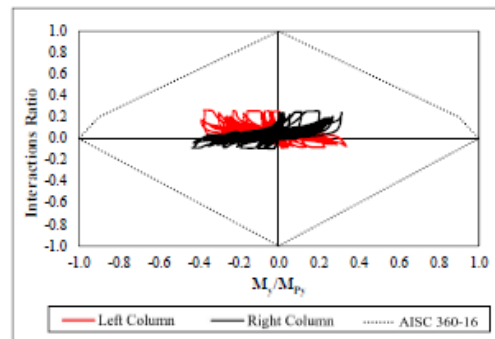
Displacement vs. Time



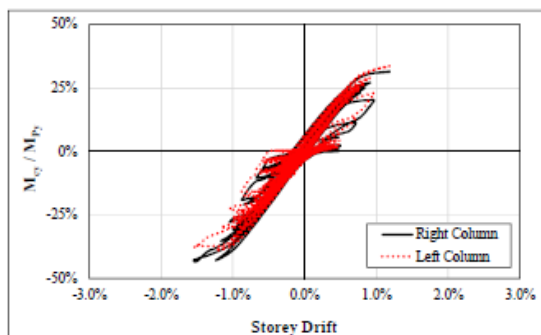
Tier Drift vs. Storey Drift



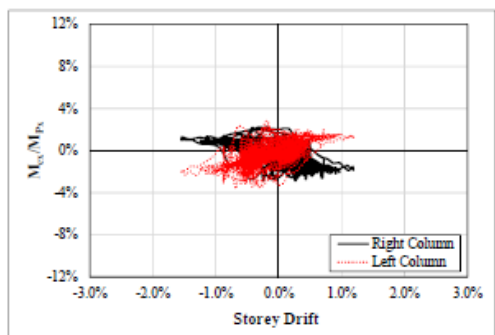
Column P-M Interaction Diagram



Column In-plane Bending Demand



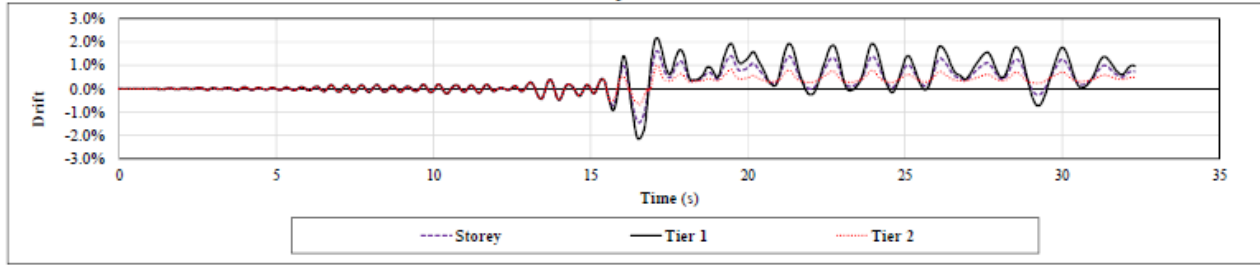
Column Out-of-plane Bending Demand



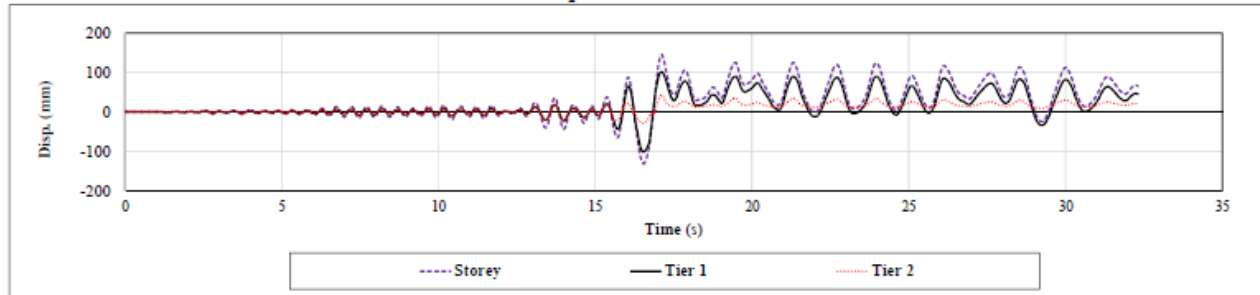
Ground Motion: SCI 21

Two-Tiered: AISC 341-16 Design

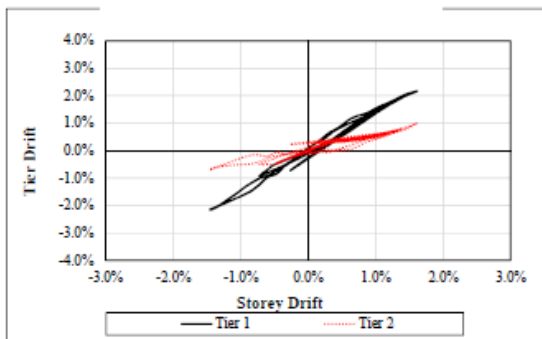
Drift vs. Time



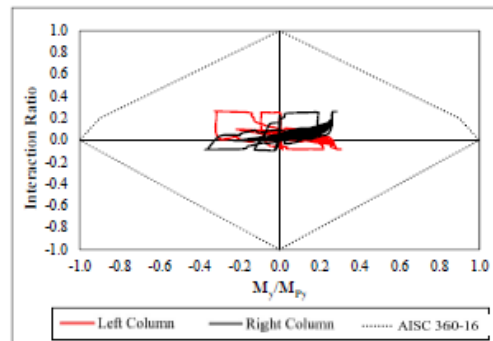
Displacement vs. Time



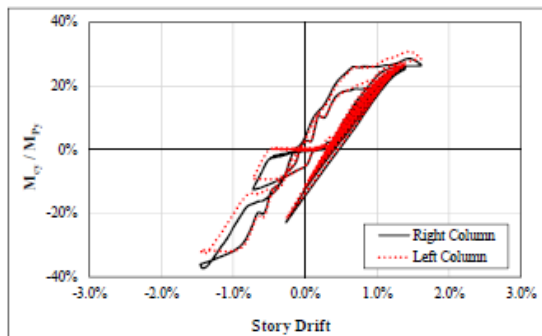
Tier Drift vs. Storey Drift



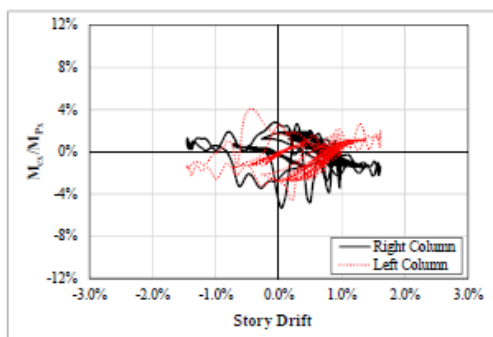
Column P-M Interaction Diagram



Column In-plane Bending Demand



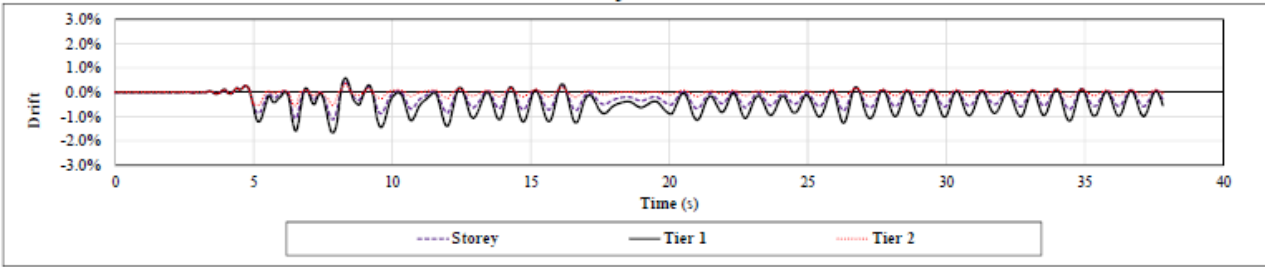
Column Out-of-plane Bending Demand



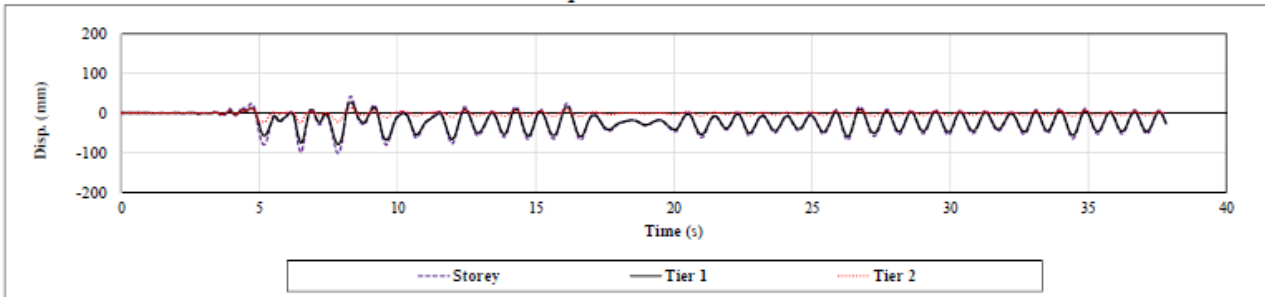
Ground Motion: SCC 1

Two-Tiered SCBF: AISC 341-16 Design

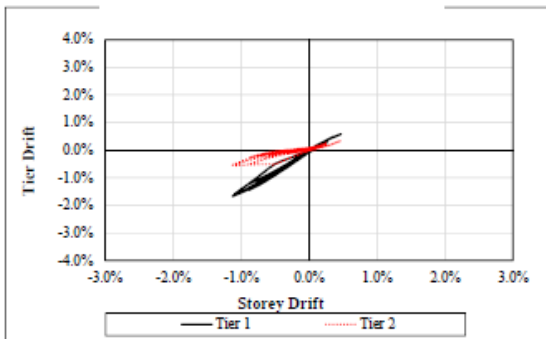
Drift vs. Time



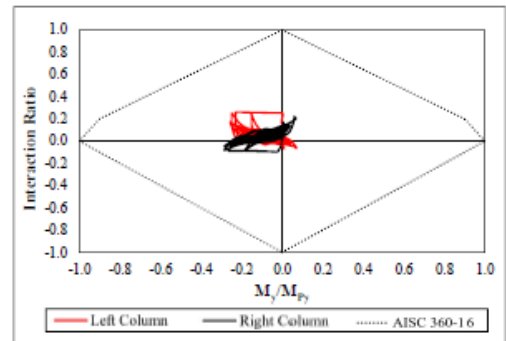
Displacement vs. Time



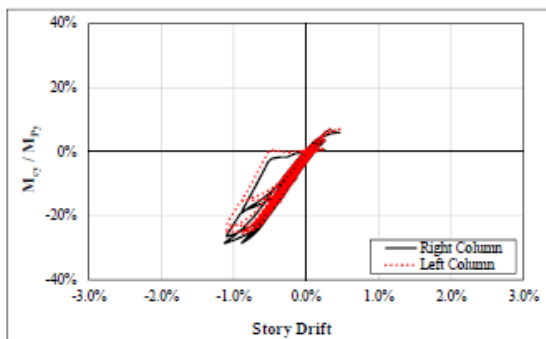
Tier Drift vs. Storey Drift



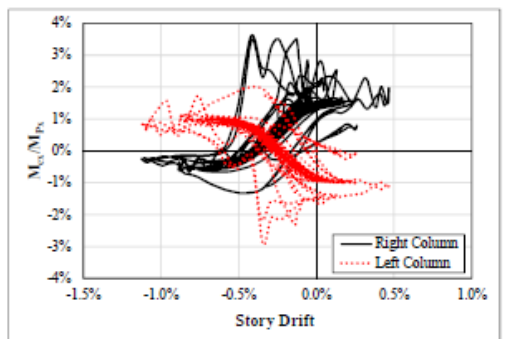
Column P-M Interaction Diagram



Column In-plane Bending Demand



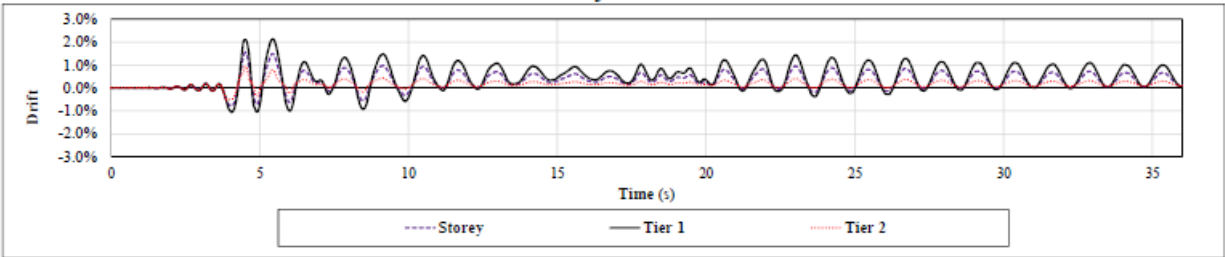
Column Out-of-plane Bending Demand



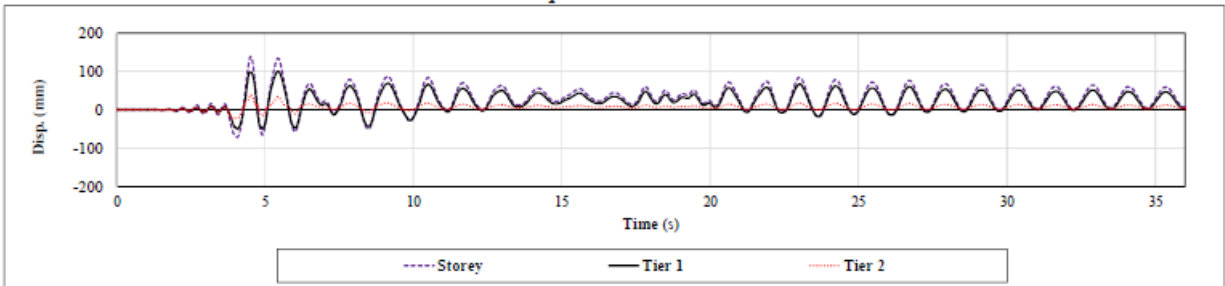
Ground Motion: SCC 2

Two-Tiered: AISC 341-16 Design

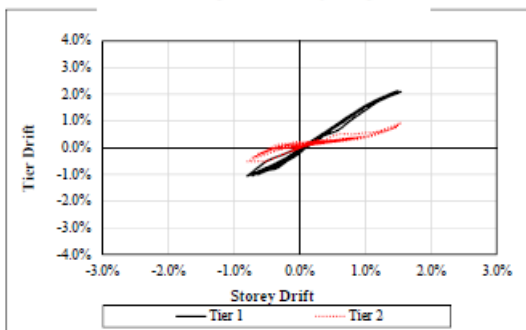
Drift vs. Time



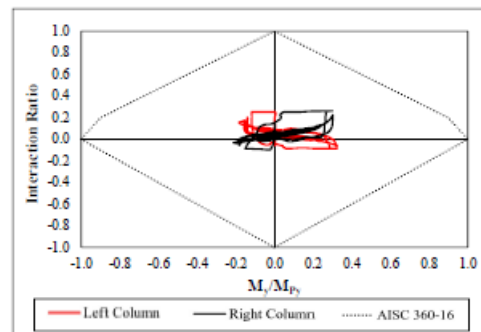
Displacement vs. Time



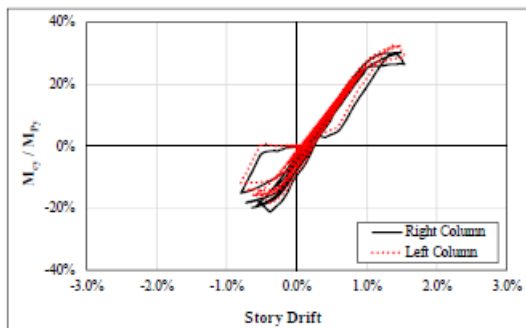
Tier Drift vs. Storey Drift



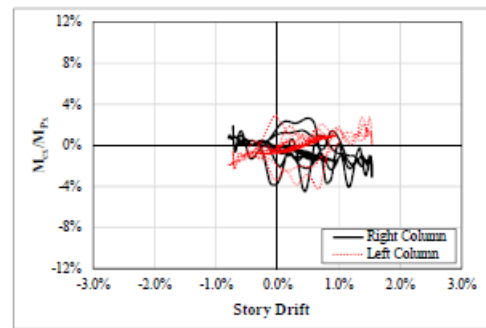
Column P-M Interaction Diagram



Column In-plane Bending Demand



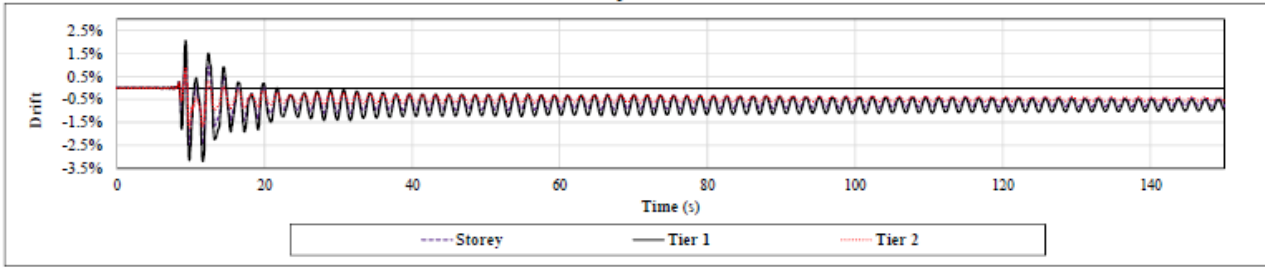
Column Out-of-plane Bending Demand



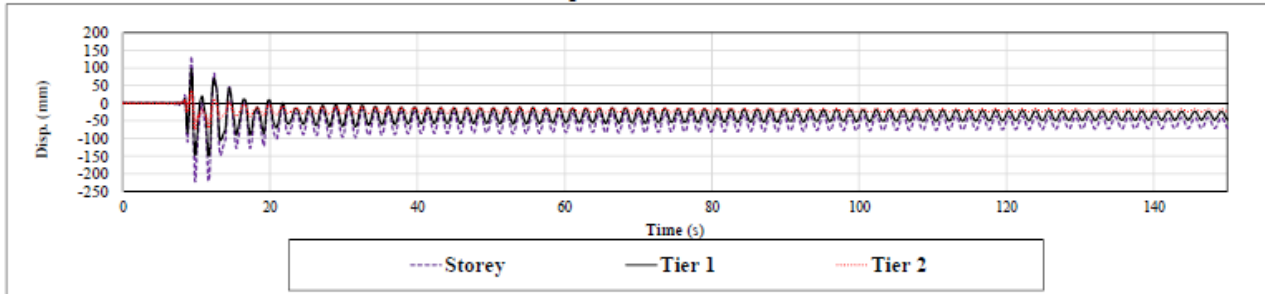
Ground Motion: SCC 3

Two-Tiered SCBF: AISC 341-16 Design

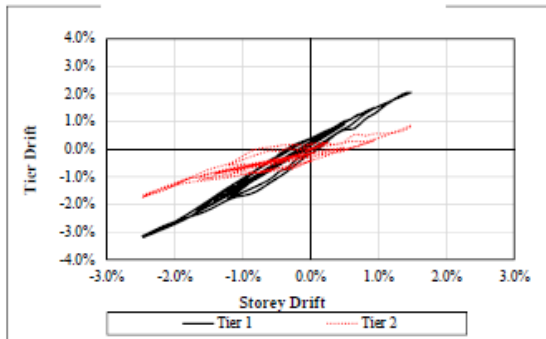
Drift vs. Time



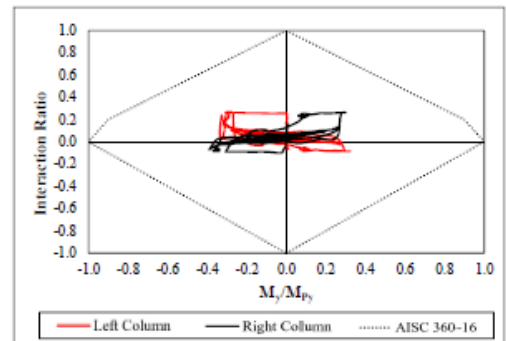
Displacement vs. Time



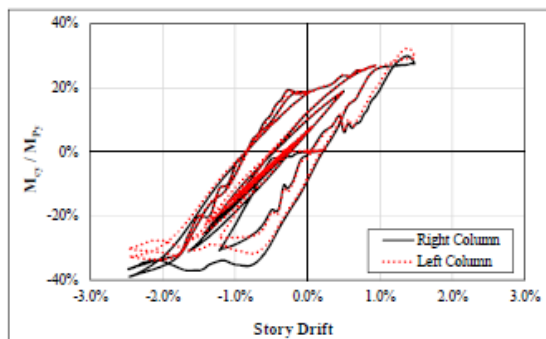
Tier Drift vs. Storey Drift



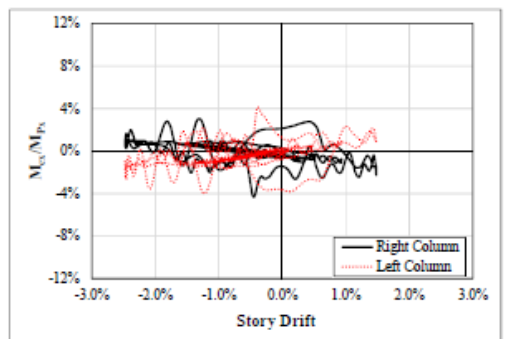
Column P-M Interaction Diagram



Column In-plane Bending Demand



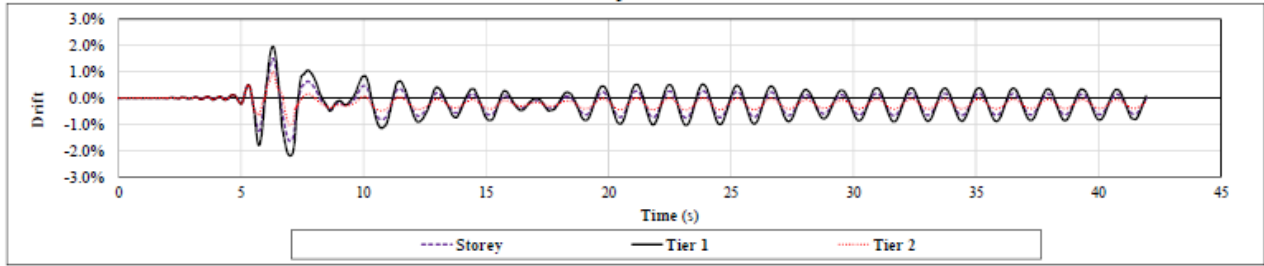
Column Out-of-plane Bending Demand



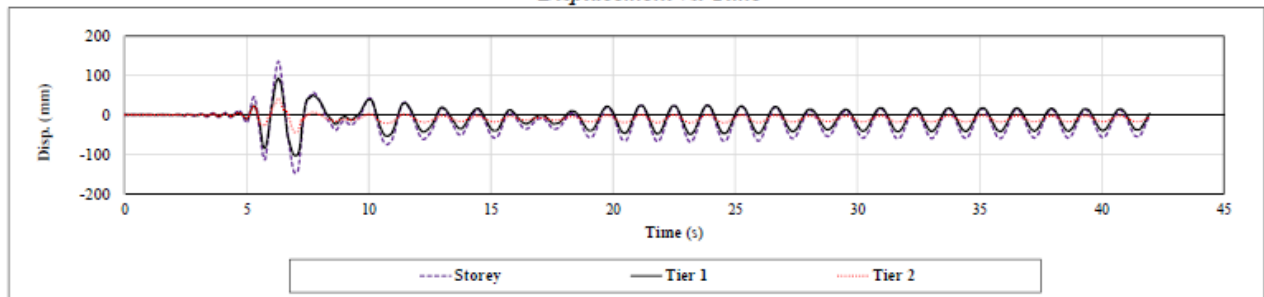
Ground Motion: SCC 4

Two-Tiered SCBF: AISC 341-16 Design

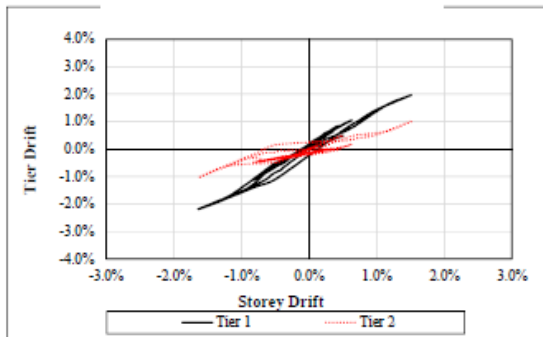
Drift vs. Time



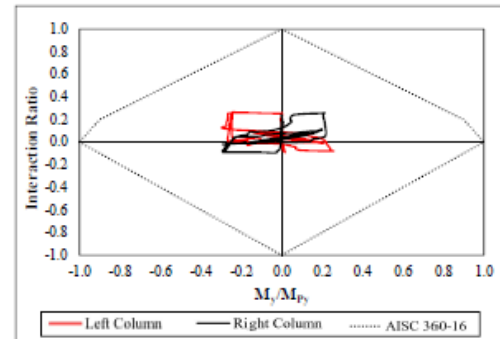
Displacement vs. Time



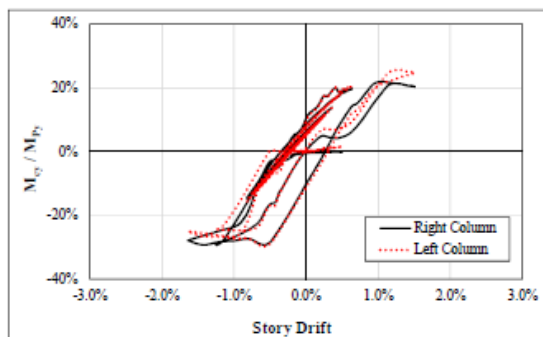
Tier Drift vs. Storey Drift



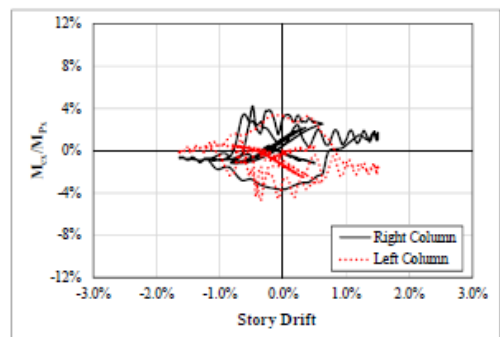
Column P-M Interaction Diagram



Column In-plane Bending Demand



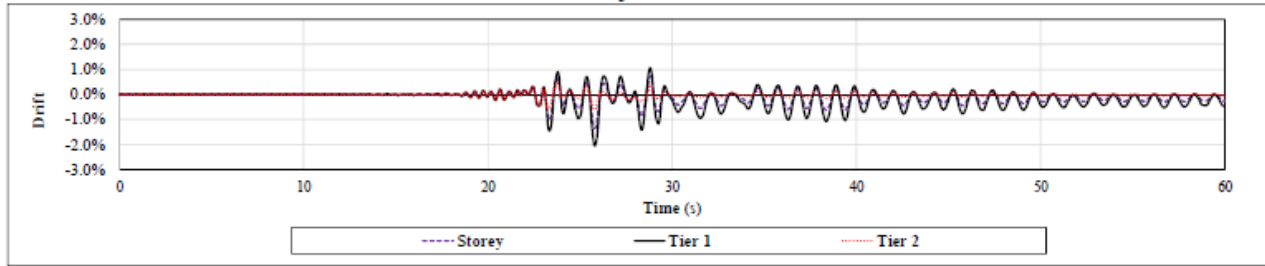
Column Out-of-plane Bending Demand



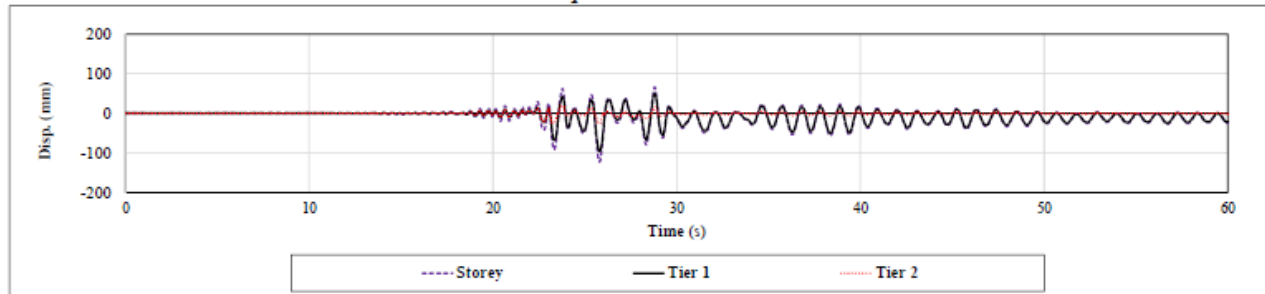
Ground Motion: SCC 5

Two-Tiered SCBF: AISC 341-16 Design

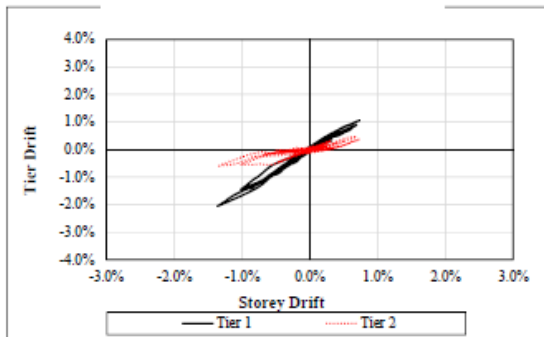
Drift vs. Time



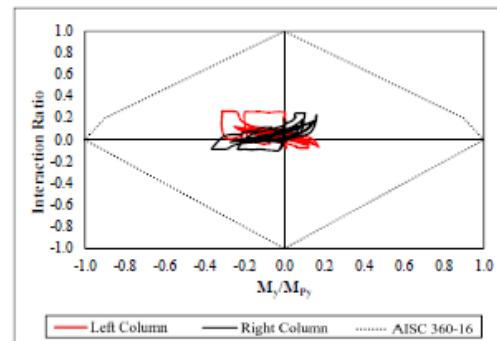
Displacement vs. Time



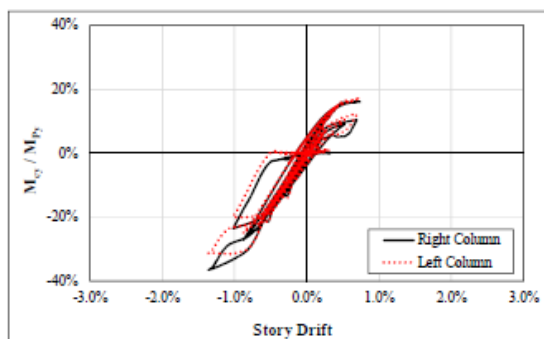
Tier Drift vs. Storey Drift



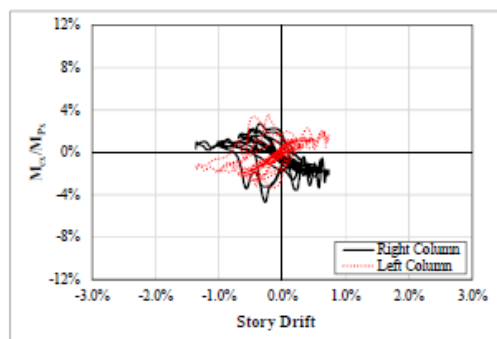
Column P-M Interaction Diagram



Column In-plane Bending Demand



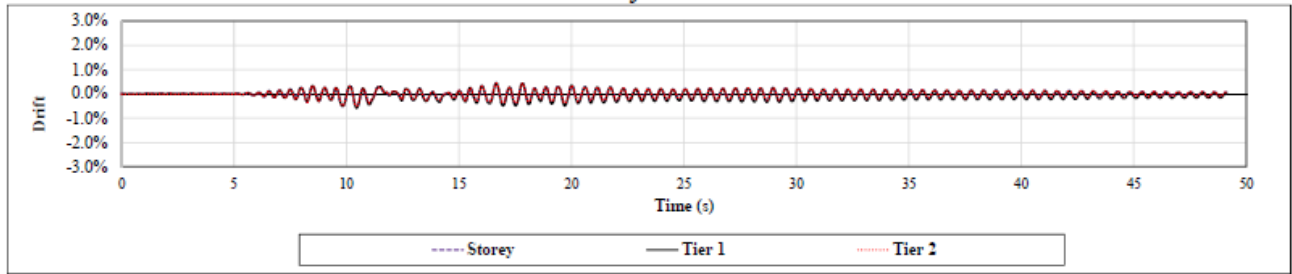
Column Out-of-plane Bending Demand



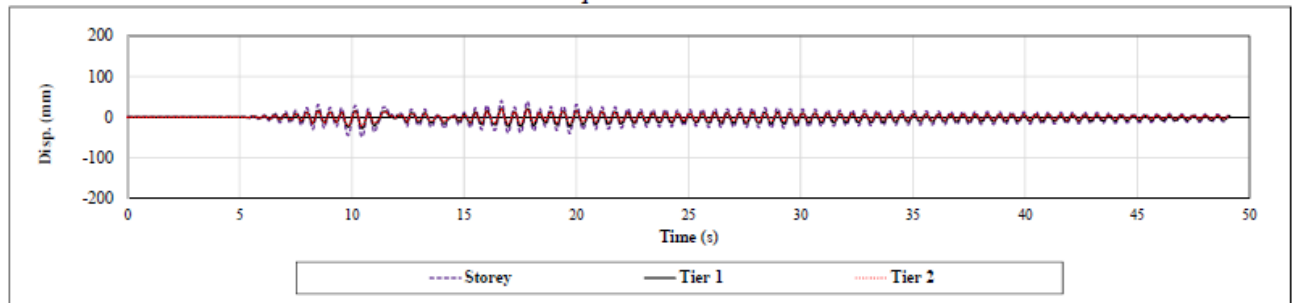
Ground Motion: SCC 6

Two-Tiered SCBF: AISC 341-16 Design

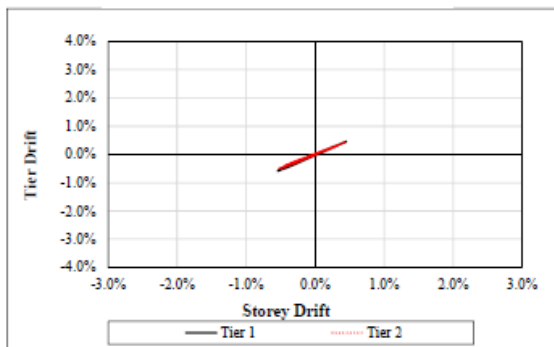
Drift vs. Time



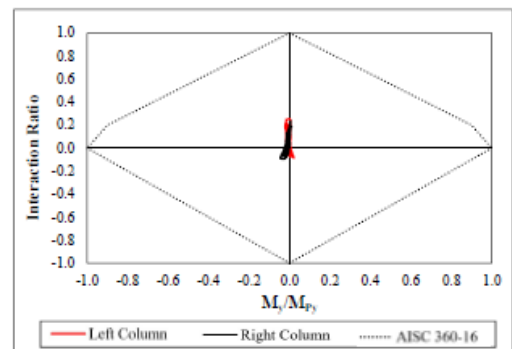
Displacement vs. Time



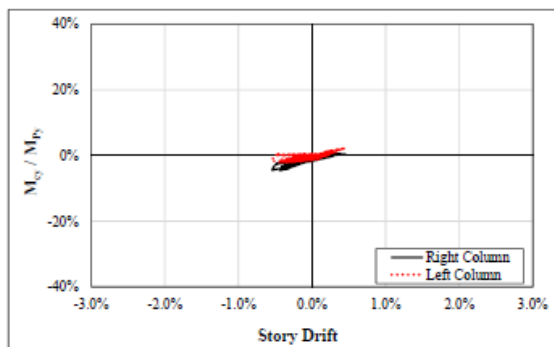
Tier Drift vs. Storey Drift



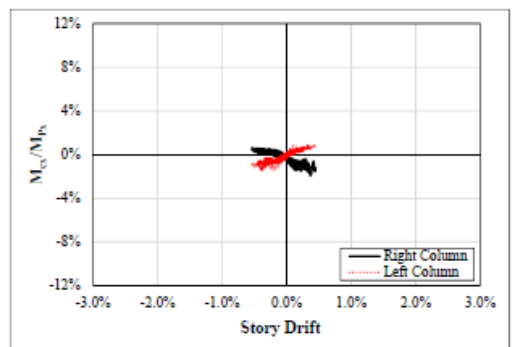
Column P-M Interaction Diagram



Column In-plane Bending Demand



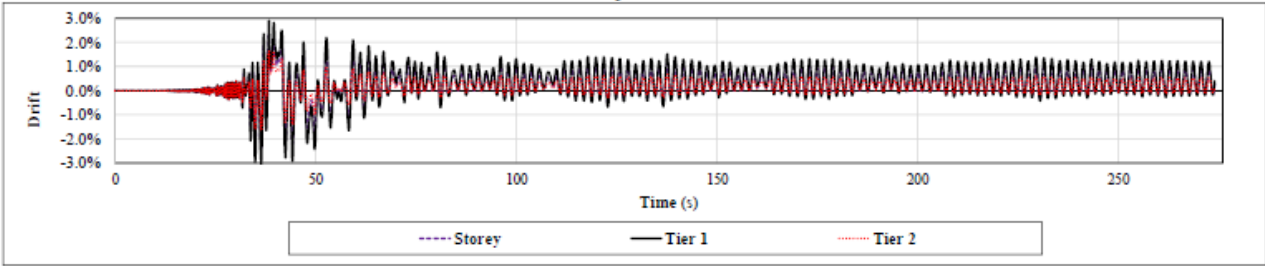
Column Out-of-plane Bending Demand



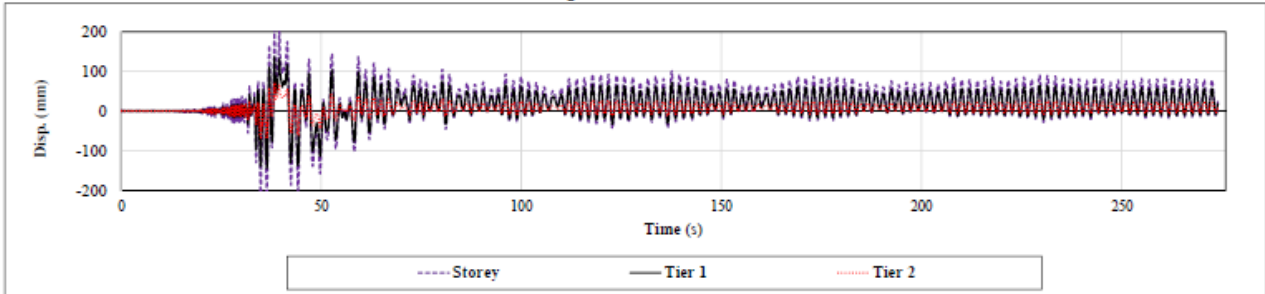
Ground Motion: SCC 7

Two-Tiered SCBF: AISC 341-16 Design

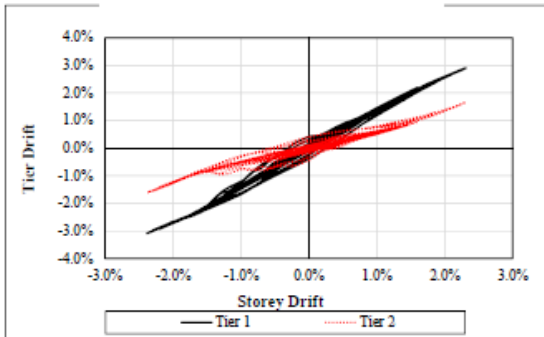
Drift vs. Time



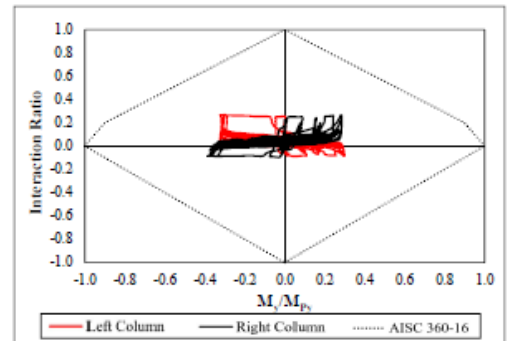
Displacement vs. Time



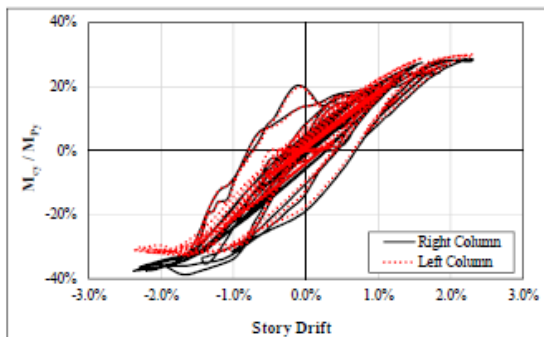
Tier Drift vs. Storey Drift



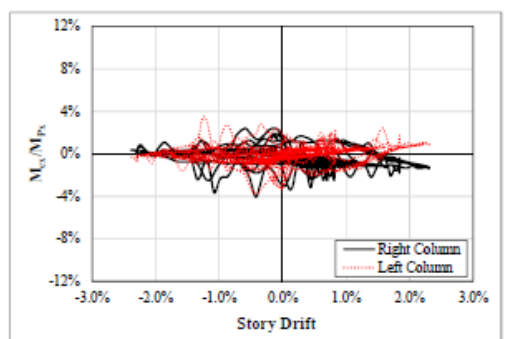
Column P-M Interaction Diagram



Column In-plane Bending Demand



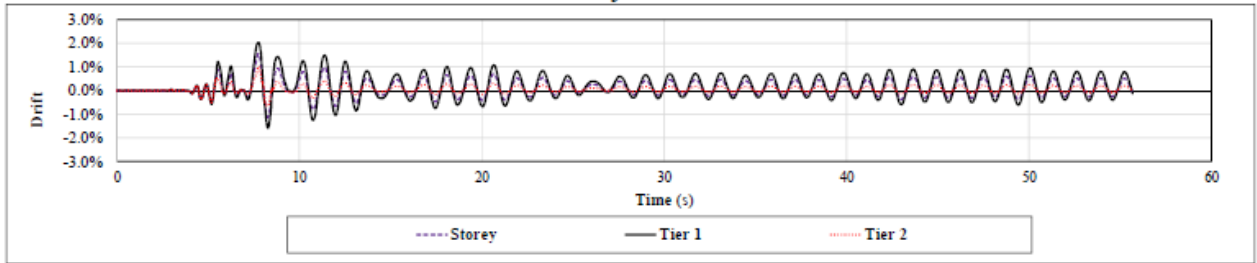
Column Out-of-plane Bending Demand



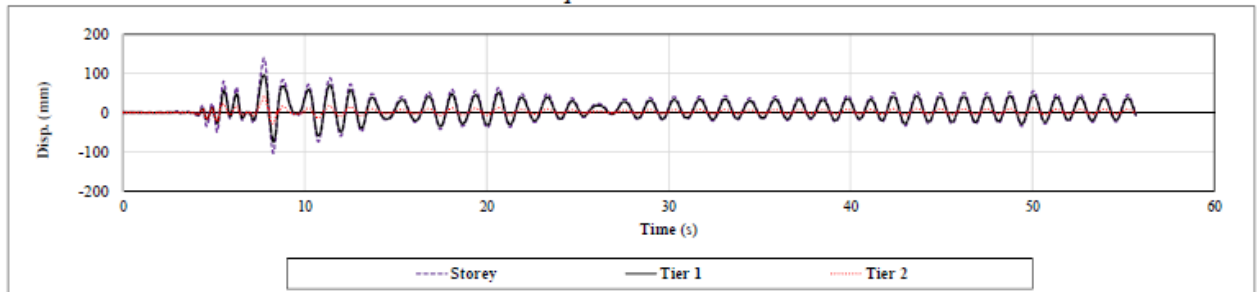
Ground Motion: SCC 8

Two-Tiered SCBF: AISC 341-16 Design

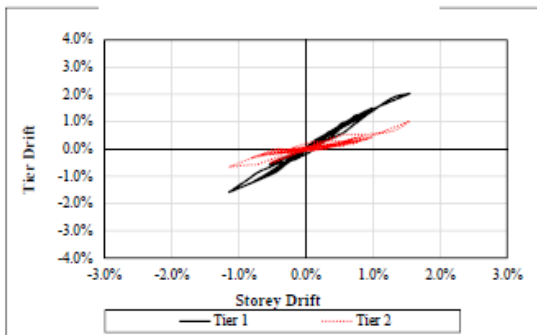
Drift vs. Time



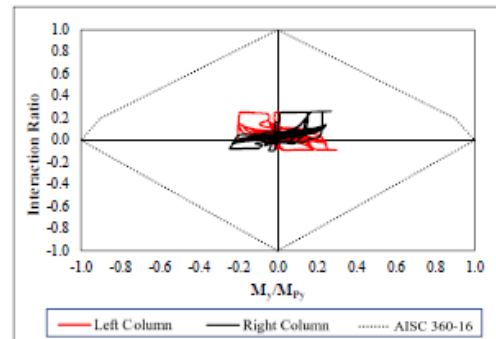
Displacement vs. Time



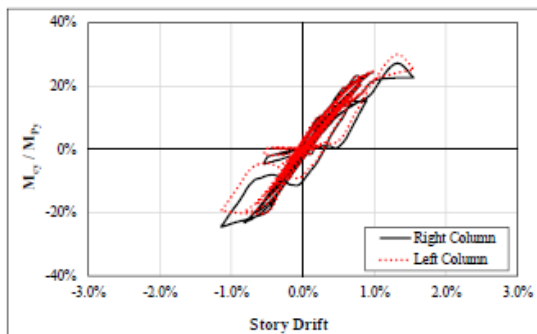
Tier Drift vs. Storey Drift



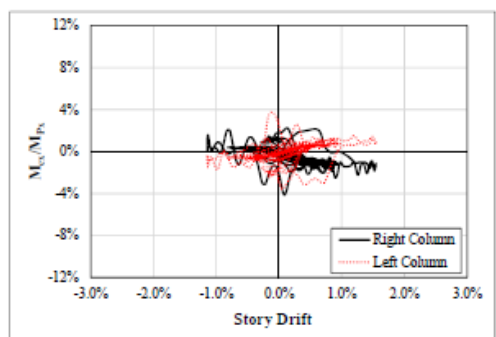
Column P-M Interaction Diagram



Column In-plane Bending Demand



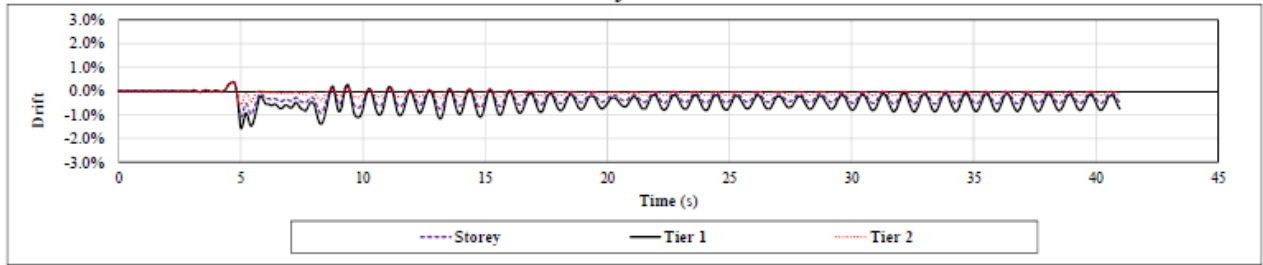
Column Out-of-plane Bending Demand



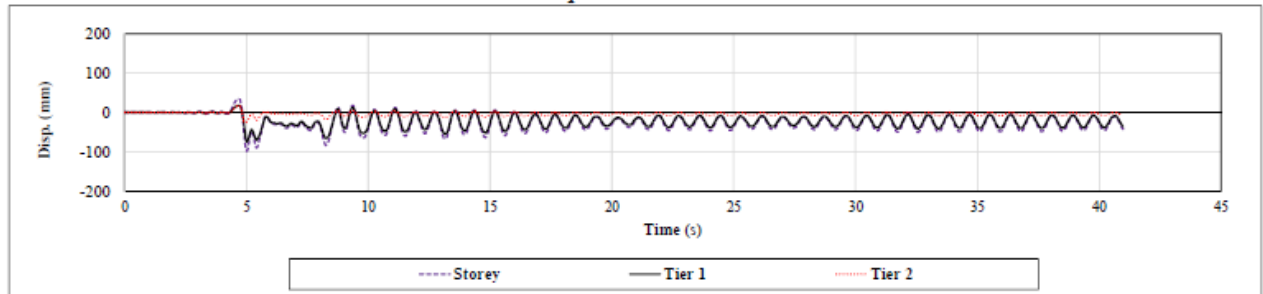
Ground Motion: SCC 9

Two-Tiered SCBF AISC 341-16 Design

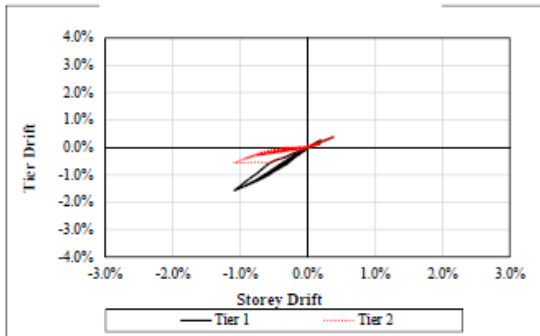
Drift vs. Time



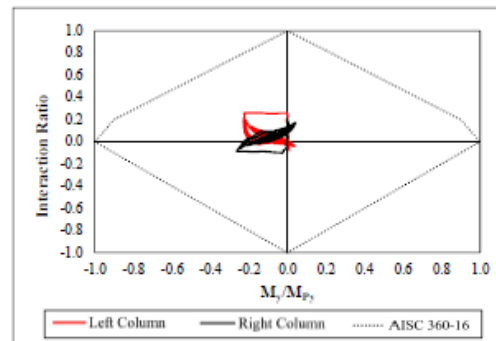
Displacement vs. Time



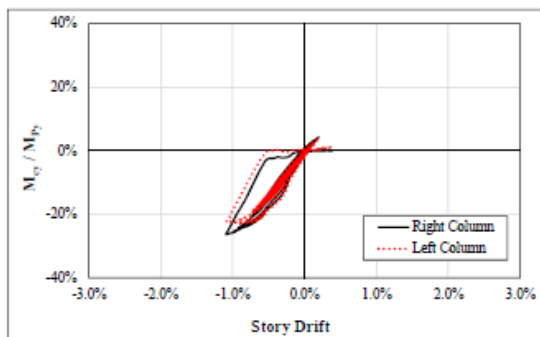
Tier Drift vs. Storey Drift



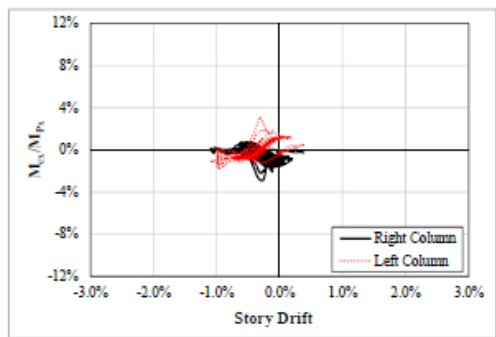
Column P-M Interaction Diagram



Column In-plane Bending Demand



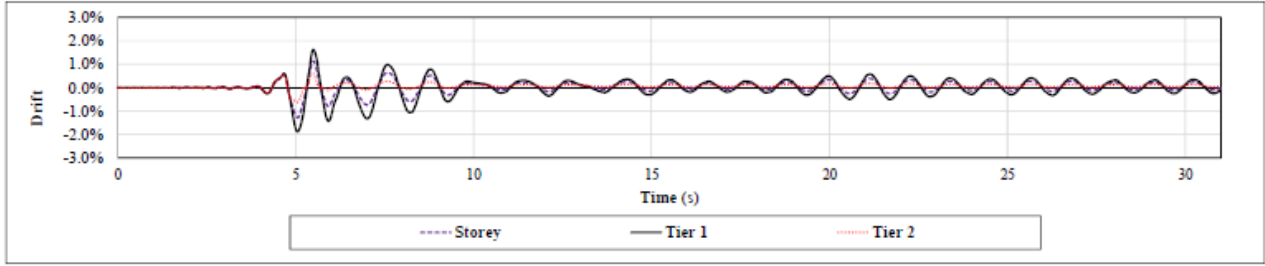
Column Out-of-plane Bending Demand



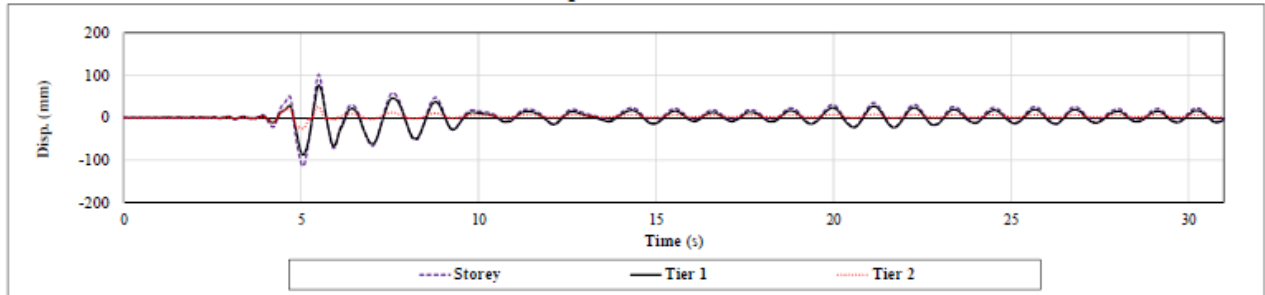
Ground Motion: SCC 10

Two-Tiered SCBF: AISC 341-16 Design

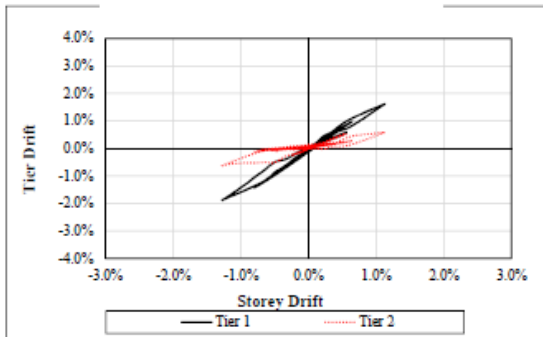
Drift vs. Time



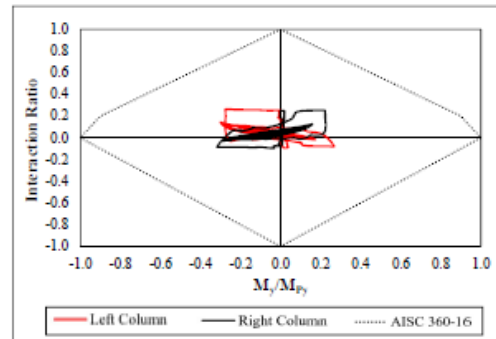
Displacement vs. Time



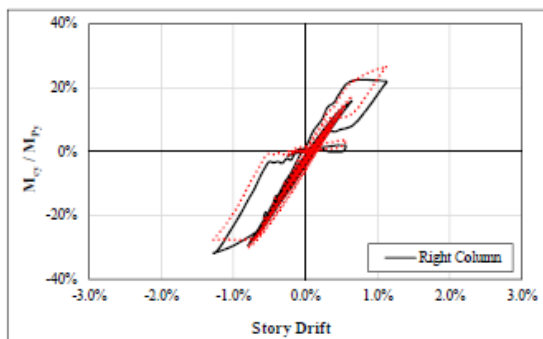
Tier Drift vs. Storey Drift



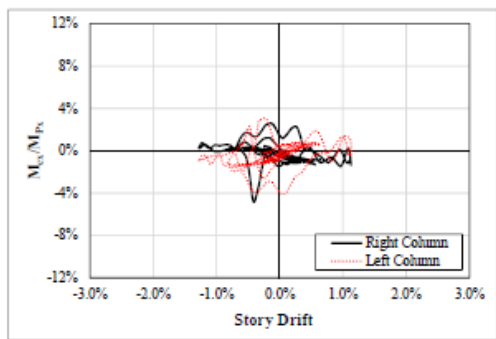
Column P-M Interaction Diagram



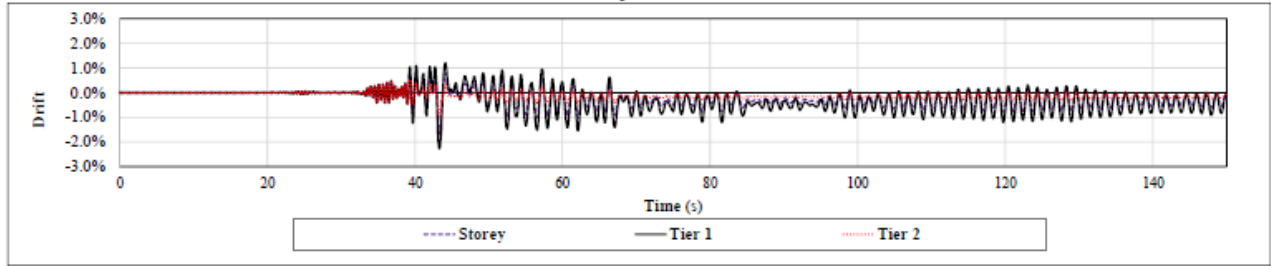
Column In-plane Bending Demand



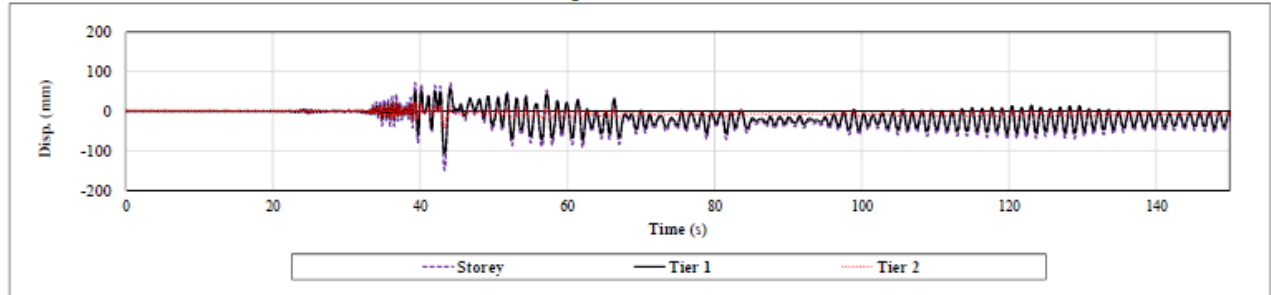
Column Out-of-plane Bending Demand



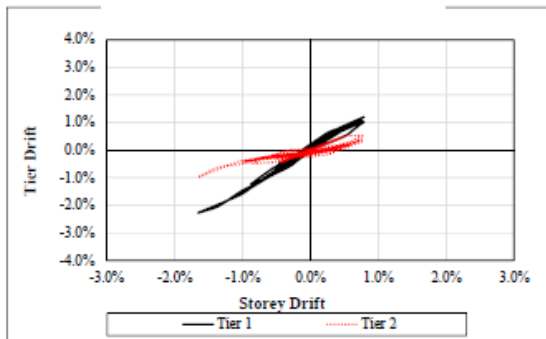
Drift vs. Time



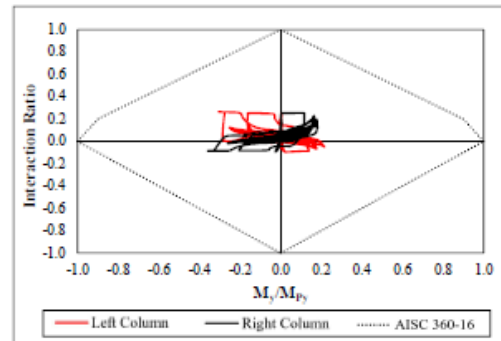
Displacement vs. Time



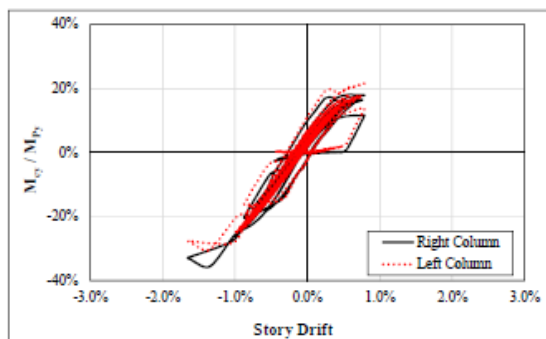
Tier Drift vs. Storey Drift



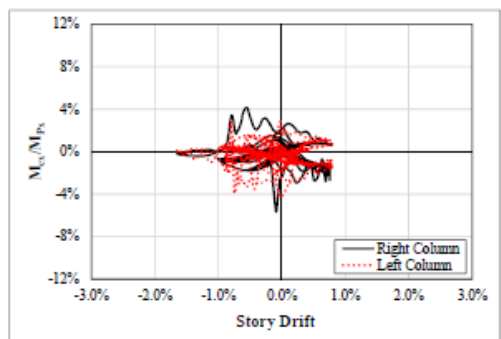
Column P-M Interaction Diagram



Column In-plane Bending Demand



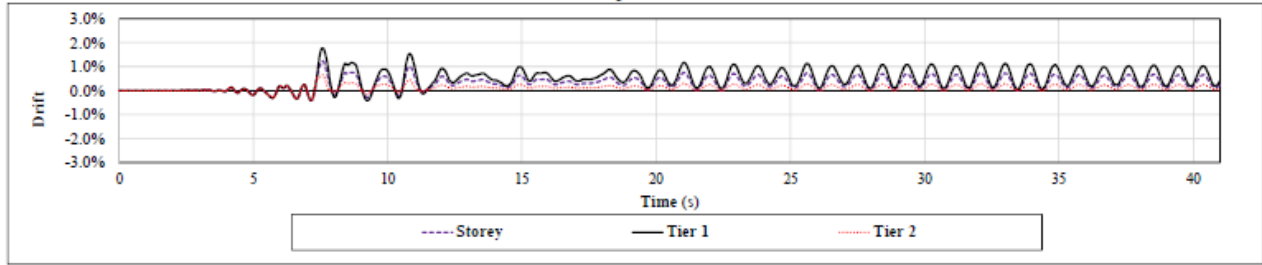
Column Out-of-plane Bending Demand



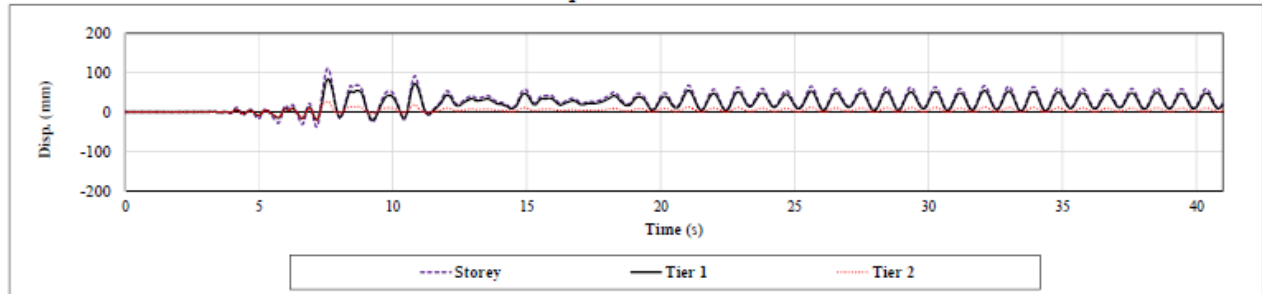
Ground Motion: SCC 12

Two-Tiered SCBF: AISC 341-16 Design

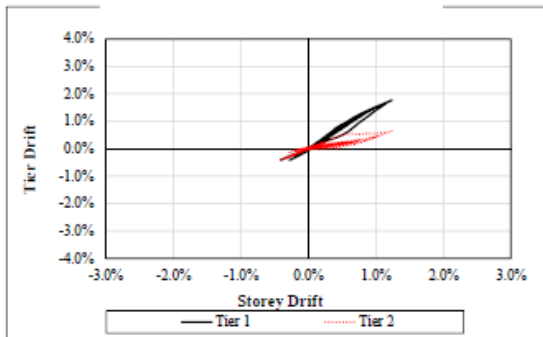
Drift vs. Time



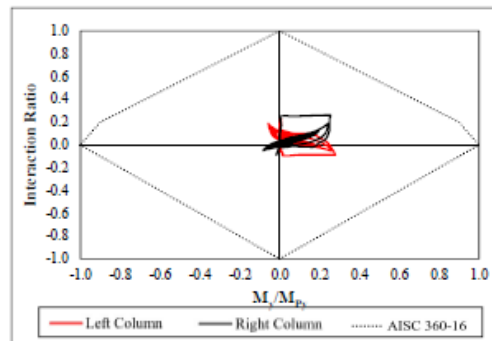
Displacement vs. Time



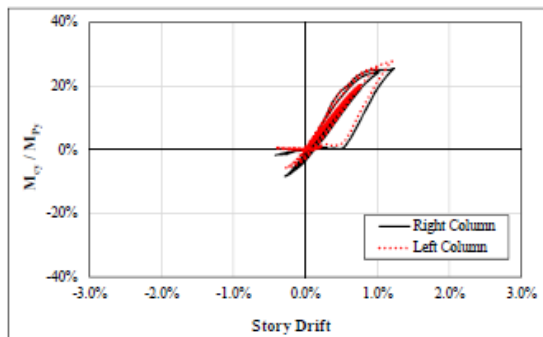
Tier Drift vs. Storey Drift



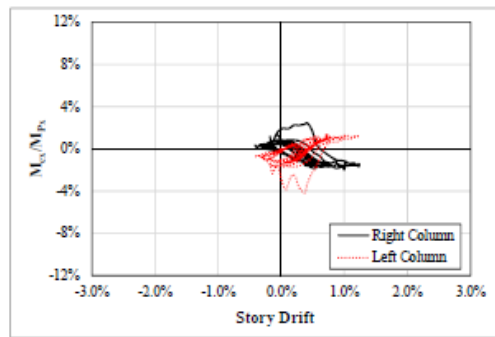
Column P-M Interaction Diagram



Column In-plane Bending Demand



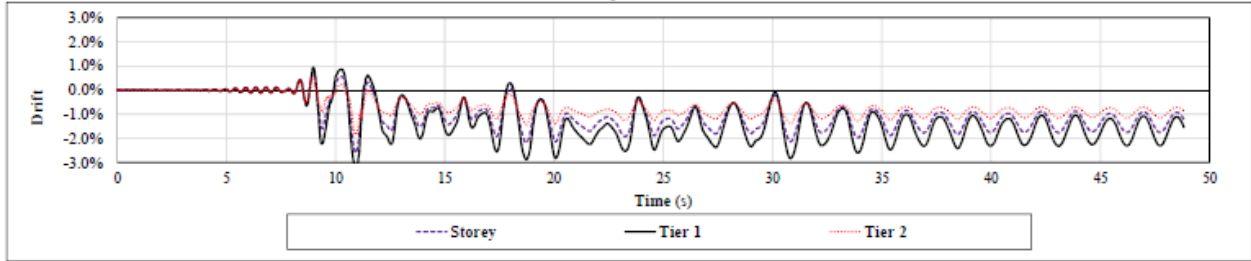
Column Out-of-plane Bending Demand



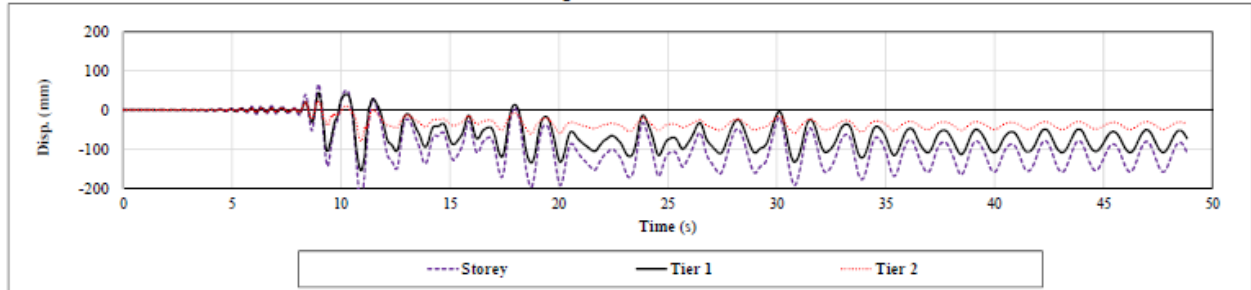
Ground Motion: SCC 13

Two-Tiered SCBF: AISC 341-16 Design

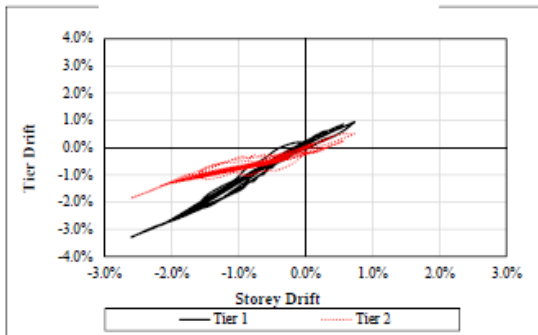
Drift vs. Time



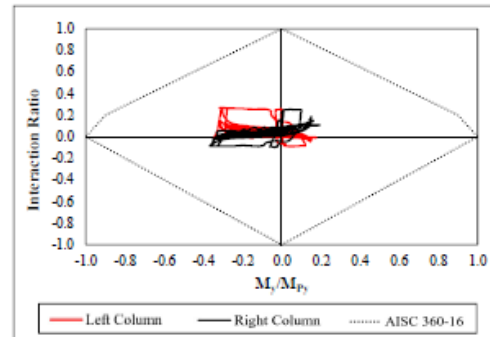
Displacement vs. Time



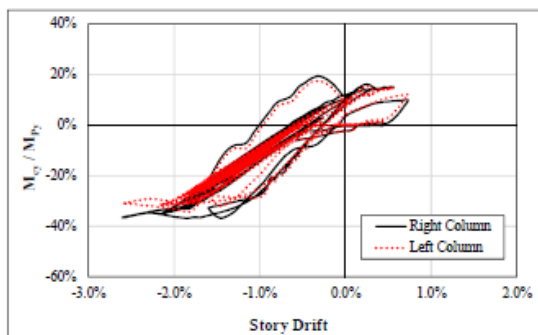
Tier Drift vs. Storey Drift



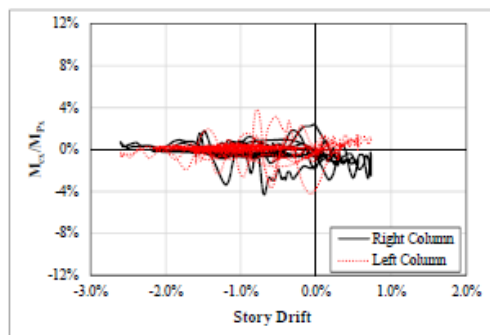
Column P-M Interaction Diagram



Column In-plane Bending Demand



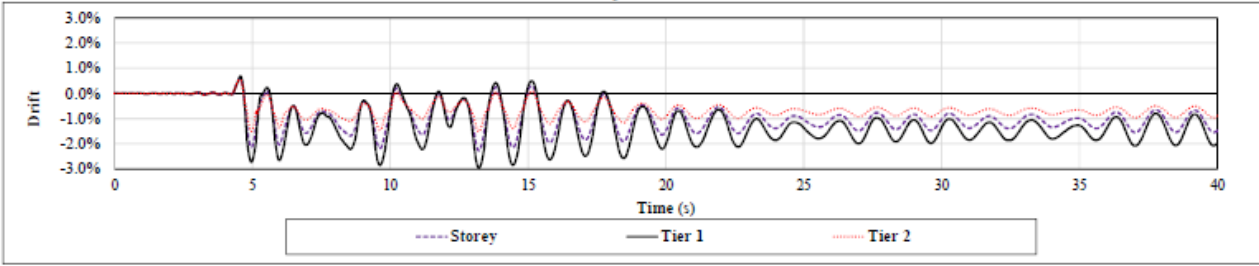
Column Out-of-plane Bending Demand



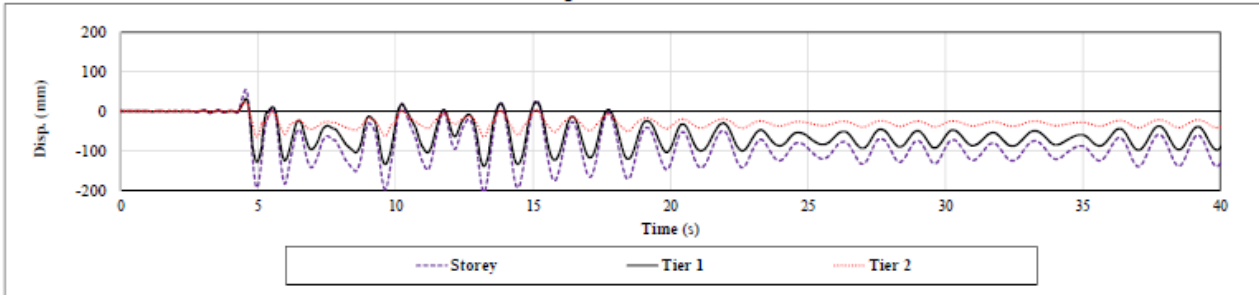
Ground Motion: SCC 14

Two-Tiered SCBF: AISC 341-16 Design

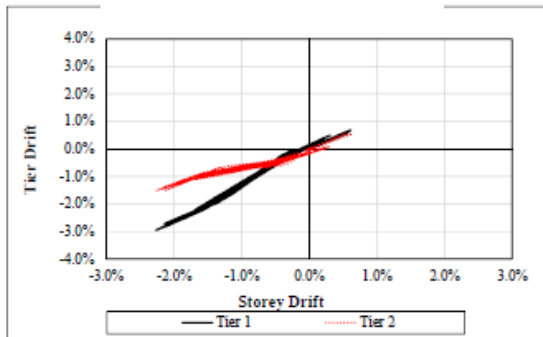
Drift vs. Time



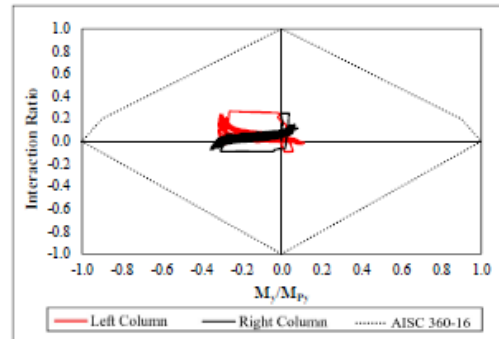
Displacement vs. Time



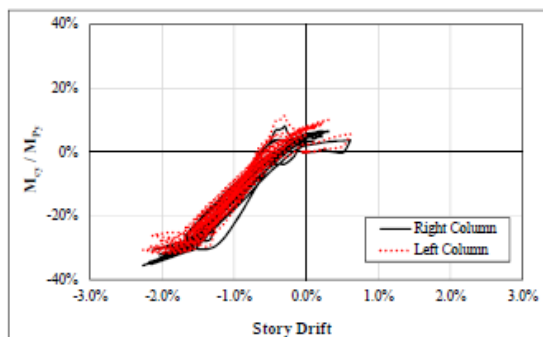
Tier Drift vs. Storey Drift



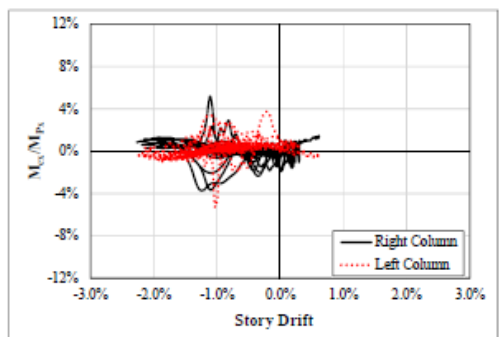
Column P-M Interaction Diagram



Column In-plane Bending Demand



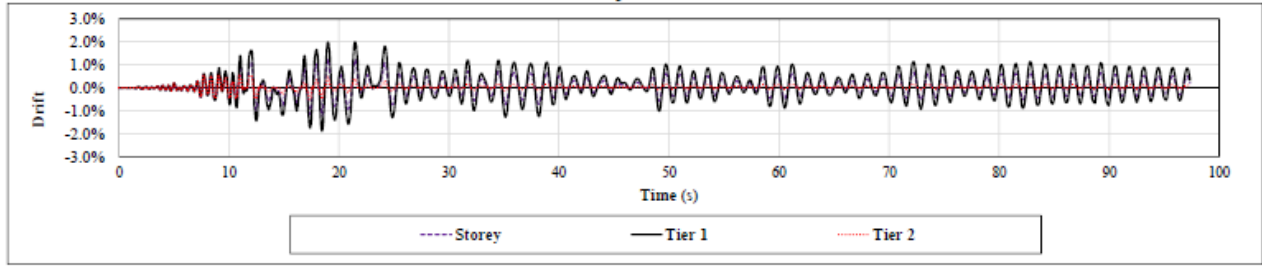
Column Out-of-plane Bending Demand



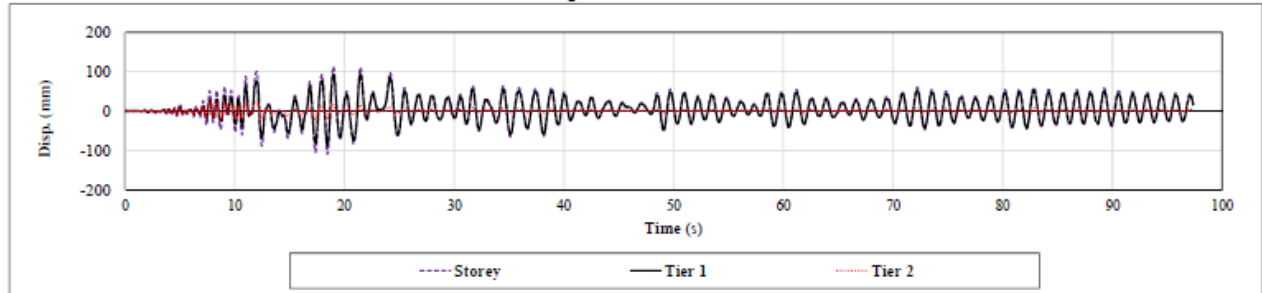
Ground Motion: SCD 1

Two-Tiered SCBF: AISC 341-16 Design

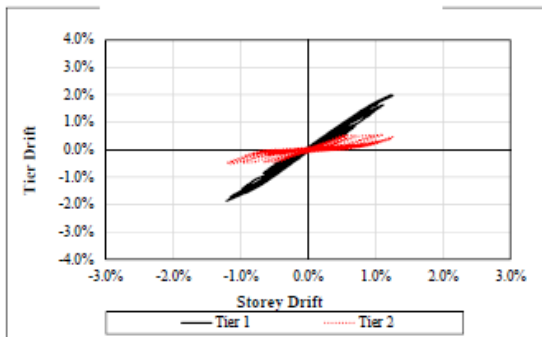
Drift vs. Time



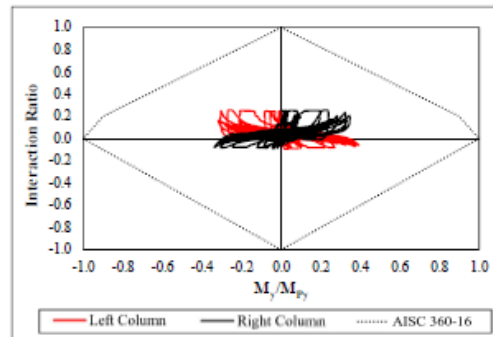
Displacement vs. Time



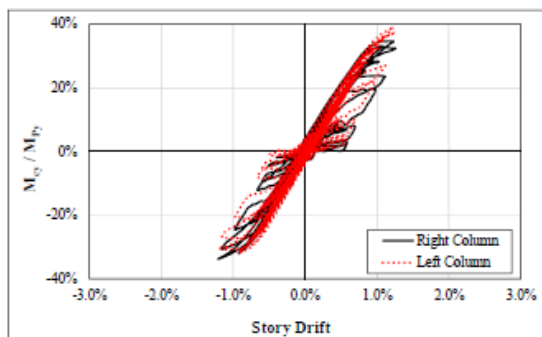
Tier Drift vs. Storey Drift



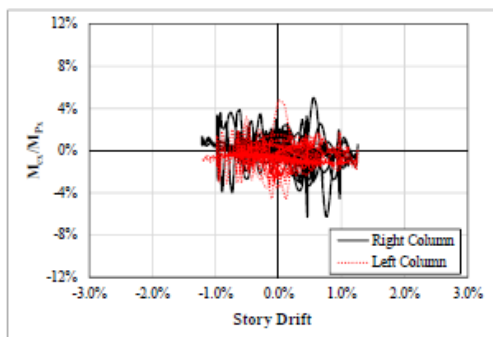
Column P-M Interaction Diagram



Column In-plane Bending Demand



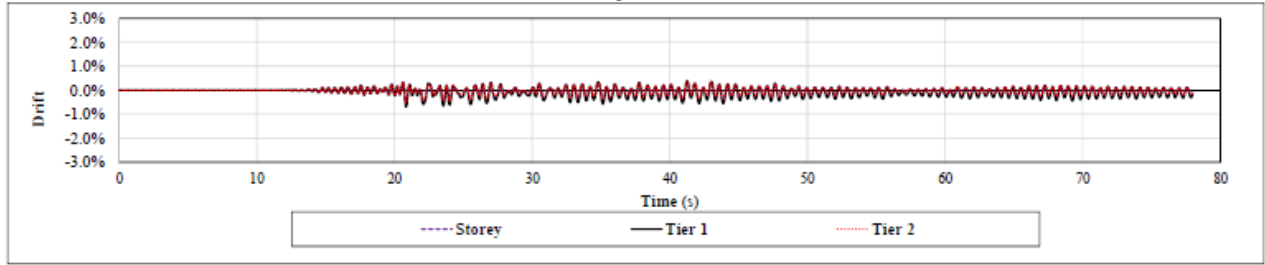
Column Out-of-plane Bending Demand



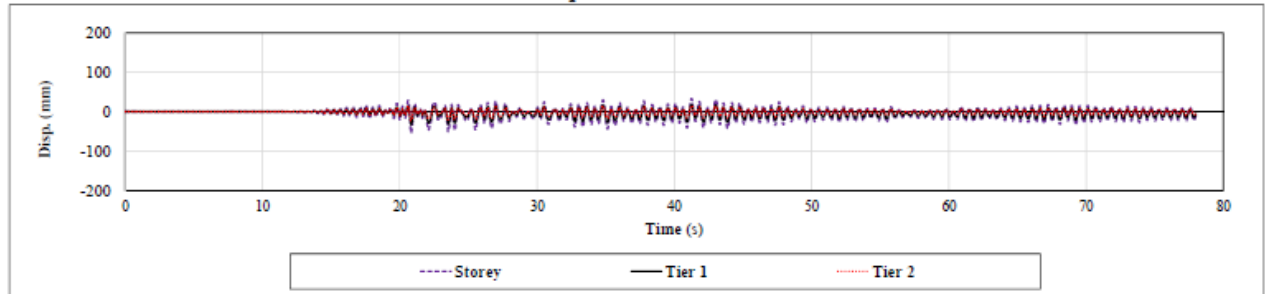
Ground Motion: SCD 2

Two-Tiered SCBF: AISC 341-16 Design

Drift vs. Time



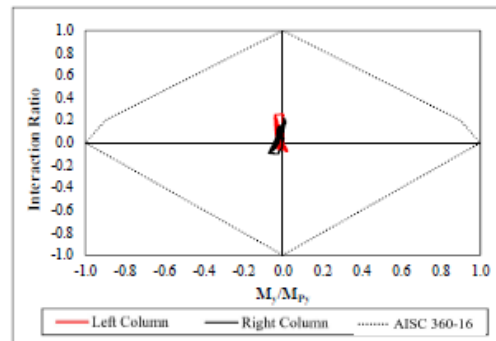
Displacement vs. Time



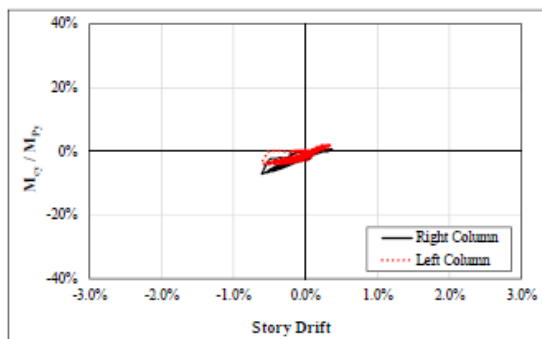
Tier Drift vs. Storey Drift



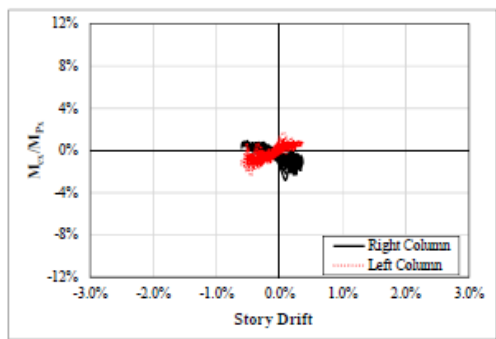
Column P-M Interaction Diagram



Column In-plane Bending Demand



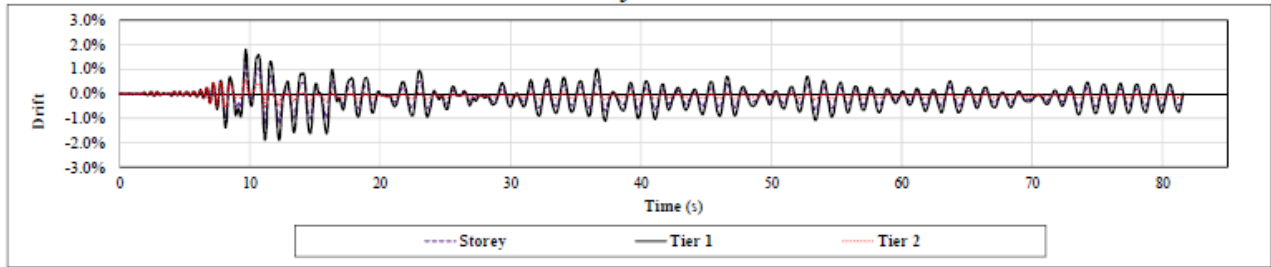
Column Out-of-plane Bending Demand



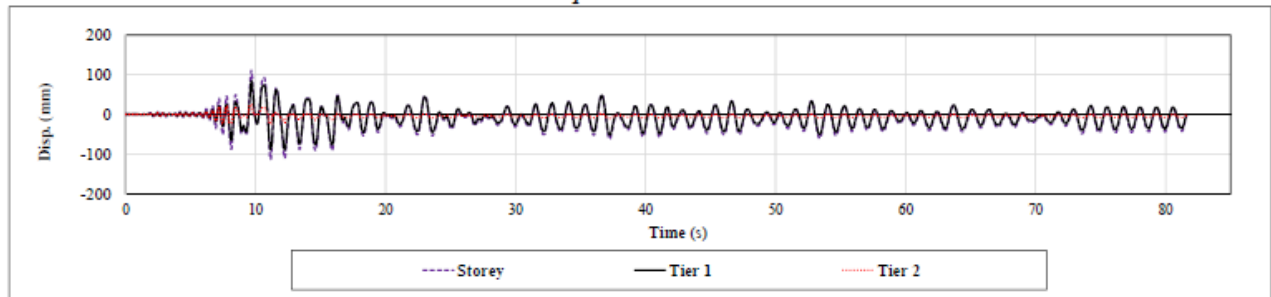
Ground Motion: SCD 3

Two-Tiered SCBF: AISC 341-16 Design

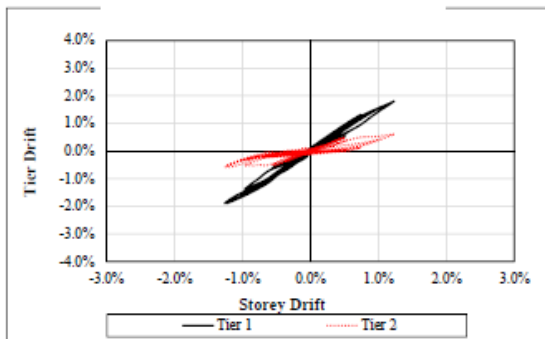
Drift vs. Time



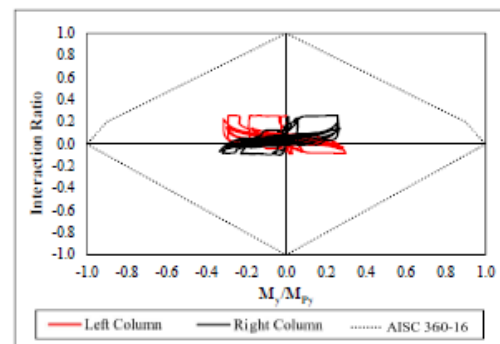
Displacement vs. Time



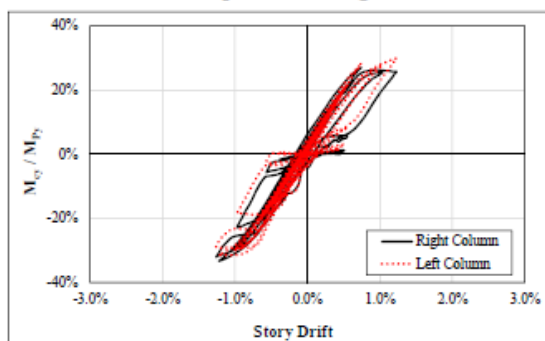
Tier Drift vs. Storey Drift



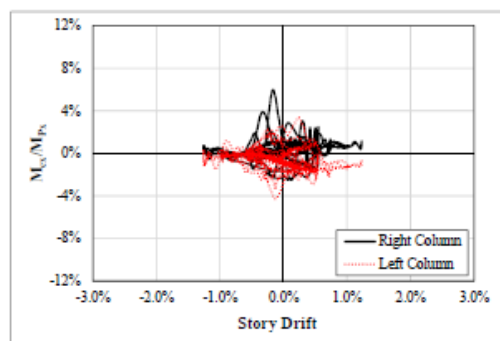
Column P-M Interaction Diagram



Column In-plane Bending Demand



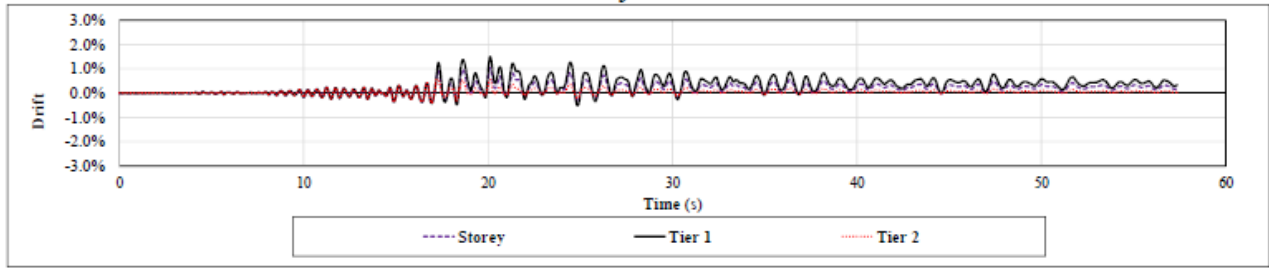
Column Out-of-plane Bending Demand



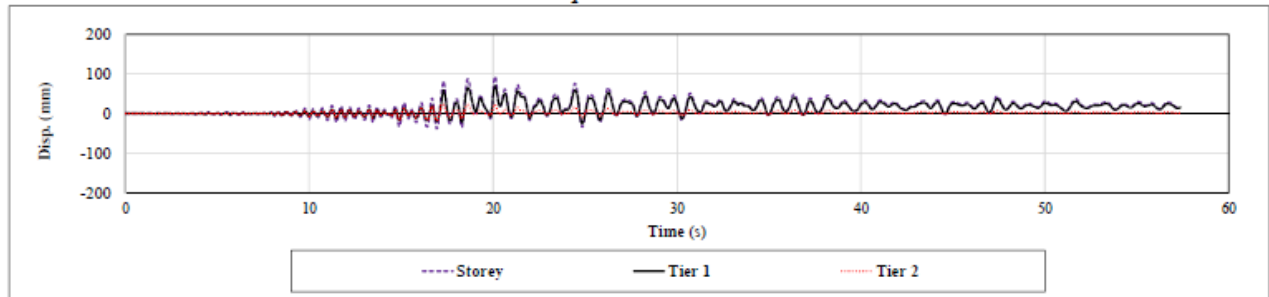
Ground Motion: SCD 4

Two-Tiered SCBF: AISC 341-16 Design

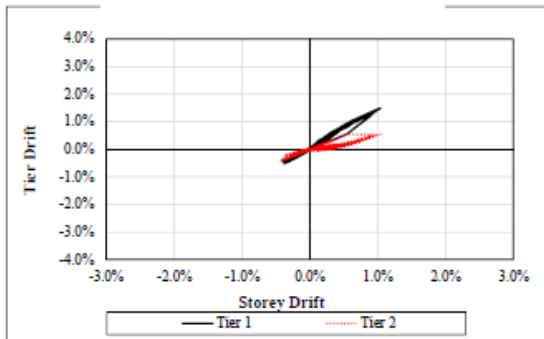
Drift vs. Time



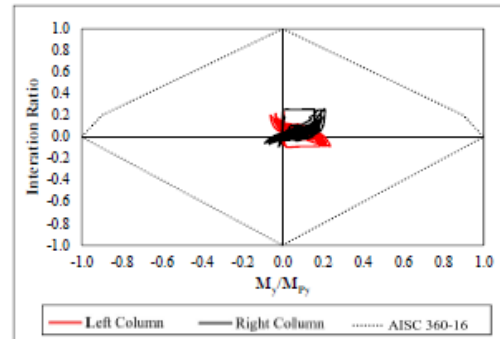
Displacement vs. Time



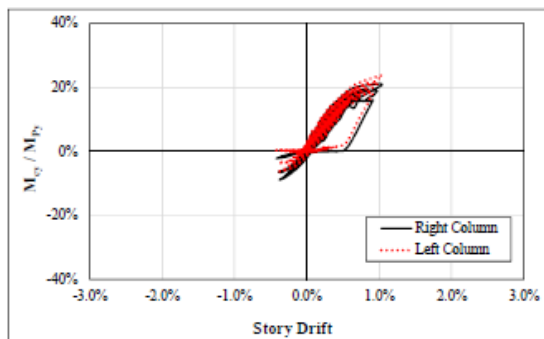
Tier Drift vs. Storey Drift



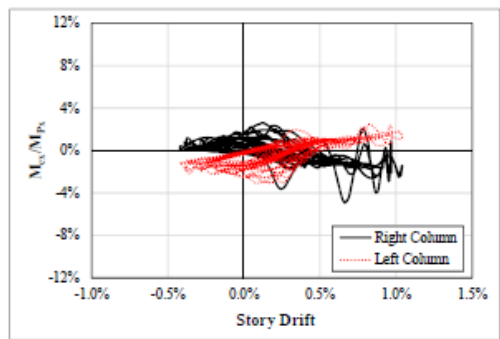
Column P-M Interaction Diagram



Column In-plane Bending Demand



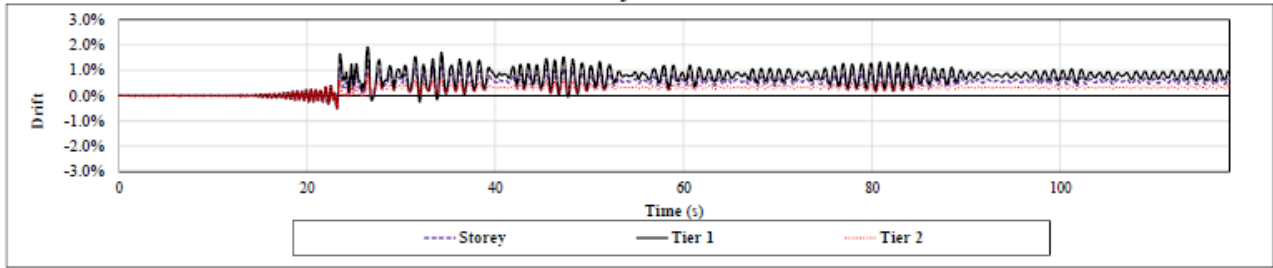
Column Out-of-plane Bending Demand



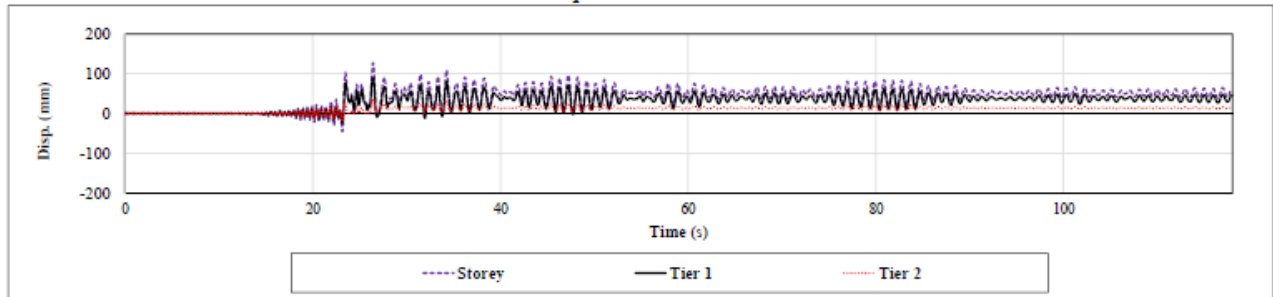
Ground Motion: SCD 5

Two-Tiered SCBF: AISC 341-16 Design

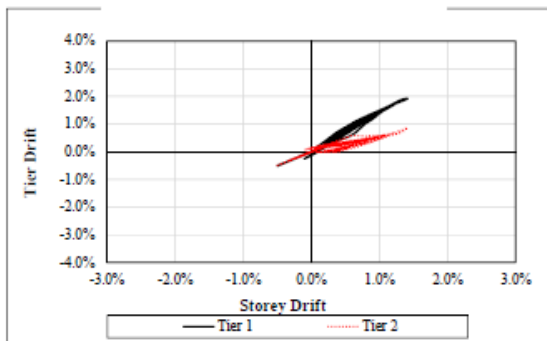
Drift vs. Time



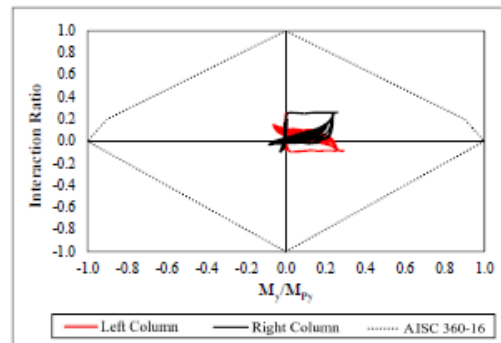
Displacement vs. Time



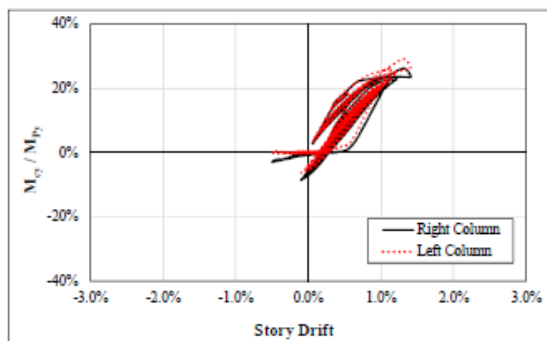
Tier Drift vs. Storey Drift



Column P-M Interaction Diagram



Column In-plane Bending Demand



Column Out-of-plane Bending Demand

